



IGAM/UniGraz Technical Report for ESA/ESTEC No. 1/2004

ESA study:

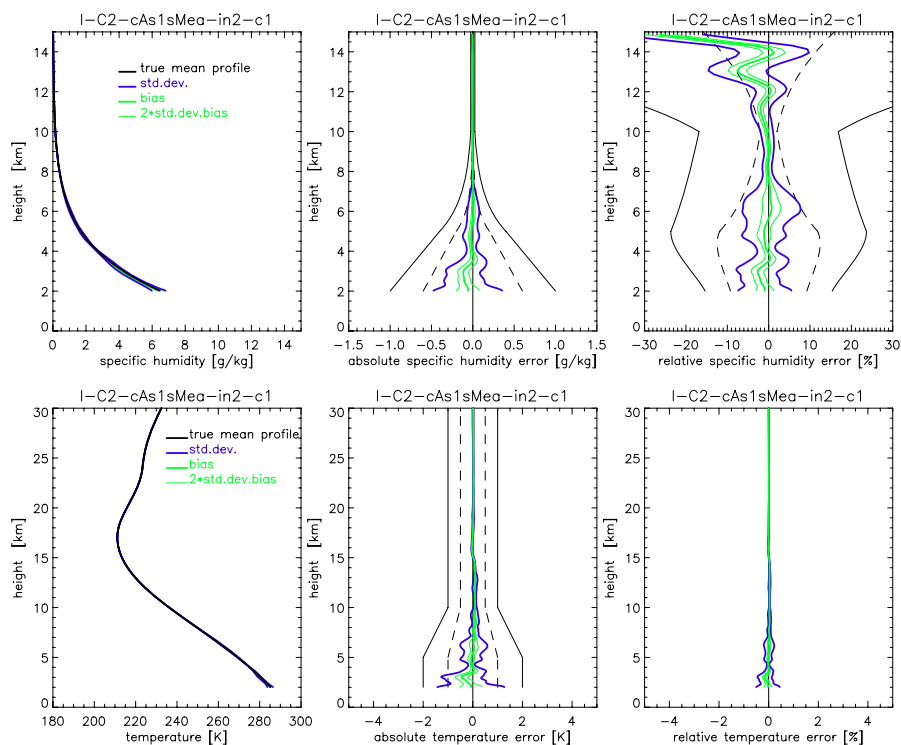
ACEPASS – LEO-LEO Occultation Characterisation Study

[ESA/ESTEC Contract No. 16743/02/NL/FF, WP 4.1: Analysis of instrumental and GOP performance impacts]

Atmospheric Profiles Retrieved from ACE+ LEO-LEO Occultation Data: Statistical Performance Analysis using Geometric Optics Processing

G. Kirchengast, S. Schweitzer, J. Ramsauer, J. Fritzer, and M. Schwaerz

IGAM/University of Graz, Graz, Austria



February 2004

(intentionally left blank, back page if double-sided print)

Table of Contents

1. INTRODUCTION	1
1.1. Study Objectives and Overview	1
1.2. Report Overview	1
2. MODELING SYSTEM FOR PERFORMANCE ANALYSIS	2
2.1. The Simulation Tool EGOPS5	2
2.2. Forward Modeling	4
2.3. Observation System and Instrumental Error Modeling	7
2.4. Retrieval Processing Chain and Retrieval Algorithms	10
3. STATISTICAL PERFORMANCE ANALYSIS RESULTS	29
3.1. Results on Retrieval Performance in Clear Air	30
3.2. Results on Retrieval Performance in Presence of Clouds	91
3.3. Results on Retrieval Performance in Presence of Clouds and Atmospheric Turbulence	104
4. SUMMARY AND CONCLUSIONS	125
REFERENCES	126
APPENDIX A.	131
A.1. ACE+ Constellation Two Line Element (TLE) Files	131
A.2. Mission Analysis/Planning input (example)	131
A.3. Forward Modeling input (example)	132
A.4. Observation System Modeling input (example)	133
A.5. Inversion/Retrieval input (example)	134

(intentionally left blank, back page if double-sided print)

1. Introduction

This report deals with Work Package 4.1 (WP 4.1) of the ACE+ Phase A Scientific Support (ACEPASS) Study on LEO-LEO Occultation Characterization (Kirchengast et al., 2002). WP 4.1 is dedicated to a performance analysis for ACE+ LEO-LEO radio occultation (RO) data with focus on assessing, based on a geometric optics retrieval processing chain, the temperature and humidity retrieval performance under reasonable system and instrumental error assumptions. For this, retrievals were carried out under diverse atmospheric conditions, from hot/wet to cold/dry and from clear moist air to cloudy and turbulent air.

1.1. Study Objectives and Overview

The overall objective of the study is the characterization of the retrieval performance achievable by atmospheric sounding with the ACE+ LEO-LEO occultation. Consolidation and refinement of the underlying observation requirements and related requirements at system level shall be obtained (ACE+ MRD, 2004). A statistical performance analysis for instrumental errors using geometric optics processing (GOP) is carried out and the retrieval results inspected for a whole range of scenarios in moist (clear) air as well as in the presence of clouds and in the presence of scintillations due to atmospheric turbulence.

In particular, the present performance analysis comprises two main lines, the characterization of instrumental errors as a function of relevant parameters and the analysis of impacts of clouds and atmospheric turbulence. In the former part, the sensitivity of humidity and temperature retrievals to various relevant instrumental error components will be analyzed under different clear air conditions using geometrics-optics (GO) processing. Also the impacts of critical parameters of the retrieval processing will thereby be investigated. The other part includes an analysis of the sensitivity of temperature, humidity and liquid-water retrievals to miscellaneous atmospheric conditions and parameters impacting the retrieval performance, assuming two different kinds of instrumental error cases. The atmospheric conditions comprise several cloudy and turbulent situations.

Based on these analyses, the study will establish and consolidate the knowledge on useful ranges of critical parameter values for acceptable mission performance and provide an assessment of the adequacy of the ACE+ requirements. The study results will establish the needed link between main system requirements, set on the bending angle/raw transmission data level, and observational requirements, set on the humidity and temperature retrieval level (ACE+ MRD, 2004).

1.2. Report Overview

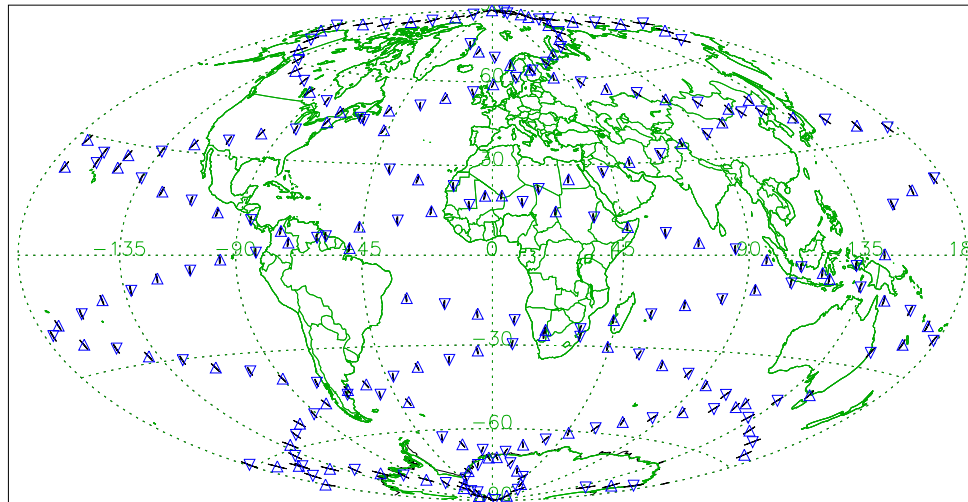
The report is structured as follows. In section 2, the performance simulation setup used for the study is presented. In particular, a description of the simulation tool EGOPS5 and a detailed description of the retrieval algorithms are provided in this section. Section 3 summarizes all analysis results and shows statistical profile retrieval performance results for a wide range of conditions. The focus is on humidity and temperature results, complementarily also results on transmission and liquid water are shown in many cases. In section 4, a brief summary and conclusions are given.

2. Modeling System for Performance Analysis

2.1. The Simulation Tool EGOPS5

EGOPS5 has been developed from EGOPS4 and is an extension and advancement of it. In contrast to EGOPS4 (Kirchengast 1998; Kirchengast et al., 2001), EGOPS5 also allows LEO-LEO occultation simulations. The baseline LEO-LEO system assumed is an ACE+ mission with two LEO satellites in an ~800 km orbit carrying LEO crosslink transmitters and two counter-rotating LEO satellites in an ~650 km orbit carrying LEO crosslink receivers (Kirchengast and Hoeg, 2004). In addition, all four satellites are baselined to carry advanced GRAS (GNSS Receiver for Atmospheric Sounding) sensors for GPS-LEO and GALILEO-LEO occultation. When working with realistic geometry, two different ACE+ satellite orbit configurations are available presently: sun-synchronous (with orbit nodes aligned in local time with the planned EPS/METOP orbit nodes) and polar (90 deg inclination). The primary baseline for ACE+ is the sun synchronous constellation. The corresponding orbital elements are listed in Appendix A.1 in the form of "Two Line Element" (TLE) sets. With such a constellation, a total of 230 occultation events is obtained during one day, and about 7000 events during one month (Figure 2.1). Appendix A.2 shows an example input file for EGOPS5 Mission Analysis/Planning simulations.

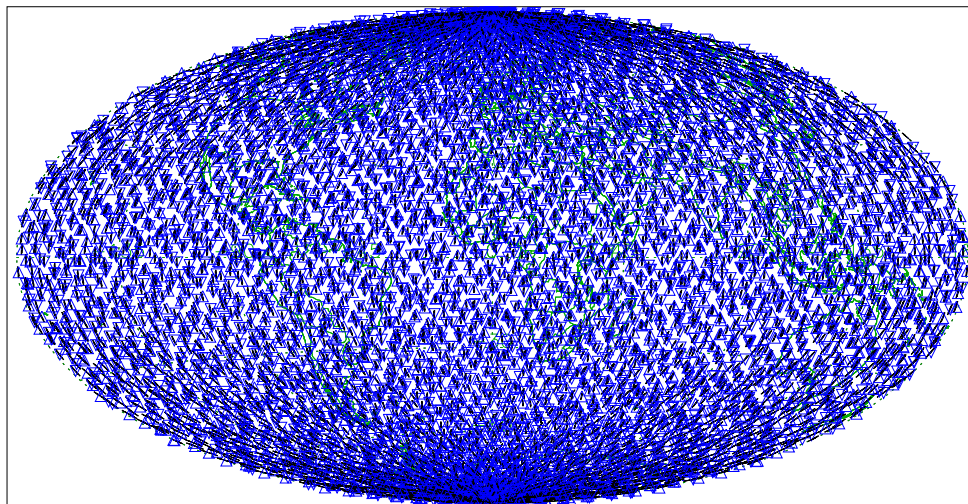
Occ. Event Distribution Data – Ground Projection Data



No.OccEv (∇ Set+ Δ Rise ACE): 232 total, 116/ 116 set/rise.
 UT Range: 990101.000000,0240000, H Levels: 2.0 12.0 10.0, 12.0 50.0 38.0
 File-Id: /ACECLIM-P2/MAnPl/S-t2h800-rA2180-1Jan1999.GrProjD01
 HRx = 650km, HTx = 800km, RxSep = 80deg, TxSep = 180deg

Produced by EGOPS⁵ V5.0a © IGAM/UC et al. 1997-2003

Occ. Event Distribution Data – Ground Projection Data



No.OccEv (∇ Set+ Δ Rise ACE): 7203 total, 3601/ 3602 set/rise.
 UT Range: 990101.000000,7440000, H Levels: 2.0 12.0 10.0, 12.0 50.0 38.0
 File-Id: /ACECLIM-P2/MAnPl/S-t2h800-rA2180-Jan1999.GrProjD01
 HRx = 650km, HTx = 800km, RxSep = 80deg, TxSep = 180deg

Produced by EGOPS⁵ V5.0a © IGAM/UC et al. 1997-2003

Fig. 2.1. ACE+ LEO-LEO occultation events during one day (upper) and one month (lower panel).

The number of LEO-LEO transmitter frequencies is three for the ACE+ system. Their nominal values, which are used in this study, are $F1 = 9.7$ GHz, $F2 = 17.25$ GHz, and $F3 = 22.6$ GHz. For realistic forward modeling beyond the gaseous atmospheric models, different cloud conditions as well as scintillations due to atmospheric turbulence can be included in EGOPS5. Various instrumental errors like thermal noise, $1/f$ amplitude noise and different amplitude drifts (polynomial and sinusoidal) can be superposed during observation system modeling.

In inversion/retrieval, the most important extension of EGOPS5 LEO-LEO over EGOPS4 GNSS-LEO is that it does not only take phases into account, but that it exploits amplitudes at

an equal footing. Besides determination of bending angles, this also allows for computation of transmission profiles at all (three) frequencies, which allows, in turn, to retrieve via complex refractivity profiles, profiles of pressure, temperature, humidity, and liquid water simultaneously.

Thus EGOPS5 will be a useful tool to carry out consistent and reliable LEO-LEO end-to-end simulations providing the basis for performing a full range of mission planning and performance analyses. This study is a first step of such analyses.

2.2. Forward Modeling

Forward Modeling and the subsequent Observation System Modeling in EGOPS are the basis for providing reasonably realistic simulated observables of phase and amplitude profiles at all relevant frequencies. LEO-LEO forward modeling in EGOPS5 consists of three main elements: the orbit arcs simulations which finds the orbit sections of the transmitter (Tx) and receiver (Rx) LEO orbits necessary for performing the forward modeling (ray-by-ray from Tx to Rx over the full occultation event, if using a ray tracer), the transmitter signal simulations and the signal propagation simulations, which also involve simulation of the atmosphere/ionosphere environment. The simulation conditions are based on user-specified input parameters like type of occultation event, atmospheric and ionospheric model and conditions, sampling rate, type of propagation simulator, etc. An example of such a forward modeling input file is shown in Appendix A.3.

Orbit arcs computations, which can be done using “ideal” or “realistic” geometry, create the so called **simulated geometry data**. This data contains the satellite positions [km] and velocities [km/s] along the orbit arcs of the specified transmitter and receiver satellites, respectively, at the specified sampling rate for the current occultation event. It is required as a geometric baseline for the subsequent signal propagation simulations. As a convenient sideline, also “true” tangent point profile estimates from ray-tracers are stored with these data.

The **transmitter signal simulations** determine the carrier-frequencies and transmitted powers of the occultation signals. In order to allow for other LEO-LEO simulations beyond ACE+, up to five frequency channels within 1 to 30 GHz are possible. The ACE+ Tx set contains the three nominal frequencies with values of $F1 = 9.7$ GHz, $F2 = 17.25$ GHz, and $F3 = 22.6$ GHz. The corresponding transmitter signal powers amount to 3 dBW for each frequency.

The **signal propagation simulations** can be carried out using the “full-3D ray tracer” (which fully accounts for the three-dimensional refractivity field and its first two derivatives), the “quasi-3D ray tracer” (which, besides the field, only accounts for vertical refractivity gradients and curvature) or the “wave optics propagator”. Currently (EGOPS5.0.3 status) and for this study, the full-3D ray tracer is the only tool to be used. The tools create the **simulated signal data**, which include the main observables excess phase [m] and atmospheric loss [dB] for each frequency at the specified sampling rates for the occultation event in consideration. Subsequently, this data is used as input data within observation system and inversion/retrieval processing. In addition, “true” bending angles [mrad] and “true” transmissions (due to absorption only) [dB] are computed as extended output, and the data also include “true” Doppler shifts [Hz] and “true” impact parameters [km] for each frequency, and the “true” linearly corrected phases LC for frequency $F1$ [m].

Rigorous modeling of atmospheric absorption loss is a new feature introduced in EGOPS5. Total atmospheric loss now consists of atmospheric loss due to defocusing and atmospheric loss due to absorption, which are considered separately. The geometric-optics computation is done in this way: For each sample in an occultation, the ray that goes from a specified transmitter position to a specified receiver position is found via precision ray-tracing. The tracking of the receiver is done with a few trials of ray paths, using Newton-Raphson's method of finding roots. After calculating initial ray parameters in degrees and total phase [km], the ray path is calculated by solving Haselgrove's three-dimensional differential equations (six equations) and the relative flux density is measured by solving twelve additional equations (Syndergaard, 1998). The eighteen equations in total are solved by numerical integration using a Runge-Kutta method and a predictor-corrector method especially designed to deal with adaptive stepsize. During the integration, in addition to the ray path calculation, the defocusing loss of the signal power is computed. After the refracted ray path is precisely known this way, along ray computation of absorption loss is done using the Bouguer-Lambert-Beer law (neglecting emission as we have strong source intensity in active limb sounding),

$$I = I_0 \cdot e^{-\int_{l_0}^{l_1} \kappa(l) dl} = e^{-\tau},$$

where I is the received signal intensity, l the coordinate along the ray path, l_0 the point of the considered part of the ray path farthest away from the sensor (to be placed above the atmosphere at ~ 80 km height so that beyond absorption is essentially negligible), l_1 the sensor-closest point of the ray path (also at ~ 80 km), I_0 the un-attenuated intensity at l_0 , κ the absorption coefficient along the ray path, which is proportional to imaginary refractivity, and τ the optical thickness (extinction coefficient, in general, but scattering is negligible in the present context). The absorption coefficient κ is calculated point-by-point along each ray for the given atmospheric conditions invoking the MPM93 imaginary refractivity model based on a selected atmospheric model (supplying temperature, water vapor, clouds,...). Using Simpson's integration rule, total optical thickness τ , and transmission (I/I_0) resp. absorption loss (I_0/I), are then calculated at the receiver end of the ray and added to the defocusing loss.

Finally, if desired, perturbations by an atmospheric turbulence/scintillation model can be superposed onto the total atmospheric loss. For further information see Kuhn (2003b).

All forward modeled events made for this study were simulated using high-precision 3D ray tracing with sub-millimetric accuracy and a sampling rate of 10 Hz. The underlying atmosphere model was the CIRA86aQ_UoG model (Kirchengast et al. 1999). Figure 2.2.1 shows a range of atmospheric temperature and humidity conditions used based on this moist air climatological model (Case1 tropical, Case2 mid-latitude summer, Case3 mid-latitude winter, Case4 high-latitude summer, Case5 high-latitude winter conditions; Case Std (standard) is mid-latitude March conditions).

Figure 2.2.2 illustrates total atmospheric loss under different conditions for an example case (mid-latitude summer), including moist but clear air, moist air plus altostratus cloud superposed, and also scintillations due to atmospheric turbulence superposed. This illustration serves to give a feeling of the atmospheric loss levels involved given the three ACE+ frequencies. In general, these losses show fairly high variation dependent on atmospheric conditions.

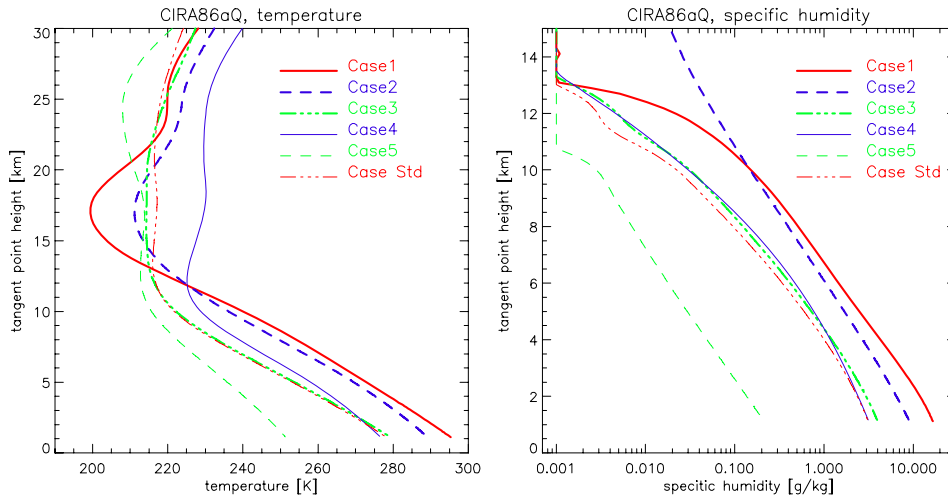


Fig. 2.2.1. Temperature and humidity profiles of the CIRA86aQ atmosphere (CIRA86aQ_UoG model) on which the simulations in this study are based.

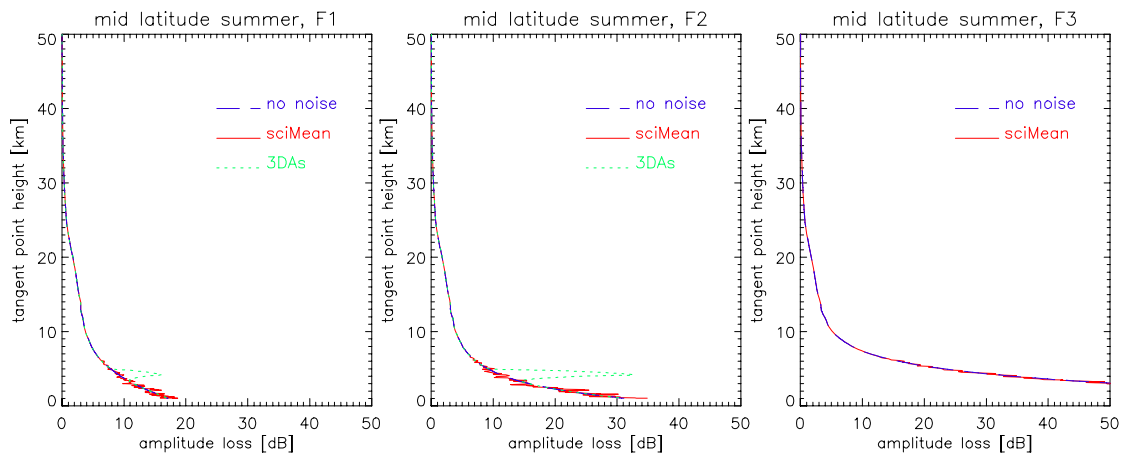


Fig. 2.2.2. Atmospheric loss at the three ACE+ frequencies for the mid-latitude summer case (dashed profiles), also with some exemplary altostratus (As) clouds (dotted profiles) as well as some “mean case” scintillation activity (solid profiles) superposed. The cloud parameters were liquid water content 0.4 g/m^3 , cloud center height 4.5 km, cloud thickness 0.6 km (with 100/200m lower/upper edges), and cloud horizontal extend 200 km. The atmos. turbulence/scintillation model parameters were $C_n^2 = 6 \times 10^{-15} \text{ m}^{-2/3}$ at surface with an exponential decrease according to a 2 km scale height, and a 200 km horizontal extend of turbulence activity (parameters based on mean turbulence conditions from radiosonde statistics, median condition turbulence is about a factor of 3 weaker; see, e.g., Kuhn, 2003a,b).

2.3. Observation System and Instrumental Error Modeling

Reasonably realistic modeling of the main LEO-LEO instrumental errors has been performed, including thermal amplitude noise, $1/f$ noise in the period domain of relevance, and linear amplitude drifts, e.g., due to slight antenna gain drift. In this context also a realistic link budget is needed in order to have a reasonable carrier-to-noise density ratio (C/N_0) input to the noise modeling. This link budget derives in EGOPS5 “automatically” from the end-to-end simulation of all link budget components from transmitter power (set to 3 dBW) via transmitter antenna gain (~25-28 dB), space loss, and receiver antennae gain (~25-28 dB) to received amplitude. Figure 2.3.1 illustrates C/N_0 profiles for an example case. With the settings used in this study, a C/N_0 figure of ~66 dBHz at 25 km height (or ~67 dBHz in “vacuum” above the atmosphere) is found. Based on the results shown in section 3, this is evidently a quite adequate figure to size the ACE+ link budget for achieving the observational requirements.

For setting the error modeling input values, we followed the specifications as laid out in the ACE+ MRD. In order to illustrate the characteristics of the different error sources, they are illustrated in Figures 2.3.2 to 2.3.5 below. As an example, an EGOPS “Observation System Modeling” input specification file is listed in Appendix A.4, which has all error models illustrated below enabled with the input settings used.

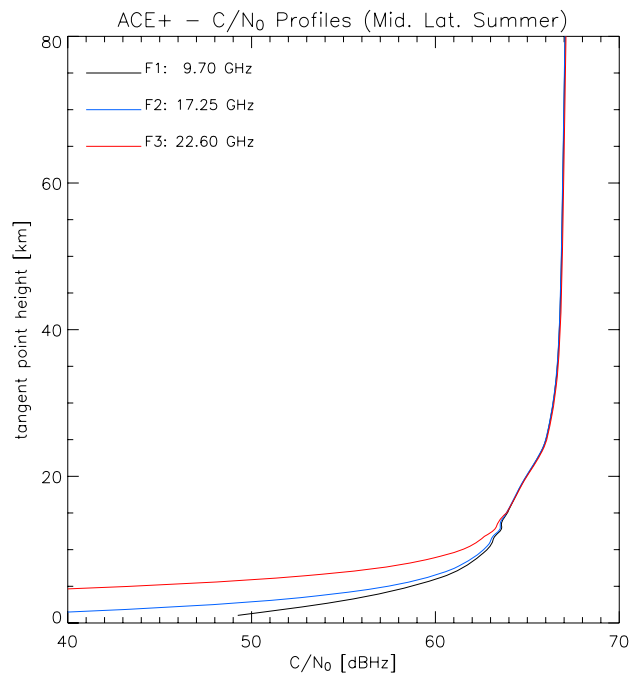


Fig. 2.3.1. Carrier-to-noise density ratio (C/N_0) profiles for the three ACE+ frequencies for the mid-latitude summer case (Case2).

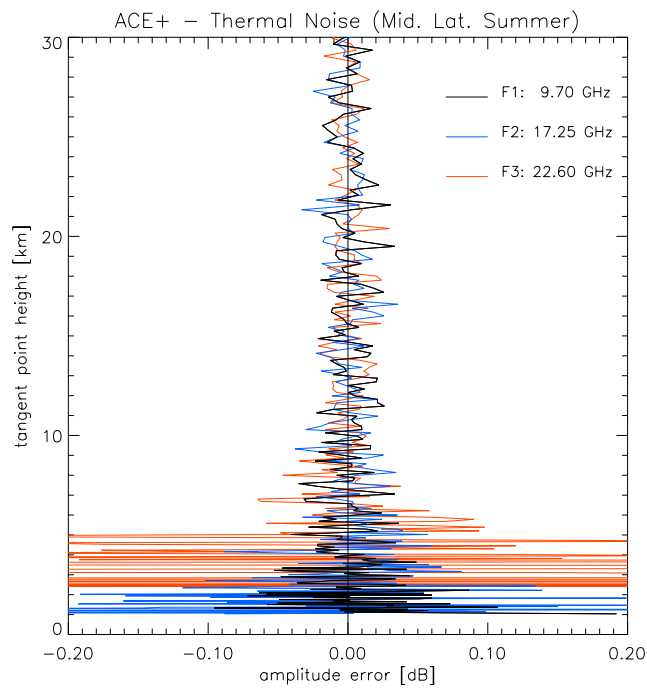


Fig. 2.3.2 Exemplary realizations of thermal amplitude noise profiles for the three ACE+ frequencies for the mid-latitude summer case. The downward increase of thermal noise with the gradual C/N_0 decrease (Figure 2.3.1) is well visible. The main thermal noise model settings were 80 K antenna noise temperature and 160 K receiver noise temperature.

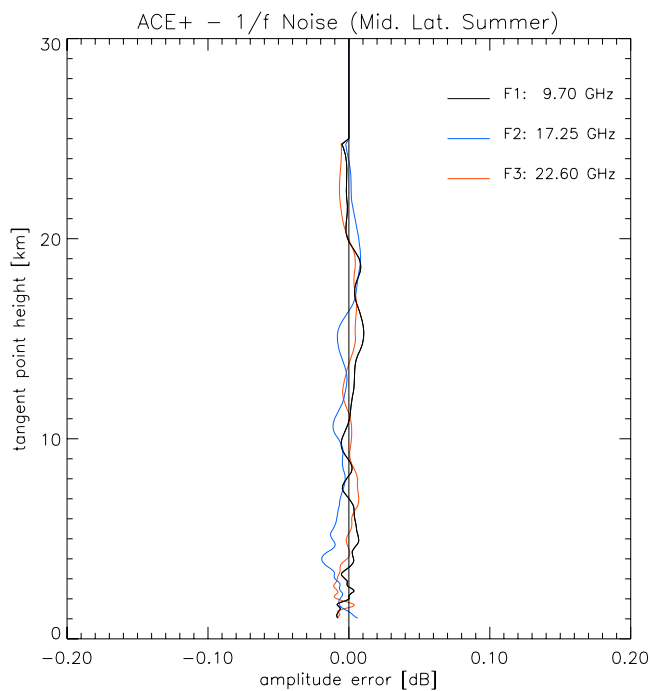


Fig. 2.3.3. Exemplary realizations of 1/f noise profiles for the three ACE+ frequencies for the mid-latitude summer case. The main 1/f noise model settings were periods from 1 to 20 sec with an error slope in the period domain of 0.050 dB/min.

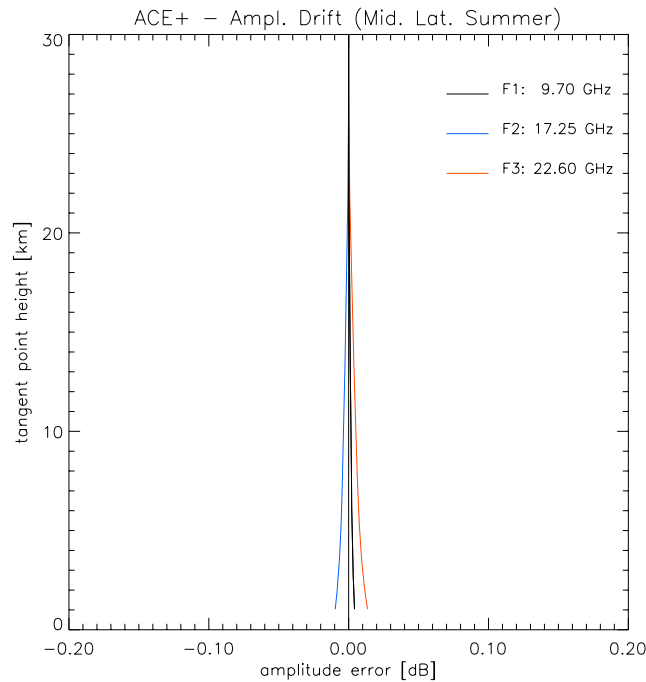


Fig. 2.3.4. Exemplary realizations of linear amplitude drift profiles for the three ACE+ frequencies for the mid-latitude summer case. The main amplitude drift model setting was a linear drift slope of 0.06 dB/min, with the drift starting at the occultation event time corresponding to a tangent height of 25 km.

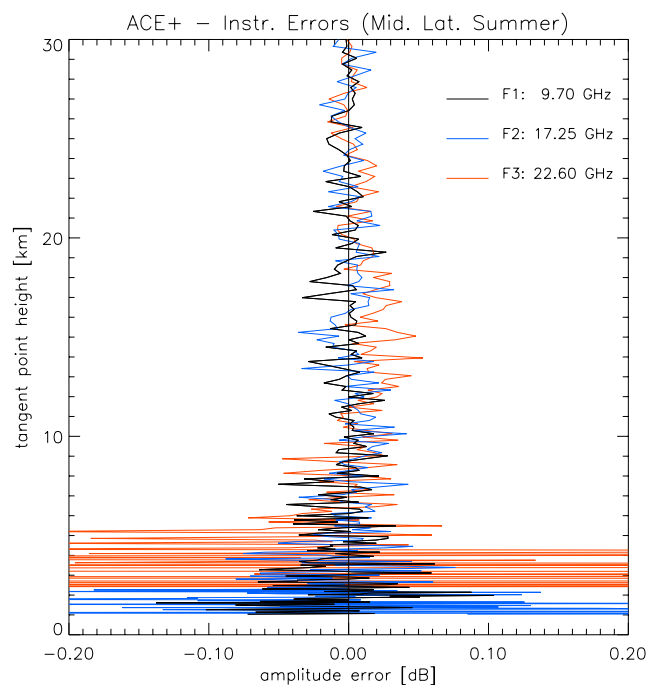


Fig. 2.3.5. Exemplary realizations of total instrumental error profiles for the three ACE+ frequencies for the mid-latitude summer case. All three error sources illustrated above in Figures 2.3.2 to 2.3.4 are included with model settings as noted in the above captions.

2.4. Retrieval Processing Chain and Retrieval Algorithms

Inversion/Retrieval of occultation data denotes the processing of simulated or observed phase and amplitude data, supplemented by the necessary geometrical information, via Doppler shifts, bending angles and transmissions down to quasi-vertical atmospheric profiles of real and imaginary refractivities, density, pressure (or geopotential height), temperature, humidity, and liquid water.

The retrieval processing strategy for LEO-LEO measurements within EGOPS5 consists of the following five main steps:

- bending angle retrieval,
- transmission retrieval,
- real refractivity retrieval,
- imaginary refractivities retrieval, and
- atmospheric profiles retrieval.

The general processing concept is illustrated in Figure 2.4.1, and the related general procedure is as follows (details on each of the five steps are given in subsections 2.4.1 to 2.4.5 below).

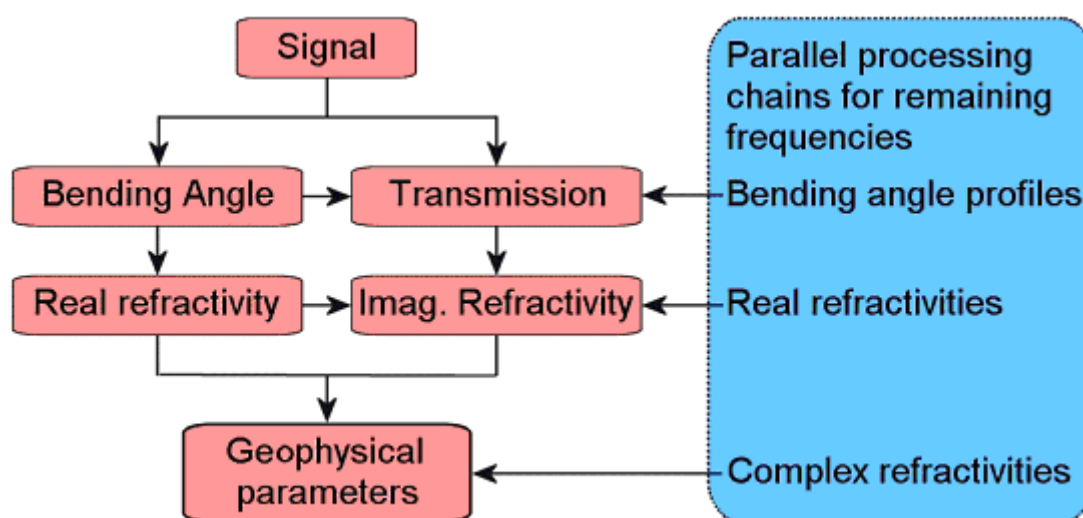


Fig. 2.4.1. LEO-LEO retrieval processing chain overview. The five upper boxes to the left represent the processing chain for a single frequency channel, whereas the box to the right represents parallel processing chains for the remaining carrier frequencies in the system. (after Nielsen et al., 2003).

First, the phase and amplitude profiles (“Signal”) are used together with the corresponding precise orbit determination (POD) data comprising positions and velocities of LEO transmitter and LEO receiver satellites to determine the atmospheric bending angle profile as a function of impact parameter in the same way as this is performed in the well-known

GNSS-LEO processing (e.g., Nielsen et al. 2003). If wave-optics processing is utilized, both phase path changes (Doppler shift profiles) and normalized amplitude profiles (raw transmission profiles) are used in this process, if only geometric-optics processing is performed only Doppler shift profiles are used. For details on this first step see subsection 2.4.1.

Second, the amplitude profiles at each LEO-LEO signal frequency (ACE+ nominal frequencies 9.7 GHz, 17.25 GHz, 22.6 GHz), the impact parameter profile, and the POD transmitter and receiver position profiles are used to compute the transmission profiles due to atmospheric absorption at each frequency. The exact way of how amplitude defocusing and spreading is subtracted from the measured amplitude profiles, in order to obtain the transmission profiles due to absorption only, depends on whether wave-optics or geometric-optics processing is utilized. For details on this second step see subsection 2.4.2.

Third, the bending angle profile as a function of impact parameter is converted to the real refractivity profile as a function of height via the classical Abel transform well-known from GNSS-LEO processing. For details on this third step see subsection 2.4.3.

Fourth, the real refractivity profile and the impact parameter profile are used together with the transmission profiles at each LEO-LEO frequency to derive the imaginary refractivity profile as a function of height at each frequency with another Abel transform akin to the classical one (same Abelian integration kernel but different in integrand). Since imaginary refractivity is proportional to the absorption coefficient, the latter can be obtained alternatively or in addition. For details on this fourth step see subsection 2.4.4.

Fifth, the real refractivity profile and the imaginary refractivity profiles at each LEO-LEO frequency, all as functions of height, are used, together with the equations relating temperature, humidity, pressure, and cloud liquid water (“geophysical parameters”) to real and imaginary refractivity, to derive the atmospheric profiles of the geophysical parameters as function of height. In addition, the geopotential height of pressure levels can be obtained from the knowledge of pressure as a function of (geometric) height. The key equations involved are the real refractivity equation (“Smith-Weintraub formula”), the hydrostatic equation, the equation of state, and the spectroscopic equations for computing the frequency-dependent absorption coefficient from the geophysical parameters (e.g., “Liebe Model”).

This geophysical parameter estimation problem is efficiently solved by downward (in height) integration of the hydrostatic equation combined with an iterative BLUE (best linear unbiased estimation) solution at each integration step for obtaining at the given height level temperature, humidity, and liquid water from the real and imaginary refractivity values. The BLUE algorithm requires the specification of covariance matrices for the refractivity data, which are formulated based on the knowledge of their respective error characteristics. If the imaginary refractivity variances grow large into the lower troposphere (e.g., under conditions of significant atmospheric turbulence) so as to render the BLUE problem effectively under-determined, it is advisable to include also adequate prior temperature values plus their variance into the estimator to ensure accurate geophysical parameter estimation also under these conditions. For details on this fifth step see subsection 2.4.5.

2.4.1. Bending Angle Retrieval

The derivation of bending angle profiles as function of the impact parameter can be performed either via a geometric-optics (GO) or a wave-optics (WO) approach. In the EGOPS5 LEO-LEO processing used for this report GO processing was employed throughout, so this avenue is described here. On the WO processing approach for bending angle retrieval see Nielsen et al. (2003) and references therein.

LEO-LEO GO bending angle retrieval uses as input observables the measured phase profiles at the LEO-LEO signal frequencies and the transmitter and receiver orbital positions and velocities from POD, and proceeds in four steps:

- smoothing (and outlier rejection)
- ionospheric correction of phases
- derivation of Doppler shift from the corrected phase delay
- derivation of bending angle and impact parameter from the Doppler shift
- statistical optimization of bending angles at high altitudes

The LEO-LEO bending angle retrieval is in general identical to the GNSS-LEO one. Extensive literature thus exists describing it in different variants, all, if properly implemented, leading to the same results. Useful general descriptions include Melbourne et al. (1994), Kursinski et al. (1997), Steiner (1998) [IGAM report], Syndergaard (1999) [DMI report], Kursinski et al. (2000) and Nielsen et al. (2003), but there are many others. Below the equations for each of the five steps are summarized with focus on their specific implementation in EGOPS5 LEO-LEO (E5L) processing.

Smoothing (and outlier rejection)

Data smoothing over ~1 sec (~2 km in height, less below 30 km) is commonly applied to simulated or measured phase path delays at sampling rates of 10 Hz (~0.2 km in height) or higher before ionospheric correction and Doppler shift derivation. This avoids unnecessary amplification of high-frequency noise. Given the countless number of digital filter possibilities, many smoothing variants are possible, the most simple one being a standard “moving average” FIR filter.

In E5L processing, a regularization smoother of the form

$$\tilde{\varphi} = \left(\mathbf{I} + \lambda \mathbf{S}^T \mathbf{S} \right)^{-1} \cdot \varphi \quad (1)$$

$$\lambda = 10^{\frac{f_s [\text{Hz}]}{10}} \quad (2)$$

φ ... N×1 measured phase delay vector $\{ \varphi_j(t_i) \}$; occultation rays $i = 1, \dots, N$;
 signal frequencies j (ACE+ baseline: $j = 1, \dots, 3$)

$\tilde{\varphi}$... N×1 smoothed phase delay vector $\{ \tilde{\varphi}_j(t_i) \}$

\mathbf{S} ... N×N smoothing matrix (third difference operator)

\mathbf{I} ... N×N unit matrix

λ ... regularization parameter

f ... sampling rate (for GO processing $f_s = 10$ Hz)

is applied to the raw $\varphi_j(t_i)$ profiles, following Syndergaard (1999), section 3.1.1 therein. A 3rd-order difference operator is used for the smoothing matrix \mathbf{S} , and $\lambda = 10$ for the GO processing sampling rate of 10 Hz. This filtering yields a vertical resolution of ~2 km above 30 km, increasing to < 1 km in the troposphere. The result in general is not very different from other filters with similar transfer function but compared to, e.g., standard “moving average” FIR filters, it is more robust against intermittent noise “spikes” in the data.

For simulated phase delay data with orderly simulated random error sources, genuine outliers (un-physical data values) do not occur. Thus currently the E5L processing has outlier rejection for $\varphi_j(t_i)$ not activated. However, a “3- σ rejection” algorithm, curing for data samples deviating by more than 3 standard deviations from the mean over a neighborhood of ± 0.5 sec, is prepared for activation as required.

Ionospheric correction of phases.

The simple linear dual-frequency combination of the form

$$\varphi(t_i) = \frac{f_1^2}{f_1^2 - f_2^2} \cdot \tilde{\varphi}_1(t_i) - \frac{f_2^2}{f_1^2 - f_2^2} \cdot \tilde{\varphi}_2(t_i) \quad (3)$$

t_i ... occultation event time, time of data sample i ; $i = 1, \dots, N$

f_1, f_2 ... LEO-LEO signal frequencies (ACE+ baseline: $f_1 = 9.7$ GHz, $f_2 = 17.25$ GHz, $f_3 = 22.6$ GHz)

$\tilde{\varphi}_1, \tilde{\varphi}_2$... smoothed phase delay at frequency f_1, f_2

φ ... atmospheric phase delay

is used to eliminate the ionospheric phase delay from the measured total phase delays, $\tilde{\varphi}_{1,2}(t)$, in order to obtain the (neutral) atmospheric phase delay $\varphi(t)$. The physical basis is the inverse-squared frequency dependence of ionospheric refractivity (e.g., Budden, 1985). Eq. (3) is sequentially applied to each individual data sample in the profile.

For the ACE+ frequencies near 10 GHz and higher, the ionospheric effects are about 2 orders of magnitude smaller than in the GNSS-LEO L-band case so more sophisticated correction schemes than Eq. (3), such as the correction of bending angles commonly used for GNSS-LEO (Vorob’ev and Krasnil’nikova, 1994), are not required. In addition, the SNR at altitudes above 30 km is much higher than in the GNSS-LEO case so that the accuracy of LEO-LEO bending angles can be expected to be significantly better in the upper stratosphere and mesosphere, potentially limited by residual clock and POD errors rather than residual ionospheric errors and thermal noise as for GNSS-LEO (Ramsauer and Kirchengast, 2001). High-quality clocks (USOs) are thus the key for realizing the much superior stratospheric performance potential of LEO-LEO phase data over GNSS-LEO as far as possible.

In E5L processing, currently the ACE+ frequencies $f_1 = 9.7$ GHz and $f_2 = 17.25$ GHz are used for the correction, and the resulting $\varphi(t)$ is assigned to f_1 . More sophisticated utilization of all pairs of f_1, f_2 , and f_3 is possible for further improved correction. Perhaps more important

practically is that they will provide useful redundant information for intrinsic quality control and verification.

Derivation of Doppler shift from the corrected phases.

Doppler shift is derived from phase delay $\varphi(t_i)$ via differentiation

$$d(t_i)[m/sec] = \frac{d\varphi(t_i)}{dt}, \quad d_j(t_i)[Hz] = -\frac{f_j}{c} d(t_i) \quad (4)$$

$d(t_i)$... Doppler shift profile

f_j ... LEO-LEO signal frequency

c ... velocity of light ($c = 299792458$ m/sec)

and is the key observable for determining the bending angle to which it is closely proportional via the sinking/rising velocity of ray paths during an occultation event (e.g., Rieder and Kirchengast, 2001a). Eq. (4) shows that absolute phase delay need not be known as the Doppler shift retains only the phase change, which is the observable to be accurately tracked over the duration of ~ 1 min during an event.

This accurate tracking is ensured by the high short-term stability (over 1–100 sec) of on-board USO frequency standards. Exactly here is the heart of the often quoted intrinsic self-calibration of refractive occultation data: each single Doppler shift profile in itself, together with its associated precise orbital position and velocity profiles from POD, is an absolute measure of height-dependent atmospheric bending angle at the time and geographic location of the event, independent of any reference or calibration data, independent of any other real or potential measurements before, in parallel, or after the 1-min event. This is also the basis, which justifies notions like “unique climate benchmark measurements” or “unique long-term stability over decades from unique short-term stability over seconds”.

In E5L processing, the phase differentiation in Eq. (4) is implemented as a space-centered finite difference, i.e., the Doppler shift of each sample is set to the difference estimate between the neighbor samples above and below (with due care for the profile boundaries). This simple scheme is possible since the regularization smoother, Eq. (1), strictly ensures smoothness of the data over each neighborhood of 3 data samples.

Derivation of bending angle and impact parameter from the Doppler shift.

The conversion equations from Doppler shift $d(t)$ and orbital positions $\mathbf{r}(t)$ and velocities $\mathbf{v}(t)$ to bending angle and impact parameter can be cast in many forms of which one is (Melbourne et al. 1994; Syndergaard, 1999)

$$d(t_i) = [v_{Rx} \cos \varphi(a_i) - v_{Tx} \cos \chi(a_i)] - \frac{dr_{RxTx}(t_i)}{dt} \quad (5)$$

$$\varphi(a_i) = \zeta - \arcsin\left(\frac{a_i}{r_{Rx}}\right) \quad (6)$$

$$\chi(a_i) = (\pi - \eta) - \arcsin\left(\frac{a_i}{r_{Tx}}\right) \quad (7)$$

$$\alpha(a_i) = \theta - \arccos\left(\frac{a_i}{r_{Rx}}\right) - \arccos\left(\frac{a_i}{r_{Tx}}\right) \quad (8)$$

- a_i ... impact parameter at data sample i (time i)
- α_i ... bending angle at data sample i
- r_{Tx} ... distance of the transmitter (Tx) from the center of local curvature
- r_{Rx} ... distance of the receiver (Rx) from the center of local curvature
- r_{RxTx} ... distance between the transmitter and receiver satellite
- v_{Tx} ... velocity of the transmitter satellite (in the occultation plane)
- v_{Rx} ... velocity of the receiver satellite (in the occultation plane)
- ζ ... angle between the Rx velocity and position vectors (in the occultation plane)
- η ... angle between the Tx velocity and position vectors (in the occultation plane)
- θ ... angle between the transmitter and the receiver position vectors

Eqs. (5) – (8) constitute the equation set used in the E5L processing, and Fig. 2.4.2 illustrates the geometrical situation in the occultation plane, the plane spanned by the Tx and Rx satellite position vectors.

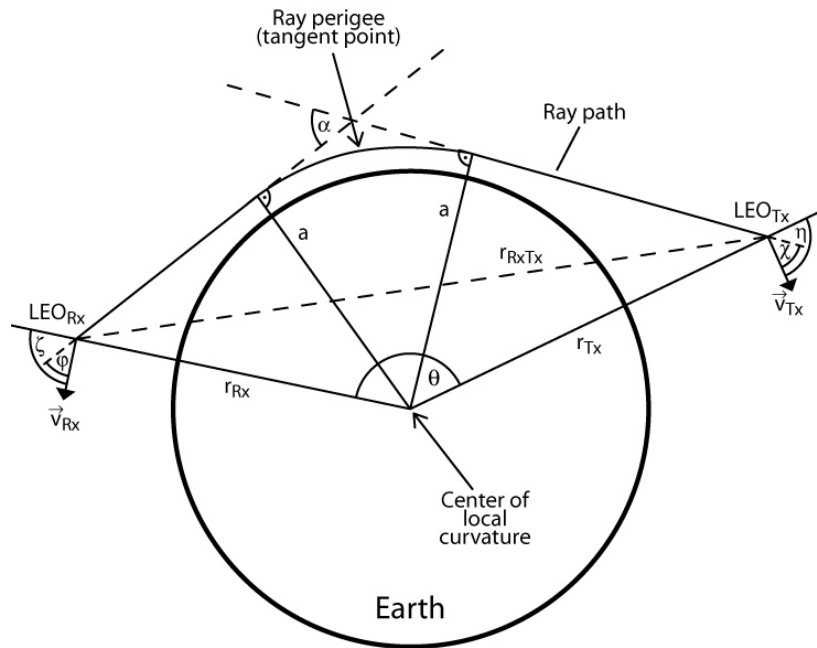


Fig. 2.4.2. LEO-LEO occultation geometry, defining various parameters used in the algorithm description.

Eqs. (5) – (8) are used either with assuming a spherical Earth (with mean radius 6371.0 km) or a realistic ellipsoidal Earth shape (WGS-84 ellipsoid; e.g., Landolt-Börnstein, 1984). In the latter case, the transmitter and receiver position vectors $r_{Tx}(t)$ and $r_{Rx}(t)$ are first transformed to originate in the ellipsoid’s center of local curvature in the occultation plane at the mean geographic location of the event rather than in the Earth’s center of mass. The details of this “oblateness correction” have been described by Syndergaard (1998) (also included as App. C.2 in Syndergaard, 1999) and are not repeated here. The essence is that the position vector’s

origin in the center of local curvature ensures that the assumption of spherical symmetry about the tangent point, implicit in Eqs. (6) – (8), is accurately valid geometrically.

A by-product of the correction is the knowledge of the mean tangent point location of the event (φ_{TP} , λ_{TP}) and of its radius of curvature at this location (R_C). In the spherical Earth case, the center of curvature and the center of mass are identical as are the radius of curvature and the Earth’s mean radius. The mean location (φ_{TP} , λ_{TP}) is computed, purely defined by geometry and independent of any atmospheric state, as the geographic location where the straight-line connection of Tx and Rx positions at a certain time during the event touches the ellipsoidal or spherical Earth’s surface. Experience with ray propagation through realistic atmospheres has shown this mean location to correspond to the location which real events typically reach near the tropopause at around 12 km, i.e., to be a very adequate mean location of any actual event though defined solely by geometry. The latter property offers the distinct advantage that purely geometrical analyses (e.g., on occultation event distributions and “true” atmospheric states at event locations) can be performed in strict consistence with forward modeling and retrieval analyses, which simulate occultation data for event locations of interest.

After the preparations described, the vectors $\mathbf{r}_{Tx}(t)$, $\mathbf{v}_{Tx}(t)$, $\mathbf{r}_{Rx}(t)$, $\mathbf{v}_{Rx}(t)$, which are utilized in the ECEF system in E5L processing, are converted by standard vector-analytical formulae to the scalar components $r_{Tx}(t)$, $v_{Tx}(t)$, $r_{Rx}(t)$, $v_{Rx}(t)$, which are the projections of the respective vectors onto the occultation plane. In case of the positions, which by definition lie in this plane, these are simply the vector magnitudes denoting the Tx and Rx distances from the Earth’s center of local curvature (see Fig. 2.4.2). To complete the input required to Eqs. (5) – (8), the angles ζ , η , and θ and the straight-line distance $r_{RxTx}(t)$ are computed from standard vector formulae as well.

Eqs. (5) – (7) demand an iterative solution for a , since a is implicitly contained only. Starting with the straight-line impact parameter as first guess for a , an accurate solution is obtained within few iterations. Given a , α is readily computed via Eq. (8).

Statistical optimization of bending angles at high altitudes.

Statistical optimization optimally combines, in an inverse-covariance-weighted least-squares sense, the measured bending angle profile with a background bending angle profile and thereby ensures adequate quality of the bending angle profiles at high altitudes (from the stratopause upwards) for the subsequent Abel transform to refractivity (subsection 2.4.3). Other more simplified methods exist to treat the upper boundary of bending angles before the Abel transform (see, e.g., Gobiet and Kirchengast, 2002; for an overview) but these are less effective and not treated here. The optimal estimation profile reads (e.g., Healy, 2001; Gobiet and Kirchengast, 2004)

$$\mathbf{\alpha}_{opt} = \mathbf{\alpha}_b + \mathbf{B}(\mathbf{B} + \mathbf{O})^{-1}(\mathbf{\alpha}_o - \mathbf{\alpha}_b) \quad (9)$$

- $\mathbf{\alpha}_{opt}$... optimized bending angle profile
- $\mathbf{\alpha}_o$... observed (retrieved) bending angle profile
- $\mathbf{\alpha}_b$... background bending angle profile
- \mathbf{O} ... observation error covariance matrix (of $\mathbf{\alpha}_o$)

\mathbf{B} ... background error covariance matrix (of a_b)

Eq. (9) assumes unbiased (Gaussian) errors and a linear problem. Linearity is fulfilled in the present case, and unbiasedness holds reasonably well for the retrieved profiles due to the self-calibrating nature of RO data (see above). Unbiasedness of background profiles needs careful selection of these profiles.

In E5L processing, the optimization is applied from 30 to 120 km height. The error covariance matrices \mathbf{O} and \mathbf{B} are formulated as

$$\mathbf{O}_{ij} = \sigma_{oi} \sigma_{oj} \cdot \exp\left(-\frac{|a_i - a_j|}{L_o}\right), \quad \mathbf{B}_{ij} = \sigma_{bi} \sigma_{bj} \cdot \exp\left(-\frac{|a_i - a_j|}{L_b}\right) \quad (10)$$

a_i, a_j ... impact parameter for data samples i and j

σ_{oi}, σ_{oj} ... observation (retrieval) standard errors at levels i and j

σ_{bi}, σ_{bj} ... background standard errors at levels i and j

L_o ... correlation length of observation errors

L_b ... correlation length of background errors

The observation standard error is estimated from the 70–80 km height segment of a_o , where the SNR < 1 , and assumed to hold for the full estimation range down to 30 km. L_o is set to 1 km in line with empirical evidence (e.g., Steiner et al., 2004 [OPAC1 paper]). The background standard error is set from experience to 15% of the a_b profile, and L_b is set to 6 km, as the smooth background profiles clearly have long-range correlation of the order of a scale height.

Suitable nearly unbiased a_b profiles are obtained from a profile search in the global MSIS90 (Hedin, 1991; S. Syndergaard, pers. communications, 1998) or CIRA86aQ (Kirchengast et al., 1999) climatology with month-to-month 5 deg latitude \times 15 deg longitude search. The a_b profile selected is the one, which best fits the retrieved profile over the stratopause region (baseline: 45 to 65 km), where retrieved data quality is still sufficiently good to allow a reasonable fit. The best-fit profile is then used up to 120 km and ensures that, via Eq. (9), a reasonable optimized bending angle profile a_{opt} is available up to 120 km, independent of the retrieved data reaching an SNR < 1 at heights of about 80 km (e.g., Rieder and Kirchengast, 2001a). This is vital for the subsequent Abel transform to induce only small error propagation from the mesospheric altitudes into the retrieval domain of interest below the stratopause (e.g., Gobiet and Kirchengast, 2002). Below about 40 km, the influence of the background profile is negligible since from the middle stratosphere downwards the retrieved data exhibit an SNR $\gg 1$ so that Eq. (9) directly yields a_o for a_{opt} .

The outputs of the bending angle retrieval are a_i (a_{opt} from Eq. 9), a_j , R_C , and $(\varphi_{TP}, \lambda_{TP})$, which are used in the subsequent steps.

2.4.2. Transmission Retrieval

Transmission retrieval starts with the amplitude profiles at each signal frequency j , $A_j(t)$, and derives transmission profiles as function of impact parameter $Tr_j(a)$, which expresses

atmospheric absorption (transmission = 1 – absorption) at frequency j due to water vapor and the background air (molecular oxygen and nitrogen). The transmission retrieval comprises two steps:

- defocusing and spreading correction
- amplitude normalization

Defocusing and spreading correction.

This correction is required since $A_j(t)$ contains besides the desired amplitude loss due to absorption also defocusing loss due to differential bending and spherical signal spreading according to the geometry (e.g., Leroy, 2001).

Both defocusing and spreading can be corrected for in using the bending angle retrieval output (see subsection 2.4.1), namely the bending angle profile $\alpha(a)$ or, alternatively, the satellite opening angle $\theta(a)$ (see Fig. 2.4.2) and the impact parameter profile a as well as the Tx and Rx satellite radial distances $r_{Tx}(a)$ and $r_{Rx}(a)$. Different variants for this correction exist (e.g., Sokolovskiy, 2000; Leroy, 2001; Jensen et al., 2003). In E5L processing the elegant one-step formulation of Jensen et al. (2003) for the defocusing and spreading model amplitude (for GO processing) is used which reads

$$A_{dsm}(a_i) = \left[\frac{a_i}{(r_{Tx} r_{Rx})^2 \sin(\theta) \sqrt{1 - \left(\frac{a_i}{r_{Tx}}\right)^2} \sqrt{1 - \left(\frac{a_i}{r_{Rx}}\right)^2} \left| \frac{d\theta}{da} \right|_i} \right]^{1/2} \quad (11)$$

$\left| \frac{d\theta}{da} \right|_i$... derivative of the satellite opening angle (Fig. 2.4.2.) after the impact parameter at level i

A_{dsm} ... defocusing and spreading model amplitude

Different formulations have to be used for WO pre-processed amplitudes (Jensen et al., 2003; Nielsen et al., 2003). $A_{dsm}(a_i)$ can be used in a next step as correction to convert the observed amplitude $A_j(t) = A_j(a)$ to the desired transmissions $Tr_j(a)$.

Amplitude normalization.

$Tr_j(a)$ being a normalized intensity, $A_j(t)$ has to be divided in some way by a normalization amplitude at some reference height besides removing the defocusing and spreading components. In E5L processing the derivation of $Tr_j(a)$ is done via

$$A_j^{dsm}(a_i) = \left(\frac{A_j}{A_{dsm}} \right)_{Z_{ref j}}^{\Delta z} \cdot A_{dsm}(a_i) \quad (12)$$

$$Tr_j(a_i) = -20 \cdot (\log A_j - \log A_j^{dsm}) \text{ [dB]} \quad (13)$$

$$\left(\frac{A_j}{A_{dsm}} \right)_{z_{refj}}^{\Delta z} \quad \dots \text{absorption amplitude at reference height } z_{refj} \text{ for frequency } j$$

(mean estimate over a height range $\pm \Delta z/2$ about z_{refj})

A_j^{dsm} ... defocusing and spreading model amplitude scaled to match the signal amplitude A_j at height z_{refj}

Eq. (12) performs the normalization in that it scales $A_{dsm}(a_i)$ to $A_j(a)$ at z_{refj} and Eq. (13) then performs the division $A_j(a)/A_j^{dsm}$, corresponding to a subtraction in [dB] space, to obtain the desired transmissions $Tr_j(a)$ pertaining to absorption only.

The z_{refj} baseline value used for the ACE+ signal frequencies is 25 km, since from about 25 km upwards $Tr_j(a)$ is unity (zero absorption) with high accuracy. This normalization to a reference height “above the absorptive atmosphere” where $Tr_j(a) = 1$ is the step where the intrinsic self-calibration of the amplitudes comes in: as for the self-calibrated bending angles it implies that as long as the transmission profiles are short-term stable over the ~30 sec of the occultation event from about 25 km towards the surface, each individual profile is a self-standing reliable measure of the atmospheric absorption at frequency j at the given place and time, independent of any other real or potential measurements before, in parallel, or after the ~30-sec event. As will be seen in subsection 2.4.4 below, the imaginary refractivity (or absorption coefficient) derived from the transmission only depends on the derivative $Tr_j(a)/da$, so that a small constant transmission residual at height z_{refj} does not matter.

In E5L processing also filtering is involved, smoothing a before use in Eq. (11) as well as $A_j(a)$ and $A_{dsm}(a)$ before use in Eqs. (12) and (13). A 3rd order polynomial filter was found adequate for this purpose with the filtering polynomial width set to ~1 km. The transmission profiles $Tr_j(a)$ are smoothed the same way. Similar to the phase delay filtering before Doppler shift deduction (subsection 2.4.1), this filtering avoids unnecessary amplification of high-frequency noise in the subsequent Abel transform to imaginary refractivity, which involves the derivative of $Tr_j(a)$ being similarly noise-sensitive as the phase delay derivation.

2.4.3. Real Refractivity Retrieval

The real refractivity profile as function of height is derived from the bending angle profile as function of impact parameter via the classical Abel transform (e.g., Fjeldbo et al., 1971; Kursinski et al., 1997; Rieder and Kirchengast, 2001b)

$$n^R(a_i) = \exp \left(\frac{1}{\pi} \int_{a_i}^{a_{top}} \frac{\alpha(a)}{\sqrt{a^2 - a_i^2}} da \right) \quad (14)$$

$$N^R(z_i) = 10^6 \left(n^R(a_i) - 1 \right), \quad z_i = r_i - R_C, \quad r_i = \frac{a_i}{n^R(a_i)} \quad (15)$$

n^R ... refractive index, real part

r_i ... radial distance of level a_i from center of local curvature

z_i ... ellipsoidal height level corresponding to a_i
 N^R ... real refractivity

In E5L processing, the top value a_{Top} of the Abelian integral, Eq. (14), which is at infinite heights theoretically (e.g., Fjeldbo et al., 1971), is set to correspond to a height of 120 km, exploiting the bending angle profile available from Eq. (9) over the full range and ensuring accurate refractivity retrieval up to the stratopause (Steiner et al., 1999). In Eq. (15) it is vital to use exactly the RC value used already in the bending angle retrieval (subsection 2.4.1) in order to ensure accurate ellipsoidal heights z_i .

2.4.4. Imaginary Refractivity Retrieval

The imaginary refractivity profile as function of height is derived by using the real refractive index profile and the impact parameter profile together with the transmission profiles at each signal frequency within another Abel transform akin to Eq. (14) (e.g., Kursinski et al., 2002)

$$k_j(z_i) = \frac{1}{\pi} \left| \frac{da}{dr} \right|_{a=a_i} \int_{a_i}^{a_j^{top}} \frac{d \ln Tr_j(a)}{da} \frac{1}{\sqrt{a^2 - a_i^2}} da \quad (16)$$

$$N_j^I(z_i) = 10^6 \cdot \frac{c}{4\pi f_j} k_j(z_i) \quad (17)$$

$Tr_j(a)$... transmission profile at frequency j (dimension less units)
 k_j ... absorption coefficient at frequency j at level z_i corresponding to a_i (cf. Eq. 15)
 f_j ... frequency at frequency channel j
 c ... velocity of light ($c = 299792458$ m/s)
 N_j^I ... imaginary refractivity at frequency j

The real refractivity information enters via the radial distance profile $r(n^R)$ evaluated according to Eq. (15), which is needed to form the derivative $|da/dr|$ in Eq. (16). Eq. (17) is the standard equation for converting the absorption coefficient to imaginary refractivity (e.g., Schanda, 1986) to which it is proportional via the wavelength.

In E5L processing, the top value a_j^{Top} of the Abelian integral Eq. (16), which is at infinite heights theoretically, is set to correspond to a height of $z_{ref j} + \Delta z/2$ (as defined for Eq. (12)). Above this height the log-transmission $\ln Tr_j(a)$ and thus its integral contribution is zero. After retrieval of the $N_j^I(z)$ profiles via Eq. (17) at each frequency j , they are filtered with a 3rd order polynomial filter with the filtering polynomial width set to ~ 1 km. As for the Doppler shift and transmission profile above, this filtering avoids potential high-frequency noise incurred by application of Eq. (16) to be transferred to further exploitation of $N_j^I(z)$ such as in the subsequent atmospheric profiles retrieval.

2.4.5. Atmospheric Profiles Retrieval

Real refractivity $N^R(z)$ and imaginary refractivities $N_j^I(z)$ are used, together with the equations relating atmospheric pressure p , temperature T , humidity q , and cloud liquid water lw to $N^R(z)$ and $N_j^I(z)$, to derive the parameters p , T , q , and lw as function of height z . In addition, the geopotential height of pressure levels, $Z(p)$, can be obtained from the knowledge of the $p(z)$ profile. The key equations involved and used in E5L processing are

- the real refractivity equation (E5L: Smith-Weintraub equation; e.g., Foelsche, 1999),

$$N^R(z) = 77.60 \frac{p(z)}{T(z)} + 3.73 \cdot 10^5 \frac{e(z)}{T(z)^2} \quad (18)$$

p ... total air pressure [hPa]
 e ... total water vapor partial pressure [hPa]
 T ... temperature [K]
 N^R ... real refractivity

- a complex (real and imaginary) refractivity model and its adjoint model (E5L: Advanced MPM93 Model and its adjoint; e.g., Liebe et al., 1993; Nielsen et al., 2003; Giering et al., 1998; ACEPASS consortium, pers. communications, 2003),

$$(N^{R\text{mod}}(z), N_j^{I\text{mod}}(z)) = N_j^{C\text{mod}}(f_j, p(z), T(z), e(z), lw(z), iw(z), rr(z)) \quad (19)$$

$$(K^{R\text{adj}}(z), K_j^{I\text{adj}}(z)) = K_j^{C\text{adj}}(f_j, p(z), T(z), e(z), lw(z), iw(z), rr(z)) \quad (20)$$

lw, iw, rr ... cloud liquid water, cloud ice water, rain rate
 $N^{R\text{mod}}$... modeled real refractivity
 $N_j^{I\text{mod}}$... modeled imaginary refractivity

$$\mathbf{K}^{R\text{adj}} = \left(\frac{\partial N^R}{\partial T}, \frac{\partial N^R}{\partial e}, \frac{\partial N^R}{\partial lw} \right)^T \dots \text{real refractivity Jacobians}$$

$$\mathbf{K}_j^{I\text{adj}} = \left(\frac{\partial N_j^I}{\partial T}, \frac{\partial N_j^I}{\partial e}, \frac{\partial N_j^I}{\partial lw} \right)^T \dots \text{imaginary refractivity Jacobians}$$

- the hydrostatic equation with the equation of state in moist air embedded (e.g., Salby, 1996),

$$\frac{d \ln p(z)}{dz} = - \frac{g(z)}{R^d T_v(z)} \quad (21)$$

R^d ... dry air gas constant ($R^d = 287.06 \text{ J kg}^{-1} \text{ K}^{-1}$)
 g ... acceleration of gravity (standard $g(z, \text{latitude})$ model; e.g., Gobiet and Kirchengast, 2002)
 T_v ... virtual temperature (see Eq. (22))

- and the equations for virtual temperature and conversion of water vapor pressure to specific humidity (e.g., Salby, 1996),

$$T_v(z) = T(z) \cdot (1 + 0.608 q(z)) \quad (22)$$

$$q(z) = 0.622 \frac{e(z)}{(p(z) - 0.378 e(z))} \quad (23)$$

Eqs. (18) and (21)–(23) are well-known fundamental equations of atmospheric physics, Eqs. (19) and (20) are a macroscopic expression of a more sophisticated spectroscopic model. The essence of the Advanced MPM93 Model, Eq. (20), for the present purpose is simple, however: it provides for any physically realistic local atmospheric state (p, T, e, lw, iw, rr) and any given X/K band signal frequency j the corresponding complex refractivity ($N^{R\text{mod}}, N^{I\text{mod}}_j$). $N^{R\text{mod}}$ is modeled for the retrieval such that $N^{R\text{mod}}$ equals N^R of Eq. (18), i.e., according to the “Smith-Weintraub” formulation.

Since the atmospheric profiles retrieval as described below requires knowledge also of the sensitivities (“Jacobians”; e.g., Rodgers, 2000) of (N^R, N^I_j) to the atmospheric state parameters (T, e, lw) at any given state (p, T, e, lw, iw, rr), also the adjoint model $\mathbf{K}^{Cadj}(f_j, p, T, e, lw, iw, rr)$ is used, the source code of which was generated in an automatic way from the source code of the model $N^{Cmod}_j(f_j, p, T, e, lw, iw, rr)$ by the Tangent-Linear and Adjoint Model Compiler TAMC (Giering et al., 1998). The Jacobians are accurate for any given state since the Advanced MPM93 model is locally linear in the neighborhood of any given state despite being non-linear if viewed over its complete relevant state space.

The problem of retrieving the atmospheric state (p, T, e, lw) from the refractivities (N^R, N^I_j) is efficiently solved by downward (in height) integration of the hydrostatic equation, Eq. (21), to sequentially obtain p , combined with an iterative BLUE (best linear unbiased estimation) solution at each integration step to obtain (T, e, lw) from (N^R, N^I_j).

The downward integration of Eq. (21) is initialized at high altitudes (E5L setting: 75 km) with some initial state ($p_{Top}, T_{Top}, e_{Top} = lw_{Top} = 0$), the accuracy of which is non-critical as any initialization errors decay quickly over the first about 3 scale heights, i.e., essentially within the mesosphere (E5L baseline: estimate of (p_{Top}, T_{Top}) from the local scale height estimated from $N^R(z)$ near 75 km and the local equation of state). 4th order Runge-Kutta integration of Eq. (21) is used (e.g., Gershenfeld, 1999; chapter 6 therein) with small integration steps (E5L setting: 100 m) to ensure accurate $p(z_i)$ values. This integration itself involves already the BLUE algorithm described below, in order to obtain, for the needed Runge-Kutta sub-steps, $T_v(z)$ in Eq. (21) from states (T, e, lw) estimated from (p, N^R, N^I_j).

After each integration step, using the value of p^i obtained at height z_i and the estimated state ($T^{i+1}, e^{i+1}, lw^{i+1}$) from the previous height z_{i+1} , the BLUE algorithm is run to obtain the state (T^i, e^i, lw^i) from the data (p^i, N^{Ri}, N^{Ii}_j) at height z_i . The pressure p^i acts as a useful “backbone” for this estimation and ensures it to be very robust and reliable. Practically, above a certain height z_{eTop} , above which water vapor has negligible effect, only T^i is estimated (E5L baseline: 20 km). Furthermore, above a certain height z_{lwTop} , above which liquid water density is negligible, only (T^i, e^i) is estimated (E5L baseline: 8.5 km). Below z_{lwTop} the full state ($T^i,$

e^i, lw^i) is estimated, which then requires at least 3 independent elements of information in (p^i, N^{Ri}, N^{Ij}) .

For the BLUE solution, an iterative Gauss-Newton algorithm of the following form is used (e.g., Rodgers, 2000; chapter 5.3 therein):

$$\mathbf{x}_{n+1} = \mathbf{x}_n + \left(\mathbf{K}_n^T \cdot \mathbf{C}_y^{-1} \cdot \mathbf{K}_n + \mathbf{C}_b^{-1} \right)^{-1} \left[\mathbf{K}_n^T \mathbf{C}_y^{-1} (\mathbf{y} - \mathbf{y}^{\text{mod}}(\mathbf{x}_n)) - \mathbf{C}_b^{-1} (\mathbf{x}_n - \mathbf{x}^b) \right] \quad (24)$$

$$\mathbf{y} = (N^R, N_j^I)^T, \quad \mathbf{y}^{\text{mod}} = (N^{R \text{mod}}, N_j^{I \text{mod}})^T \quad (25)$$

$$\mathbf{C}_y = \text{Diag}(\sigma_{N^R}^2, \sigma_{N_j^I}^2) \quad (26)$$

$$\sigma_{N^R} = \begin{cases} N^R [f_{15} \cdot \exp(f_{hi}(z - 15\text{km}))] & \text{for } z \geq 15\text{km} \\ N^R \left[f_{15} + f_{lo} \left(\frac{1}{\text{Max}(z, 1\text{km})} - \frac{1}{15\text{km}} \right) \right] & \text{for } z < 15\text{km} \end{cases} \quad (27)$$

$$\sigma_{N_j^I} = \sigma_{N_j^I}^0 \cdot \left[f_w \cdot \left(\frac{1}{\text{Max}(Tr_j(z_i), 10^{-6})} + f_c \cdot \frac{1}{\text{Max}(Pt_j(z_i), 10^{-6})} \right) \right] \cdot f_{T^{\text{fit}}} \quad (28)$$

$$\mathbf{K} = (\mathbf{K}^{R \text{adj}}, \mathbf{K}_j^{I \text{adj}})^T \quad (29)$$

$$\mathbf{x} = (T, e, lw)^T, \quad \mathbf{x}^b = \mathbf{x}(z_{i+1}) = (T^b, e^{i+1}, lw^{i+1})^T, \quad \mathbf{x}_0 = \mathbf{x}^b \quad (30)$$

$$T^b = \begin{cases} T^{i-1} & \text{for } z > z_{\text{fit min}} \\ T^{\text{fit}} & \text{for } z < z_{\text{fit min}} \end{cases} \quad (31)$$

$$\mathbf{C}_b = \text{Diag}(\sigma_T^2, \sigma_e^2, \sigma_{lw}^2) \quad (32)$$

$$\sigma_T = \begin{cases} \text{const. for } z > z_{\text{fit min}} \\ s_T^{z_{\text{fit min}}} + \left(\frac{ds_T}{dz} \right) |z - z_{\text{fit min}}| & \text{for } z < z_{\text{fit min}} \end{cases}; \quad \sigma_e, \sigma_{lw} = \text{const.} \quad (33)$$

- n ... iteration index for the iterative BLUE estimator ($n = 0, \dots, \text{Min}(n_{\text{converged}}, 12)$)
- \mathbf{y} ... measurement vector (real and imag. refractivities; ACE+ baseline $j = 1, 2, 3$, i.e., four elements N^R, N_1^I, N_2^I, N_3^I)
- \mathbf{y}^{mod} ... forward modeled measurement vector, updated at each iteration n (from call of Advanced MPM93 Model Eq. (19))
- \mathbf{C}_y ... measurement (and forward modeling) error covariance matrix (set as diagonal matrix)

- σ_{N^R} ... standard error of real refractivity (formulation following Steiner and Kirchengast, 2004; baseline E5L parameters: $f_{15} = 0.001$, $f_{hi} = 0.02$, $f_{lo} = 0.01$)
- $\sigma_{N_j^I}$... standard error of imaginary refractivity at frequency j
- $\sigma_{N_j^0}$... standard error estimate for N_j^I within the $z_{refj} \pm \Delta z/2$ height range (cf. Eq. (12))
- Pt_j ... amplitude *rms* error estimate from high-pass filtered data (with ~ 1 km filter bandwidth) for optional up-scaling of $\sigma_{N_j^I}$ in presence of scintillations (f_c is set to switch this term to unity if the optional up-scaling shall be disabled)
- f_w ... weighting factor (baseline E5L setting is to unity)
- $f_{T^{fit}}$... factor with nominal value of unity; if $z_i < z_{fit\ min}$ $f_{T^{fit}}$ set to $5 + \text{Min}(2.5 |z_i - z_{fit\ min}|, 10)$ (baseline E5L setting to down-weight N_j^I influence on the estimated \mathbf{x})
- \mathbf{K} ... Jacobian weighting matrix (dimension: no. of elements in $\mathbf{y} \times$ no. of elements in \mathbf{x}), updated at each iteration n (from call of adjoint model to Advanced MPM93 Model, Eq. (20))
- \mathbf{x} ... state vector to be estimated, updated at each iteration n
- \mathbf{x}^b ... background (a priori) state vector (set nominally to state of previous state estimate on previous height level z_{i+1})
- \mathbf{x}_0 ... initial guess state vector (used as starting point for iteration of Eq. (24))
- T^b ... background (a priori) temperature, given $z_{fit\ min} > z_0$ (bottom level of profile) a “best-fit background profile” temperature T^{fit} is used at $z_i < z_{fit\ min}$ instead of T^{i+1} from previous height level z_{i+1}
- C_b ... background (a priori) error covariance matrix (set as diagonal matrix)
- $\sigma_T, \sigma_e, \sigma_{lw}$... standard errors of temperature, water vapor pressure, liquid water density (set nominally to high values so that the influence of the background state \mathbf{x}^b on the estimated \mathbf{x} is negligible; given T^{fit} at $z_i < z_{fit\ min}$ is used, σ_T is set to a smaller standard error consistent with the uncertainty of $T^{fit}(z_i)$ so that in this case – and only in this case – T^b exerts influence on the estimated \mathbf{x})
- $s_T^{z_{fit\ min}}$... background standard error estimate for best-fit profile temperature at level $z_{fit\ min}$ (baseline E5L setting: 0.75 K)
- $\left(\frac{ds_T}{dz}\right)$... downward increase of background standard error estimate with increasing distance from $z_{fit\ min}$ (baseline E5L setting: 0.25 K/km)
- $z_{fit\ min}$... threshold height for $N_j^I(z_i)$ quality below which a best-fit background temperature T^b is enabled to exert influence on \mathbf{x} ; above influence of background \mathbf{x}^b is negligible

Because the estimation problem is slightly over-determined for the ACE+ baseline of 3 signal frequencies, it is possible to retrieve the state (T^i, e^i, lw^i) even if one of the independent information pieces is lost, as will frequently be the case at any given height level, where only two of the three frequencies provide amplitude data in a useful dynamic range. Even if, for example, the information from two imaginary refractivities is lost, which can happen for

example in very wet regions, pressure, humidity and temperature still can be calculated if concentration of liquid water can be neglected or some information component (e.g., temperature) is known to some degree from background data. Information of real refractivity at lowest ACE+ frequency (9.7 GHz) will get lost only in extreme (and rare) situations, in which case atmospheric profiles retrieval in the lower troposphere is compromised.

2.4.6. Example results for illustration of inversion/retrieval processing chain output

As an example for the results of inversion retrieval and to illustrate the functioning of the whole retrieval chain, Figures 2.4.3 to 2.4.6 show the sequence of retrieved parameters, from transmission via refractivities to atmospheric parameters, for the mid-latitude summer case (Case 2). In each figure are shown three different panels (left, parameter profile; middle, absolute retrieval error; right, relative retrieval error), which depict four different profiles for different observation system errors involved (no error, thermal noise, 1/f amplitude noise, and linear amplitude drift). The corresponding inversion/retrieval input specifications for the mid-latitude summer case without errors are listed as an example in Appendix A.5.

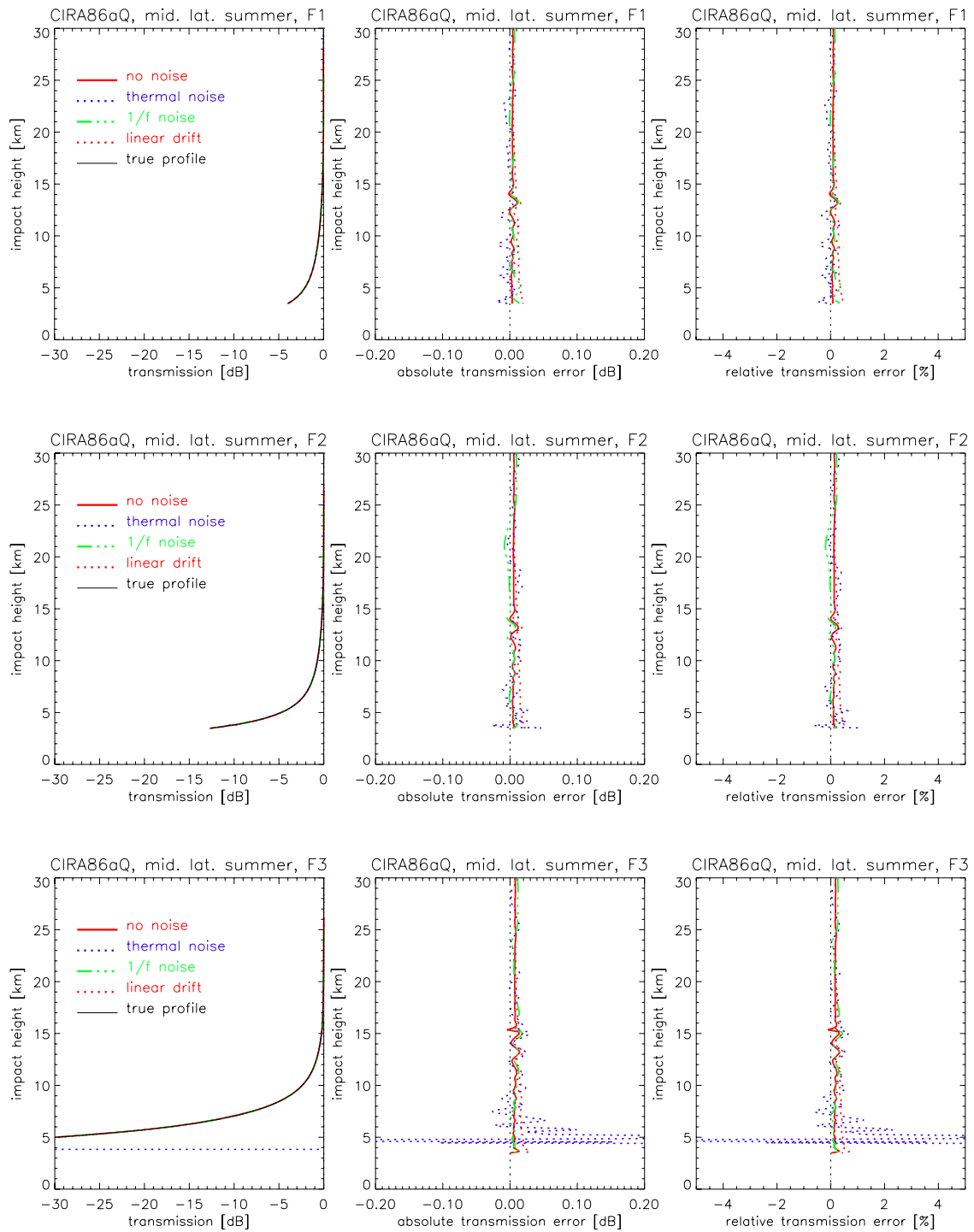


Fig. 2.4.3. Exemplary transmission retrieval results for the three ACE+ frequencies F1 to F3 for the mid-latitude summer case. Retrievals based on assuming the different instrumental error sources discussed above (subsection 2.3) are illustrated.

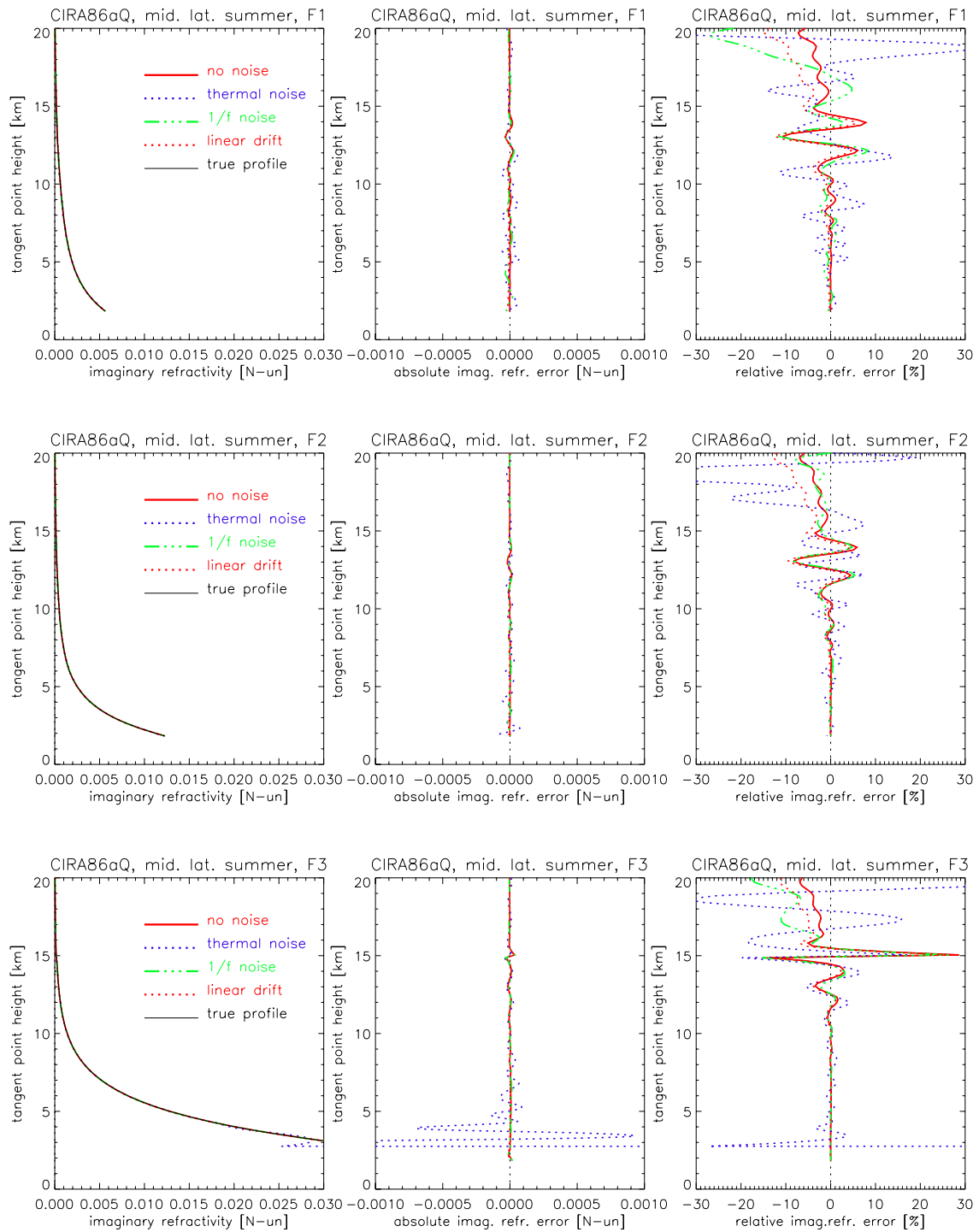


Fig. 2.4.4. Exemplary imaginary refractivity retrieval results for the three ACE+ frequencies F1 to F3 for the mid-latitude summer case. Retrievals based on assuming the different instrumental error sources discussed above (subsection 2.3) are illustrated.

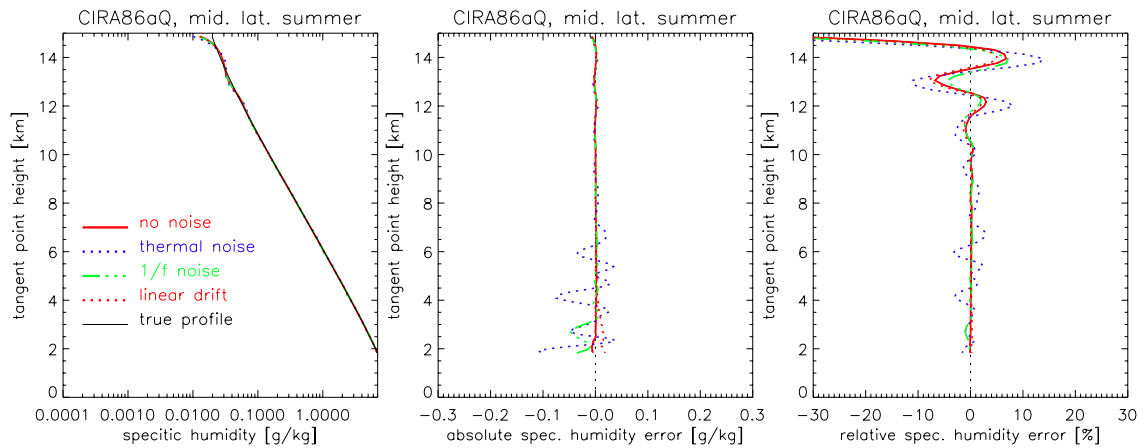


Fig. 2.4.5. Exemplary humidity retrieval results for the mid-latitude summer case. Retrievals based on assuming the different instrumental error sources discussed above (subsection 2.3) are illustrated.

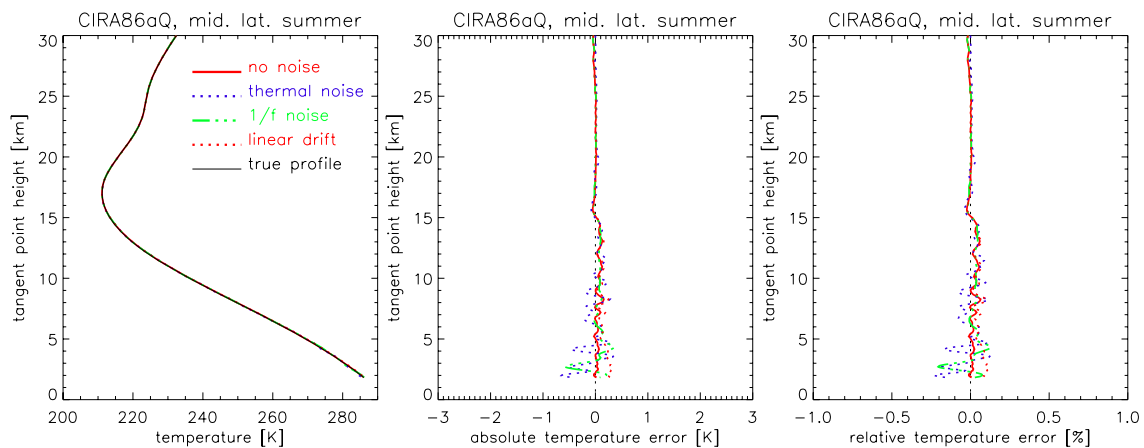


Fig. 2.4.6. Exemplary temperature retrieval results for the mid-latitude summer case. Retrievals based on assuming the different instrumental error sources discussed above (subsection 2.3) are illustrated.

3. Statistical Performance Analysis Results

The three subsections below, sections 3.1 to 3.3, show retrieval results, for different kinds of instrumental errors and under different conditions, as follows:

- **Section 3.1** shows clear/moist-air transmission, humidity and temperature retrieval results for various instrumental error assumptions under five different atmospheric conditions, tropical (Case 1, "C1"), mid-latitude summer (Case 2, "C2"), mid-latitude winter (Case 3, "C3"), high-latitude summer (Case 4, "C4") and high-latitude winter (Case 5, "C5"), ranging from tropically wet to very dry conditions (see Figure 2.2.1). The following six error cases are defined:
 1. no instrumental noise
 2. C/N_0 67 dBHz, ampl. drift 0.33%/20 sec, no 1/f noise
 3. C/N_0 67 dBHz, ampl. drift 0.33%/20 sec, 1/f noise $0.01 \cdot T\%$ | $T = 1-20\text{sec}$
 4. C/N_0 67 dBHz, ampl. drift 0.33%/20 sec, 1/f noise $0.02 \cdot T\%$ | $T = 1-20\text{sec}$
 5. C/N_0 67 dBHz, ampl. drift 0.62%/20 sec, 1/f noise $0.01 \cdot T\%$ | $T = 1-20\text{sec}$
 6. C/N_0 67 dBHz, ampl. drift 0.62%/20 sec, 1/f noise $0.02 \cdot T\%$ | $T = 1-20\text{sec}$

The notations of the several error components, in the headers of the figure panels, are 't67' for thermal noise with a C/N_0 in vacuum "above the atmosphere" of 67 dBHz, 'd04' for a linear drift slope of 0.04 dB/min ($\sim 0.33\%/20$ sec), 'd08' for a linear drift slope of 0.08 dB/min ($\sim 0.62\%/20$ sec), 'f25' for an 1/f noise with an error slope of 0.025 dB/min ($\sim 0.01 \cdot T\%$ in 1-20 sec) and 'f50' for an 1/f noise with an error slope of 0.050 dB/min ($\sim 0.02 \cdot T\%$ in 1-20 sec). In modeling all these amplitude errors, the parameter values have been set to cover a range of requirements roughly consistent with the main system requirements in the ACE+ MRD (2004).

For each of these 5×6 observation system modeling scenarios (5 atmospheres, each 6 error scenarios) an ensemble of 40 realizations was run to enable statistical error estimates on the retrieval results.

- **Section 3.2** shows transmission, humidity, temperature and liquid water retrieval results for the mid-latitude summer case ("C2") in presence of clouds (LWC ... Liquid water content of cloud; Height ... center height of cloud, Thickness ... thickness of cloud, with content LWC, about center height):
 1. *Randomized 3D As Clouds:*
 $LWC = 0.2 \text{ g/m}^3 \pm 0.1 \text{ g/m}^3$ (rms bounds: 0–0.4 g/m^3)
 $Height = 4.5 \text{ km} \pm 0.25 \text{ km}$ (rms bounds: 4–5 km)
 $Thickness = 0.6 \text{ km} \pm 0.15 \text{ km}$ (rms bounds: 0.3–0.9 km)
 2. *Randomized 3D Cu Clouds:*
 $LWC = 0.5 \text{ g/m}^3 \pm 0.25 \text{ g/m}^3$ (rms bounds: 0–1 g/m^3)
 $Height = 2.5 \text{ km} \pm 0.25 \text{ km}$ (rms bounds: 2–3 km)
 $Thickness = 0.3 \text{ km} \pm 0.05 \text{ km}$ (rms bounds: 0.2–0.4 km)

Randomized selection of the cloud parameters within the given bounds was performed to obtain different clouds for the individual realizations in a profiles ensemble, mimicking cloud variability. For each of the two forward modeling cases above (3D As and 3D Cu case) an ensemble of 40 realizations was run to enable statistical error estimates on the retrieval results.

The retrieval results for these two 40 realization ensembles were computed assuming two kinds of total instrumental errors, ‘in1’ with C/N_0 67 dBHz, ampl. drift 0.33%/20 sec, 1/f noise 0.01·T% for T=1-20sec, and ‘in2’ with C/N_0 67 dBHz, ampl. drift 0.62%/20 sec, 1/f noise 0.02·T% for T=1-20sec. The inversion/retrieval used the standard p+T+q+w (cloudy air) retrieval of EGOPS5.0.3r2.

- **Section 3.3** shows transmission, humidity, temperature and liquid water retrieval results for the mid-latitude summer case (“C2”) in presence of randomized clouds — using the 3D *As* and the 3D *Cu* case as in section 3.2 — but now with “mean” scintillations (“*Mea*”) due to atmospheric turbulence superposed in addition. The settings for this *Mea* scintillation case were $C_n^2 = 6 \cdot 10^{-15} \text{ m}^{-2/3}$, scale height = 2 km, horizontal extend = 200 km, C_n^2 height shape exponential, and outer scale of turbulence 100 m, consistent with mid-latitude “mean” (average) scintillation strengths. The turbulence parameters are based on turbulence statistics from radiosondes (e.g., Kuhn, 2003a; and references therein).

For each of the two forward modeling cases (*As* clouds + *Mea* scintillations, *Cu* clouds + *Mea* scintillations) an ensemble of 40 realizations was run to enable statistical error estimates on the retrieval results.

The retrieval results for the two 40 realization ensembles were computed assuming two kinds of total instrumental errors, ‘in1’ and ‘in2’, the same ones as for section 3.2 (see above), using the following two retrieval algorithms:

1. standard p+T+q+w (cloudy air) retrieval of EGOPS5.0.3r2
2. advanced p+T+q+w (cloudy air) retrieval of EGOPS5.0.4r1 (including best-fit temperature extrapolation below ~6 km into the lower troposphere)

All retrieval error results are illustrated in terms of standard deviation, bias, and bias uncertainty (2·x standard deviation of bias). The figures aim to give a quantitative visual estimate of the magnitudes at which the humidity and temperature retrieval errors are to be expected and how they compare to the observational requirements laid out in the ACE+ MRD (2004), which are depicted at error plot panels for visual reference.

Overall, the EGOPS5 end-to-end simulation system and the retrieval algorithms in their current version (embodied in the EGOPS5.0.3r2 and EGOPS5.0.4r1 versions used) proved to be adequately mature for the required performance analysis. Clearly, still many further extensions and improvements to the system need to be performed in the future, however.

3.1. Results on Retrieval Performance in Clear Air

This section shows clear/moist air transmission, humidity, and temperature retrieval results for six kinds of instrumental errors under five different atmospheric conditions (detailed specifications see in the introduction above).

The results of all 5×6 clear air scenarios are shown on the following pages 31 – 90.

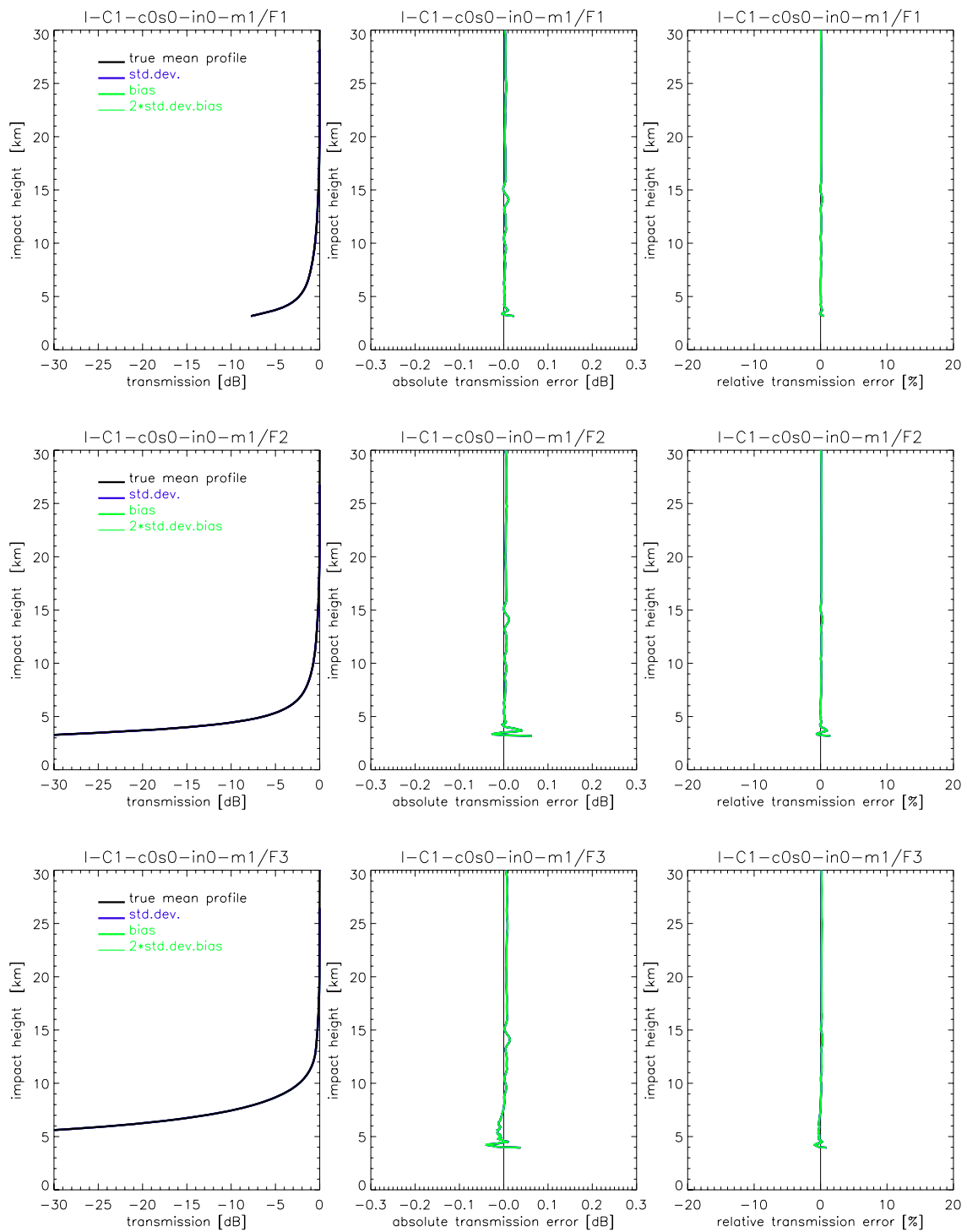


Fig. 3.1.1. Transmission retrieval results for the ACE+ frequencies F1 = 9.7 GHz (top panels), F2 = 17.25 GHz (middle panels), and F3 = 22.6 GHz (bottom panels) for the tropical case (C1), no instrumental errors (in0) scenario. Statistics performance results (standard deviation, bias, 2 x std.deviation of bias) for an ensemble of 40 profiles are shown. The std.deviation is shown as +/- envelopes about the bias profile.

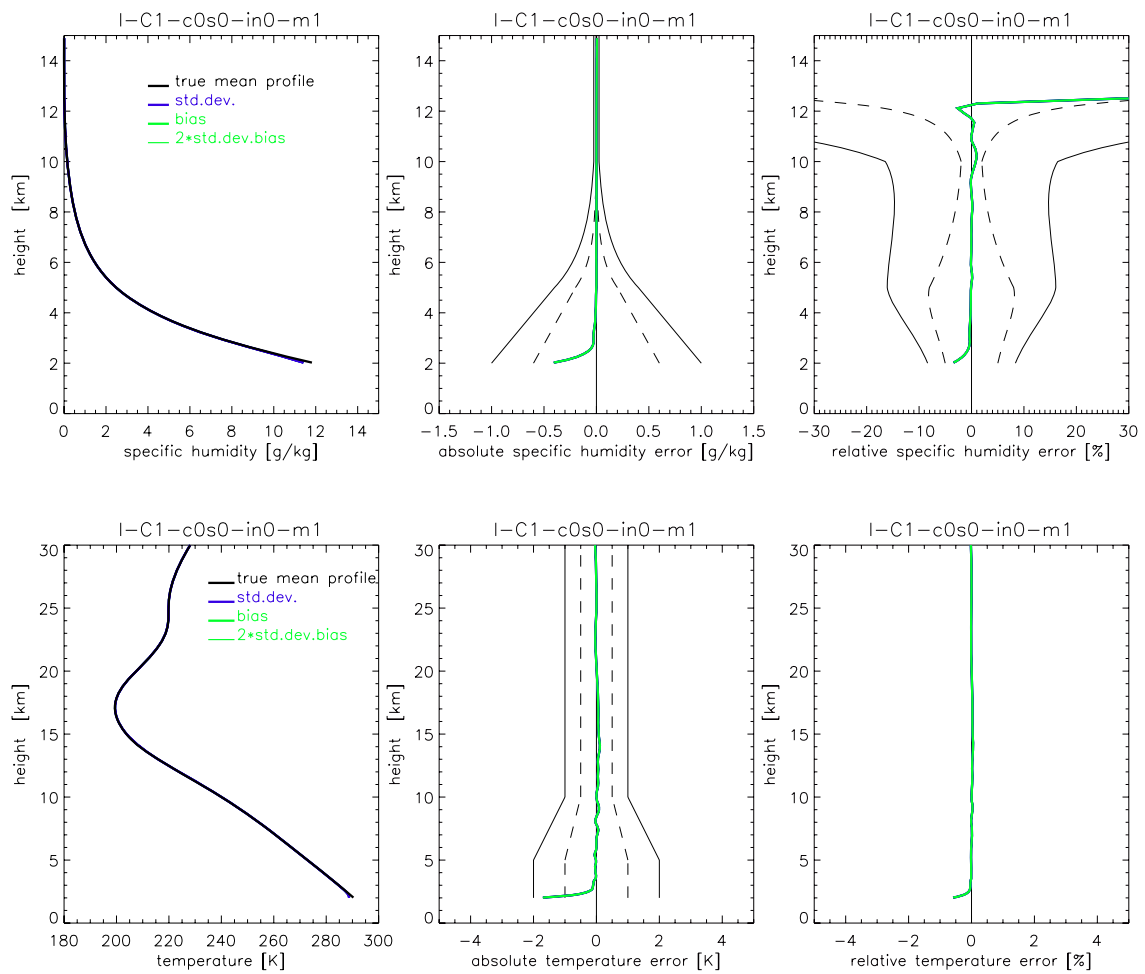


Fig. 3.1.2. Humidity (upper panels) and temperature (lower panels) retrieval results for the tropical case (C1), no instrumental errors (in0) scenario. Statistics performance results (standard deviation, bias, 2 x std.deviation of bias) for an ensemble of 40 profiles are shown. The std.deviation is shown as +/- envelopes about the bias profiles. In the middle panels (for humidity and temperature) and the right panel (for humidity) the observational requirements, as set by the ACE+ MRD (v2.1/Jan 2004), are shown for reference (solid black, threshold requirements; dashed black, target requirements).

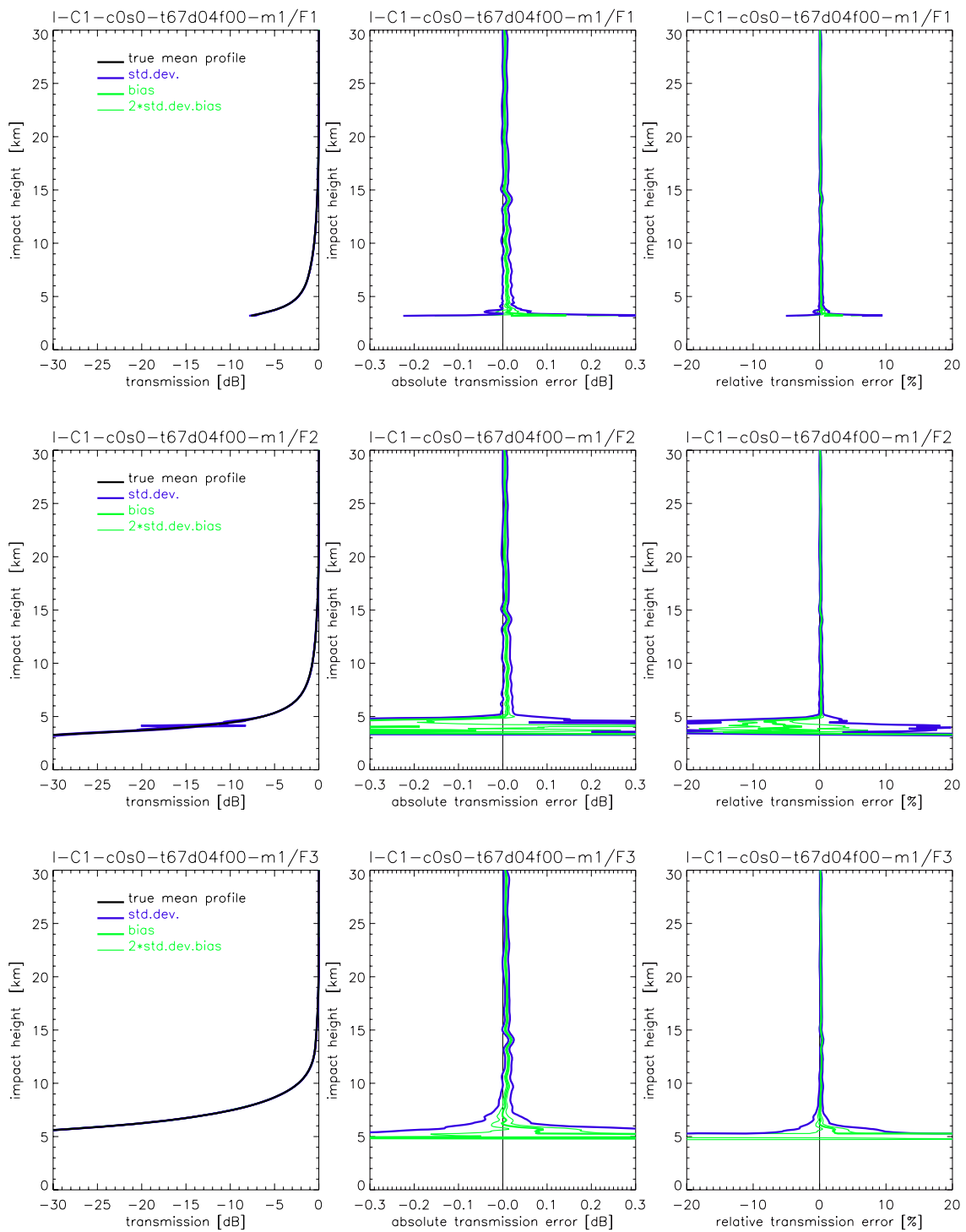


Fig. 3.1.3. Transmission retrieval results for the ACE+ frequencies F1 = 9.7 GHz (top panels), F2 = 17.25 GHz (middle panels), and F3 = 22.6 GHz (bottom panels) for the tropical case (C1), instrumental errors (ine) scenario (therm. noise, C/No 67 dBHz, ampl. drift 0.33%/20sec, no 1/f noise). Statistics performance results (standard deviation, bias, 2 x std.deviation of bias) for an ensemble of 40 profiles are shown. The std.deviation is shown as +/- envelopes about the bias profile.

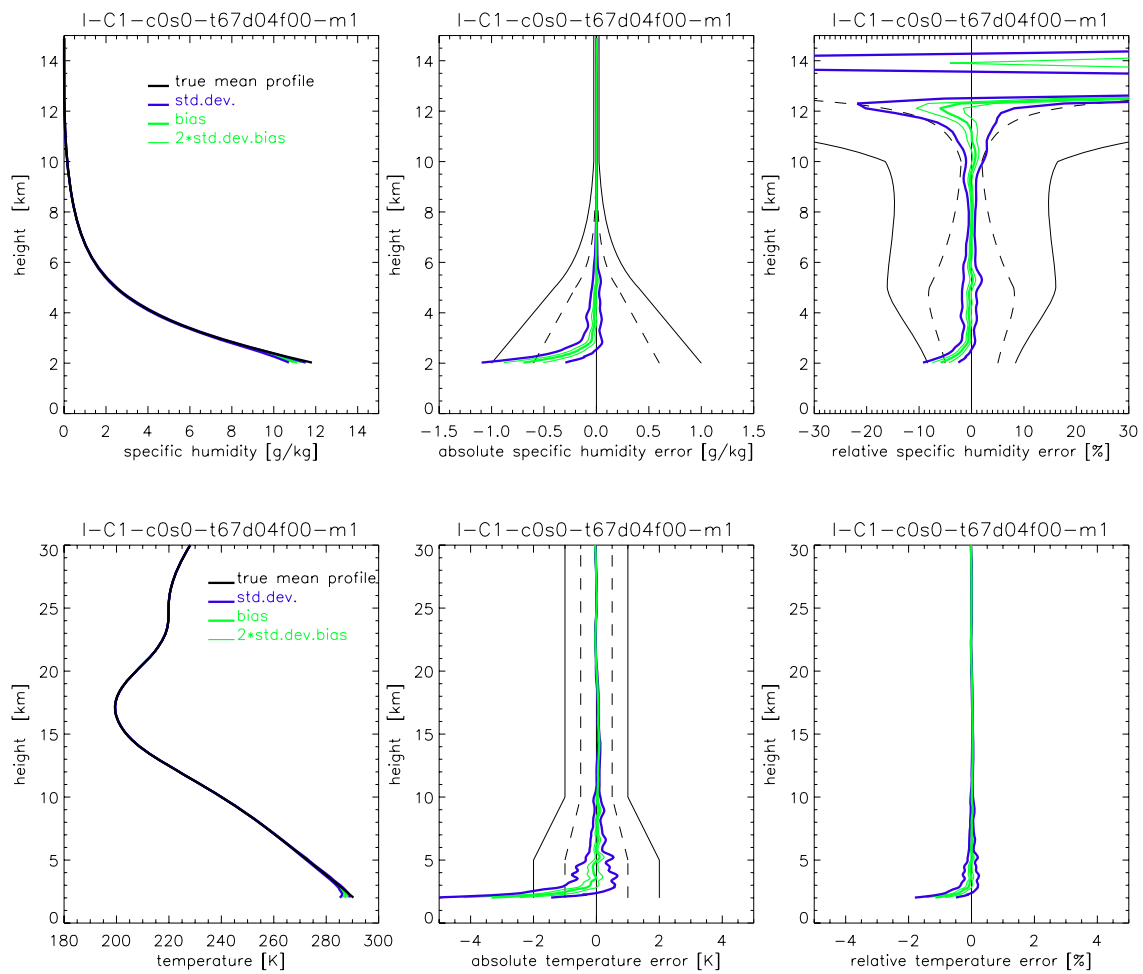


Fig. 3.1.4. Humidity (upper panels) and temperature (lower panels) retrieval results for the tropical case (C1), instrumental errors (ine) scenario (therm. noise, C/No 67 dBHz, ampl. drift 0.33%/20sec, no 1/f noise). Statistics performance results (standard deviation, bias, 2 x std.deviation of bias) for an ensemble of 40 profiles are shown. The std.deviation is shown as +/- envelopes about the bias profiles. In the middle panels (for humidity and temperature) and the right panel (for humidity) the observational requirements, as set by the ACE+ MRD (v2.1/Jan 2004), are shown for reference (solid black, threshold requirements; dashed black, target requirements).

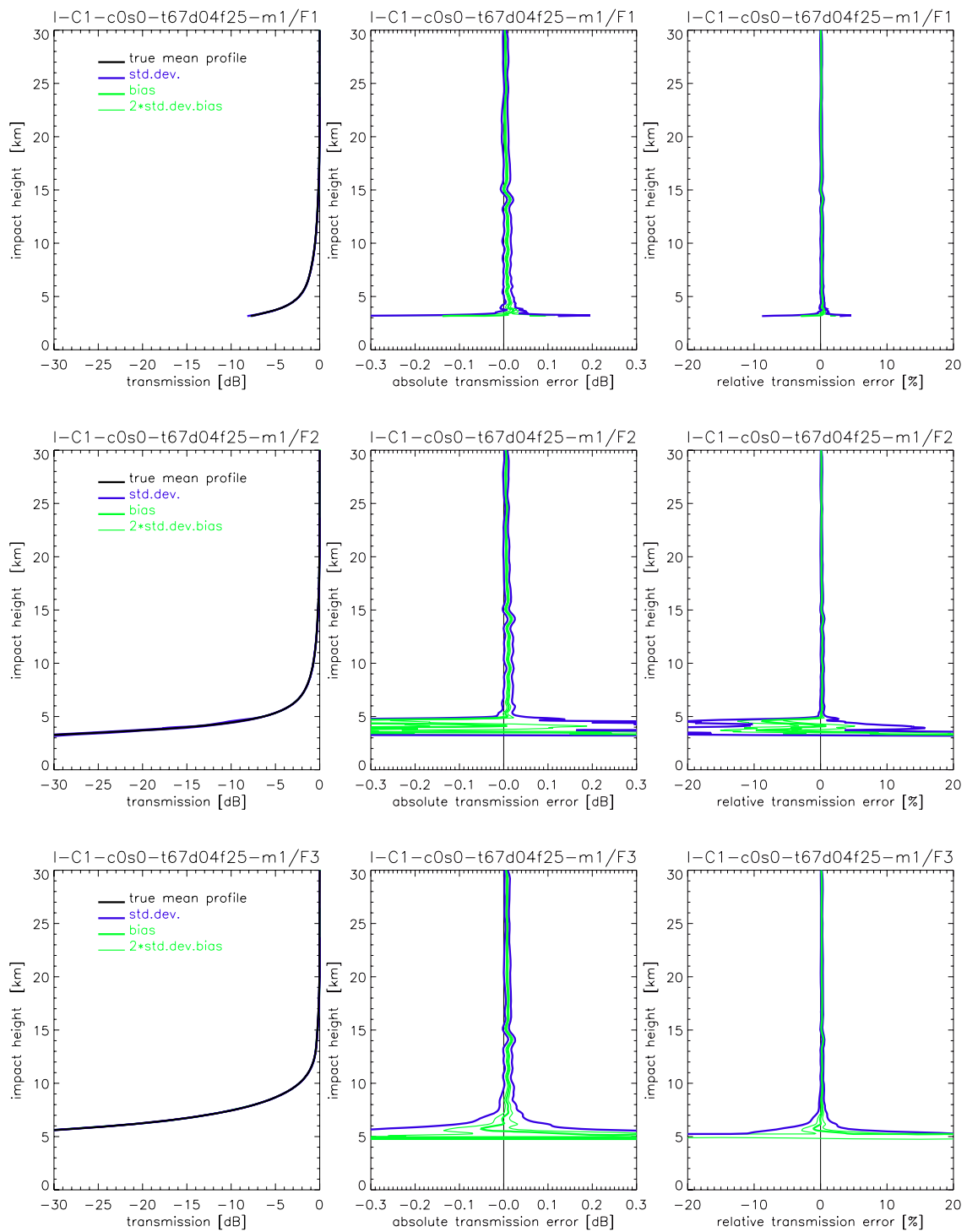


Fig. 3.1.5. Transmission retrieval results for the ACE+ frequencies F1 = 9.7 GHz (top panels), F2 = 17.25 GHz (middle panels), and F3 = 22.6 GHz (bottom panels) for the tropical case (C1), instrumental errors (ine) scenario (therm. noise, C/No 67 dBHz, ampl. drift 0.33%/20sec, 1/f noise 0.01*T%, T=1-20sec). Statistics performance results (standard deviation, bias, 2 x std.deviation of bias) for an ensemble of 40 profiles are shown. The std.deviation is shown as +/- envelopes about the bias profile.

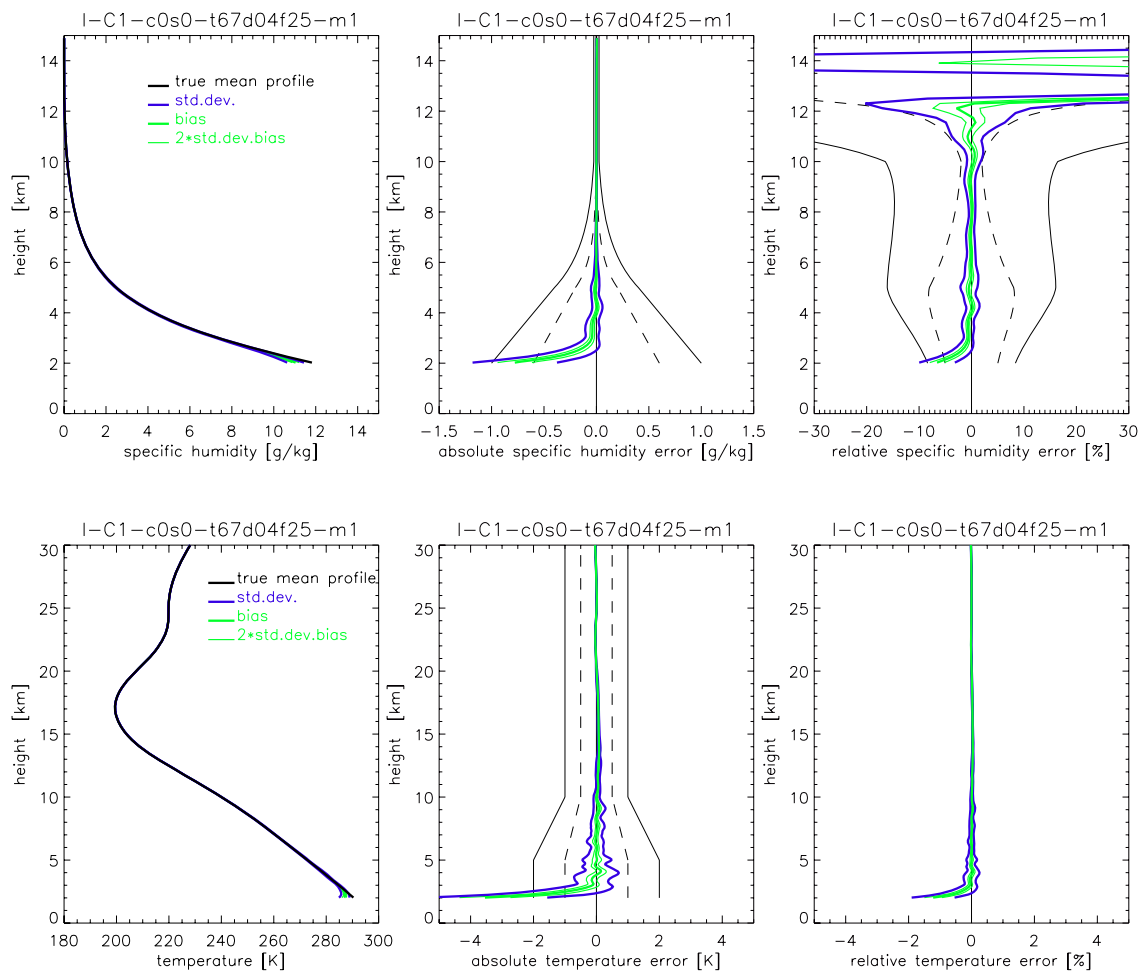


Fig. 3.1.6. Humidity (upper panels) and temperature (lower panels) retrieval results for the tropical case (C1), instrumental errors (ine) scenario (therm. noise, C/No 67 dBHz, ampl. drift 0.33%/20sec, 1/f noise 0.01*T%, T=1-20sec). Statistics performance results (standard deviation, bias, 2 x std.deviation of bias) for an ensemble of 40 profiles are shown. The std.deviation is shown as +/- envelopes about the bias profiles. In the middle panels (for humidity and temperature) and the right panel (for humidity) the observational requirements, as set by the ACE+ MRD (v2.1/Jan 2004), are shown for reference (solid black, threshold requirements; dashed black, target requirements).

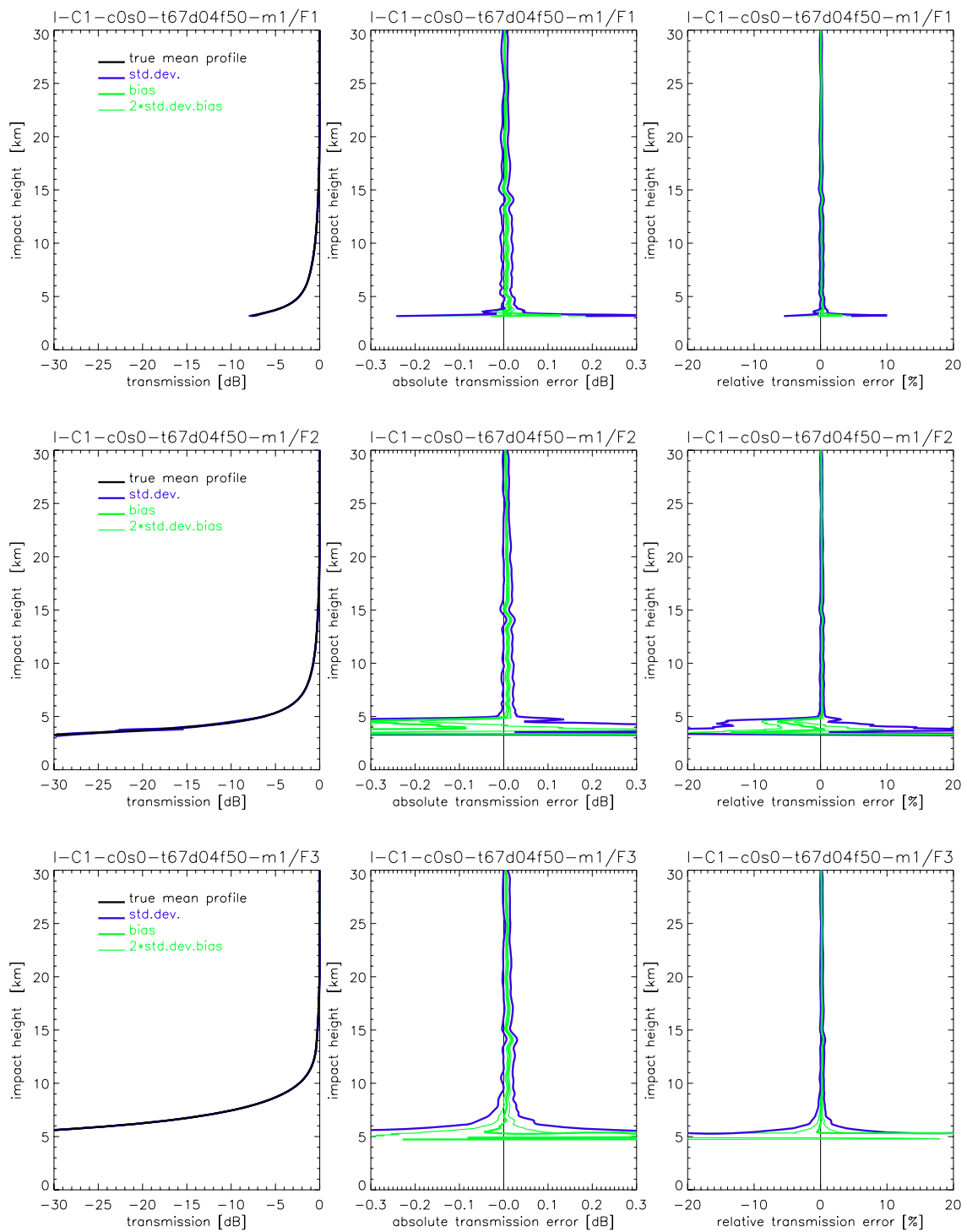


Fig. 3.1.7. Transmission retrieval results for the ACE+ frequencies F1 = 9.7 GHz (top panels), F2 = 17.25 GHz (middle panels), and F3 = 22.6 GHz (bottom panels) for the tropical case (C1), instrumental errors (ine) scenario (therm. noise, C/No 67 dBHz, ampl. drift 0.33%/20sec, 1/f noise 0.02*T%, T=1-20sec). Statistics performance results (standard deviation, bias, 2 x std.deviation of bias) for an ensemble of 40 profiles are shown. The std.deviation is shown as +/- envelopes about the bias profile.

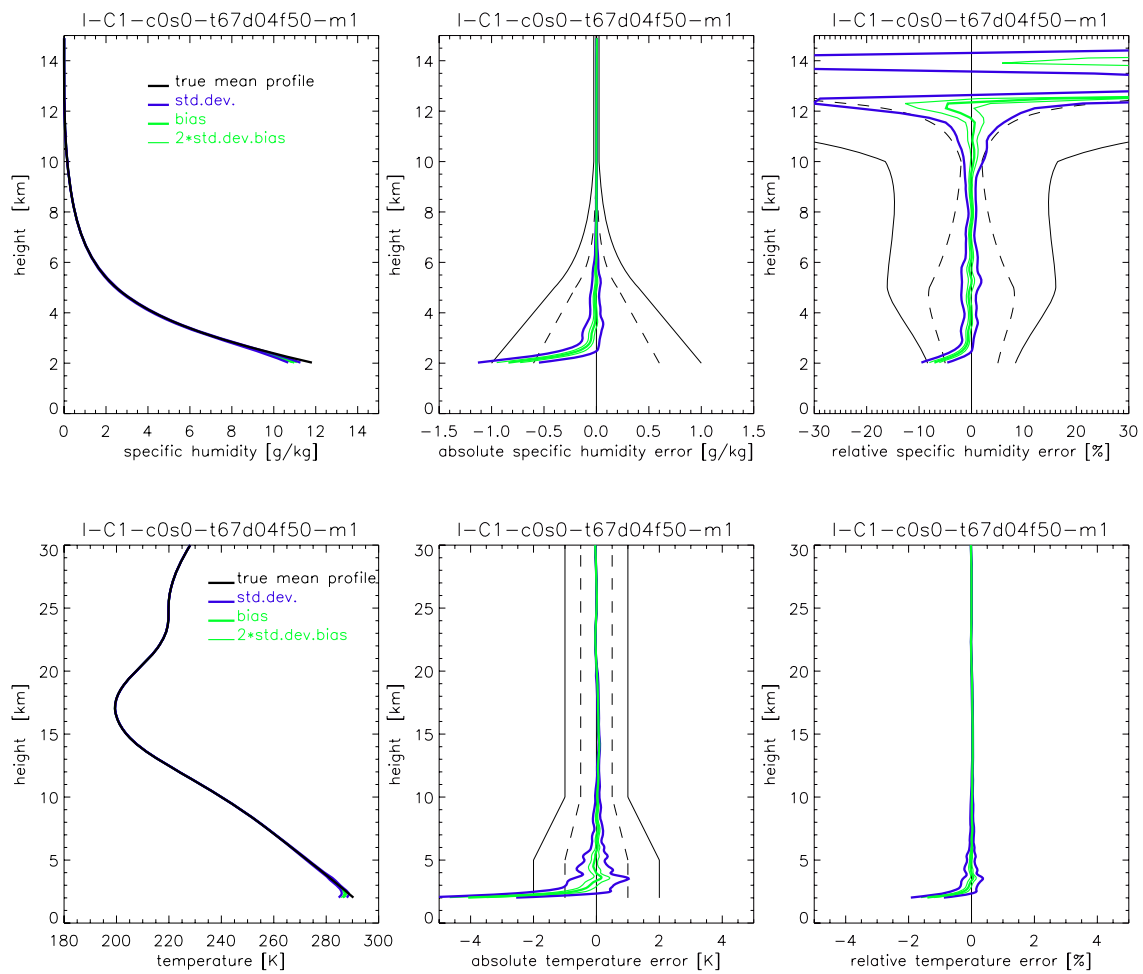


Fig. 3.1.8. Humidity (upper panels) and temperature (lower panels) retrieval results for the tropical case (C1), instrumental errors (ine) scenario (therm. noise, C/No 67 dBHz, ampl. drift 0.33%/20sec, 1/f noise 0.02*T%, T=1-20sec). Statistics performance results (standard deviation, bias, 2 x std.deviation of bias) for an ensemble of 40 profiles are shown. The std.deviation is shown as +/- envelopes about the bias profiles. In the middle panels (for humidity and temperature) and the right panel (for humidity) the observational requirements, as set by the ACE+ MRD (v2.1/Jan 2004), are shown for reference (solid black, threshold requirements; dashed black, target requirements).

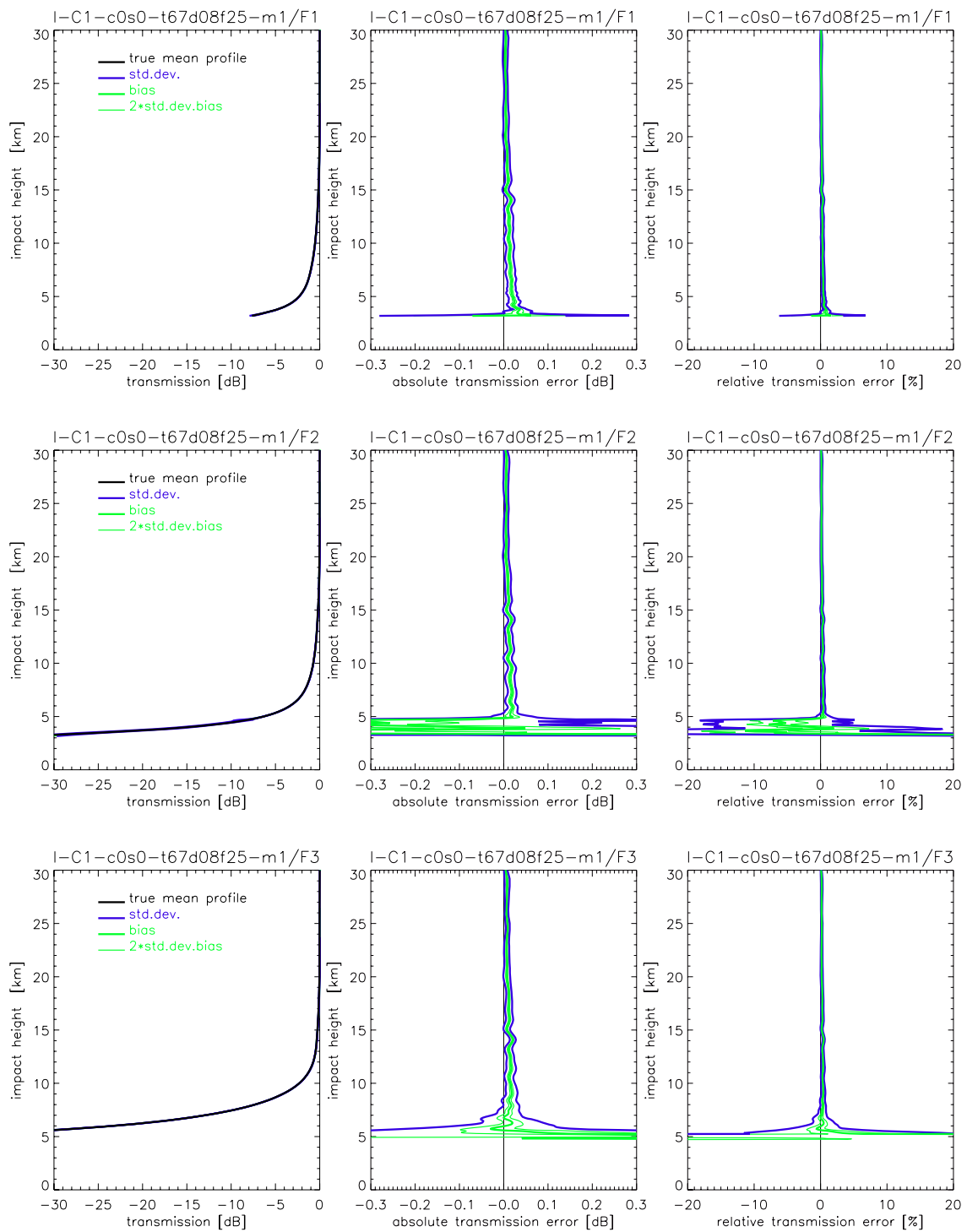


Fig. 3.1.9. Transmission retrieval results for the ACE+ frequencies F1 = 9.7 GHz (top panels), F2 = 17.25 GHz (middle panels), and F3 = 22.6 GHz (bottom panels) for the tropical case (C1), instrumental errors (ine) scenario (therm. noise, C/No 67 dBHz, ampl. drift 0.62%/20sec, 1/f noise 0.01*T%, T=1-20sec). Statistics performance results (standard deviation, bias, 2 x std.deviation of bias) for an ensemble of 40 profiles are shown. The std.deviation is shown as +/- envelopes about the bias profile.

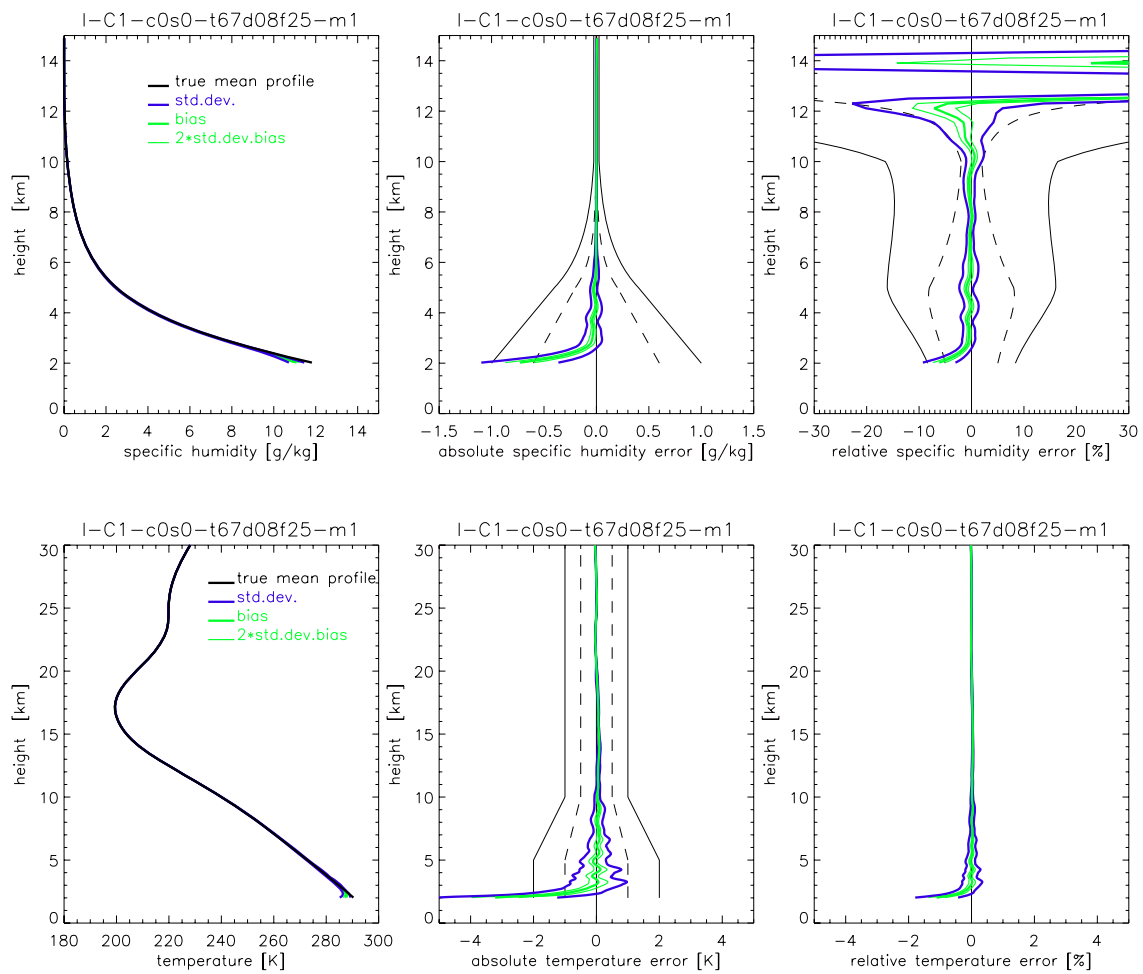


Fig. 3.1.10. Humidity (upper panels) and temperature (lower panels) retrieval results for the tropical case (C1), instrumental errors (ine) scenario (therm. noise, C/No 67 dBHz, ampl. drift 0.62%/20sec, 1/f noise 0.01*T%, T=1-20sec). Statistics performance results (standard deviation, bias, 2 x std.deviation of bias) for an ensemble of 40 profiles are shown. The std.deviation is shown as +/- envelopes about the bias profiles. In the middle panels (for humidity and temperature) and the right panel (for humidity) the observational requirements, as set by the ACE+ MRD (v2.1/Jan 2004), are shown for reference (solid black, threshold requirements; dashed black, target requirements).

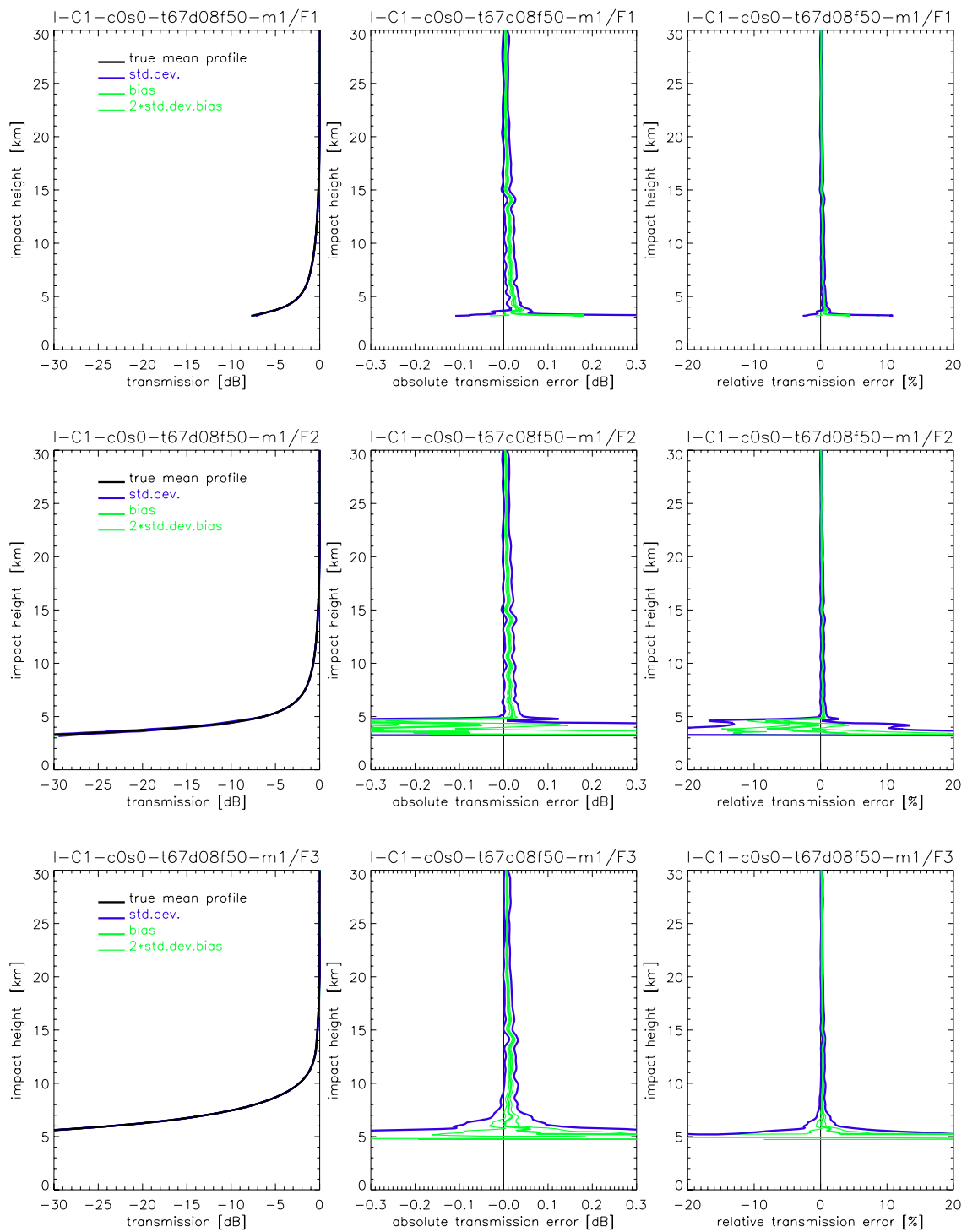


Fig. 3.1.11. Transmission retrieval results for the ACE+ frequencies F1 = 9.7 GHz (top panels), F2 = 17.25 GHz (middle panels), and F3 = 22.6 GHz (bottom panels) for the tropical case (C1), instrumental errors (ine) scenario (therm. noise, C/No 67 dBHz, ampl. drift 0.62%/20sec, 1/f noise 0.02*T%, T=1-20sec). Statistics performance results (standard deviation, bias, 2 x std.deviation of bias) for an ensemble of 40 profiles are shown. The std.deviation is shown as +/- envelopes about the bias profile.

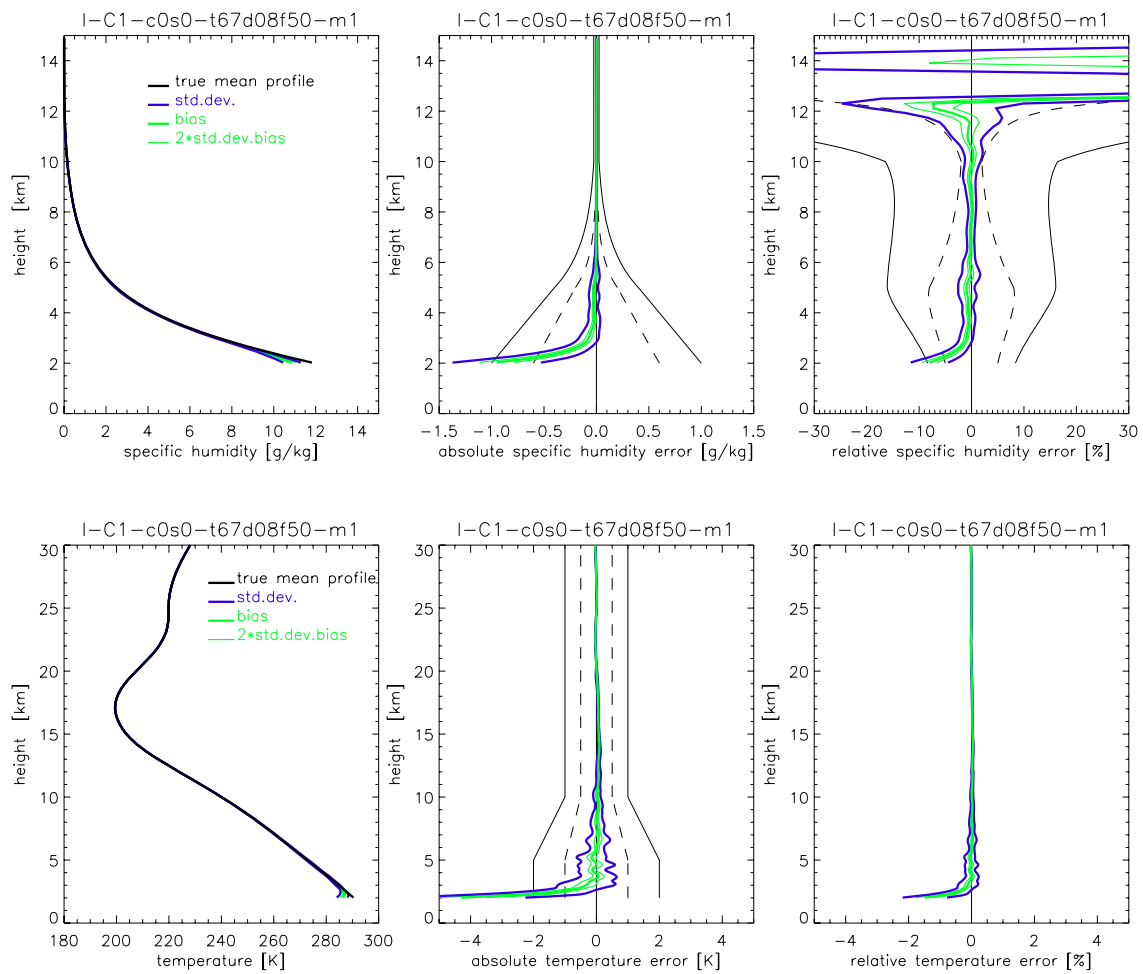


Fig. 3.1.12. Humidity (upper panels) and temperature (lower panels) retrieval results for the tropical case (C1), instrumental errors (ine) scenario (therm. noise, C/No 67 dBHz, ampl. drift 0.62%/20sec, 1/f noise 0.02*T%, T=1-20sec). Statistics performance results (standard deviation, bias, 2 x std.deviation of bias) for an ensemble of 40 profiles are shown. The std.deviation is shown as +/- envelopes about the bias profiles. In the middle panels (for humidity and temperature) and the right panel (for humidity) the observational requirements, as set by the ACE+ MRD (v2.1/Jan 2004), are shown for reference (solid black, threshold requirements; dashed black, target requirements).

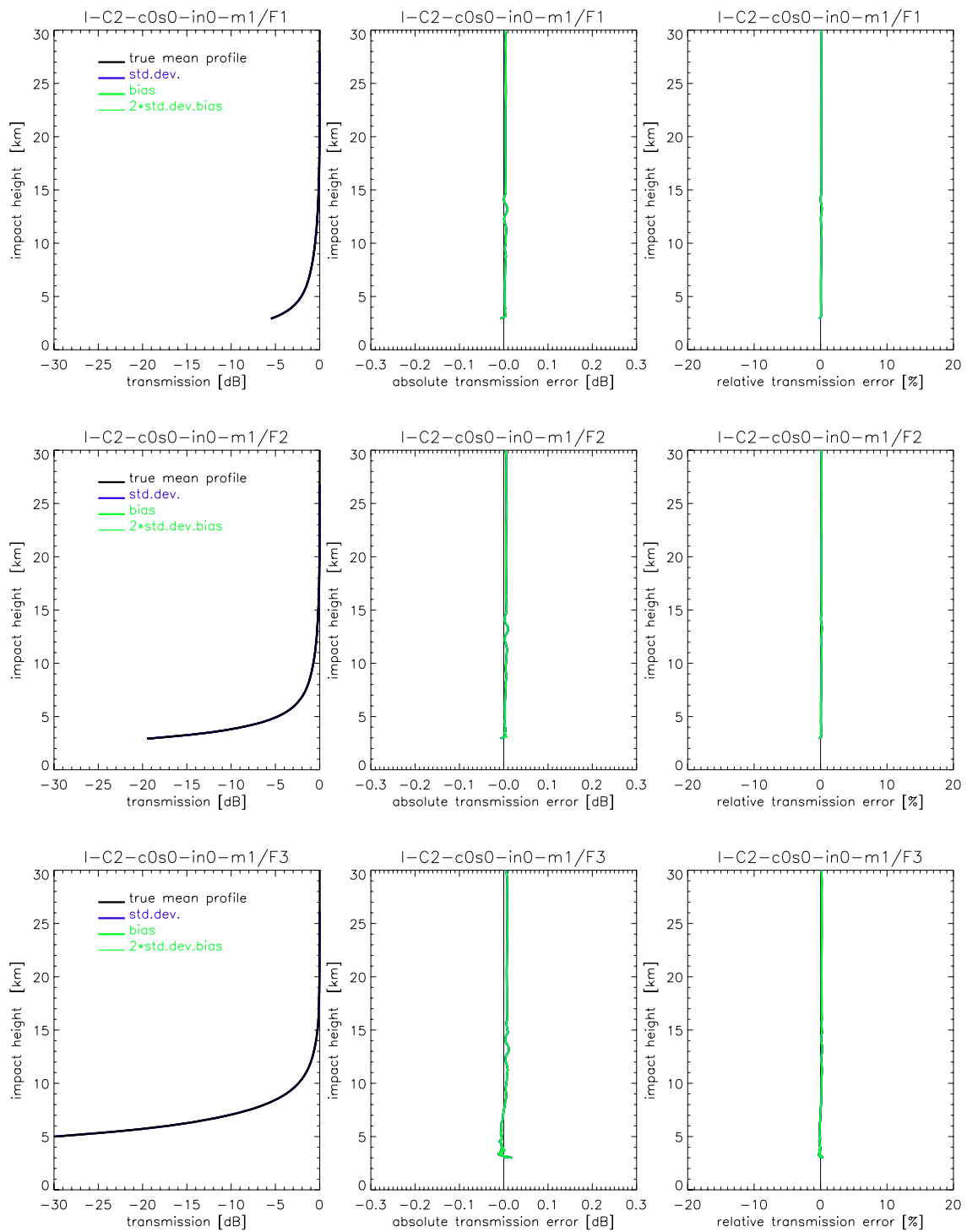


Fig. 3.1.13. Transmission retrieval results for the ACE+ frequencies F1 = 9.7 GHz (top panels), F2 = 17.25 GHz (middle panels), and F3 = 22.6 GHz (bottom panels) for the mid-lat summer case (C2), no instrumental errors (in0) scenario. Statistics performance results (standard deviation, bias, 2 x std.deviation of bias) for an ensemble of 40 profiles are shown. The std.deviation is shown as +/- envelopes about the bias profile.

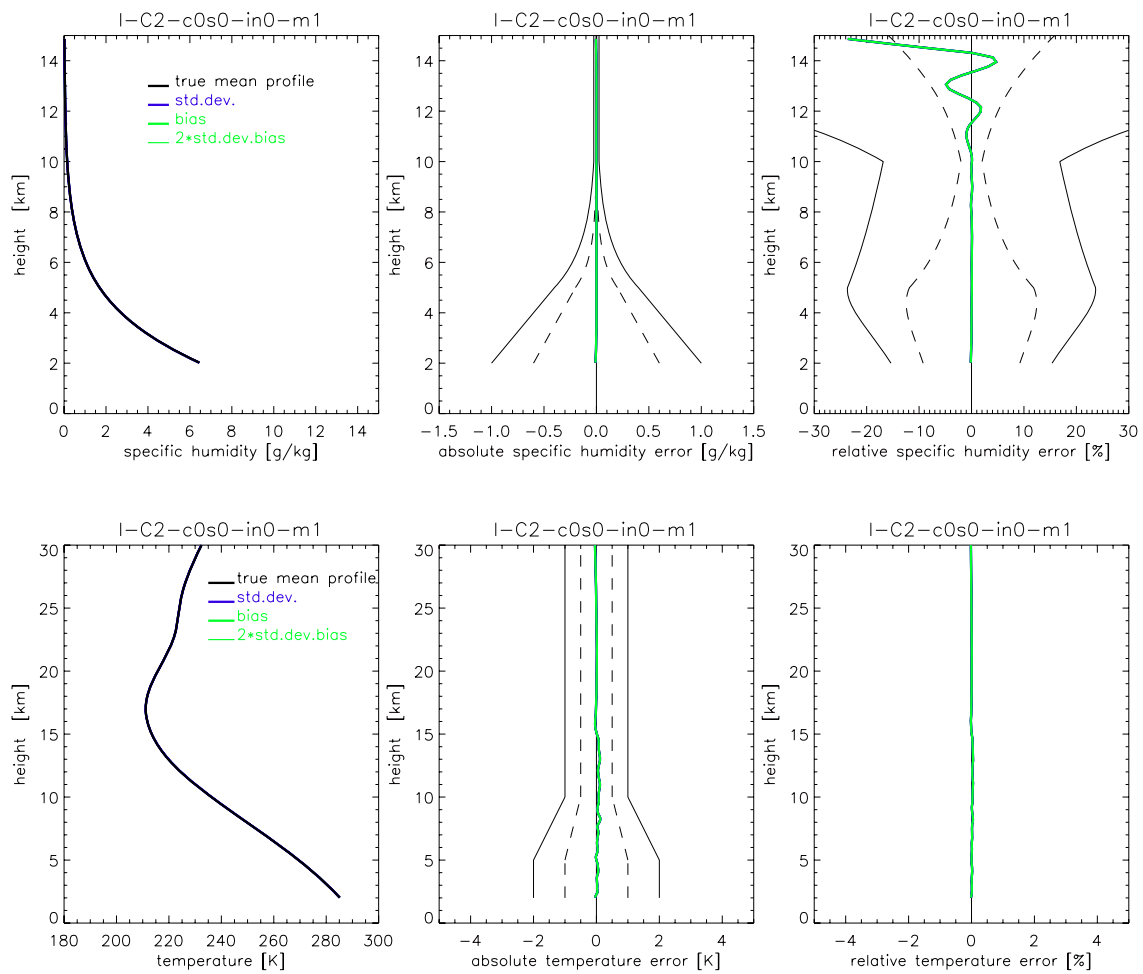


Fig. 3.1.14. Humidity (upper panels) and temperature (lower panels) retrieval results for the mid-lat summer case (C2), no instrumental errors (in0) scenario. Statistics performance results (standard deviation, bias, 2 x std.deviation of bias) for an ensemble of 40 profiles are shown. The std.deviation is shown as +/- envelopes about the bias profiles. In the middle panels (for humidity and temperature) and the right panel (for humidity) the observational requirements, as set by the ACE+ MRD (v2.1/Jan 2004), are shown for reference (solid black, threshold requirements; dashed black, target requirements).

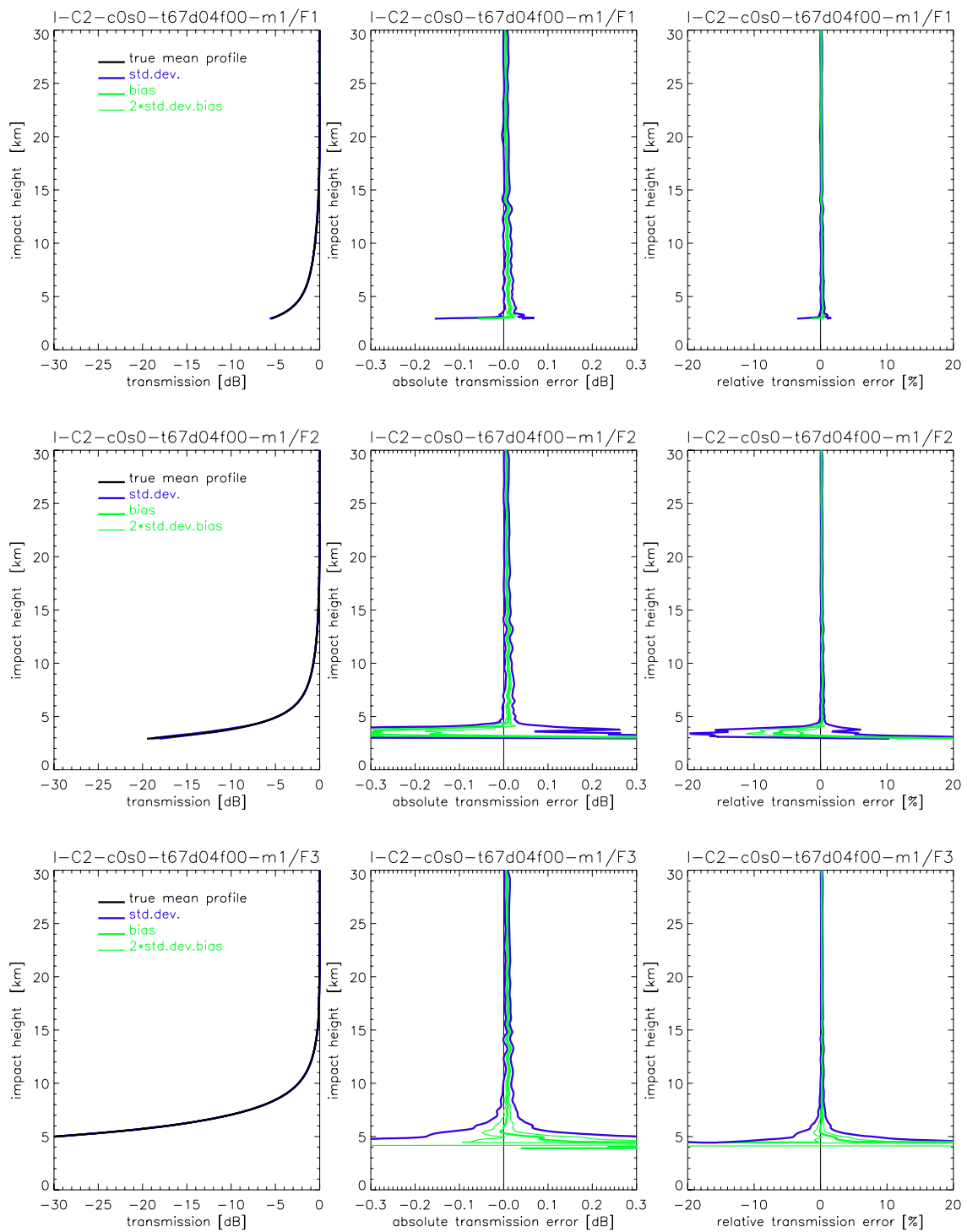


Fig. 3.1.15. Transmission retrieval results for the ACE+ frequencies F1 = 9.7 GHz (top panels), F2 = 17.25 GHz (middle panels), and F3 = 22.6 GHz (bottom panels) for the mid-lat summer case (C2), instrumental errors (ine) scenario (therm. noise, C/No 67 dBHz, ampl. drift 0.33%/20sec, no 1/f noise). Statistics performance results (standard deviation, bias, 2 x std.deviation of bias) for an ensemble of 40 profiles are shown. The std.deviation are shown as +/- envelopes about the bias profile.

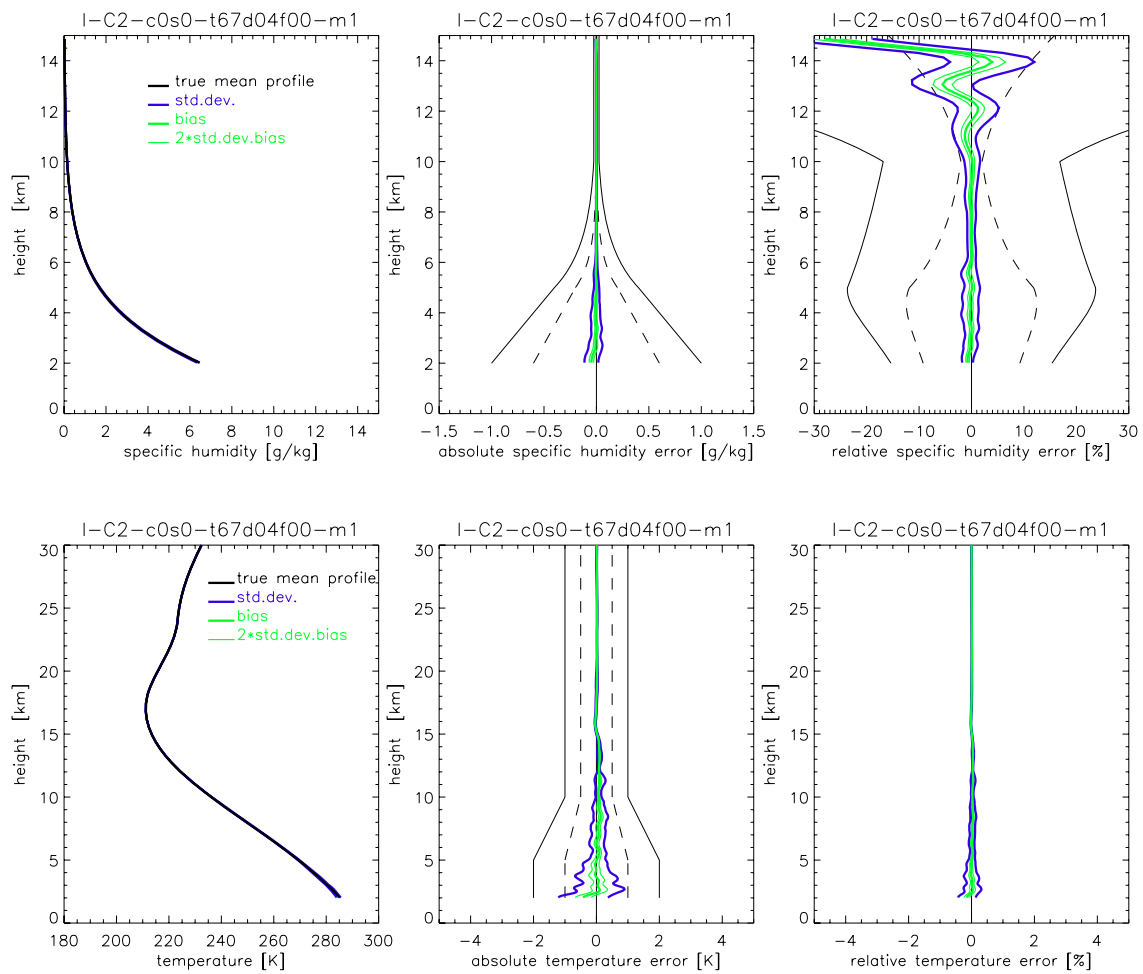


Fig. 3.1.16. Humidity (upper panels) and temperature (lower panels) retrieval results for the mid-lat summer case (C2), instrumental errors (ine) scenario (therm. noise, C/No 67 dBHz, ampl. drift 0.33%/20sec, no 1/f noise). Statistics performance results (standard deviation, bias, 2 x std.deviation of bias) for an ensemble of 40 profiles are shown. The std.deviation is shown as +/- envelopes about the bias profiles. In the middle panels (for humidity and temperature) and the right panel (for humidity) the observational requirements, as set by the ACE+ MRD (v2.1/Jan 2004), are shown for reference (solid black, threshold requirements; dashed black, target requirements).

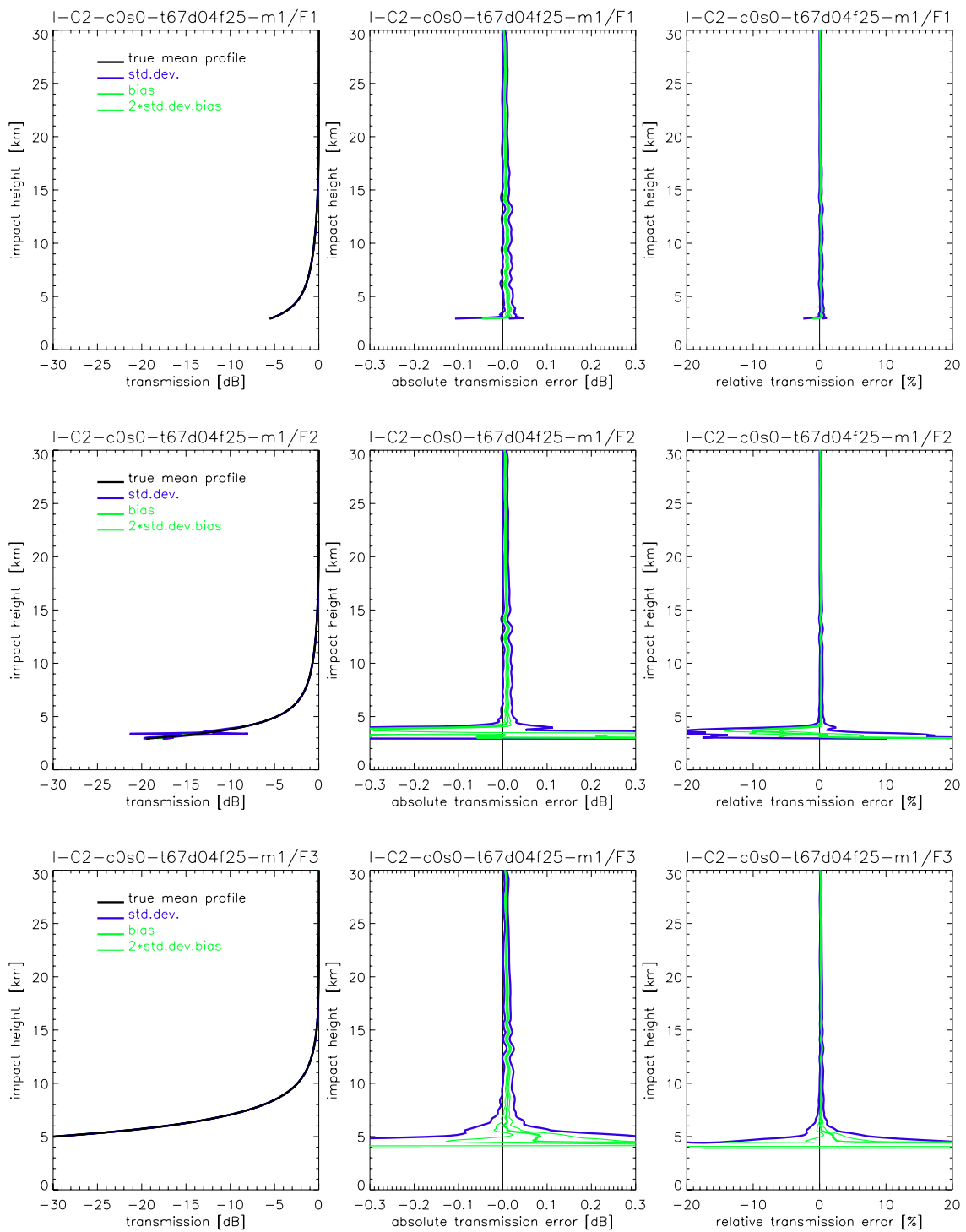


Fig. 3.1.17. Transmission retrieval results for the ACE+ frequencies F1 = 9.7 GHz (top panels), F2 = 17.25 GHz (middle panels), and F3 = 22.6 GHz (bottom panels) for the mid-lat summer case (C2), instrumental errors (ine) scenario (therm. noise, C/No 67 dBHz, ampl. drift 0.33%/20sec, 1/f noise 0.01*T%, T=1-20sec). Statistics performance results (standard deviation, bias, 2 x std.deviation of bias) for an ensemble of 40 profiles are shown. The std.deviation is shown as +/- envelopes about the bias profile.

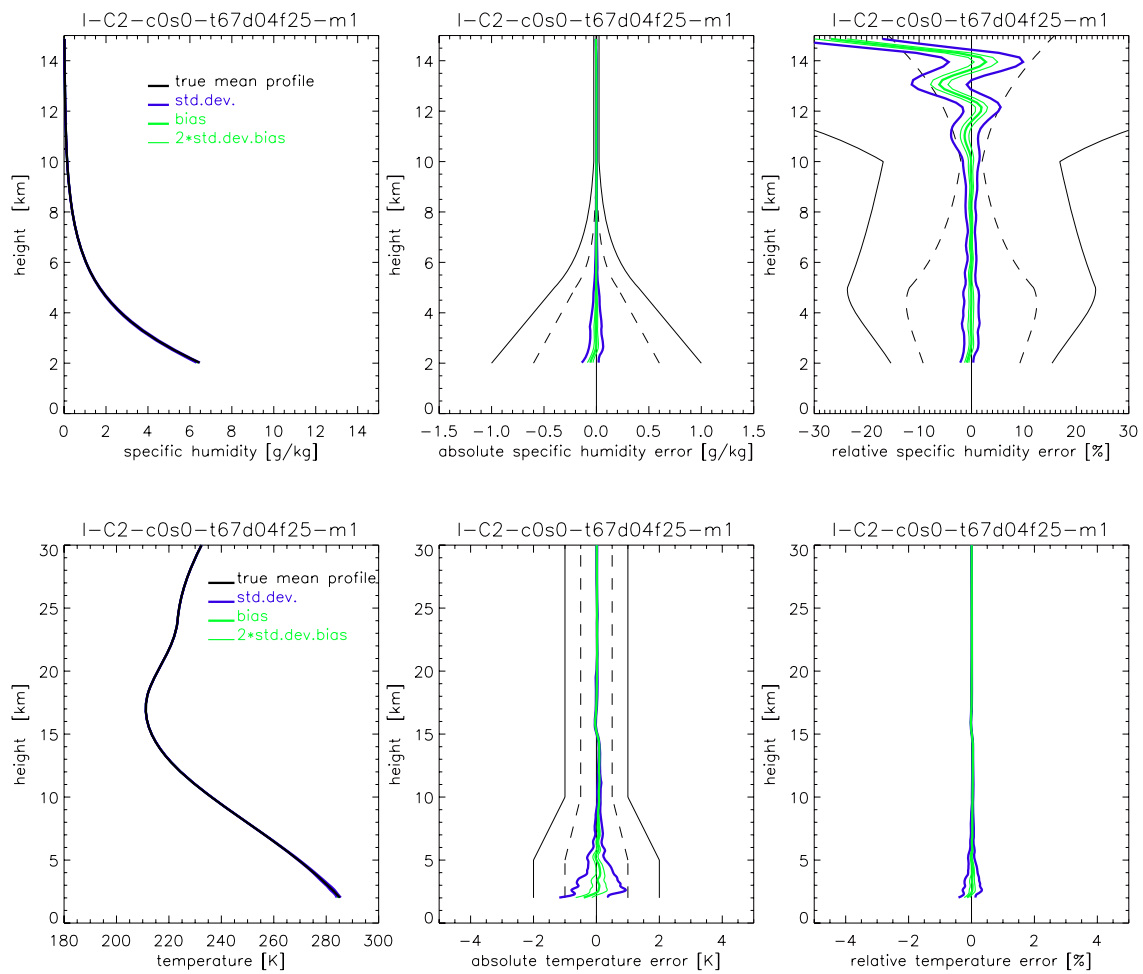


Fig. 3.1.18. Humidity (upper panels) and temperature (lower panels) retrieval results for the mid-lat summer case (C2), instrumental errors (ine) scenario (therm. noise, C/No 67 dBHz, ampl. drift 0.33%/20sec, 1/f noise 0.01*T%, T=1-20sec). Statistics performance results (standard deviation, bias, 2 x std.deviation of bias) for an ensemble of 40 profiles are shown. The std.deviation is shown as +/- envelopes about the bias profiles. In the middle panels (for humidity and temperature) and the right panel (for humidity) the observational requirements, as set by the ACE+ MRD (v2.1/Jan 2004), are shown for reference (solid black, threshold requirements; dashed black, target requirements).

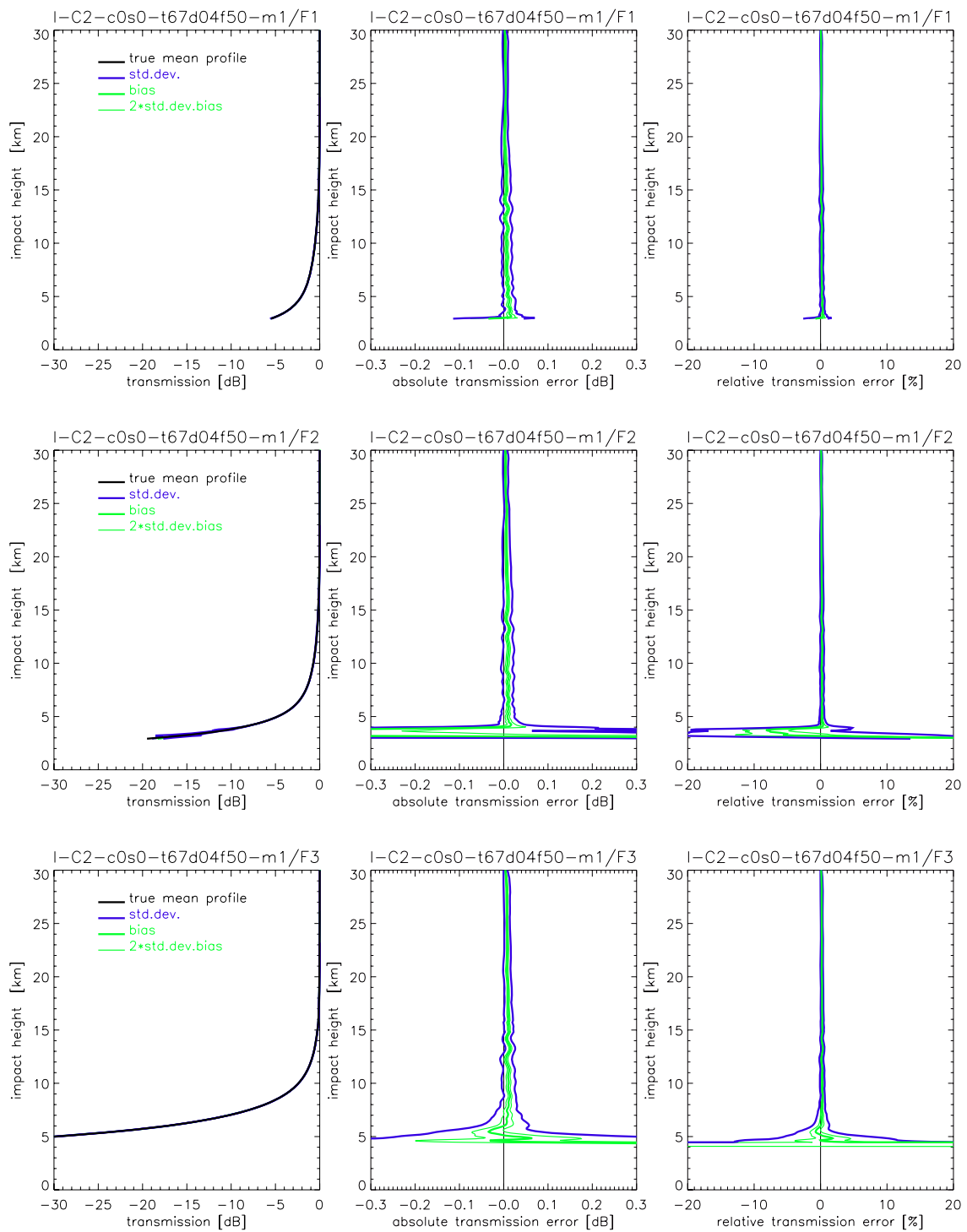


Fig. 3.1.19. Transmission retrieval results for the ACE+ frequencies F1 = 9.7 GHz (top panels), F2 = 17.25 GHz (middle panels), and F3 = 22.6 GHz (bottom panels) for the mid-lat summer case (C2), instrumental errors (ine) scenario (therm. noise, C/No 67 dBHz, ampl. drift 0.33%/20sec, 1/f noise 0.02*T%, T=1-20sec). Statistics performance results (standard deviation, bias, 2 x std.deviation of bias) for an ensemble of 40 profiles are shown. The std.deviation is shown as +/- envelopes about the bias profile.

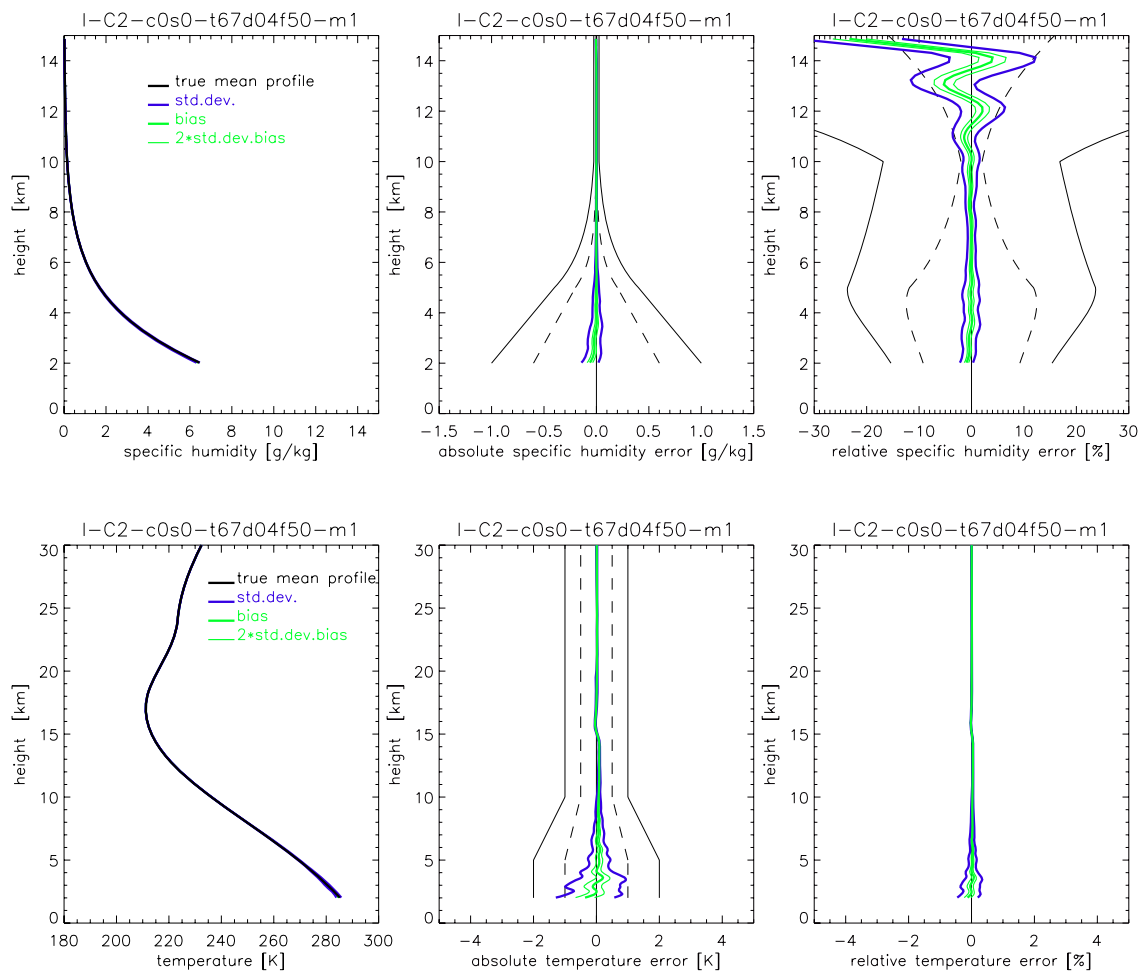


Fig. 3.1.20. Humidity (upper panels) and temperature (lower panels) retrieval results for the mid-lat summer case (C2), instrumental errors (ine) scenario (therm. noise, C/No 67 dBHz, ampl. drift 0.33%/20sec, 1/f noise 0.02*T%, T=1-20sec). Statistics performance results (standard deviation, bias, 2 x std.deviation of bias) for an ensemble of 40 profiles are shown. The std.deviation is shown as +/- envelopes about the bias profiles. In the middle panels (for humidity and temperature) and the right panel (for humidity) the observational requirements, as set by the ACE+ MRD (v2.1/Jan 2004), are shown for reference (solid black, threshold requirements; dashed black, target requirements).

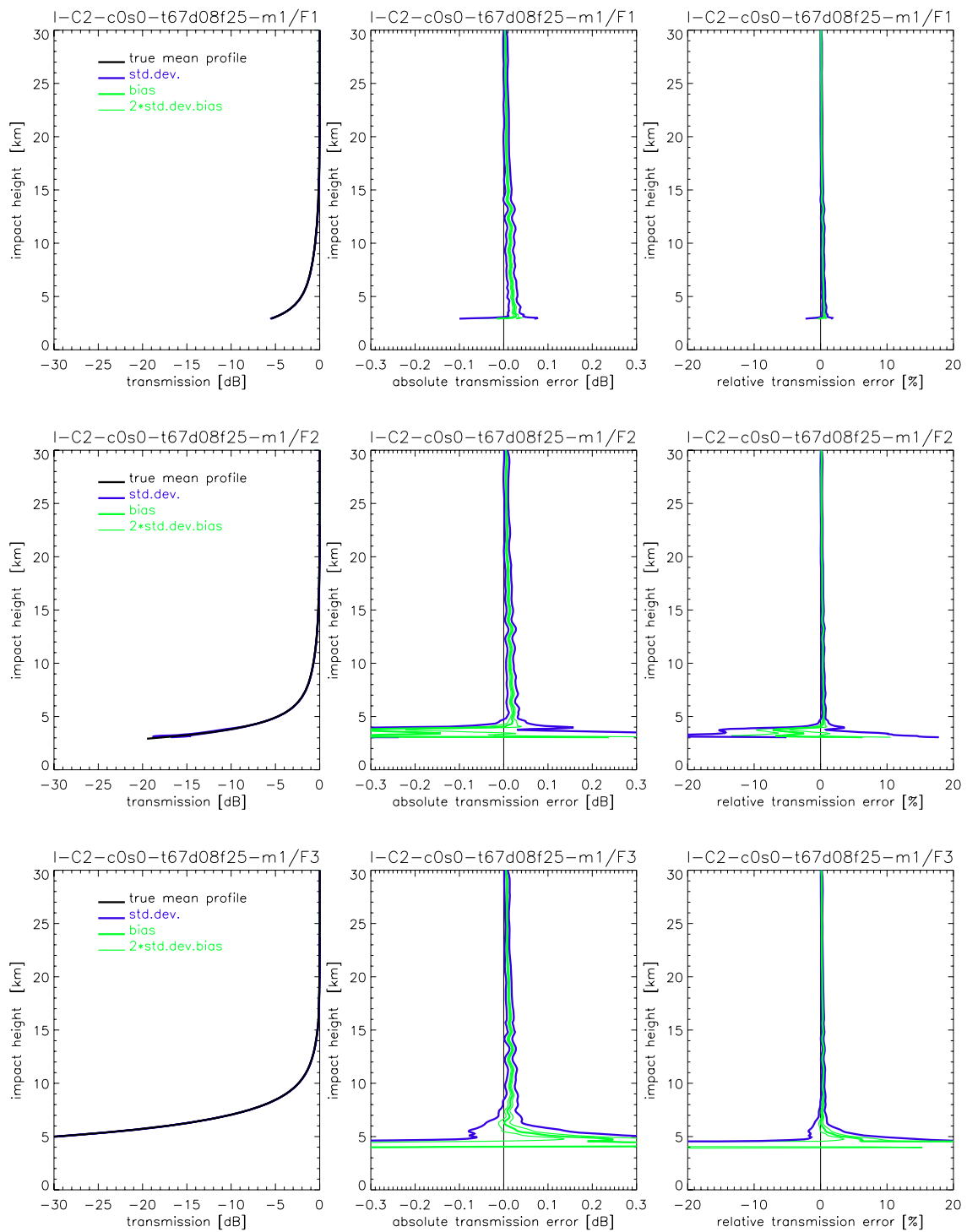


Fig. 3.1.21. Transmission retrieval results for the ACE+ frequencies F1 = 9.7 GHz (top panels), F2 = 17.25 GHz (middle panels), and F3 = 22.6 GHz (bottom panels) for the mid-lat summer case (C2), instrumental errors (ine) scenario (therm. noise, C/No 67 dBHz, ampl. drift 0.62%/20sec, 1/f noise 0.01*T%, T=1-20sec). Statistics performance results (standard deviation, bias, 2 x std.deviation of bias) for an ensemble of 40 profiles are shown. The std.deviation is shown as +/- envelopes about the bias profile.

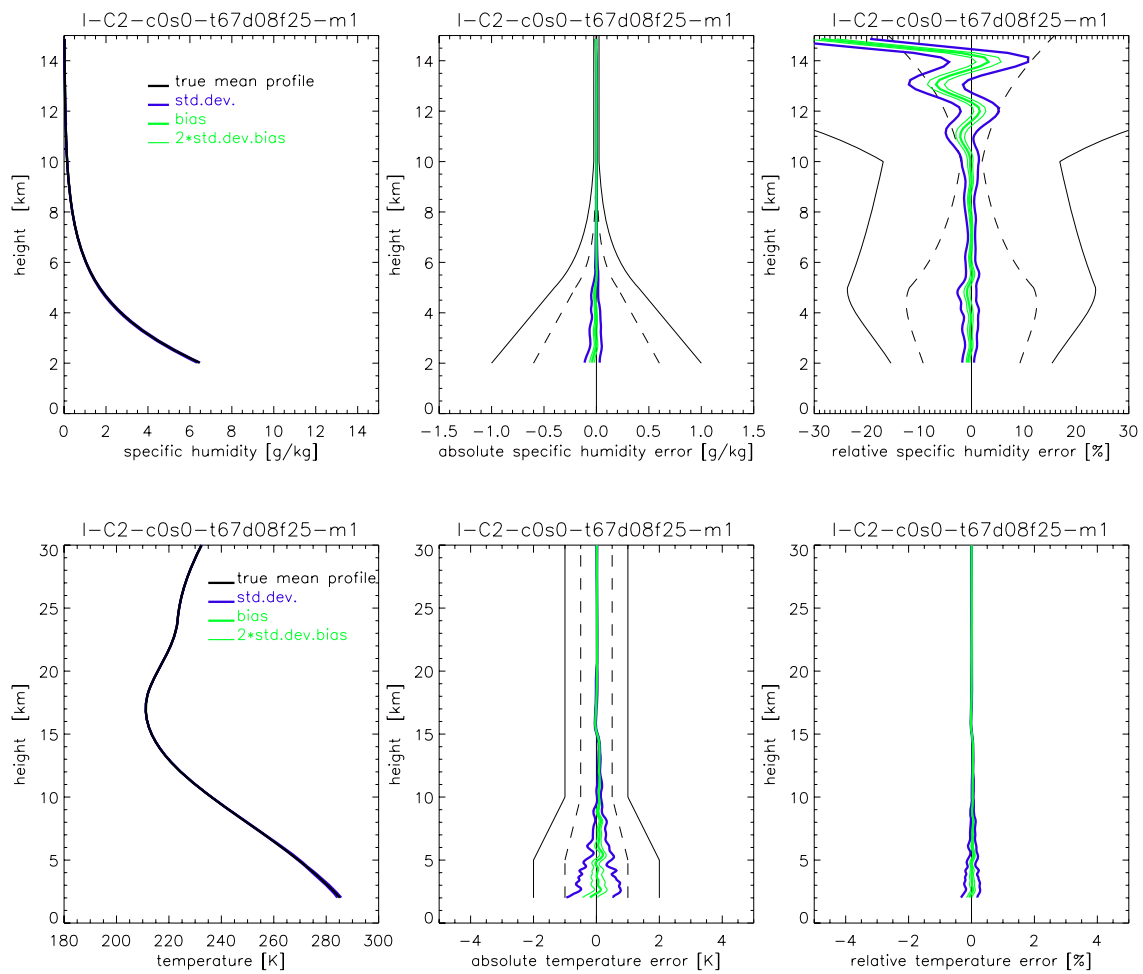


Fig. 3.1.22. Humidity (upper panels) and temperature (lower panels) retrieval results for the mid-lat summer case (C2), instrumental errors (ine) scenario (therm. noise, C/No 67 dBHz, ampl. drift 0.62%/20sec, 1/f noise 0.01*T%, T=1-20sec). Statistics performance results (standard deviation, bias, 2 x std.deviation of bias) for an ensemble of 40 profiles are shown. The std.deviation is shown as +/- envelopes about the bias profiles. In the middle panels (for humidity and temperature) and the right panel (for humidity) the observational requirements, as set by the ACE+ MRD (v2.1/Jan 2004), are shown for reference (solid black, threshold requirements; dashed black, target requirements).

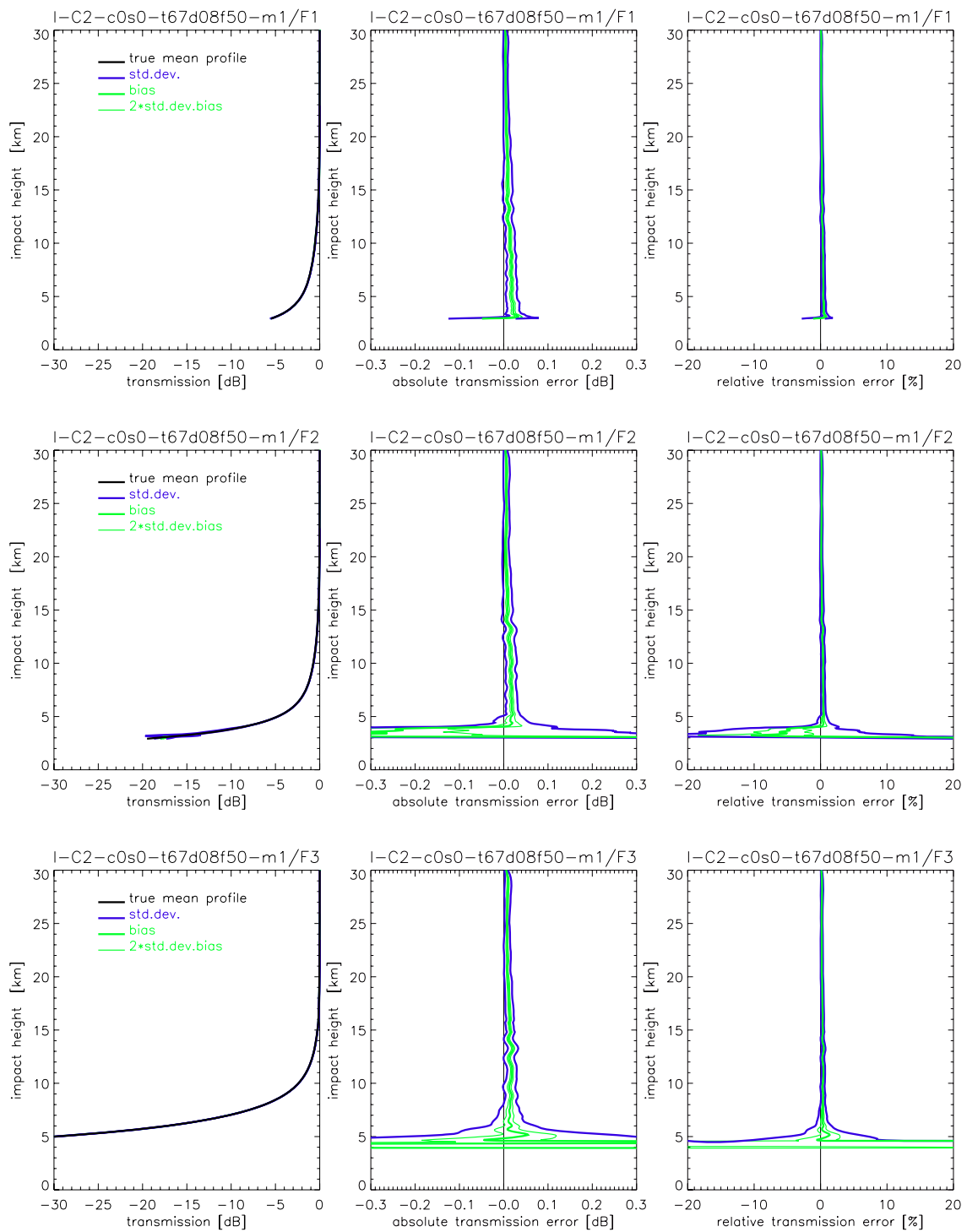


Fig. 3.1.23. Transmission retrieval results for the ACE+ frequencies F1 = 9.7 GHz (top panels), F2 = 17.25 GHz (middle panels), and F3 = 22.6 GHz (bottom panels) for the mid-lat summer case (C2), instrumental errors (ine) scenario (therm. noise, C/No 67 dBHz, ampl. drift 0.62%/20sec, 1/f noise 0.02*T%, T=1-20sec). Statistics performance results (standard deviation, bias, 2 x std.deviation of bias) for an ensemble of 40 profiles are shown. The std.deviation are shown as +/- envelopes about the bias profile.

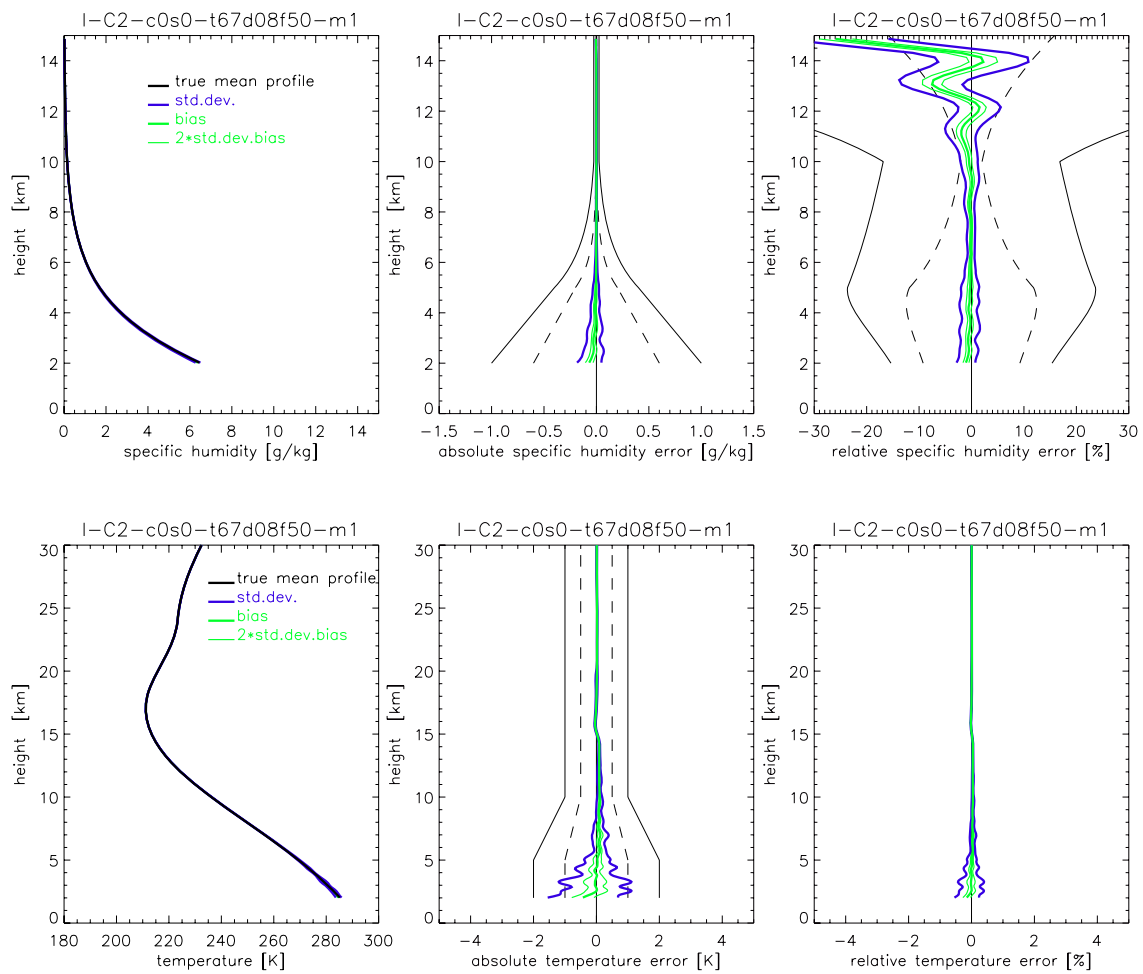


Fig. 3.1.24. Humidity (upper panels) and temperature (lower panels) retrieval results for the mid-lat summer case (C2), instrumental errors (ine) scenario (therm. noise, C/No 67 dBHz, ampl. drift 0.62%/20sec, 1/f noise 0.02*T%, T=1-20sec). Statistics performance results (standard deviation, bias, 2 x std.deviation of bias) for an ensemble of 40 profiles are shown. The std.deviation is shown as +/- envelopes about the bias profiles. In the middle panels (for humidity and temperature) and the right panel (for humidity) the observational requirements, as set by the ACE+ MRD (v2.1/Jan 2004), are shown for reference (solid black, threshold requirements; dashed black, target requirements).

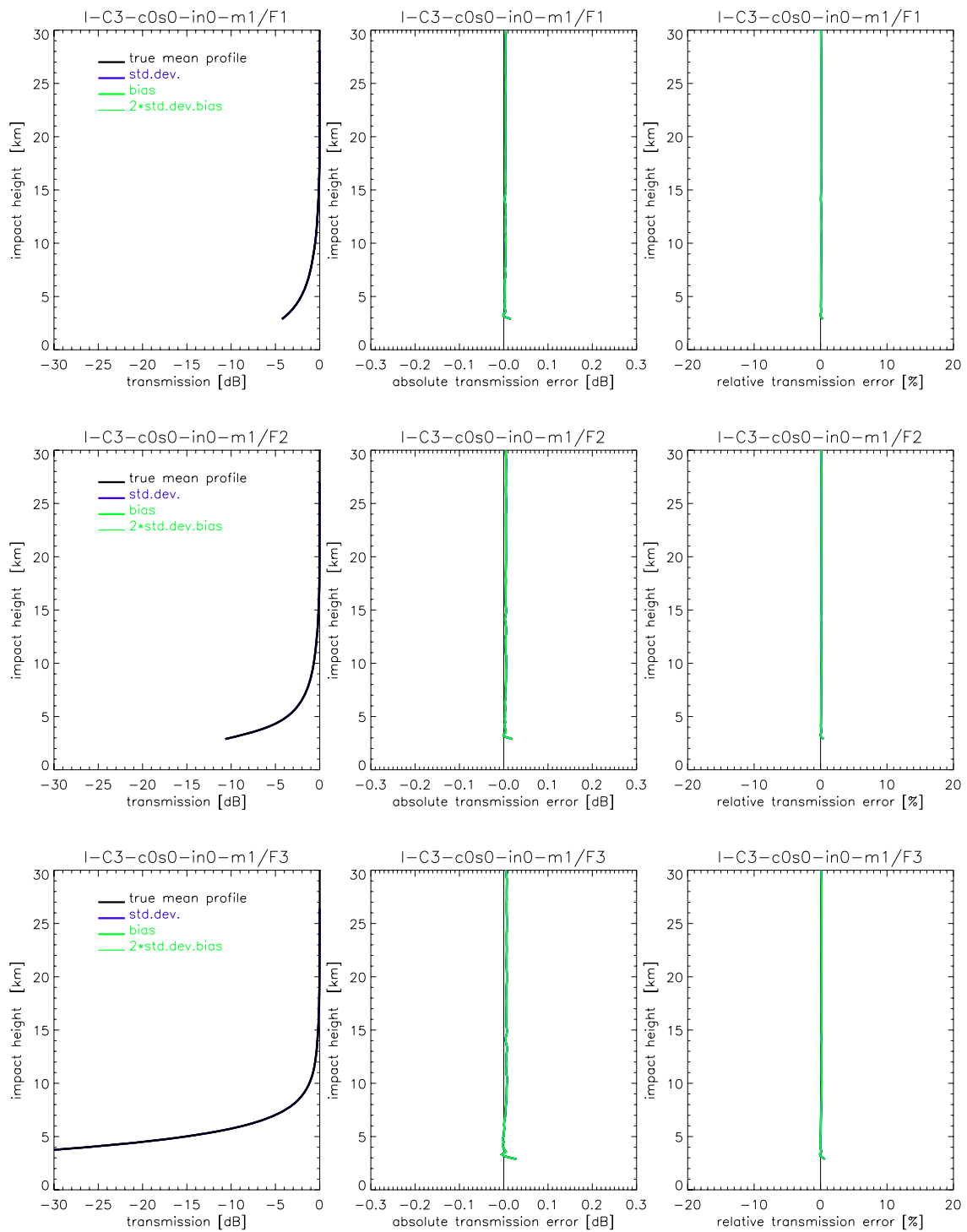


Fig. 3.1.25. Transmission retrieval results for the ACE+ frequencies F1 = 9.7 GHz (top panels), F2 = 17.25 GHz (middle panels), and F3 = 22.6 GHz (bottom panels) for the mid-lat winter case (C3), no instrumental errors (in0) scenario. Statistics performance results (standard deviation, bias, 2 x std.deviation of bias) for an ensemble of 40 profiles are shown. The std.deviation is shown as +/- envelopes about the bias profile.

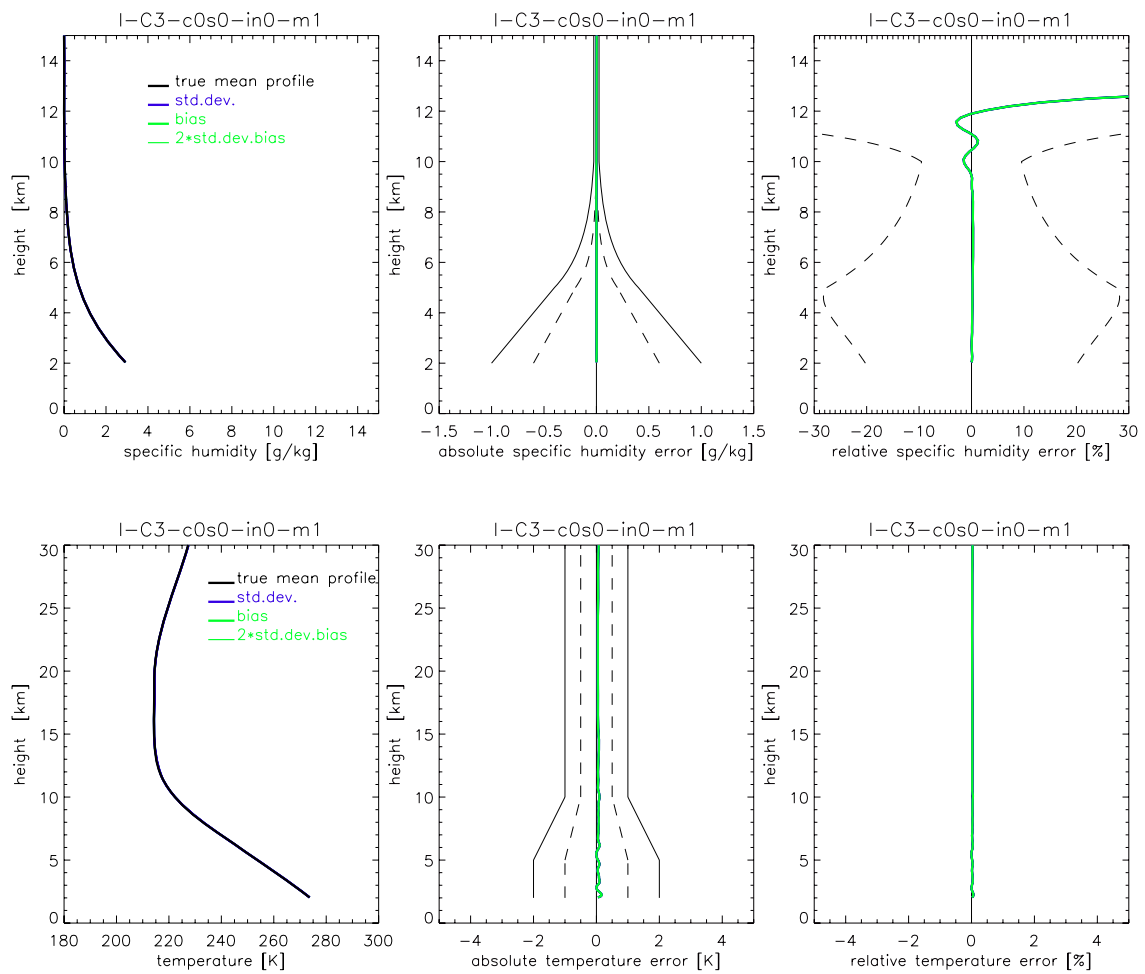


Fig. 3.1.26. Humidity (upper panels) and temperature (lower panels) retrieval results for the mid-lat winter case (C3), no instrumental errors (in0) scenario. Statistics performance results (standard deviation, bias, 2 x std.deviation of bias) for an ensemble of 40 profiles are shown. The std.deviation is shown as +/- envelopes about the bias profiles. In the middle panels (for humidity and temperature) and the right panel (for humidity) the observational requirements, as set by the ACE+ MRD (v2.1/Jan 2004), are shown for reference (solid black, threshold requirements; dashed black, target requirements).

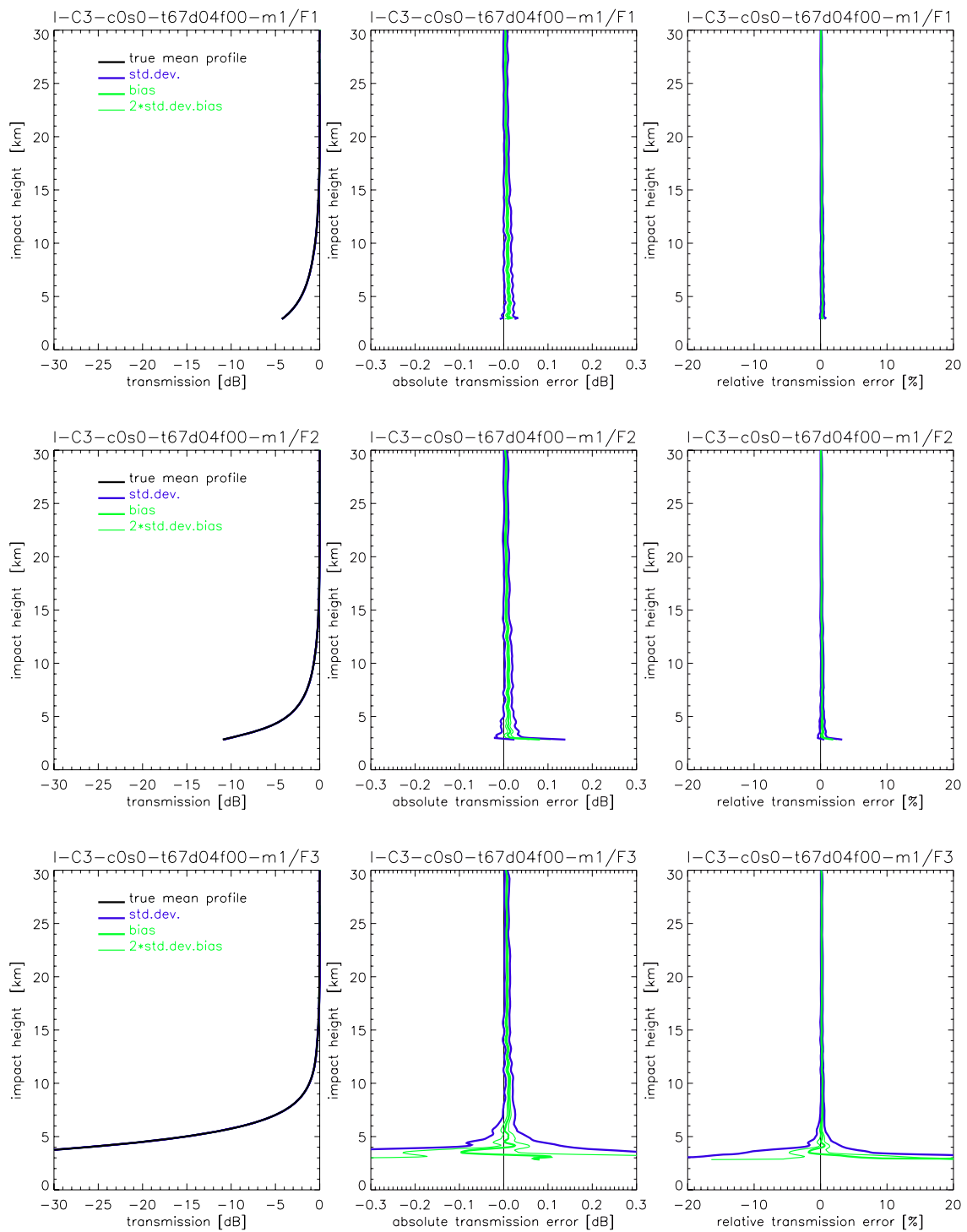


Fig. 3.1.27. Transmission retrieval results for the ACE+ frequencies F1 = 9.7 GHz (top panels), F2 = 17.25 GHz (middle panels), and F3 = 22.6 GHz (bottom panels) for the mid-lat winter case (C3), instrumental errors (ine) scenario (therm. noise, C/No 67 dBHz, ampl. drift 0.33%/20sec, no 1/f noise). Statistics performance results (standard deviation, bias, 2 x std.deviation of bias) for an ensemble of 40 profiles are shown. The std.deviation are shown as +/- envelopes about the bias profile.

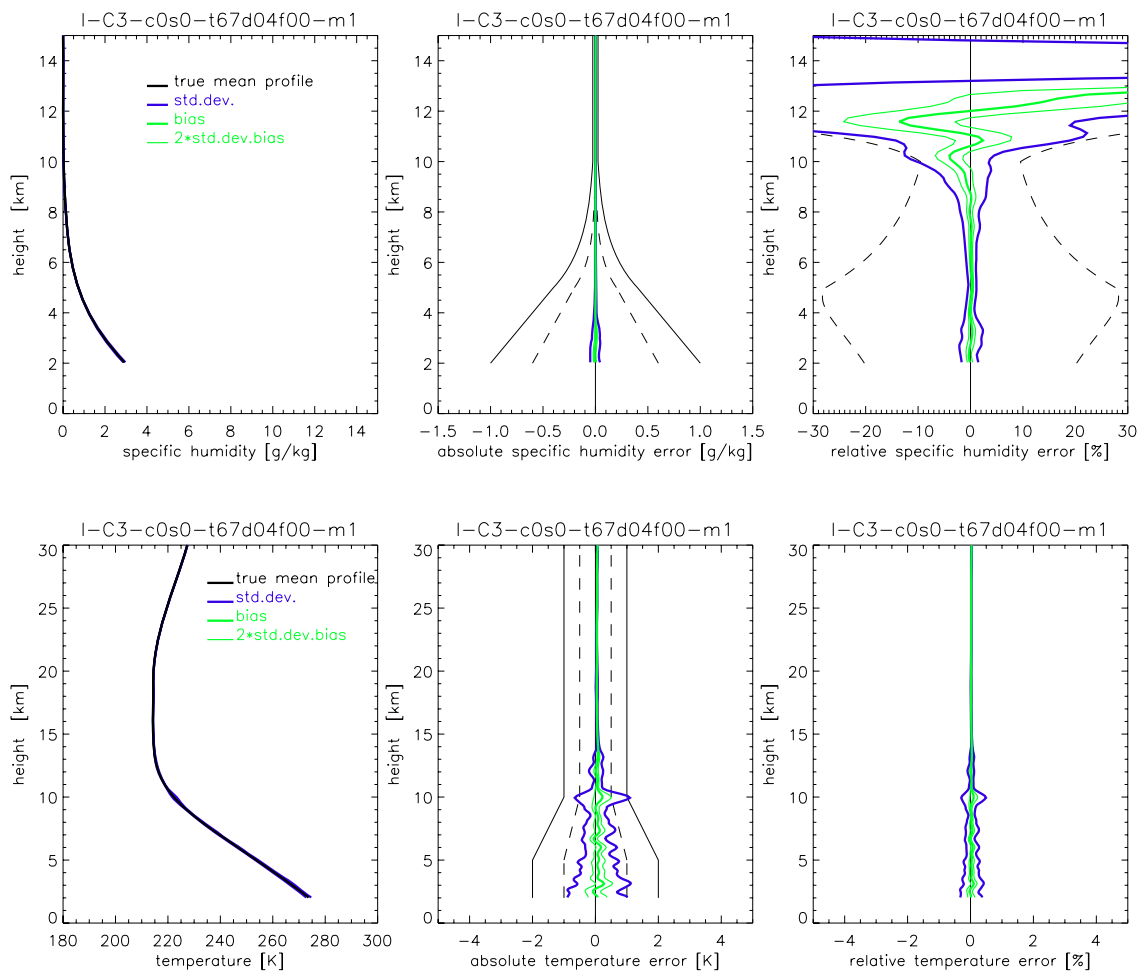


Fig. 3.1.28. Humidity (upper panels) and temperature (lower panels) retrieval results for the mid-lat winter case (C3), instrumental errors (ine) scenario (therm. noise, C/No 67 dBHz, ampl. drift 0.33%/20sec, no 1/f noise). Statistics performance results (standard deviation, bias, 2 x std.deviation of bias) for an ensemble of 40 profiles are shown. The std.deviation is shown as +/- envelopes about the bias profiles. In the middle panels (for humidity and temperature) and the right panel (for humidity) the observational requirements, as set by the ACE+ MRD (v2.1/Jan 2004), are shown for reference (solid black, threshold requirements; dashed black, target requirements).

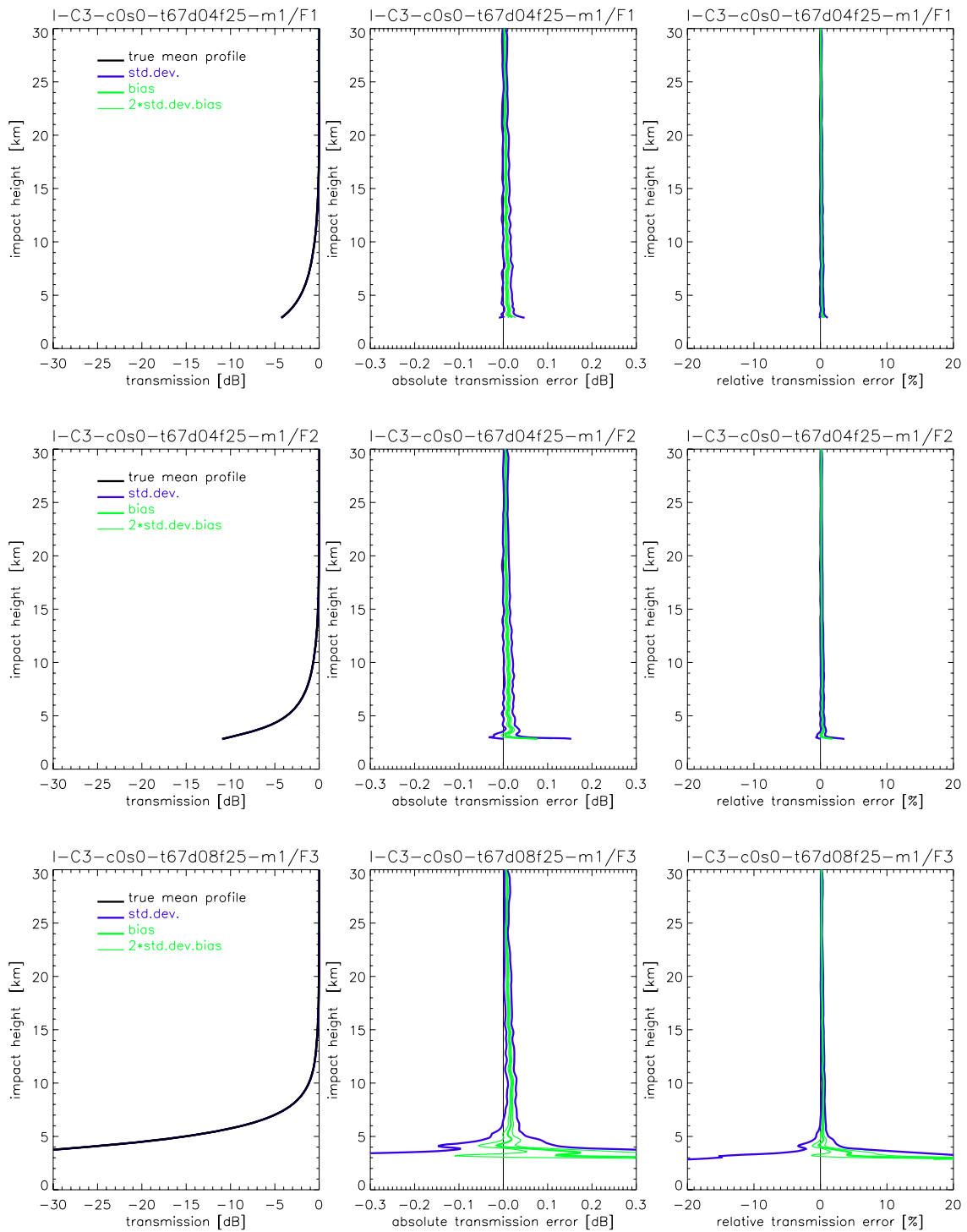


Fig. 3.1.29. Transmission retrieval results for the ACE+ frequencies F1 = 9.7 GHz (top panels), F2 = 17.25 GHz (middle panels), and F3 = 22.6 GHz (bottom panels) for the mid-lat winter case (C3), instrumental errors (ine) scenario (therm. noise, C/No 67 dBHz, ampl. drift 0.33%/20sec, 1/f noise 0.01*T%, T=1-20sec). Statistics performance results (standard deviation, bias, 2 x std.deviation of bias) for an ensemble of 40 profiles are shown. The std.deviation is shown as +/- envelopes about the bias profile.

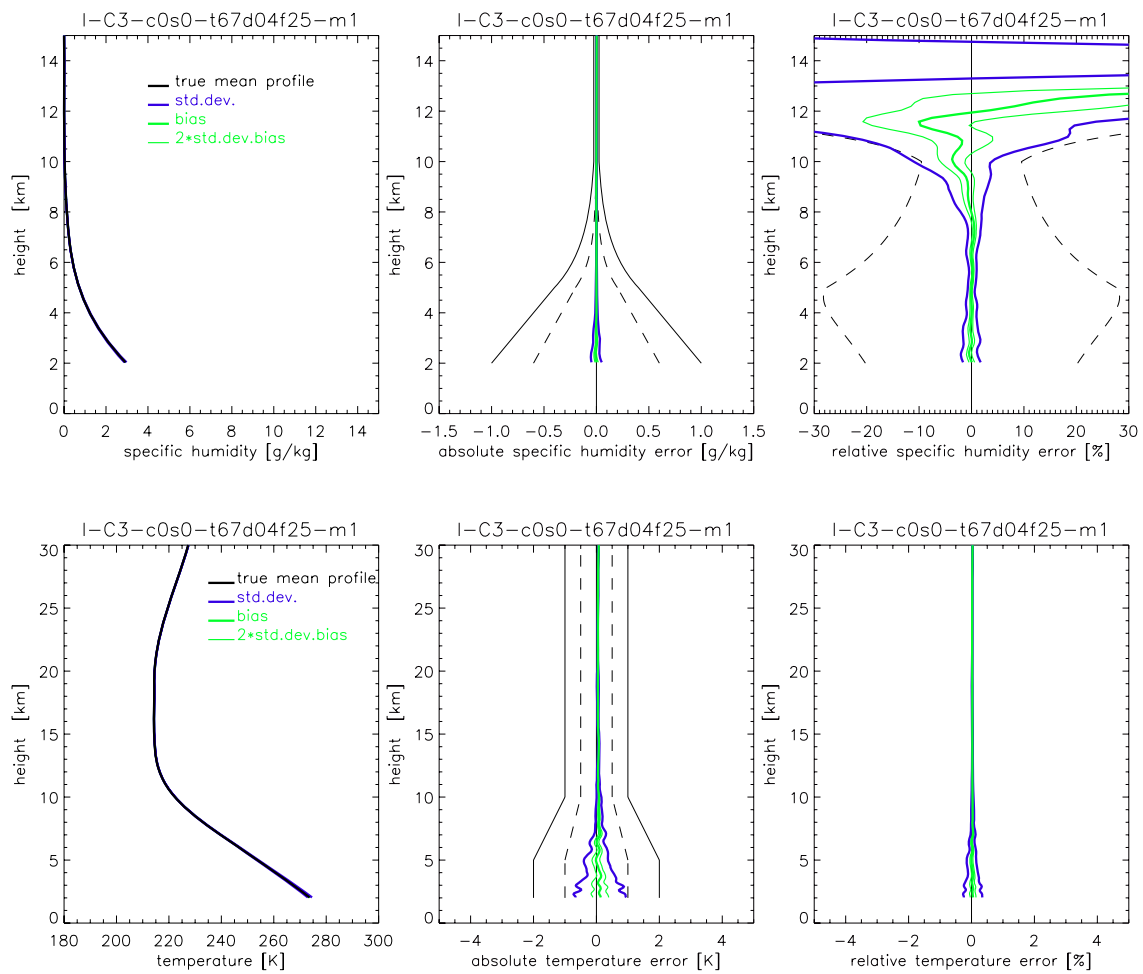


Fig. 3.1.30. Humidity (upper panels) and temperature (lower panels) retrieval results for the mid-lat winter case (C3), instrumental errors (ine) scenario (therm. noise, C/No 67 dBHz, ampl. drift 0.33%/20sec, 1/f noise 0.01*T%, T=1-20sec). Statistics performance results (standard deviation, bias, 2 x std.deviation of bias) for an ensemble of 40 profiles are shown. The std.deviation is shown as +/- envelopes about the bias profiles. In the middle panels (for humidity and temperature) and the right panel (for humidity) the observational requirements, as set by the ACE+ MRD (v2.1/Jan 2004), are shown for reference (solid black, threshold requirements; dashed black, target requirements).

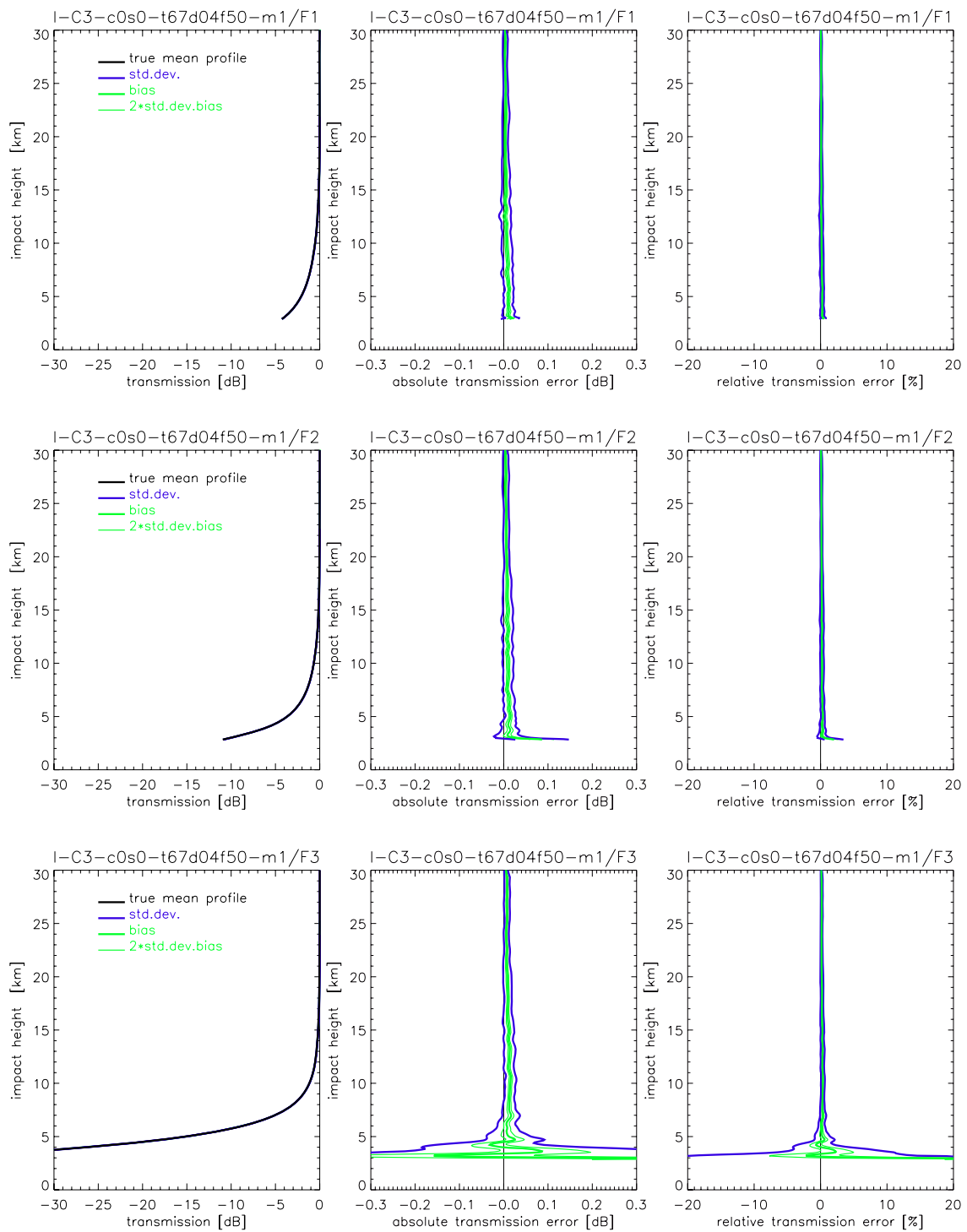


Fig. 3.1.31. Transmission retrieval results for the ACE+ frequencies F1 = 9.7 GHz (top panels), F2 = 17.25 GHz (middle panels), and F3 = 22.6 GHz (bottom panels) for the mid-lat winter case (C3), instrumental errors (ine) scenario (therm. noise, C/No 67 dBHz, ampl. drift 0.33%/20sec, 1/f noise 0.02*T%, T=1-20sec). Statistics performance results (standard deviation, bias, 2 x std.deviation of bias) for an ensemble of 40 profiles are shown. The std.deviation is shown as +/- envelopes about the bias profile.

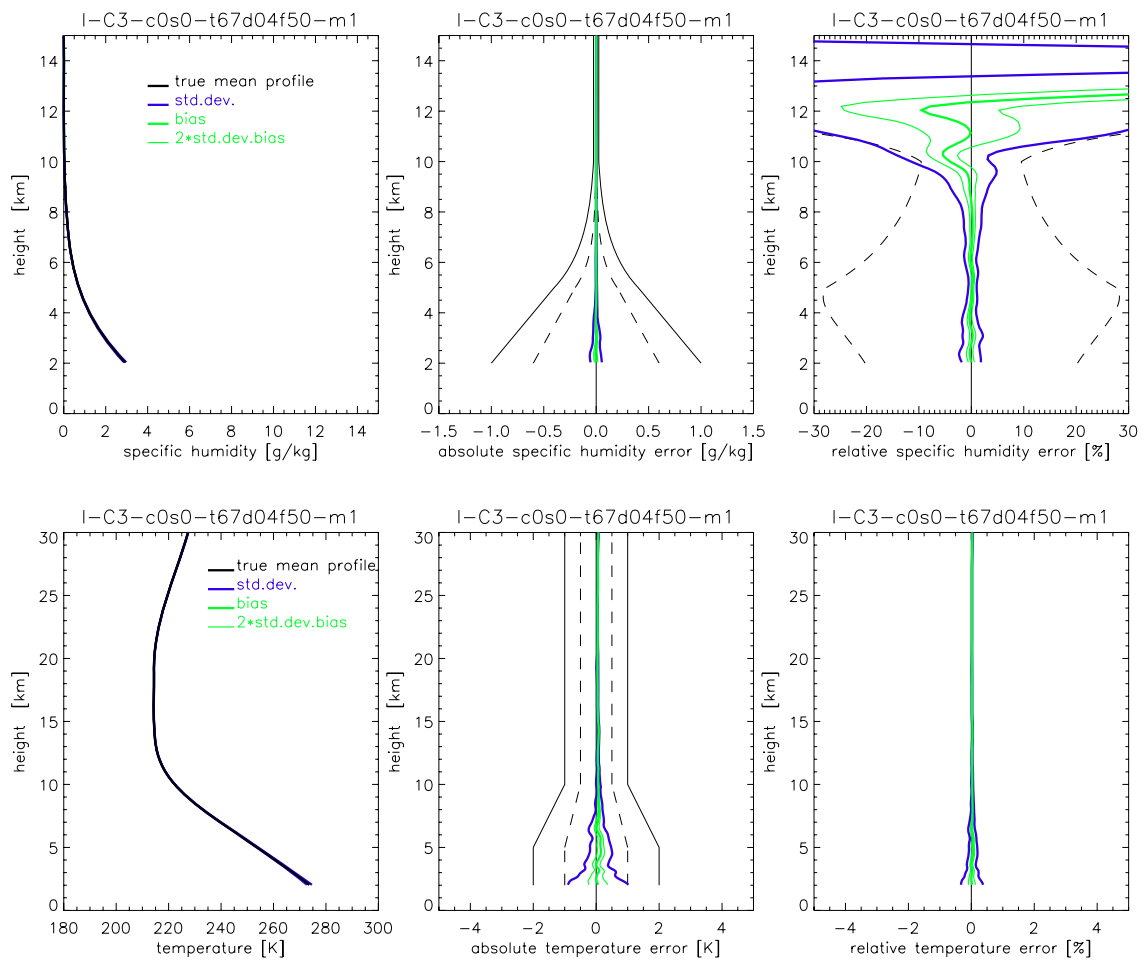


Fig. 3.1.32. Humidity (upper panels) and temperature (lower panels) retrieval results for the mid-lat winter case (C3), instrumental errors (ine) scenario (therm. noise, C/No 67 dBHz, ampl. drift 0.33%/20sec, 1/f noise 0.02*T%, T=1-20sec). Statistics performance results (standard deviation, bias, 2 x std.deviation of bias) for an ensemble of 40 profiles are shown. The std.deviations are shown as +/- envelopes about the bias profiles. In the middle panels (for humidity and temperature) and the right panel (for humidity) the observational requirements, as set by the ACE+ MRD (v2.1/Jan 2004), are shown for reference (solid black, threshold requirements; dashed black, target requirements).

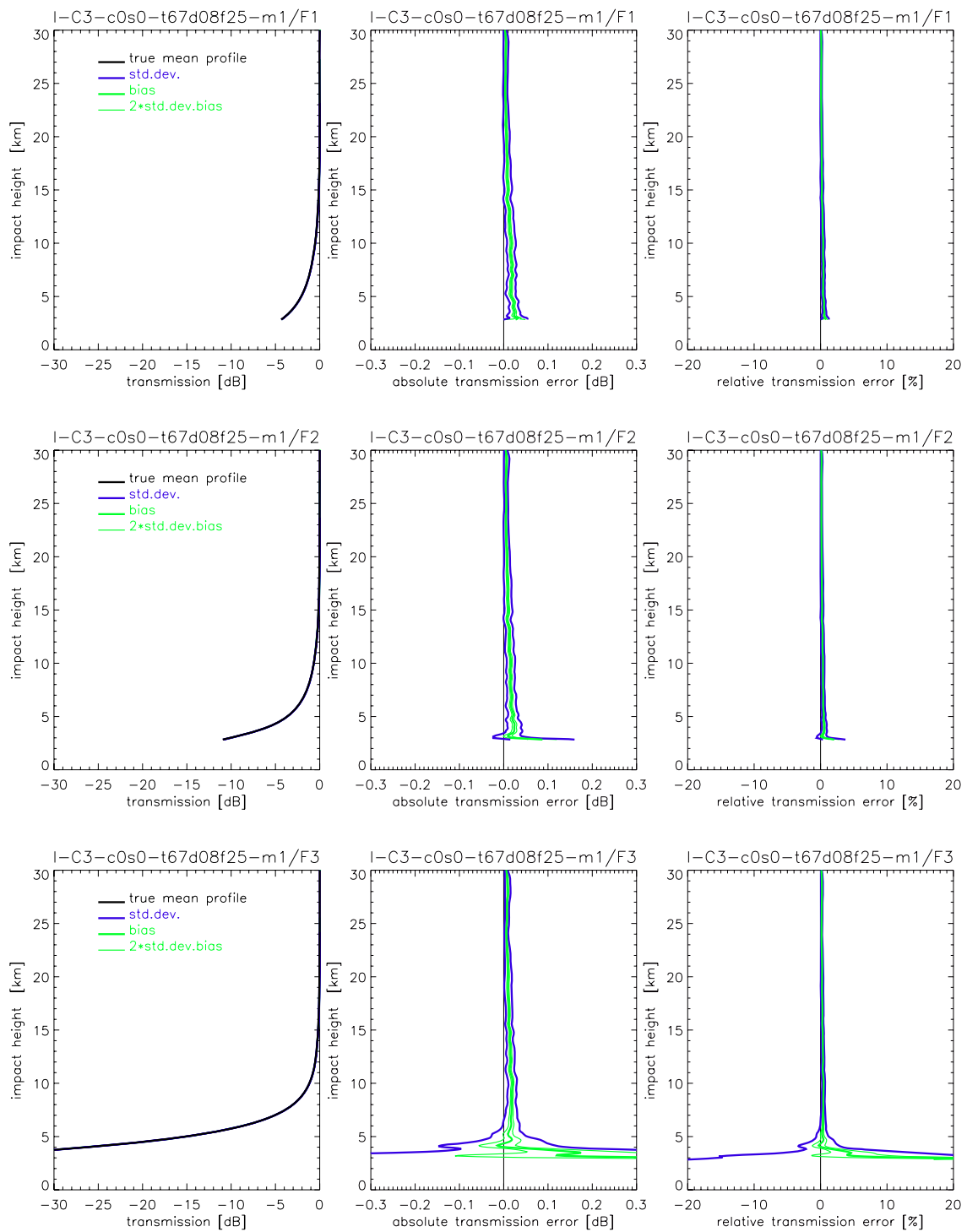


Fig. 3.1.33. Transmission retrieval results for the ACE+ frequencies F1 = 9.7 GHz (top panels), F2 = 17.25 GHz (middle panels), and F3 = 22.6 GHz (bottom panels) for the mid-lat winter case (C3), instrumental errors (ine) scenario (therm. noise, C/No 67 dBHz, ampl. drift 0.62%/20sec, 1/f noise 0.01*T%, T=1-20sec). Statistics performance results (standard deviation, bias, 2 x std.deviation of bias) for an ensemble of 40 profiles are shown. The std.deviation is shown as +/- envelopes about the bias profile.

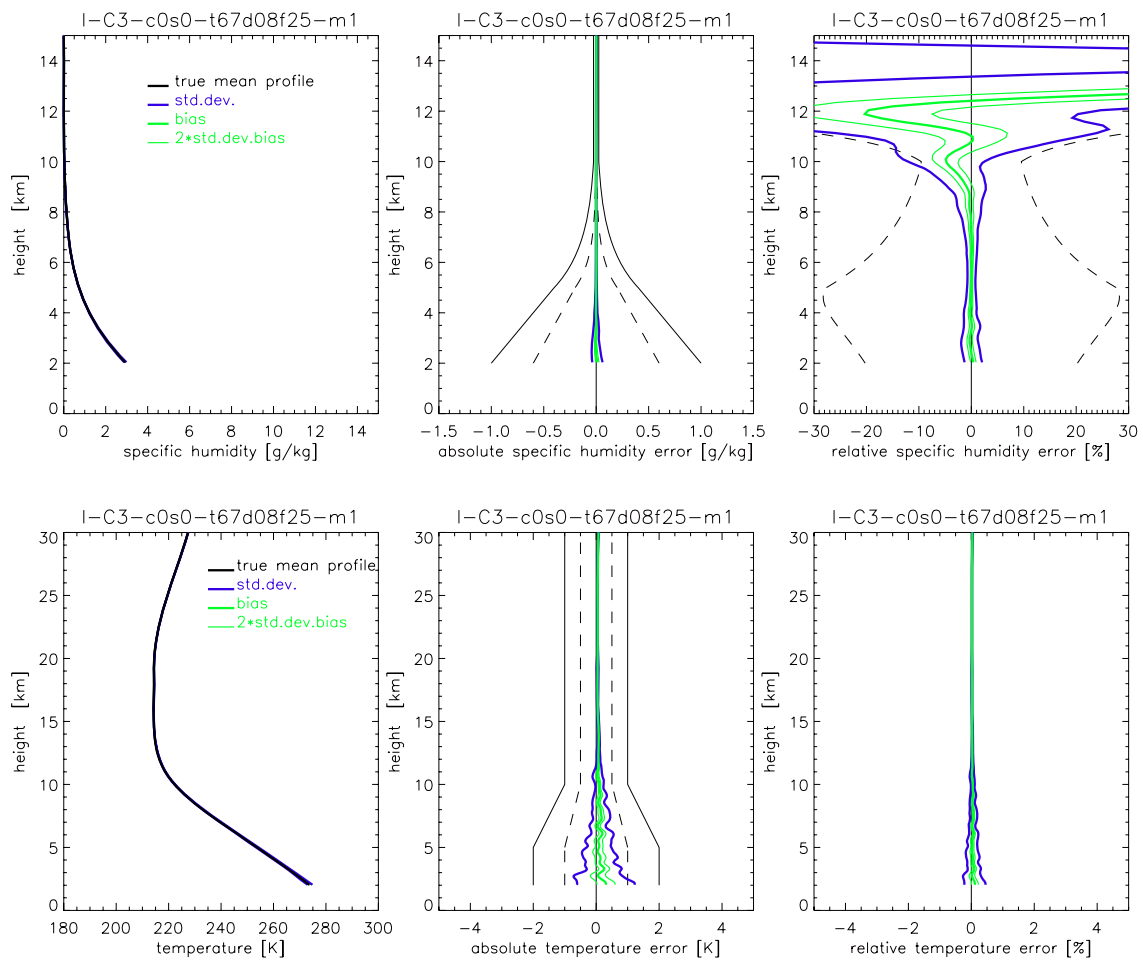


Fig. 3.1.34. Humidity (upper panels) and temperature (lower panels) retrieval results for the mid-lat winter case (C3), instrumental errors (ine) scenario (therm. noise, C/No 67 dBHz, ampl. drift 0.62%/20sec, 1/f noise 0.01*T%, T=1-20sec). Statistics performance results (standard deviation, bias, 2 x std.deviation of bias) for an ensemble of 40 profiles are shown. The std.deviation is shown as +/- envelopes about the bias profiles. In the middle panels (for humidity and temperature) and the right panel (for humidity) the observational requirements, as set by the ACE+ MRD (v2.1/Jan 2004), are shown for reference (solid black, threshold requirements; dashed black, target requirements).

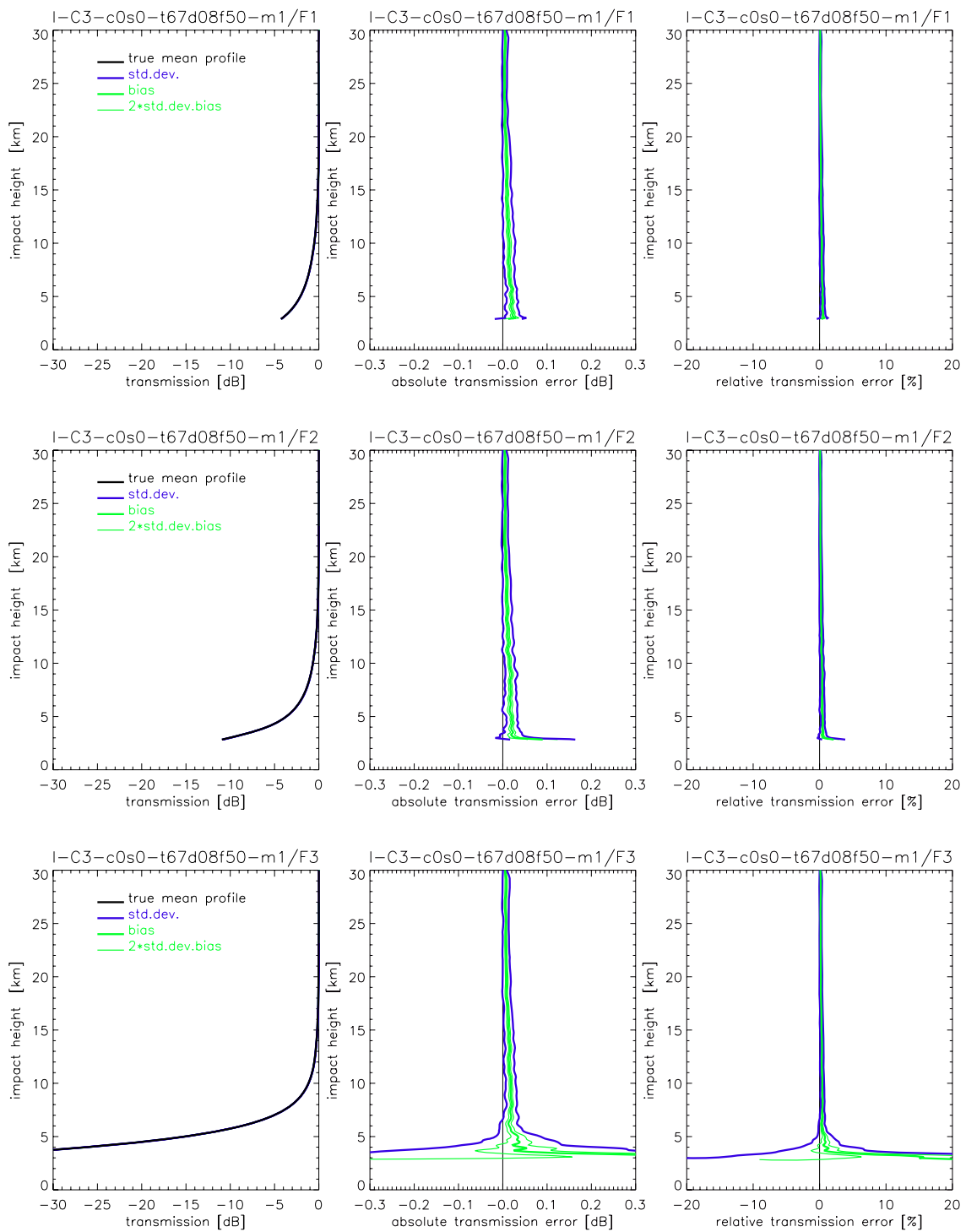


Fig. 3.1.35. Transmission retrieval results for the ACE+ frequencies F1 = 9.7 GHz (top panels), F2 = 17.25 GHz (middle panels), and F3 = 22.6 GHz (bottom panels) for the mid-lat winter case (C3), instrumental errors (ine) scenario (therm. noise, C/No 67 dBHz, ampl. drift 0.62%/20sec, 1/f noise 0.02*T%, T=1-20sec). Statistics performance results (standard deviation, bias, 2 x std.deviation of bias) for an ensemble of 40 profiles are shown. The std.deviation is shown as +/- envelopes about the bias profile.

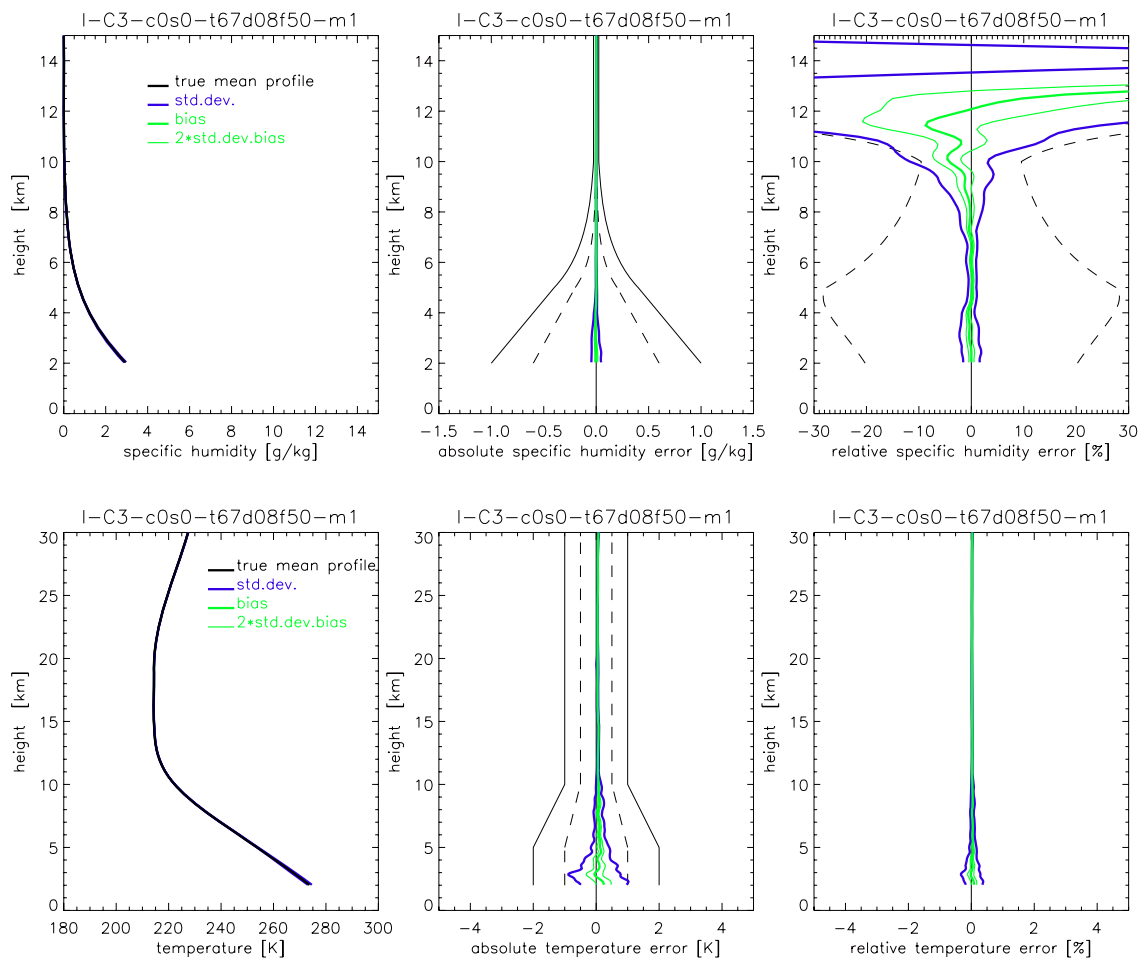


Fig. 3.1.36. Humidity (upper panels) and temperature (lower panels) retrieval results for the mid-lat winter case (C3), instrumental errors (ine) scenario (therm. noise, C/No 67 dBHz, ampl. drift 0.62%/20sec, 1/f noise 0.02*T%, T=1-20sec). Statistics performance results (standard deviation, bias, 2 x std.deviation of bias) for an ensemble of 40 profiles are shown. The std.deviation is shown as +/- envelopes about the bias profiles. In the middle panels (for humidity and temperature) and the right panel (for humidity) the observational requirements, as set by the ACE+ MRD (v2.1/Jan 2004), are shown for reference (solid black, threshold requirements; dashed black, target requirements).

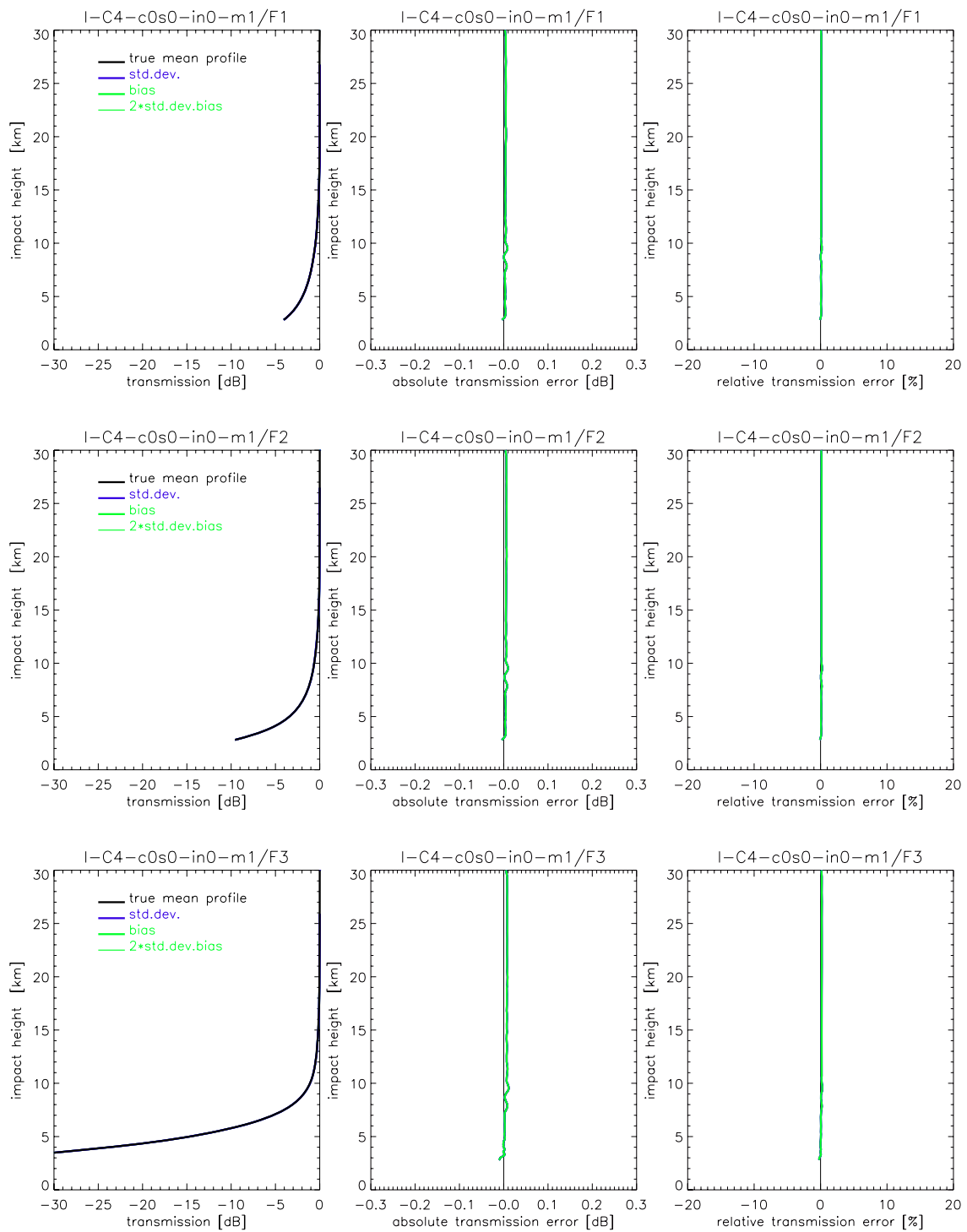


Fig. 3.1.37. Transmission retrieval results for the ACE+ frequencies F1 = 9.7 GHz (top panels), F2 = 17.25 GHz (middle panels), and F3 = 22.6 GHz (bottom panels) for the high-lat summer case (C4), no instrumental errors (in0) scenario. Statistics performance results (standard deviation, bias, 2 x std.deviation of bias) for an ensemble of 40 profiles are shown. The std.deviation is shown as +/- envelopes about the bias profile.

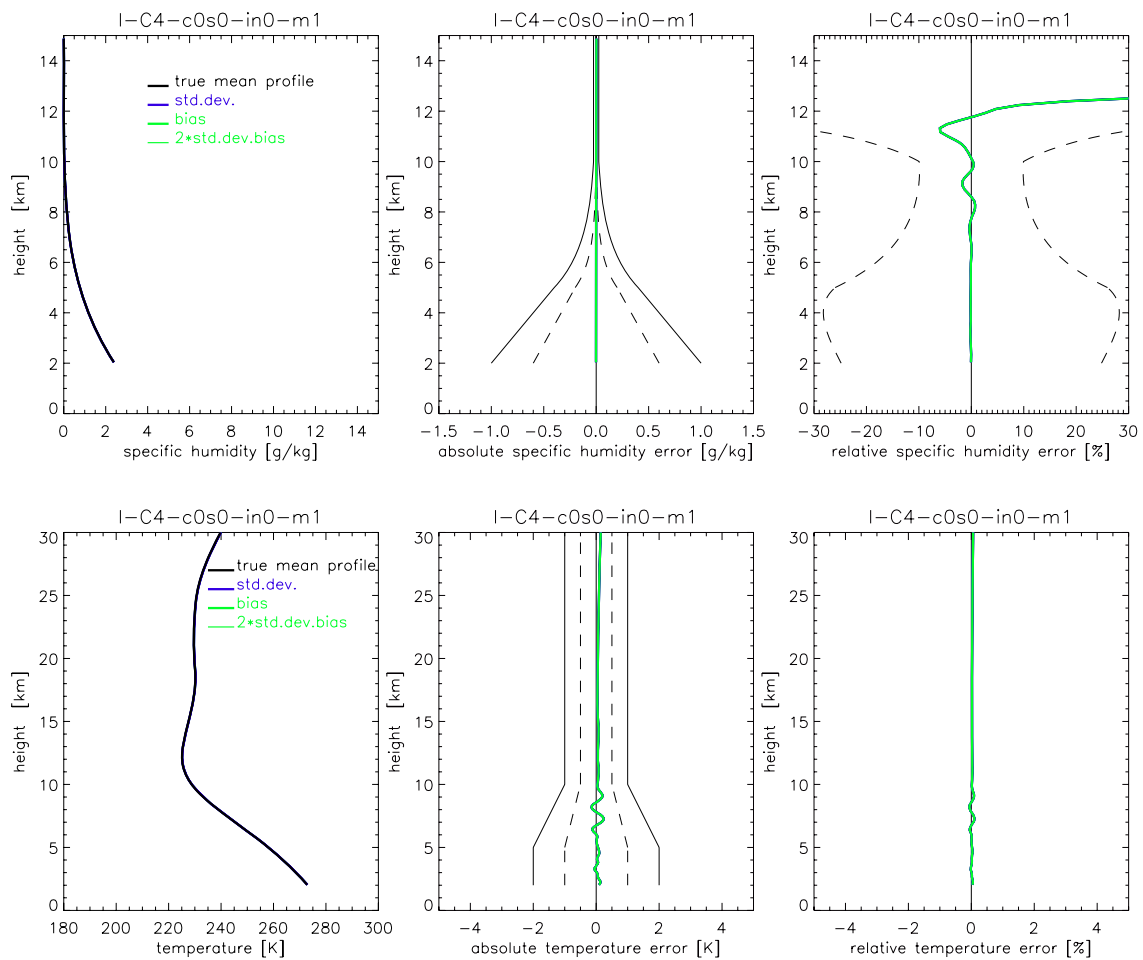


Fig. 3.1.38. Humidity (upper panels) and temperature (lower panels) retrieval results for the high-lat summer case (C4), no instrumental errors (in0) scenario. Statistics performance results (standard deviation, bias, 2 x std.deviation of bias) for an ensemble of 40 profiles are shown. The std.deviation is shown as +/- envelopes about the bias profiles. In the middle panels (for humidity and temperature) and the right panel (for humidity) the observational requirements, as set by the ACE+ MRD (v2.1/Jan 2004), are shown for reference (solid black, threshold requirements; dashed black, target requirements).

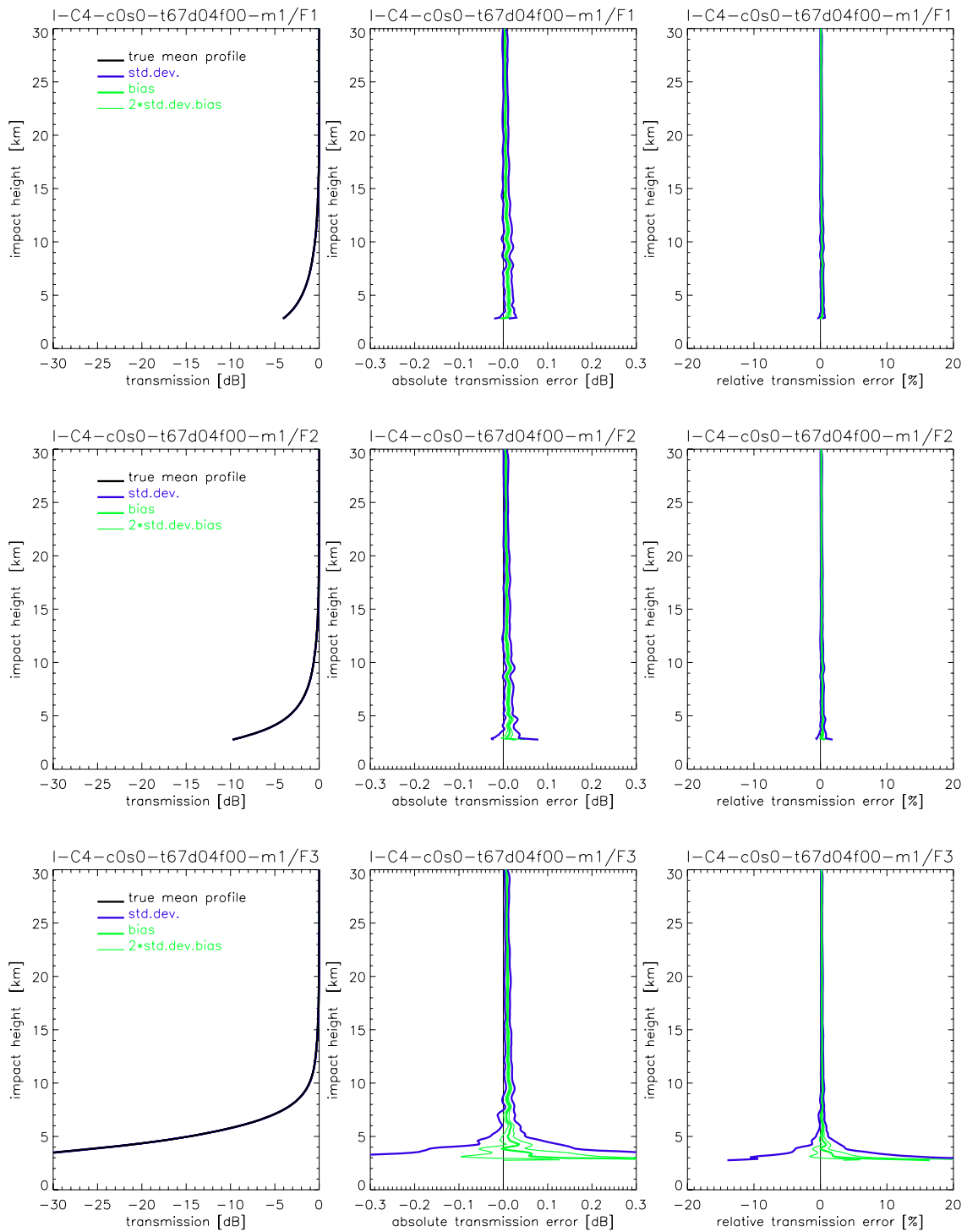


Fig. 3.1.39. Transmission retrieval results for the ACE+ frequencies F1 = 9.7 GHz (top panels), F2 = 17.25 GHz (middle panels), and F3 = 22.6 GHz (bottom panels) for the high-lat summer case (C4), instrumental errors (ine) scenario (therm. noise, C/No 67 dBHz, ampl. drift 0.33%/20sec, no 1/f noise). Statistics performance results (standard deviation, bias, 2 x std.deviation of bias) for an ensemble of 40 profiles are shown. The std.deviation are shown as +/- envelopes about the bias profile.

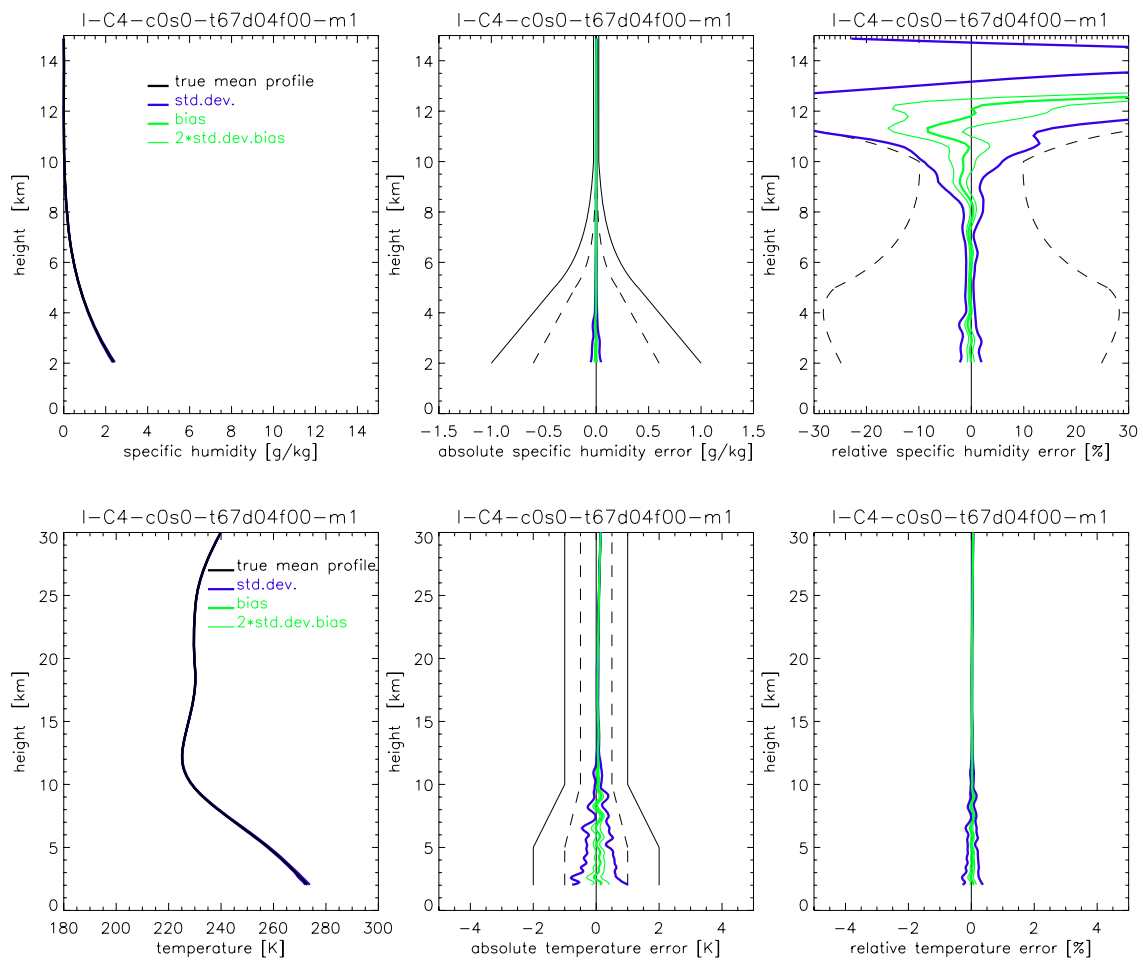


Fig. 3.1.40. Humidity (upper panels) and temperature (lower panels) retrieval results for the high-lat summer case (C4), instrumental errors (ine) scenario (therm. noise, C/No 67 dBHz, ampl. drift 0.33%/20sec, no 1/f noise). Statistics performance results (standard deviation, bias, 2 x std.deviation of bias) for an ensemble of 40 profiles are shown. The std.deviation is shown as +/- envelopes about the bias profiles. In the middle panels (for humidity and temperature) and the right panel (for humidity) the observational requirements, as set by the ACE+ MRD (v2.1/Jan 2004), are shown for reference (solid black, threshold requirements; dashed black, target requirements).

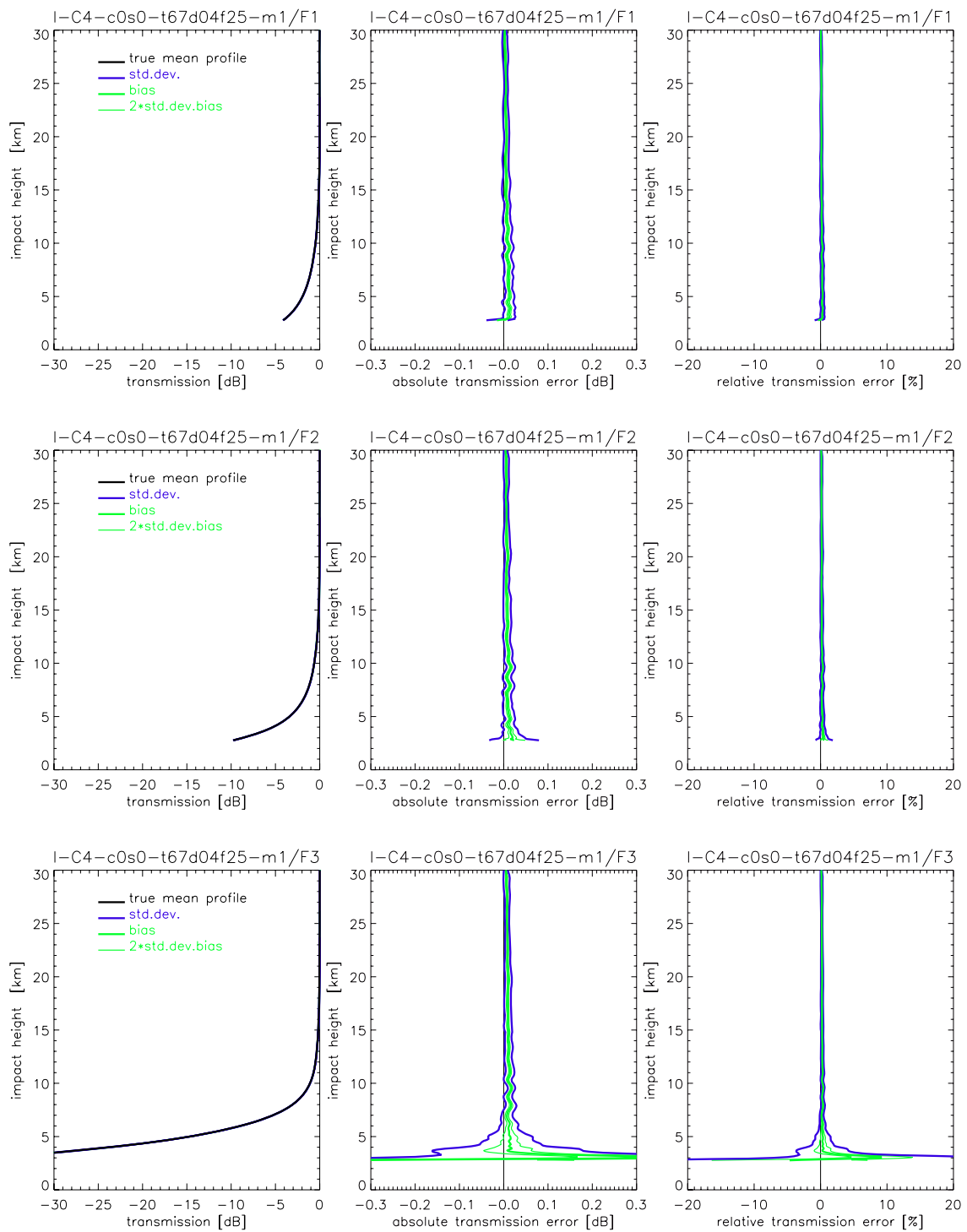


Fig. 3.1.41. Transmission retrieval results for the ACE+ frequencies F1 = 9.7 GHz (top panels), F2 = 17.25 GHz (middle panels), and F3 = 22.6 GHz (bottom panels) for the high-lat summer case (C4), instrumental errors (ine) scenario (therm. noise, C/No 67 dBHz, ampl. drift 0.33%/20sec, 1/f noise 0.01*T%, T=1-20sec). Statistics performance results (standard deviation, bias, 2 x std.deviation of bias) for an ensemble of 40 profiles are shown. The std.deviation is shown as +/- envelopes about the bias profile.

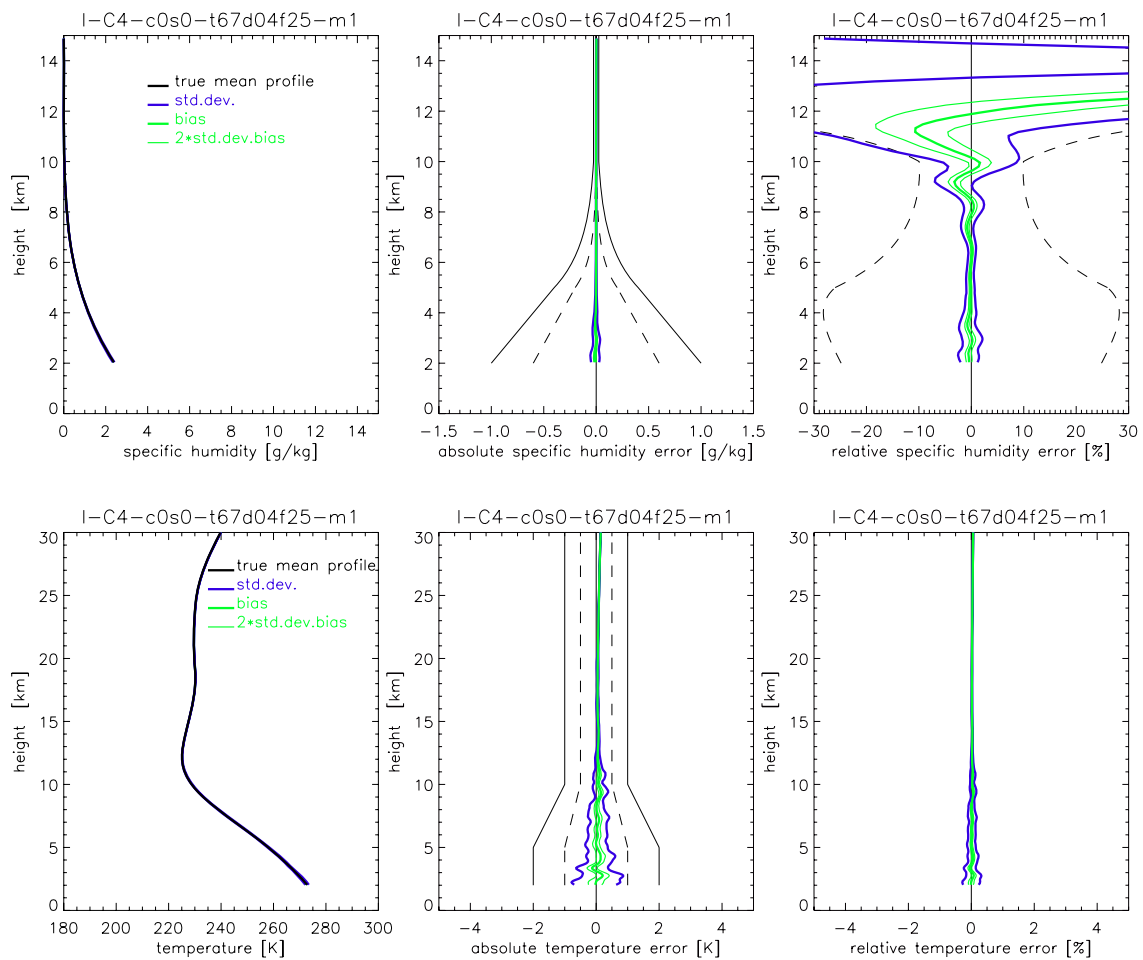


Fig. 3.1.42. Humidity (upper panels) and temperature (lower panels) retrieval results for the high-lat summer case (C4), instrumental errors (ine) scenario (therm. noise, C/No 67 dBHz, ampl. drift 0.33%/20sec, 1/f noise 0.01*T%, T=1-20sec). Statistics performance results (standard deviation, bias, 2 x std.deviation of bias) for an ensemble of 40 profiles are shown. The std.deviation is shown as +/- envelopes about the bias profiles. In the middle panels (for humidity and temperature) and the right panel (for humidity) the observational requirements, as set by the ACE+ MRD (v2.1/Jan 2004), are shown for reference (solid black, threshold requirements; dashed black, target requirements).

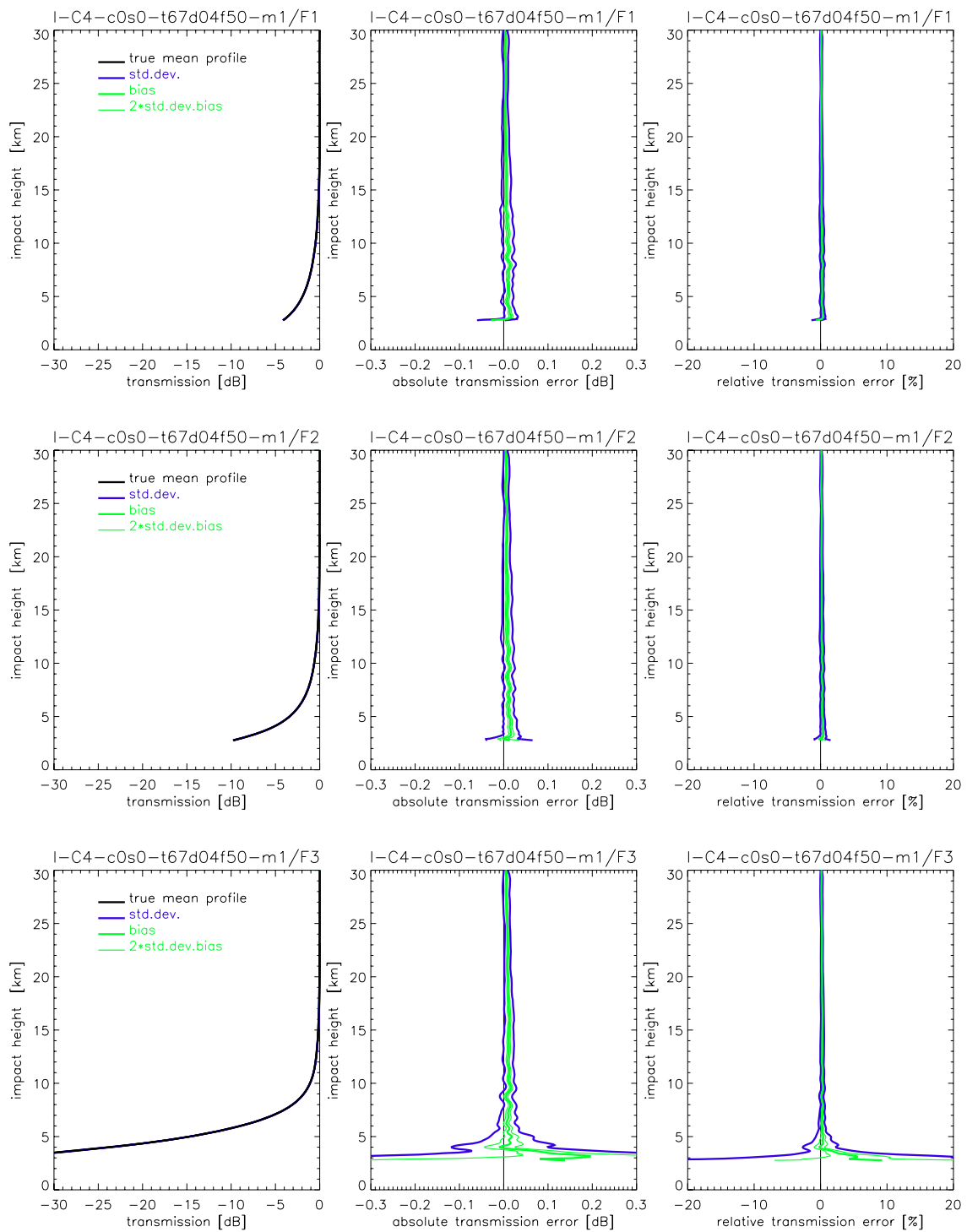


Fig. 3.1.43. Transmission retrieval results for the ACE+ frequencies F1 = 9.7 GHz (top panels), F2 = 17.25 GHz (middle panels), and F3 = 22.6 GHz (bottom panels) for the high-lat summer case (C4), instrumental errors (ine) scenario (therm. noise, C/No 67 dBHz, ampl. drift 0.33%/20sec, 1/f noise 0.02*T%, T=1-20sec). Statistics performance results (standard deviation, bias, 2 x std.deviation of bias) for an ensemble of 40 profiles are shown. The std.deviation is shown as +/- envelopes about the bias profile.

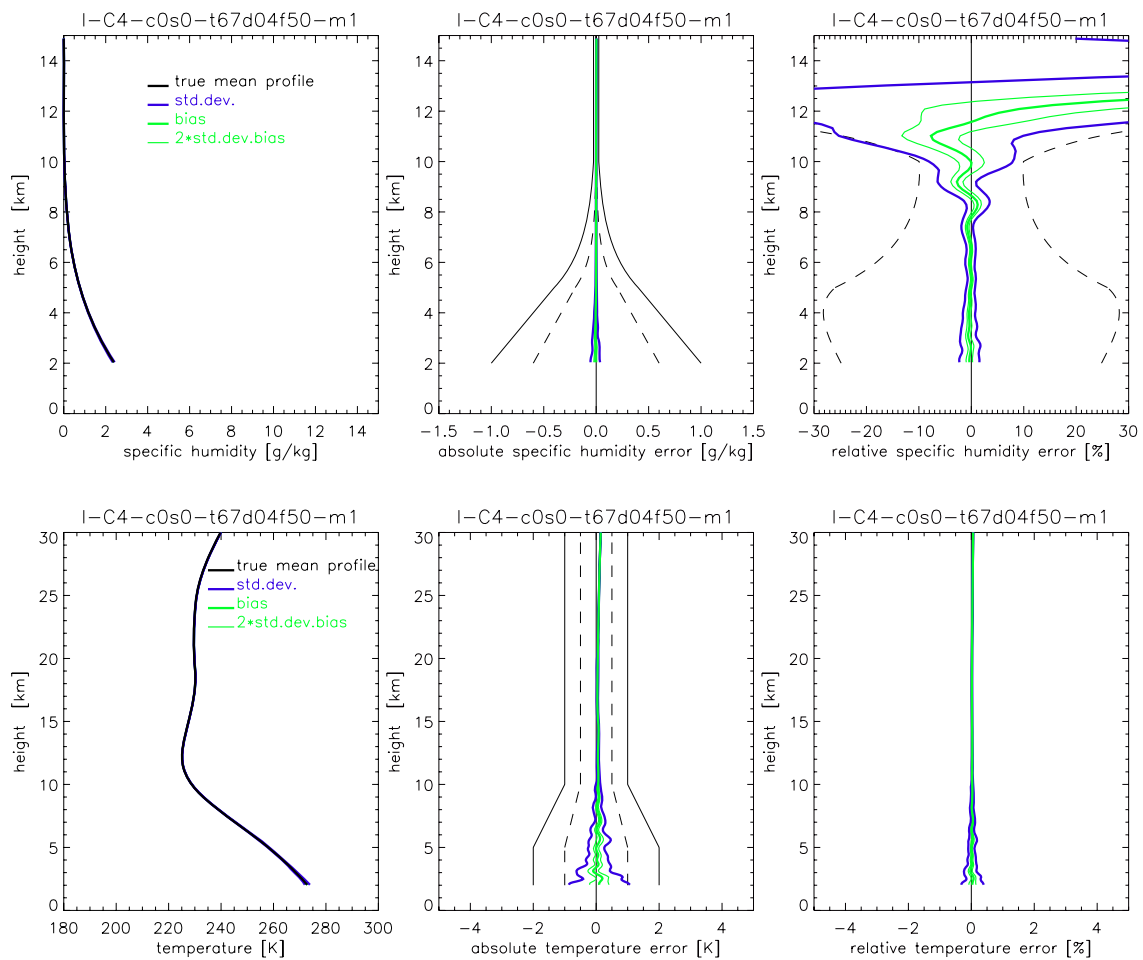


Fig. 3.1.44. Humidity (upper panels) and temperature (lower panels) retrieval results for the high-lat summer case (C4), instrumental errors (ine) scenario (therm. noise, C/No 67 dBHz, ampl. drift 0.33%/20sec, 1/f noise 0.02*T%, T=1-20sec). Statistics performance results (standard deviation, bias, 2 x std.deviation of bias) for an ensemble of 40 profiles are shown. The std.deviation is shown as +/- envelopes about the bias profiles. In the middle panels (for humidity and temperature) and the right panel (for humidity) the observational requirements, as set by the ACE+ MRD (v2.1/Jan 2004), are shown for reference (solid black, threshold requirements; dashed black, target requirements).

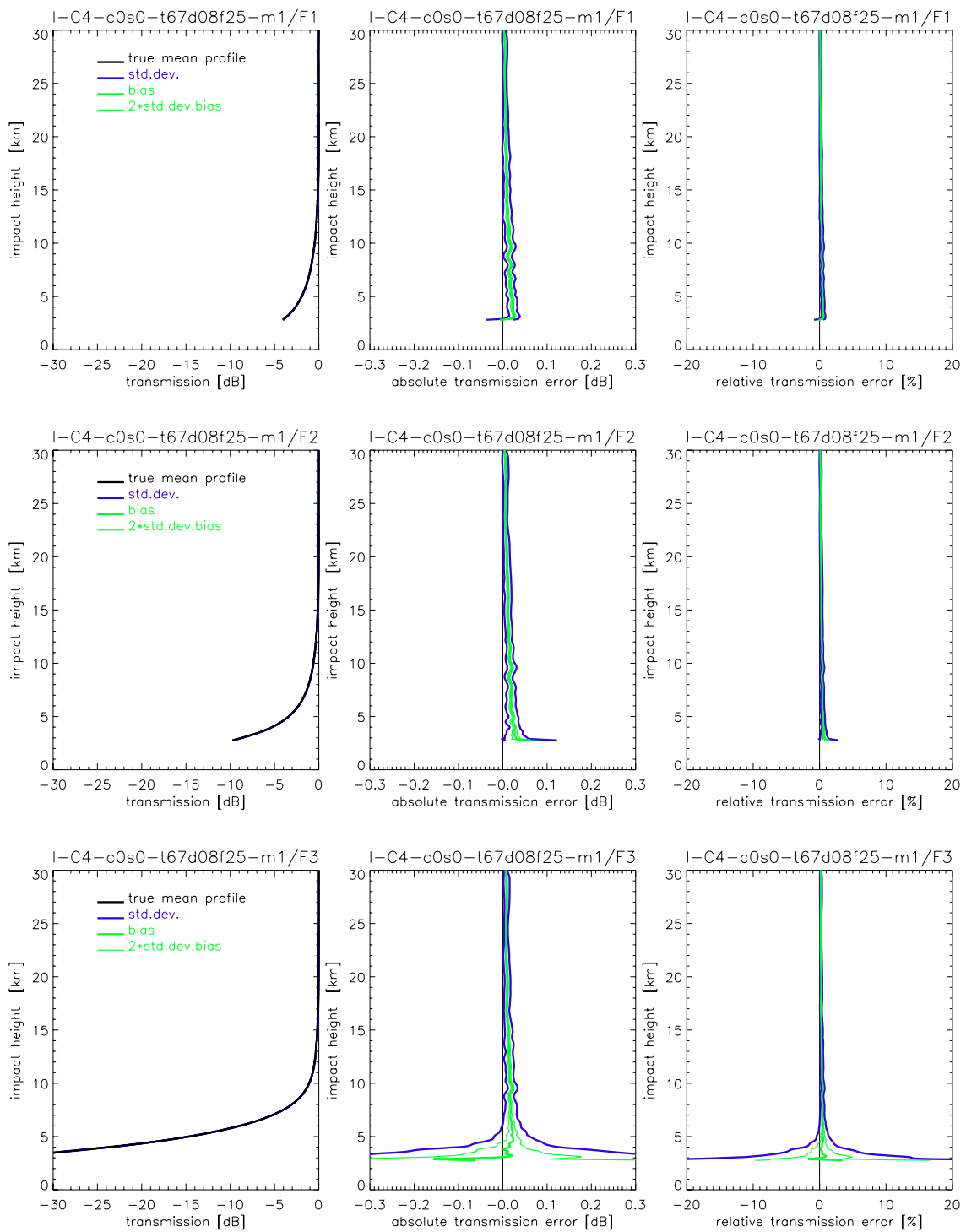


Fig. 3.1.45. Transmission retrieval results for the ACE+ frequencies F1 = 9.7 GHz (top panels), F2 = 17.25 GHz (middle panels), and F3 = 22.6 GHz (bottom panels) for the high-lat summer case (C4), instrumental errors (ine) scenario (therm. noise, C/No 67 dBHz, ampl. drift 0.62%/20sec, 1/f noise 0.01*T%, T=1-20sec). Statistics performance results (standard deviation, bias, 2 x std.deviation of bias) for an ensemble of 40 profiles are shown. The std.deviation is shown as +/- envelopes about the bias profile.

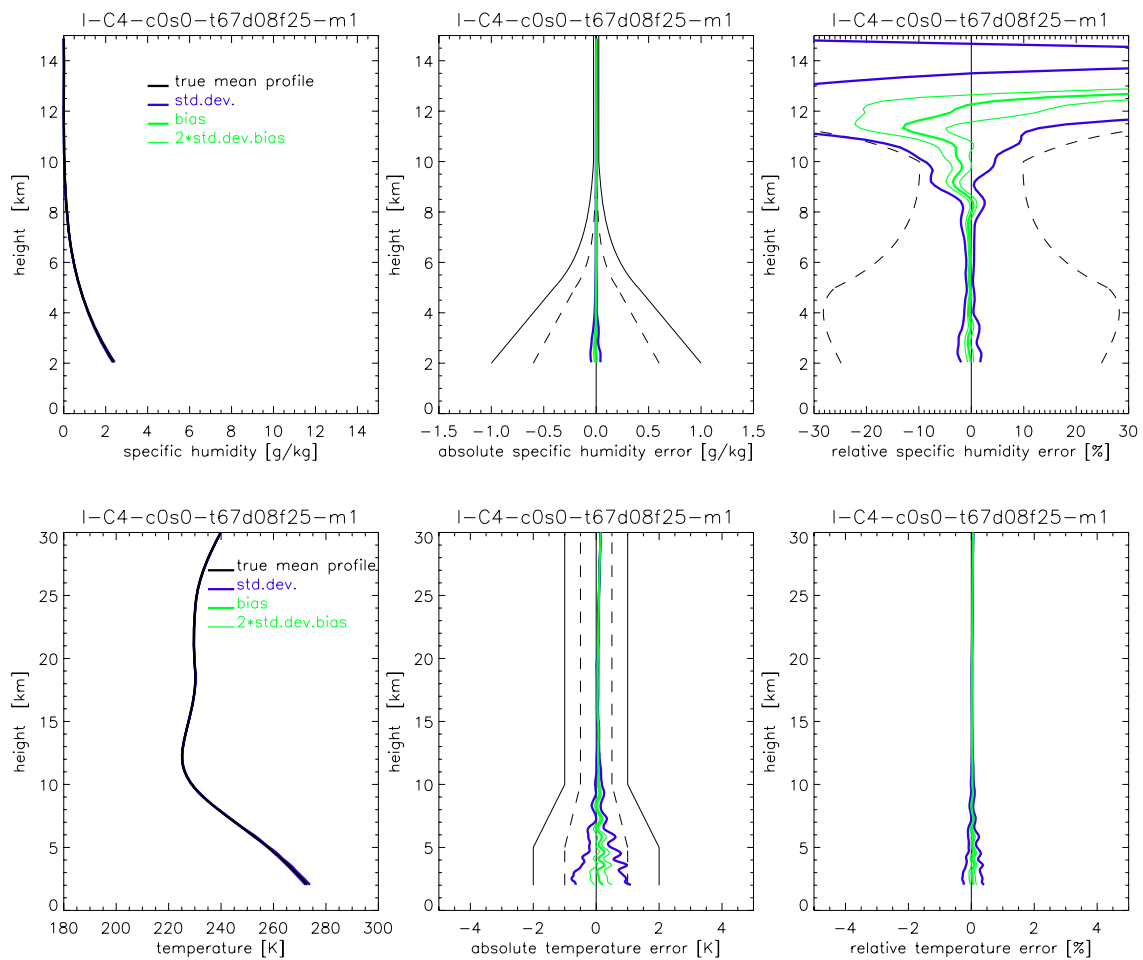


Fig. 3.1.46. Humidity (upper panels) and temperature (lower panels) retrieval results for the high-lat summer case (C4), instrumental errors (ine) scenario (therm. noise, C/No 67 dBHz, ampl. drift 0.62%/20sec, 1/f noise 0.01*T%, T=1-20sec). Statistics performance results (standard deviation, bias, 2 x std.deviation of bias) for an ensemble of 40 profiles are shown. The std.deviation is shown as +/- envelopes about the bias profiles. In the middle panels (for humidity and temperature) and the right panel (for humidity) the observational requirements, as set by the ACE+ MRD (v2.1/Jan 2004), are shown for reference (solid black, threshold requirements; dashed black, target requirements).

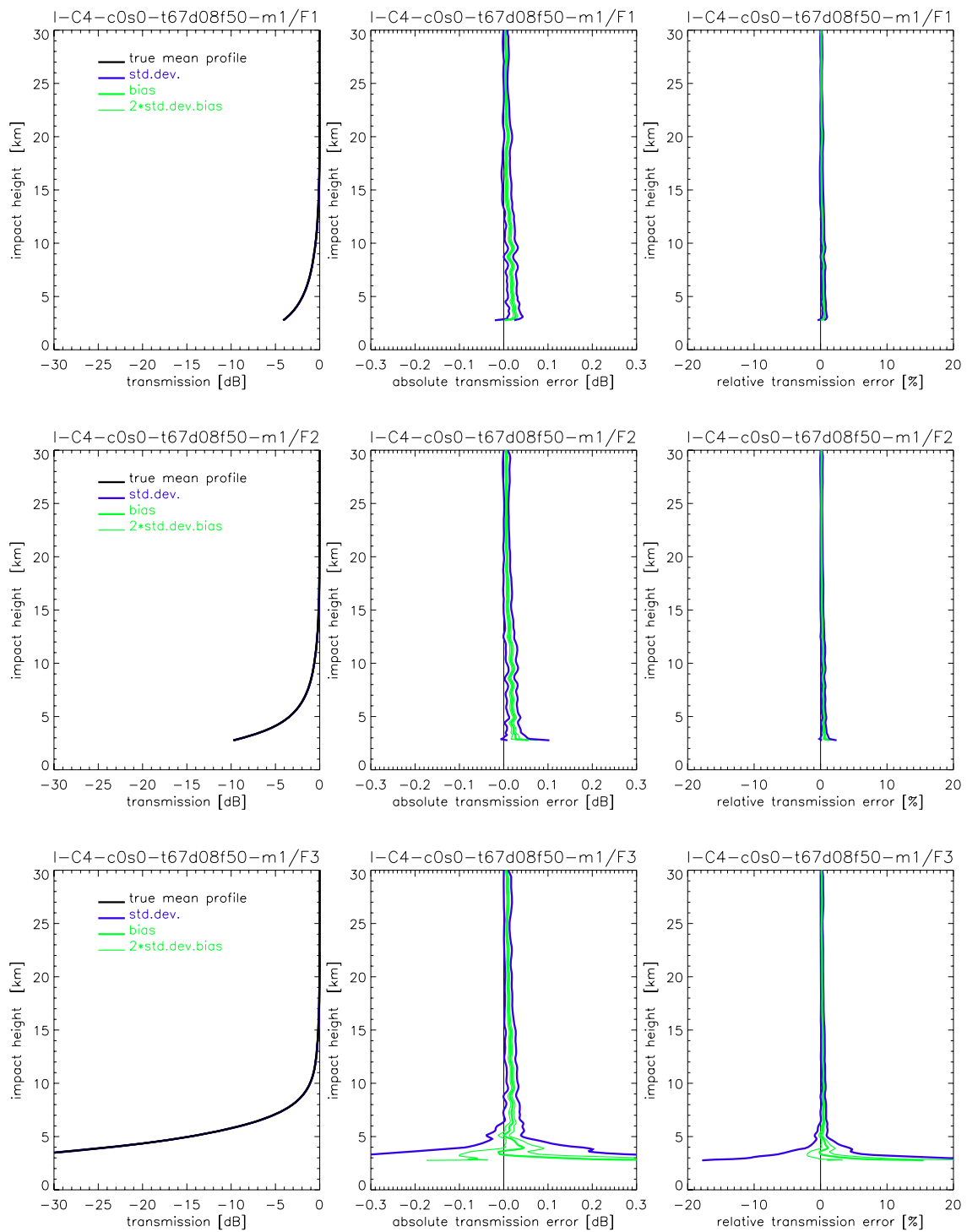


Fig. 3.1.47. Transmission retrieval results for the ACE+ frequencies F1 = 9.7 GHz (top panels), F2 = 17.25 GHz (middle panels), and F3 = 22.6 GHz (bottom panels) for the high-lat summer case (C4), instrumental errors (ine) scenario (therm. noise, C/No 67 dBHz, ampl. drift 0.62%/20sec, 1/f noise 0.02*T%, T=1-20sec). Statistics performance results (standard deviation, bias, 2 x std.deviation of bias) for an ensemble of 40 profiles are shown. The std.deviation is shown as +/- envelopes about the bias profile.

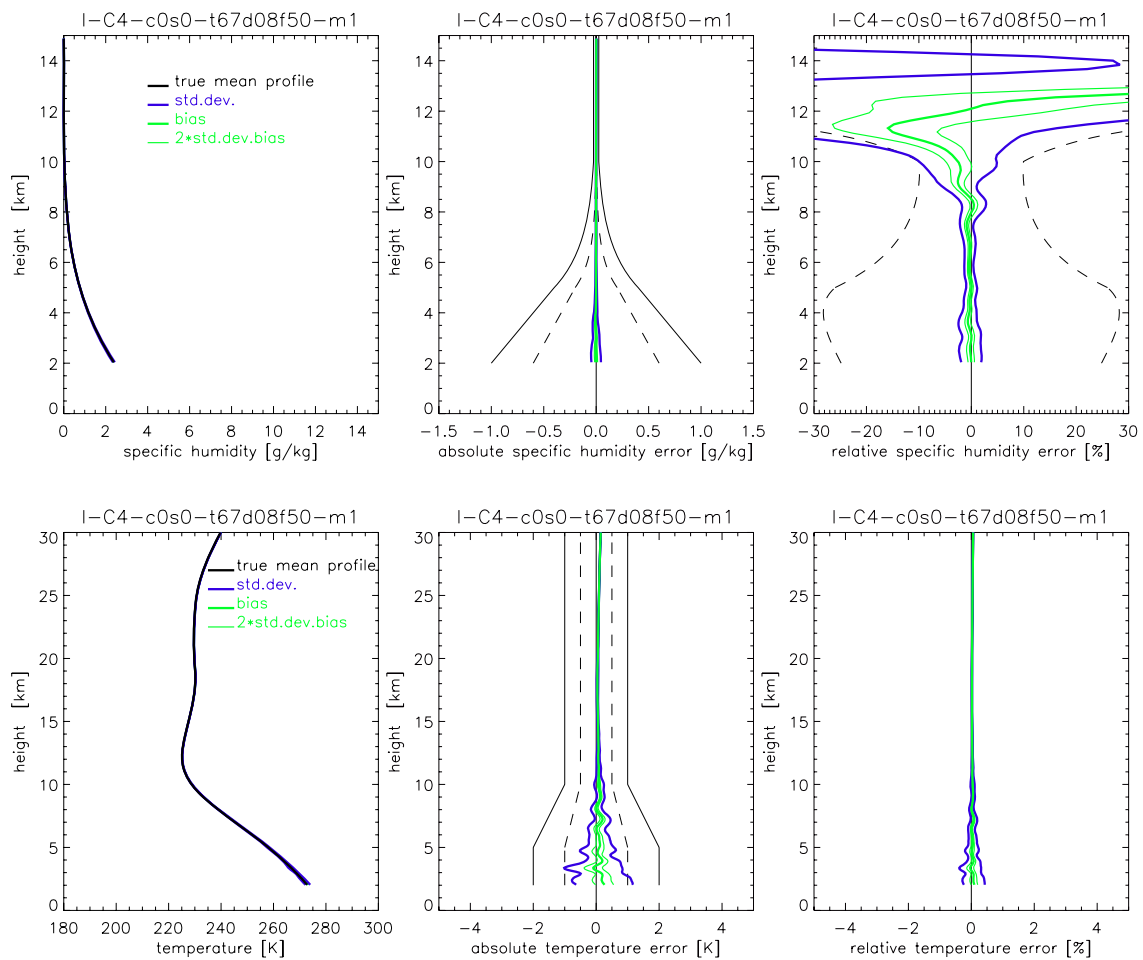


Fig. 3.1.48. Humidity (upper panels) and temperature (lower panels) retrieval results for the high-lat summer case (C4), instrumental errors (ine) scenario (therm. noise, C/No 67 dBHz, ampl. drift 0.62%/20sec, 1/f noise 0.02*T%, T=1-20sec). Statistics performance results (standard deviation, bias, 2 x std.deviation of bias) for an ensemble of 40 profiles are shown. The std.deviation is shown as +/- envelopes about the bias profiles. In the middle panels (for humidity and temperature) and the right panel (for humidity) the observational requirements, as set by the ACE+ MRD (v2.1/Jan 2004), are shown for reference (solid black, threshold requirements; dashed black, target requirements).

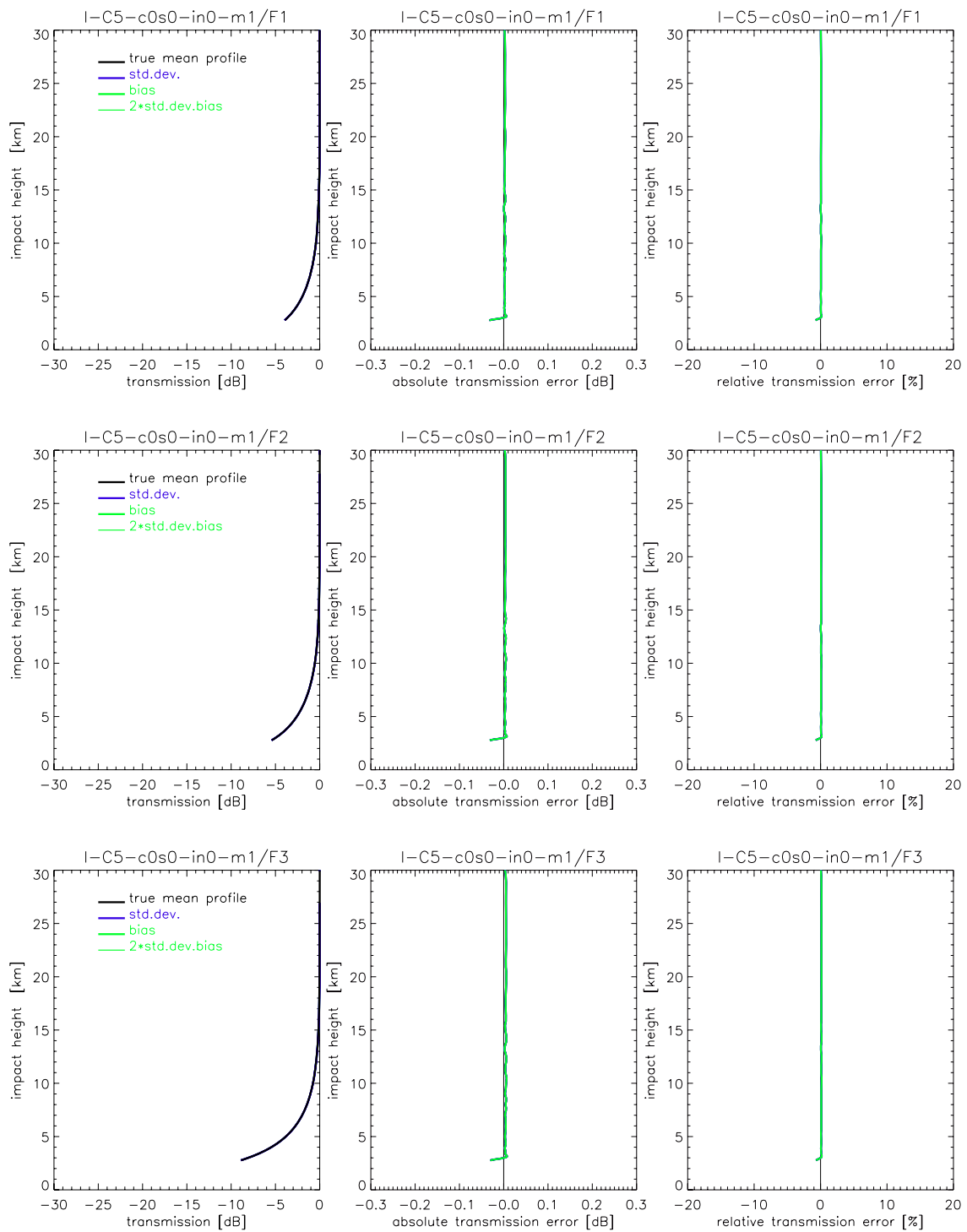


Fig. 3.1.49. Transmission retrieval results for the ACE+ frequencies F1 = 9.7 GHz (top panels), F2 = 17.25 GHz (middle panels), and F3 = 22.6 GHz (bottom panels) for the high-lat winter case (C5), no instrumental errors (in0) scenario. Statistics performance results (standard deviation, bias, 2 x std.deviation of bias) for an ensemble of 40 profiles are shown. The std.deviation is shown as +/- envelopes about the bias profile.

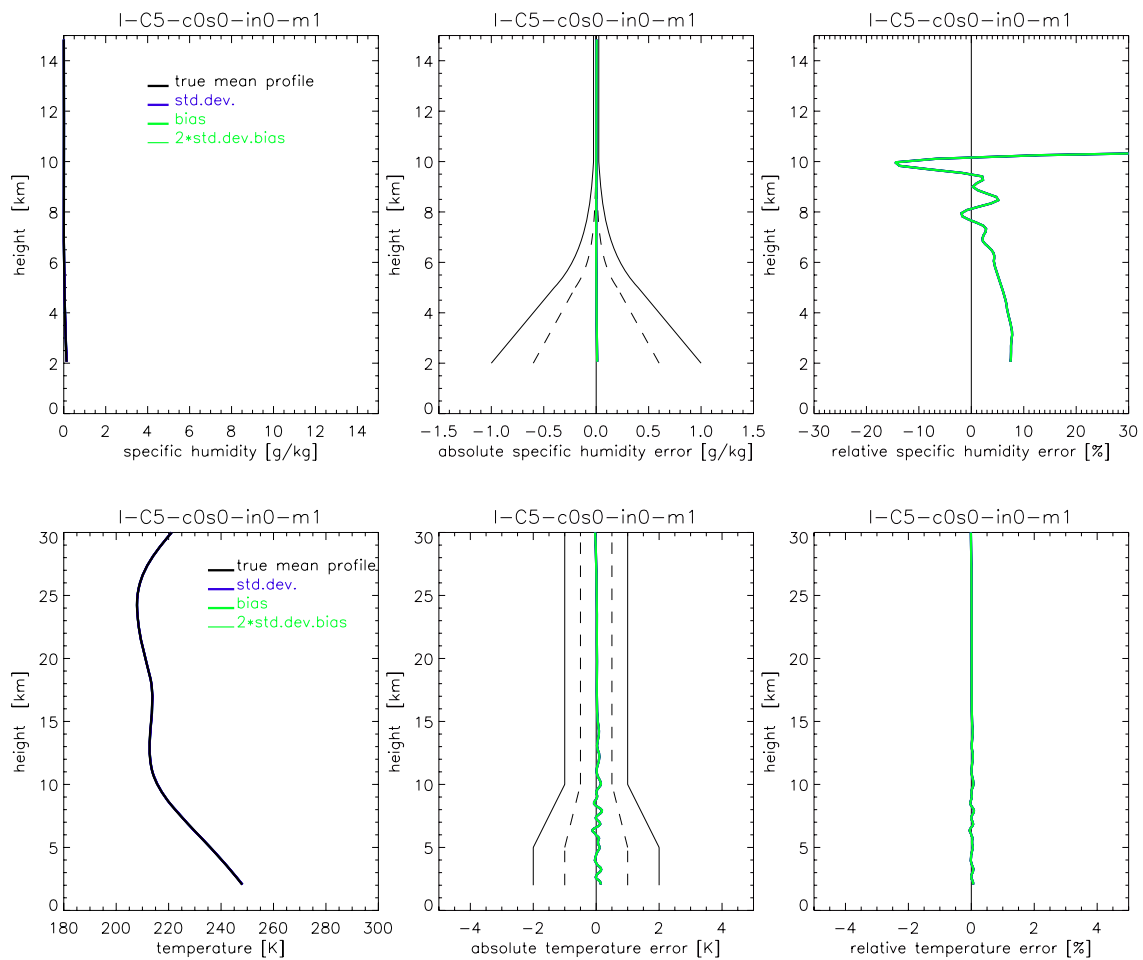


Fig. 3.1.50. Humidity (upper panels) and temperature (lower panels) retrieval results for the high-lat winter case (C5), no instrumental errors (in0) scenario. Statistics performance results (standard deviation, bias, 2 x std.deviation of bias) for an ensemble of 40 profiles are shown. The std.deviation is shown as +/- envelopes about the bias profiles. In the middle panels (for humidity and temperature) and the right panel (for humidity) the observational requirements, as set by the ACE+ MRD (v2.1/Jan 2004), are shown for reference (solid black, threshold requirements; dashed black, target requirements).

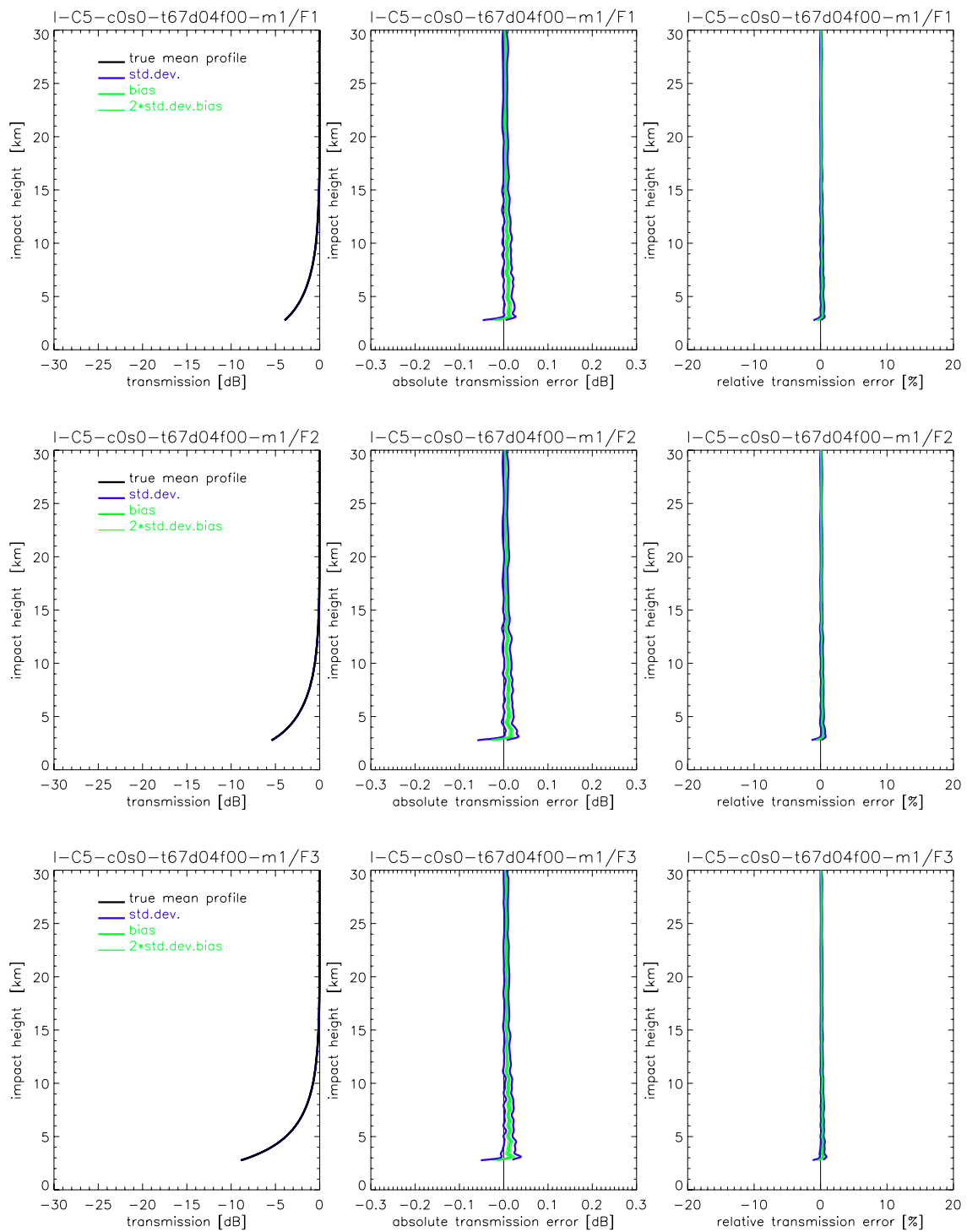


Fig. 3.1.51. Transmission retrieval results for the ACE+ frequencies F1 = 9.7 GHz (top panels), F2 = 17.25 GHz (middle panels), and F3 = 22.6 GHz (bottom panels) for the high-lat winter case (C5), instrumental errors (ine) scenario (therm. noise, C/No 67 dBHz, ampl. drift 0.33%/20sec, no 1/f noise). Statistics performance results (standard deviation, bias, 2 x std.deviation of bias) for an ensemble of 40 profiles are shown. The std.deviation are shown as +/- envelopes about the bias profile.

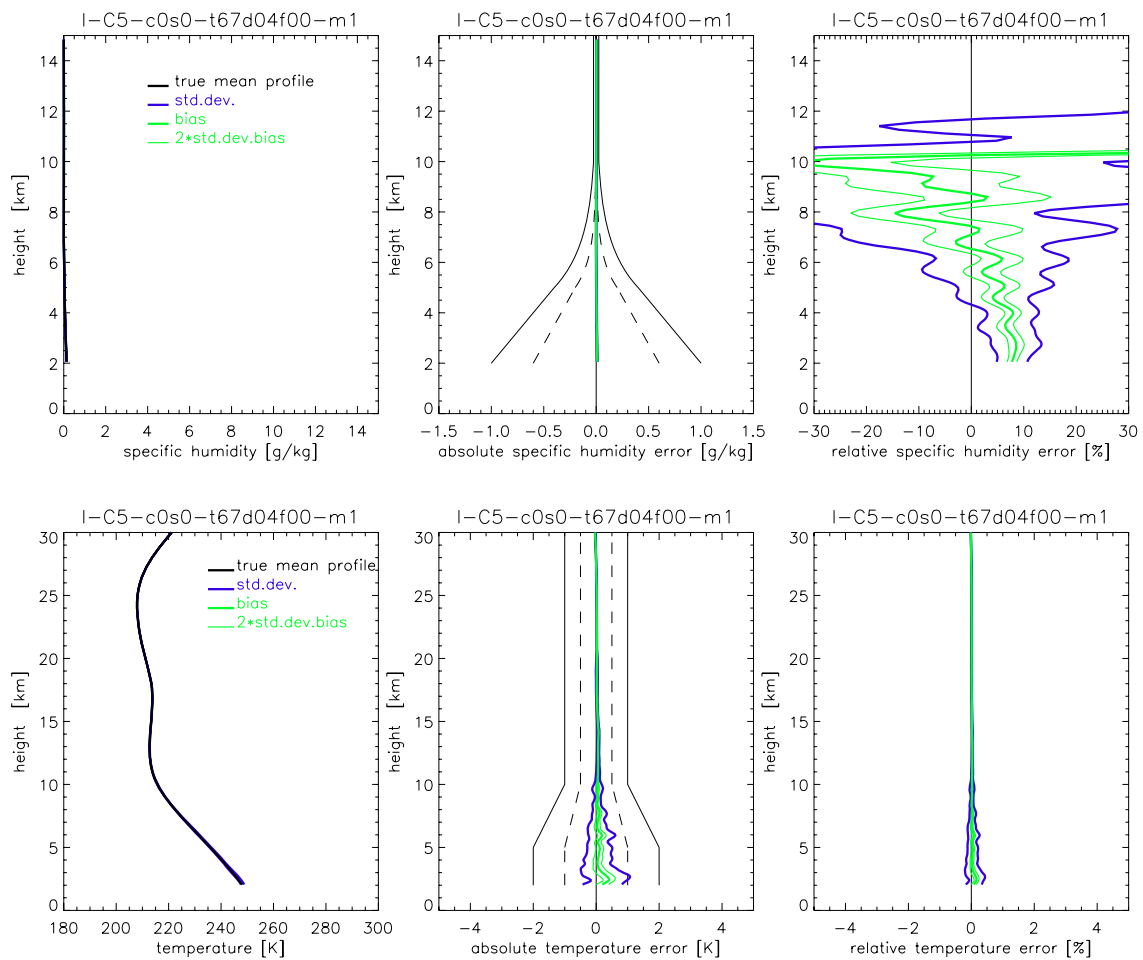


Fig. 3.1.52. Humidity (upper panels) and temperature (lower panels) retrieval results for the high-lat winter case (C5), instrumental errors (ine) scenario (therm. noise, C/No 67 dBHz, ampl. drift 0.33%/20sec, no 1/f noise). Statistics performance results (standard deviation, bias, 2 x std.deviation of bias) for an ensemble of 40 profiles are shown. The std.deviation is shown as +/- envelopes about the bias profiles. In the middle panels (for humidity and temperature) and the right panel (for humidity) the observational requirements, as set by the ACE+ MRD (v2.1/Jan 2004), are shown for reference (solid black, threshold requirements; dashed black, target requirements).

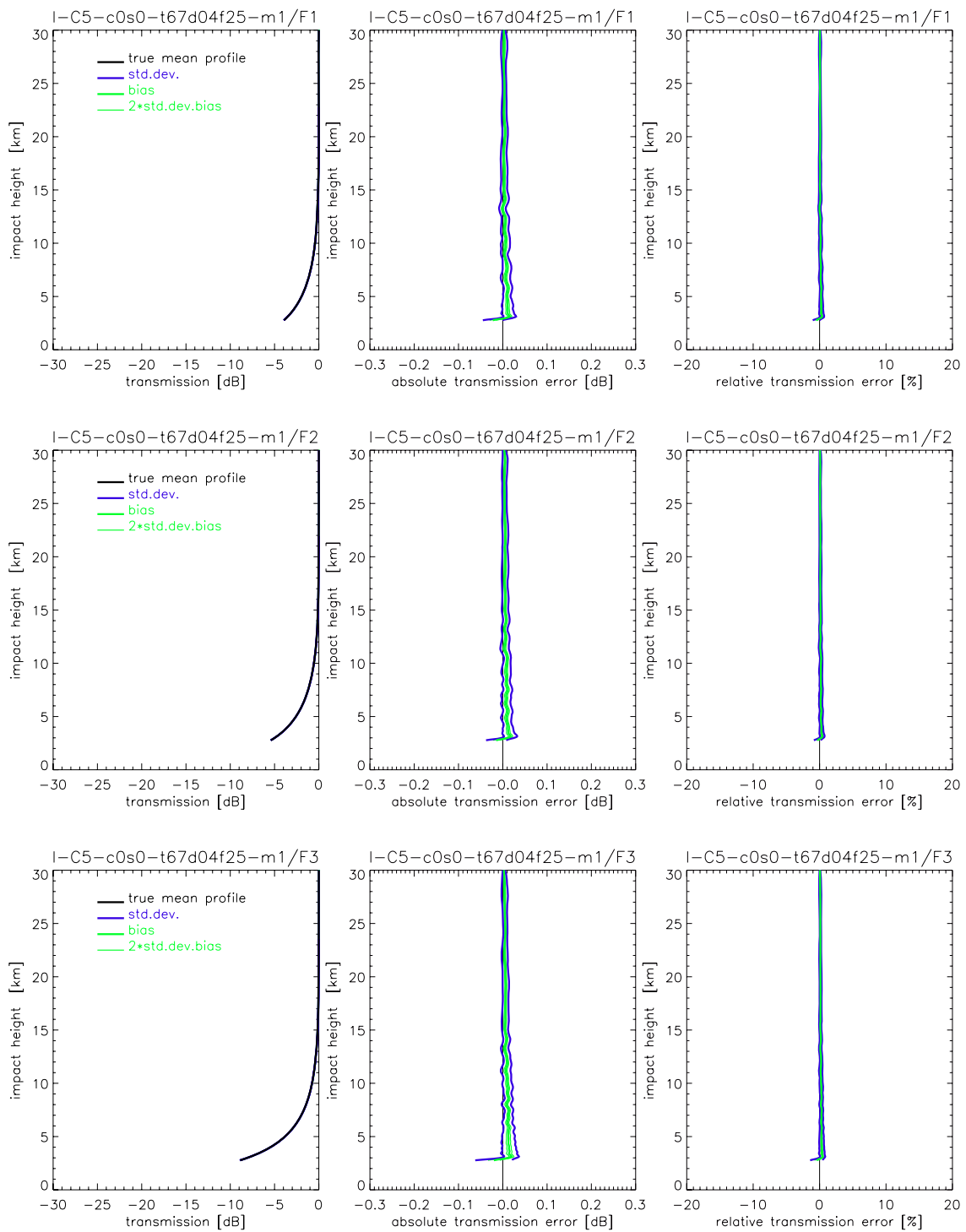


Fig. 3.1.53. Transmission retrieval results for the ACE+ frequencies F1 = 9.7 GHz (top panels), F2 = 17.25 GHz (middle panels), and F3 = 22.6 GHz (bottom panels) for the high-lat winter case (C5) instrumental errors (ine) scenario (therm. noise, C/No 67 dBHz, ampl. drift 0.33%/20sec, 1/f noise 0.01*T%, T=1-20sec). Statistics performance results (standard deviation, bias, 2 x std.deviation of bias) for an ensemble of 40 profiles are shown. The std.deviation are shown as +/- envelopes about the bias profile.

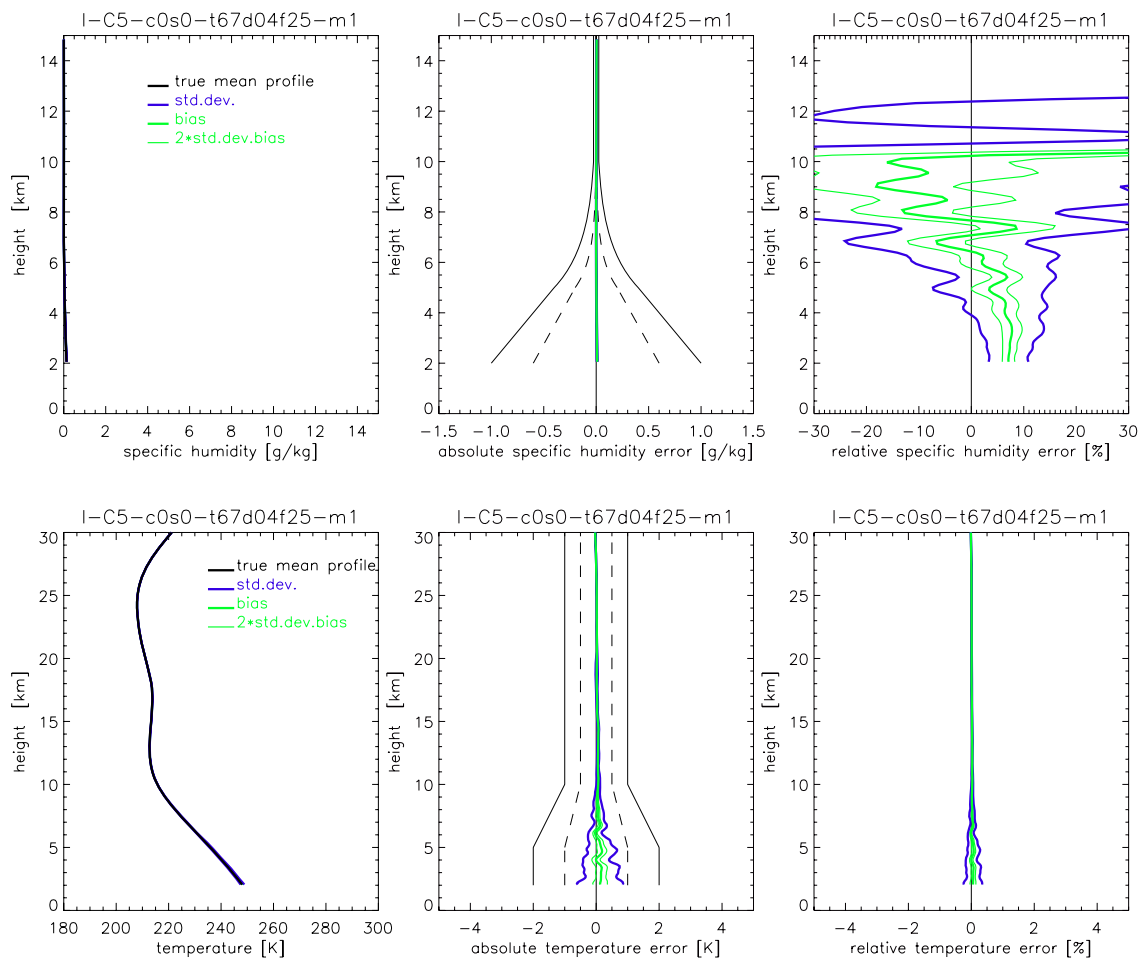


Fig. 3.1.54. Humidity (upper panels) and temperature (lower panels) retrieval results for the high-lat winter case (C5), instrumental errors (ine) scenario (therm. noise, C/No 67 dBHz, ampl. drift 0.33%/20sec, 1/f noise 0.01*T%, T=1-20sec). Statistics performance results (standard deviation, bias, 2 x std.deviation of bias) for an ensemble of 40 profiles are shown. The std.deviation is shown as +/- envelopes about the bias profiles. In the middle panels (for humidity and temperature) and the right panel (for humidity) the observational requirements, as set by the ACE+ MRD (v2.1/Jan 2004), are shown for reference (solid black, threshold requirements; dashed black, target requirements).

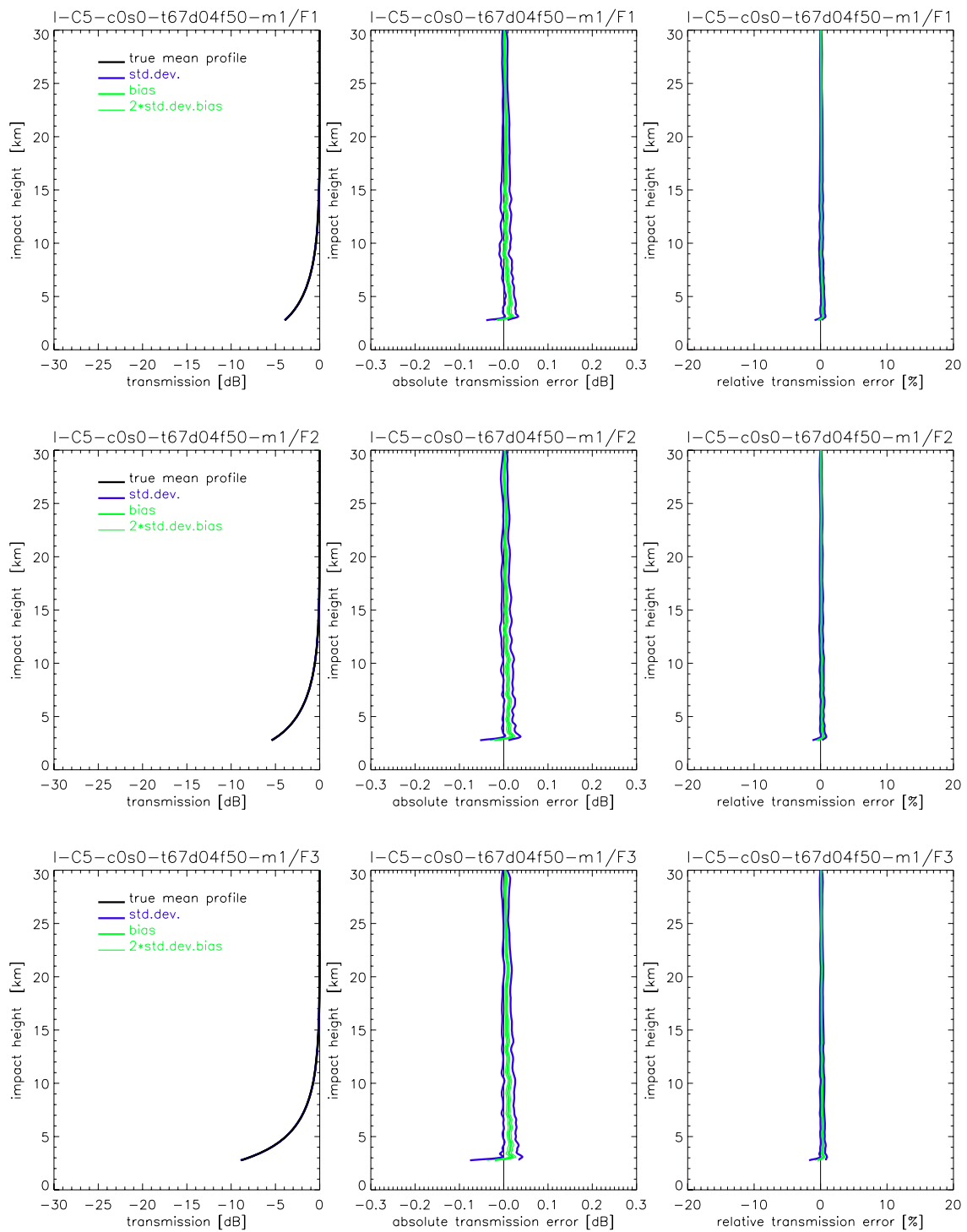


Fig. 3.1.55. Transmission retrieval results for the ACE+ frequencies F1 = 9.7 GHz (top panels), F2 = 17.25 GHz (middle panels), and F3 = 22.6 GHz (bottom panels) for the high-lat winter case (C5), instrumental errors (ine) scenario (therm. noise, C/No 67 dBHz, ampl. drift 0.33%/20sec, 1/f noise 0.02*T%, T=1-20sec). Statistics performance results (standard deviation, bias, 2 x std.deviation of bias) for an ensemble of 40 profiles are shown. The std.deviation is shown as +/- envelopes about the bias profile.

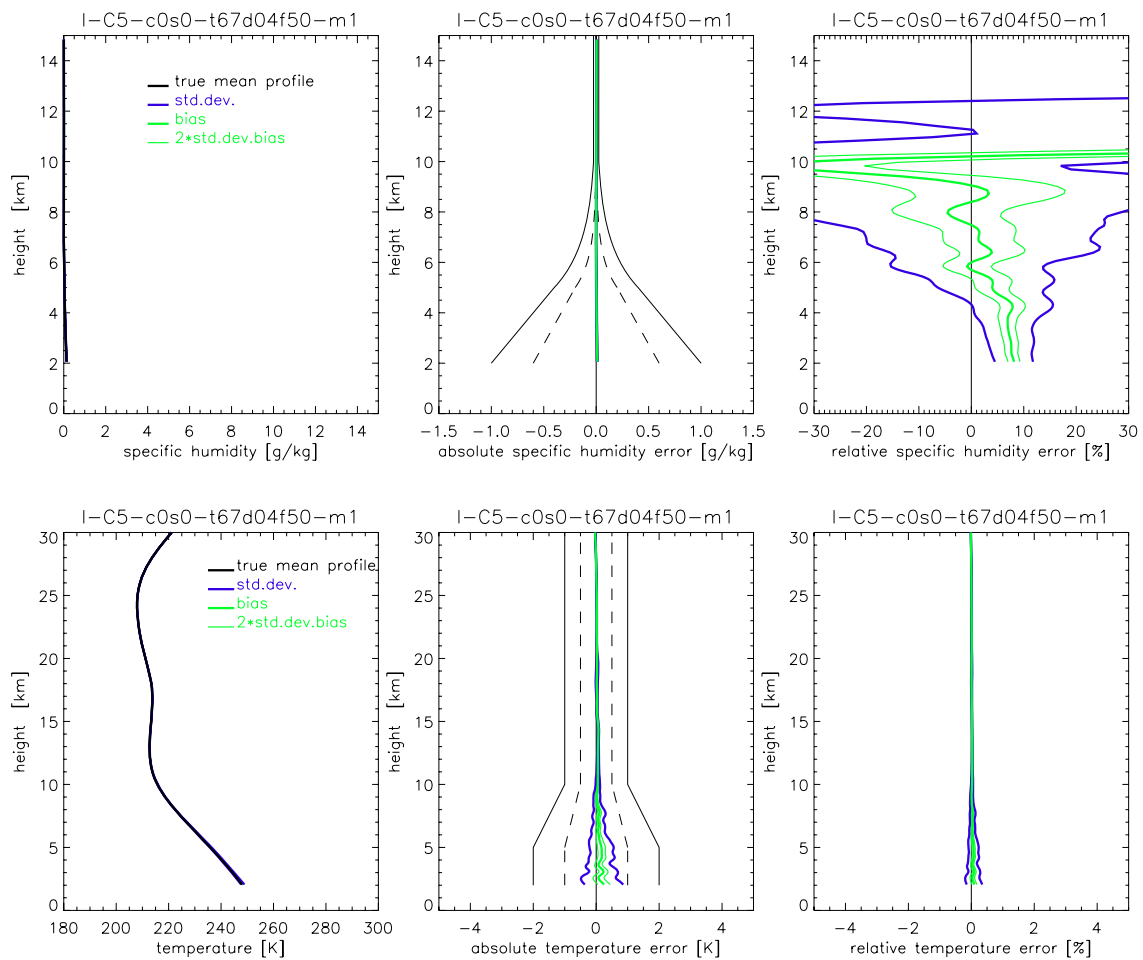


Fig. 3.1.56. Humidity (upper panels) and temperature (lower panels) retrieval results for the high-lat winter case (C5), instrumental errors (ine) scenario (therm. noise, C/No 67 dBHz, ampl. drift 0.33%/20sec, 1/f noise 0.02*T%, T=1-20sec). Statistics performance results (standard deviation, bias, 2 x std.deviation of bias) for an ensemble of 40 profiles are shown. The std.deviation is shown as +/- envelopes about the bias profiles. In the middle panels (for humidity and temperature) and the right panel (for humidity) the observational requirements, as set by the ACE+ MRD (v2.1/Jan 2004), are shown for reference (solid black, threshold requirements; dashed black, target requirements).

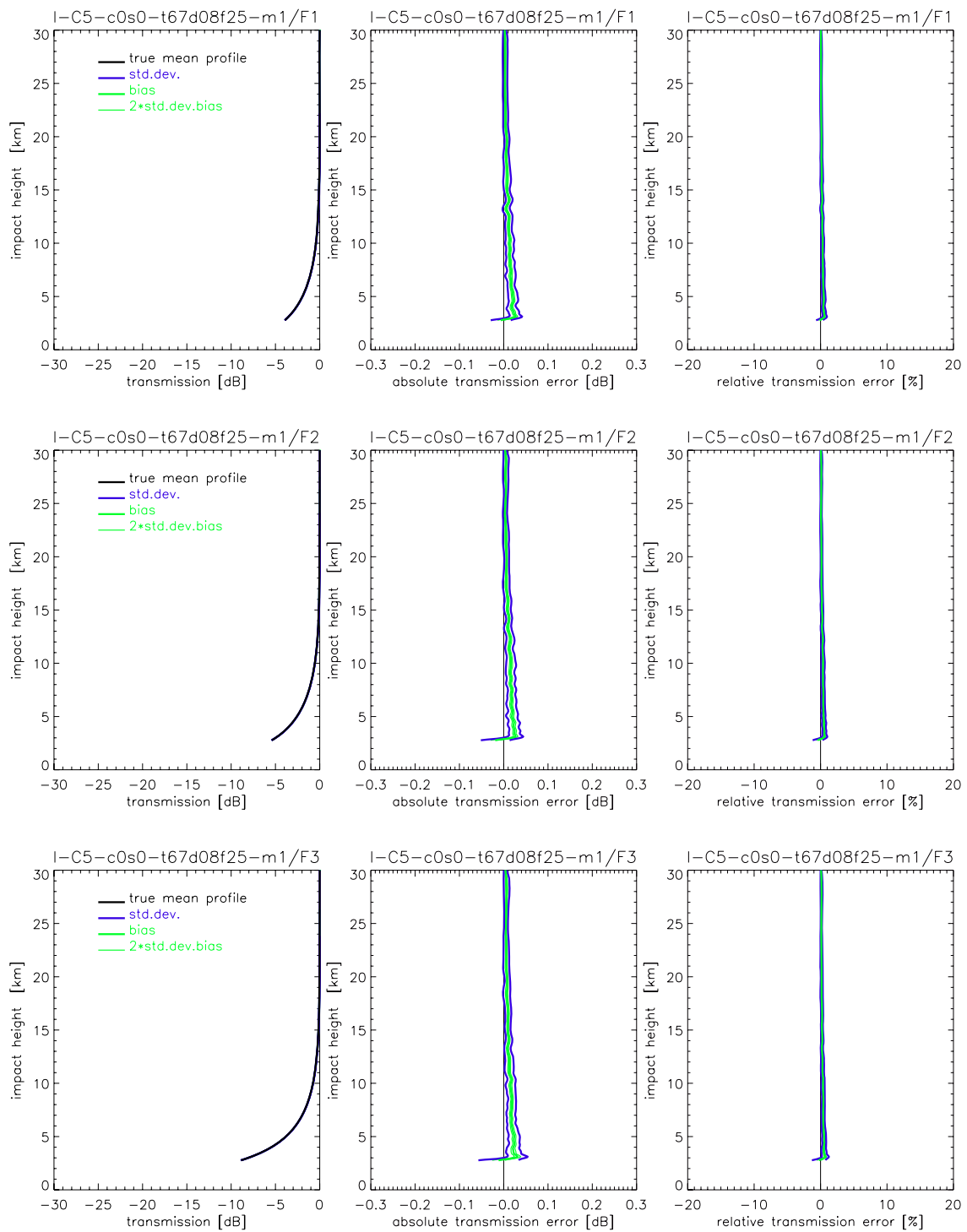


Fig. 3.1.57. Transmission retrieval results for the ACE+ frequencies F1 = 9.7 GHz (top panels), F2 = 17.25 GHz (middle panels), and F3 = 22.6 GHz (bottom panels) for the high-lat winter case (C5), instrumental errors (ine) scenario (therm. noise, C/No 67 dBHz, ampl. drift 0.62%/20sec, 1/f noise 0.01*T%, T=1-20sec). Statistics performance results (standard deviation, bias, 2 x std.deviation of bias) for an ensemble of 40 profiles are shown. The std.deviation is shown as +/- envelopes about the bias profile.

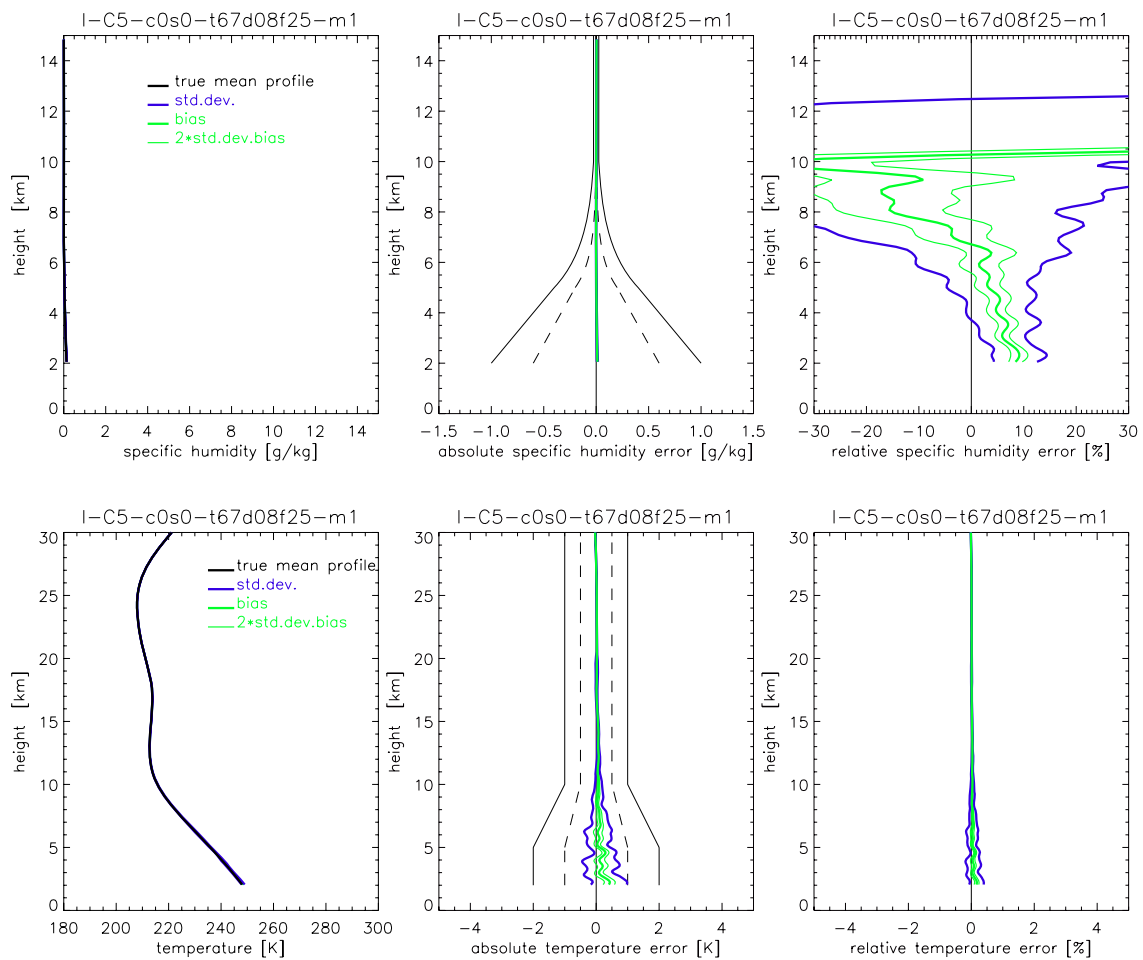


Fig. 3.1.58. Humidity (upper panels) and temperature (lower panels) retrieval results for the high-lat winter case (C5), instrumental errors (ine) scenario (therm. noise, C/No 67 dBHz, ampl. drift 0.62%/20sec, 1/f noise 0.01*T%, T=1-20sec). Statistics performance results (standard deviation, bias, 2 x std.deviation of bias) for an ensemble of 40 profiles are shown. The std.deviation is shown as +/- envelopes about the bias profiles. In the middle panels (for humidity and temperature) and the right panel (for humidity) the observational requirements, as set by the ACE+ MRD (v2.1/Jan 2004), are shown for reference (solid black, threshold requirements; dashed black, target requirements).

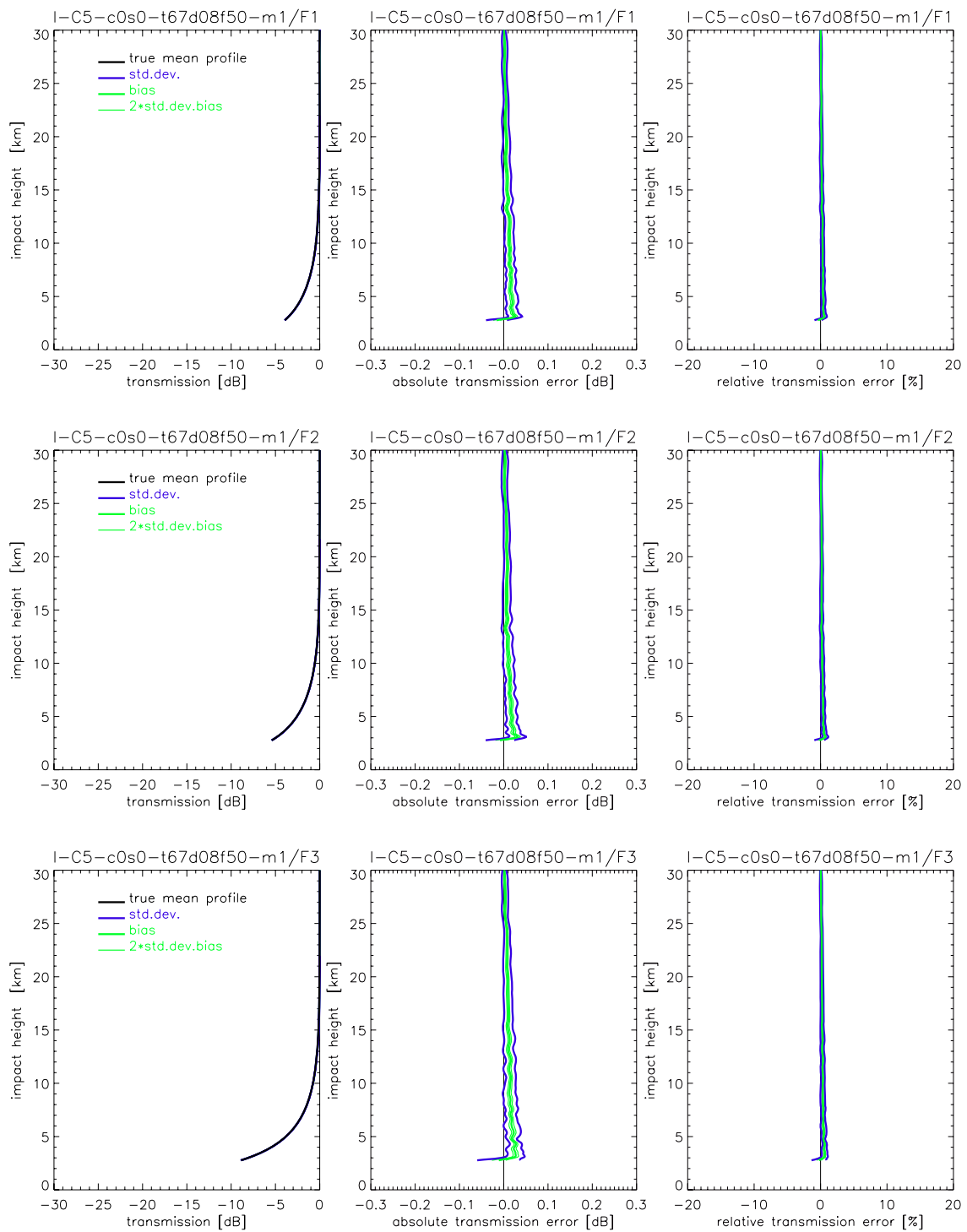


Fig. 3.1.59. Transmission retrieval results for the ACE+ frequencies F1 = 9.7 GHz (top panels), F2 = 17.25 GHz (middle panels), and F3 = 22.6 GHz (bottom panels) for the high-lat winter case (C5), instrumental errors (ine) scenario (therm. noise, C/No 67 dBHz, ampl. drift 0.62%/20sec, 1/f noise 0.02*T%, T=1-20sec). Statistics performance results (standard deviation, bias, 2 x std.deviation of bias) for an ensemble of 40 profiles are shown. The std.deviation is shown as +/- envelopes about the bias profile.

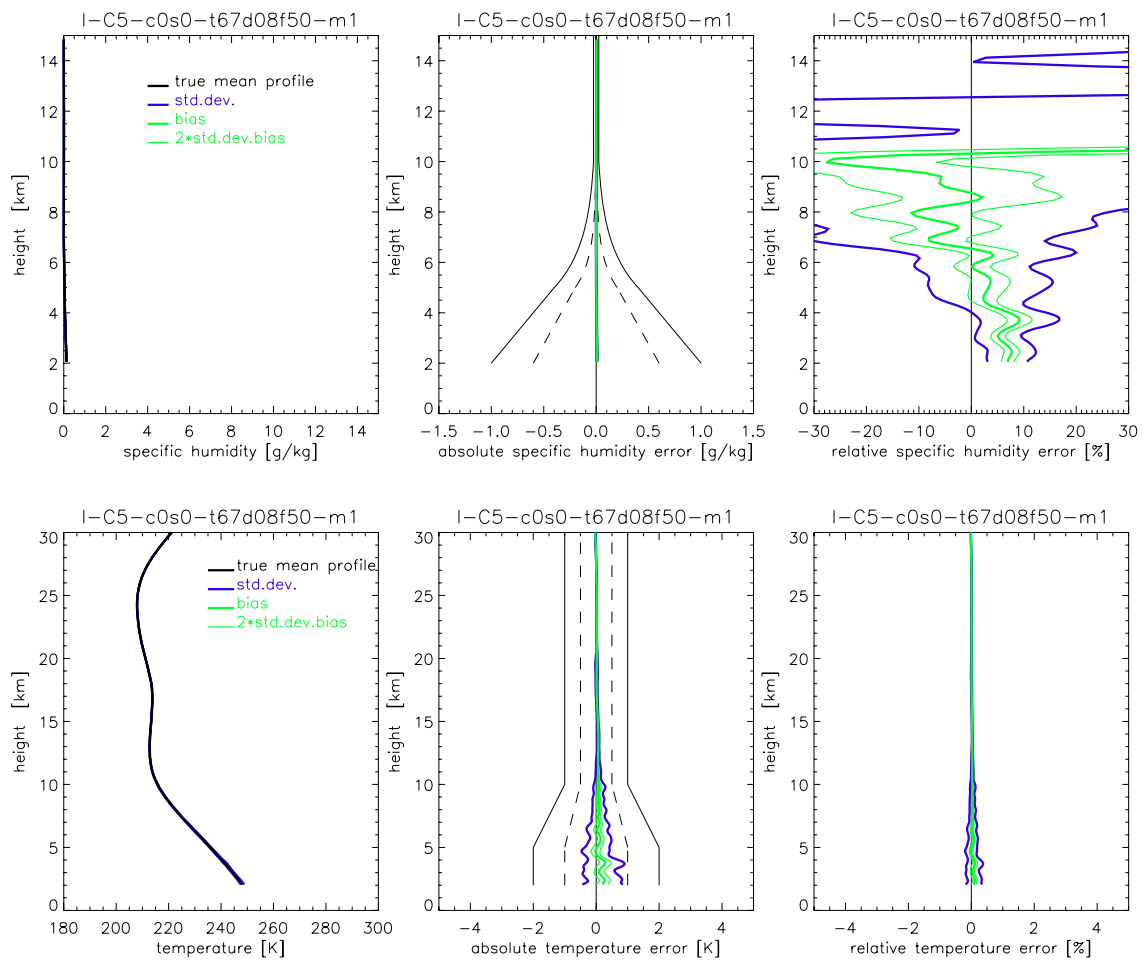


Fig. 3.1.60. Humidity (upper panels) and temperature (lower panels) retrieval results for the high-lat winter case (C5), instrumental errors (ine) scenario (therm. noise, C/No 67 dBHz, ampl. drift 0.62%/20sec, 1/f noise 0.02*T%, T=1-20sec). Statistics performance results (standard deviation, bias, 2 x std.deviation of bias) for an ensemble of 40 profiles are shown. The std.deviations are shown as +/- envelopes about the bias profiles. In the middle panels (for humidity and temperature) and the right panel (for humidity) the observational requirements, as set by the ACE+ MRD (v2.1/Jan 2004), are shown for reference (solid black, threshold requirements; dashed black, target requirements).

3.2. Results on Retrieval Performance in Presence of Clouds

This subsection shows transmission, humidity, temperature, and liquid water retrieval results for the mid-latitude summer case (C2) in presence of randomized 3D As and 3D Cu clouds, respectively. Furthermore, two kinds of total instrumental errors were superposed on each case. For a detailed description of the specifications for these scenarios see the introduction to section 3 on pages 29 – 30.

The results of the 2×2 cloudy air scenarios are shown on the following pages 92 – 103.

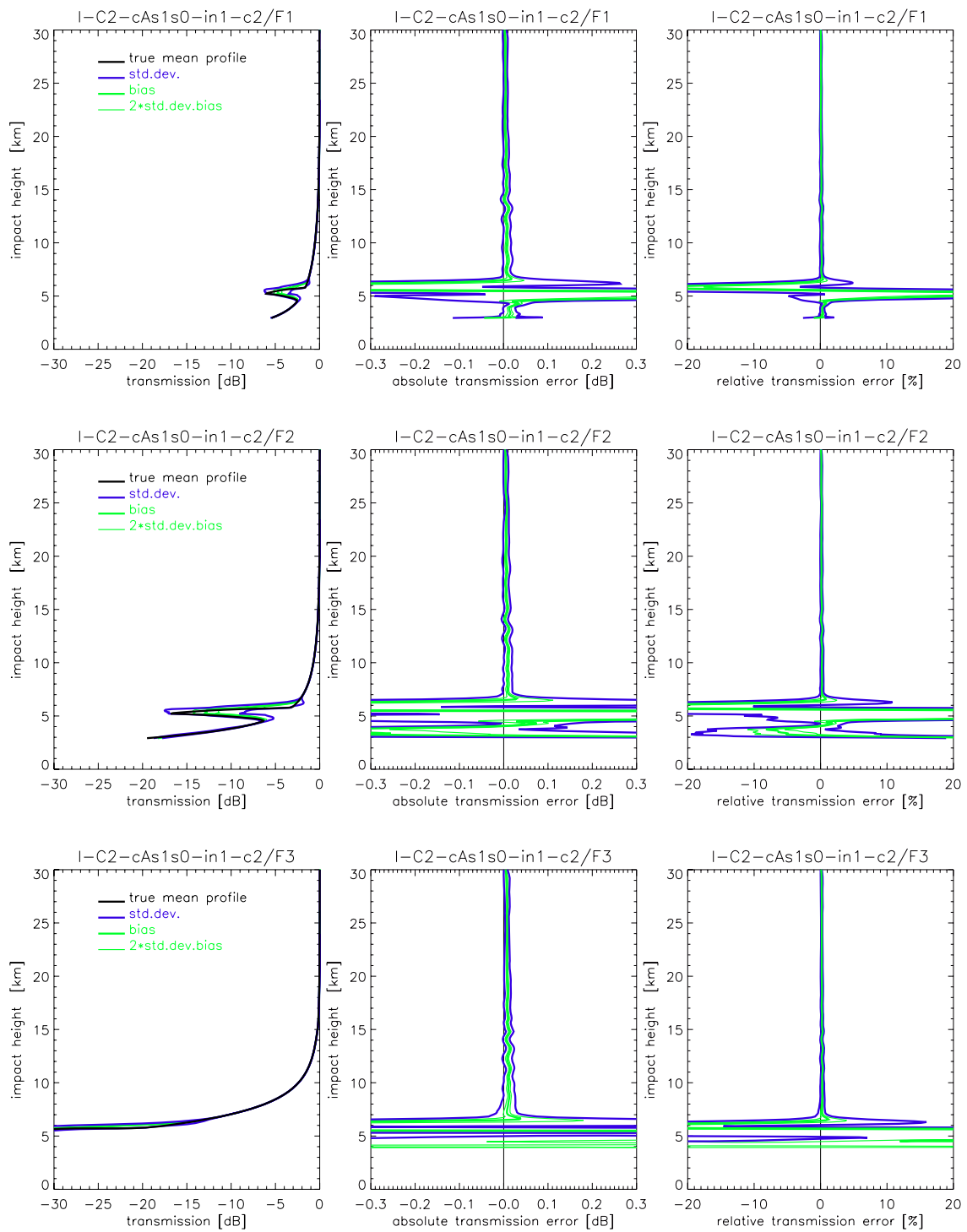


Fig. 3.2.1 Transmission retrieval results for the ACE+ frequencies F1 = 9.7 GHz (top panels), F2 = 17.25 GHz (middle panels), and F3 = 22.6 GHz (bottom panels) for the mid-lat summer case (C2), instrumental errors (ine) scenario (therm. noise, C/No 67 dBHz, ampl. drift 0.33%/20sec, 1/f noise 0.01*T%, T=1-20sec). Statistics performance results (standard deviation, bias, 2 x std.deviation of bias) for an ensemble of 40 profiles are shown. The std.deviation are shown as +/- envelopes about the bias profile.

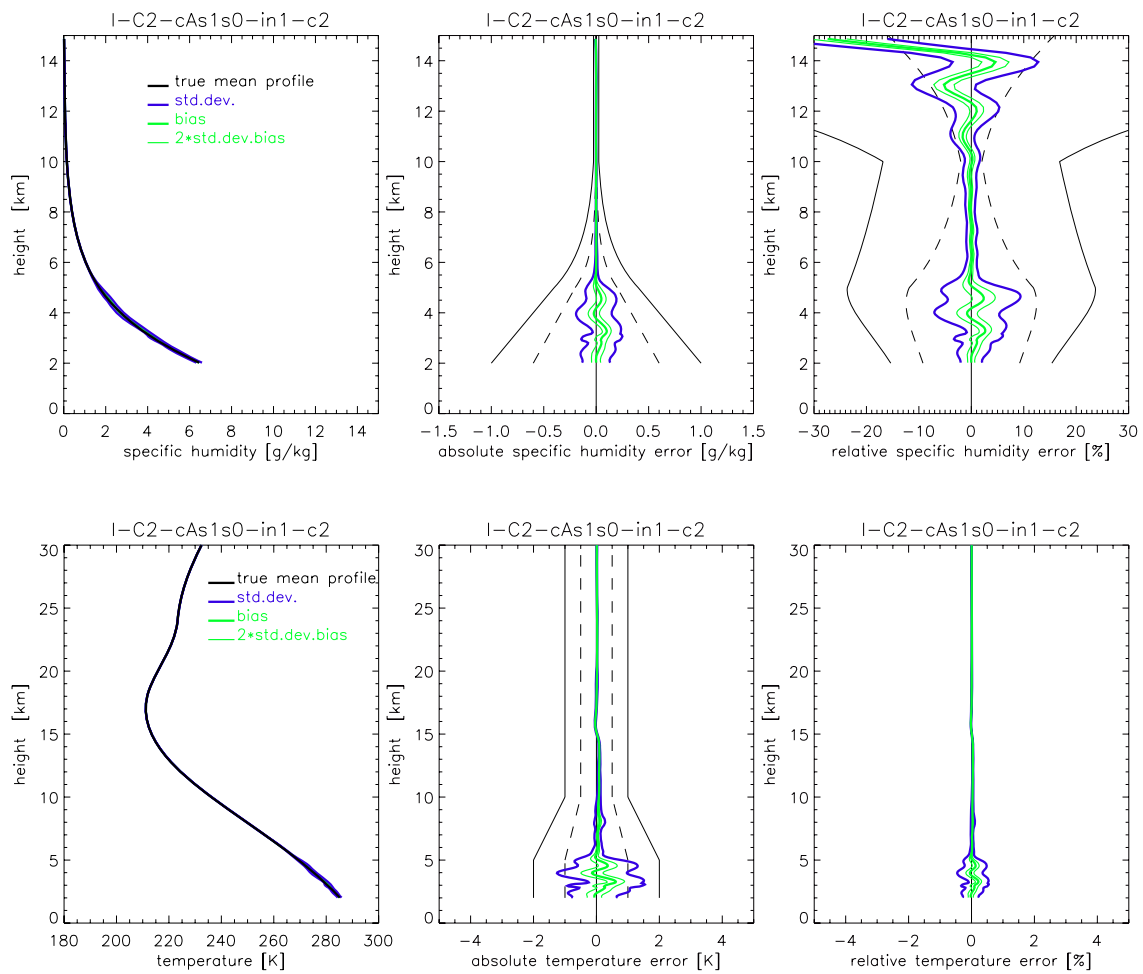


Fig. 3.2.2. Humidity (upper panels) and temperature (lower panels) retrieval results for the mid-lat summer case (C2), instrumental errors (ine) scenario (therm. noise, C/No 67 dBHz, ampl. drift 0.33%/20sec, 1/f noise 0.01*T%, T=1-20sec). Statistics performance results (standard deviation, bias, 2 x std.deviation of bias) for an ensemble of 40 profiles are shown. The std.deviation is shown as +/- envelopes about the bias profiles. In the middle panels (for humidity and temperature) and the right panel (for humidity) the observational requirements, as set by the ACE+ MRD (v2.1/Jan 2004), are shown for reference (solid black, threshold requirements; dashed black, target requirements).

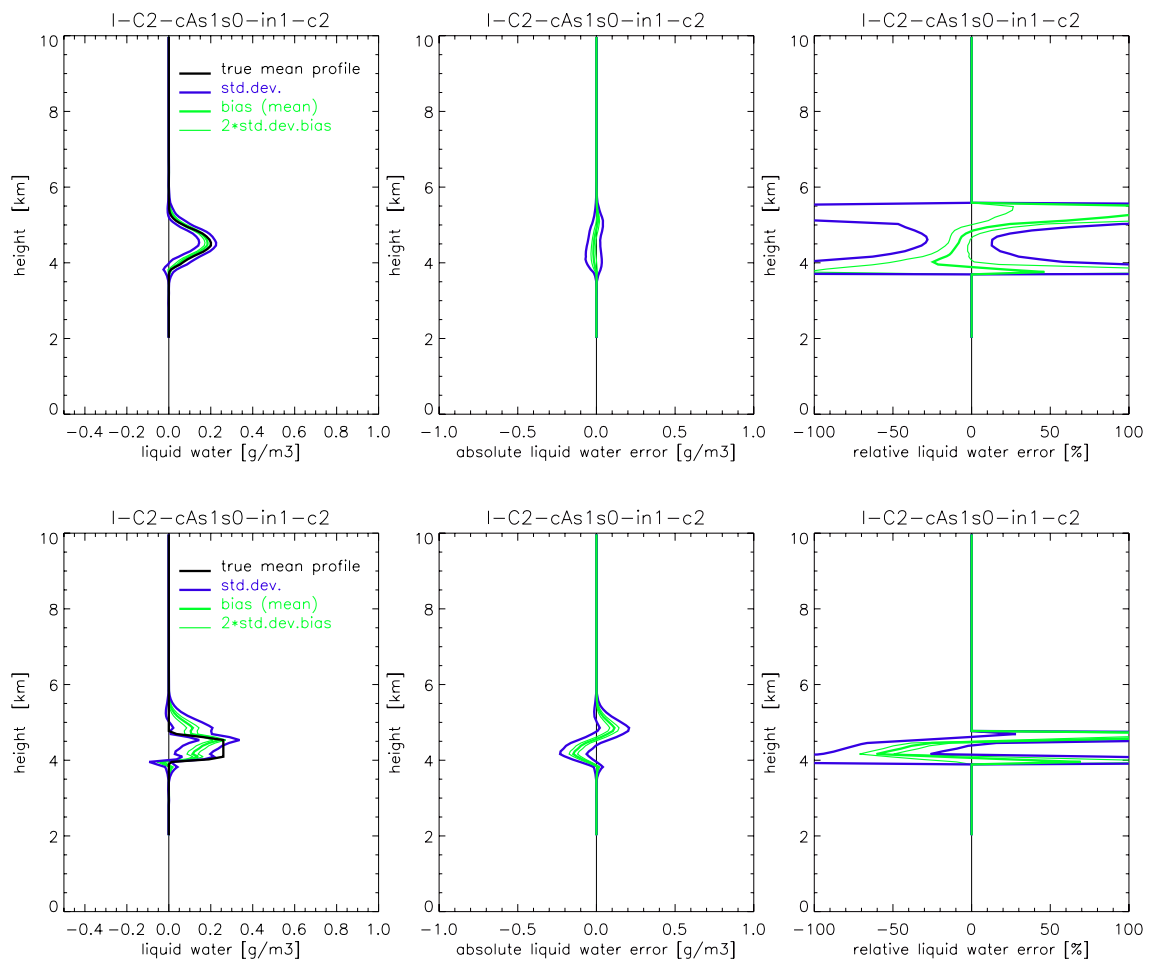


Fig. 3.2.3. Liquid water sample of reference profiles (upper panels) and single reference profile (lower panels) retrieval results for the mid-lat summer case (C2), instrumental errors (ine) scenario (therm. noise, C/No 67 dBHz, ampl. drift 0.33%/20sec, 1/f noise 0.01*T%, T=1-20sec). Statistics performance results (standard deviation, bias, 2 x std.deviation of bias) for an ensemble of 40 profiles are shown. The std.deviation are shown as +/- envelopes about the bias profiles. In the middle panels (for humidity and temperature) and the right panel (for humidity) the observational requirements, as set by the ACE+ MRD (v2.1/Jan 2004), are shown for reference (solid black, threshold requirements; dashed black, target requirements).

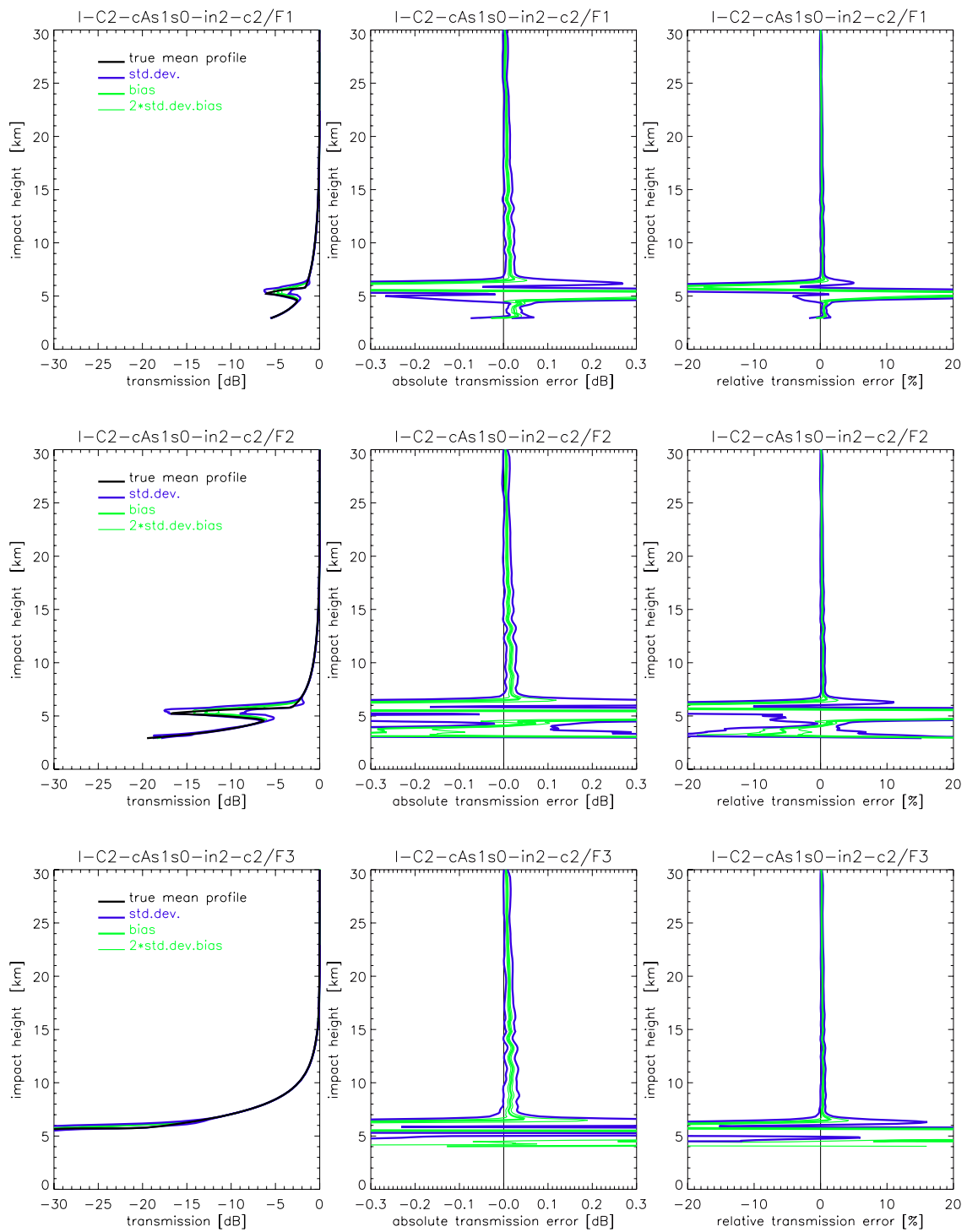


Fig. 3.2.4 Transmission retrieval results for the ACE+ frequencies F1 = 9.7 GHz (top panels), F2 = 17.25 GHz (middle panels), and F3 = 22.6 GHz (bottom panels) for the mid-lat summer case (C2), instrumental errors (ine) scenario (therm. noise, C/No 67 dBHz, ampl. drift 0.62%/20sec, 1/f noise 0.02*T%, T=1-20sec). Statistics performance results (standard deviation, bias, 2 x std.deviation of bias) for an ensemble of 40 profiles are shown. The std.deviation are shown as +/- envelopes about the bias profile.

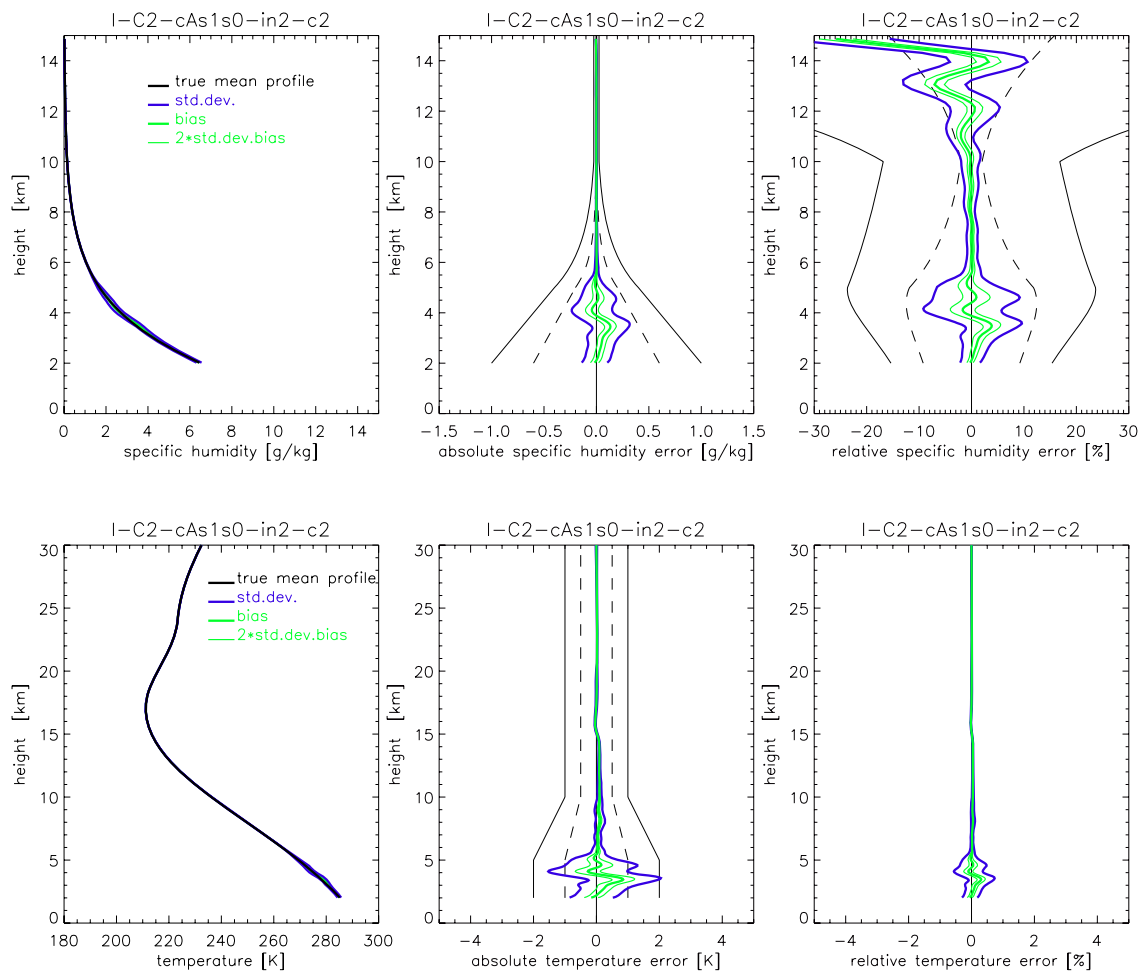


Fig. 3.2.5. Humidity (upper panels) and temperature (lower panels) retrieval results for the mid-lat summer case (C2), instrumental errors (ine) scenario (therm. noise, C/No 67 dBHz, ampl. drift 0.62%/20sec, 1/f noise 0.02*T%, T=1-20sec). Statistics performance results (standard deviation, bias, 2 x std.deviation of bias) for an ensemble of 40 profiles are shown. The std.deviation is shown as +/- envelopes about the bias profiles. In the middle panels (for humidity and temperature) and the right panel (for humidity) the observational requirements, as set by the ACE+ MRD (v2.1/Jan 2004), are shown for reference (solid black, threshold requirements; dashed black, target requirements).

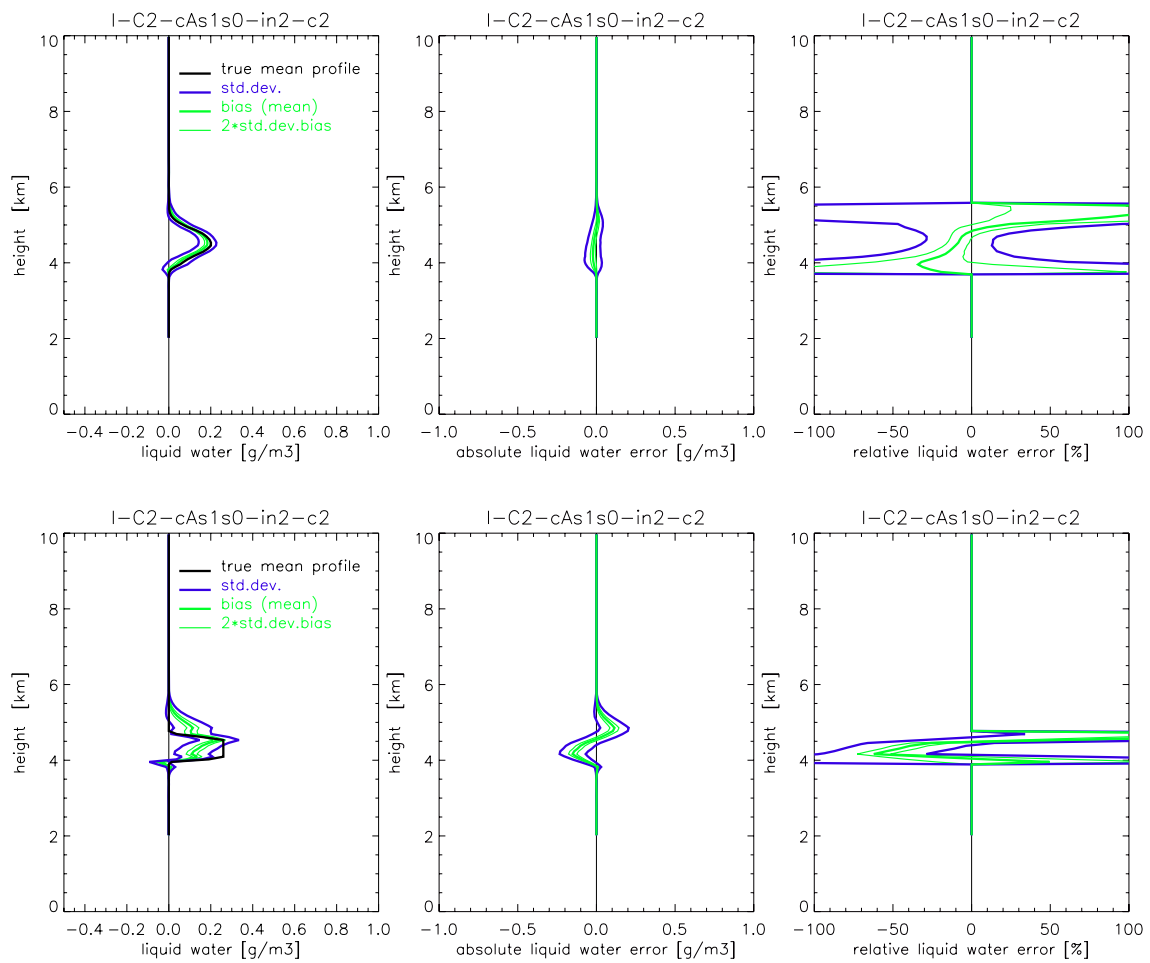


Fig. 3.2.6. Liquid water sample of reference profiles (upper panels) and single reference profile (lower panels) retrieval results for the mid-lat summer case (C2), instrumental errors (ine) scenario (therm. noise, C/No 67 dBHz, ampl. drift 0.62%/20sec, 1/f noise 0.02*T%, T=1-20sec). Statistics performance results (standard deviation, bias, 2 x std.deviation of bias) for an ensemble of 40 profiles are shown. The std.deviation are shown as +/- envelopes about the bias profiles. In the middle panels (for humidity and temperature) and the right panel (for humidity) the observational requirements, as set by the ACE+ MRD (v2.1/Jan 2004), are shown for reference (solid black, threshold requirements; dashed black, target requirements).

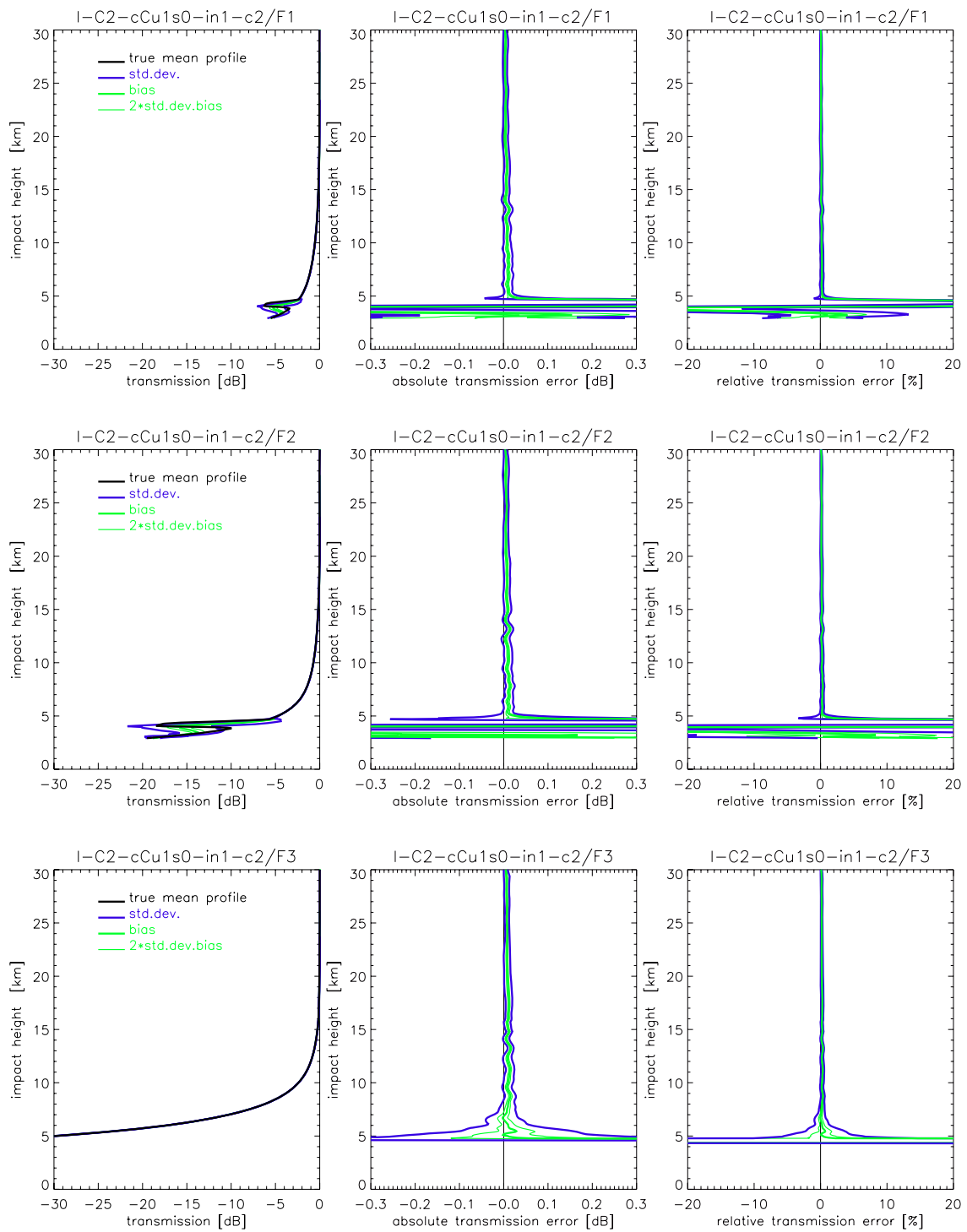


Fig. 3.2.7 Transmission retrieval results for the ACE+ frequencies F1 = 9.7 GHz (top panels), F2 = 17.25 GHz (middle panels), and F3 = 22.6 GHz (bottom panels) for the mid-lat summer case (C2), instrumental errors (ine) scenario (therm. noise, C/No 67 dBHz, ampl. drift 0.33%/20sec, 1/f noise 0.01*T%, T=1-20sec). Statistics performance results (standard deviation, bias, 2 x std.deviation of bias) for an ensemble of 40 profiles are shown. The std.deviation is shown as +/- envelopes about the bias profile.

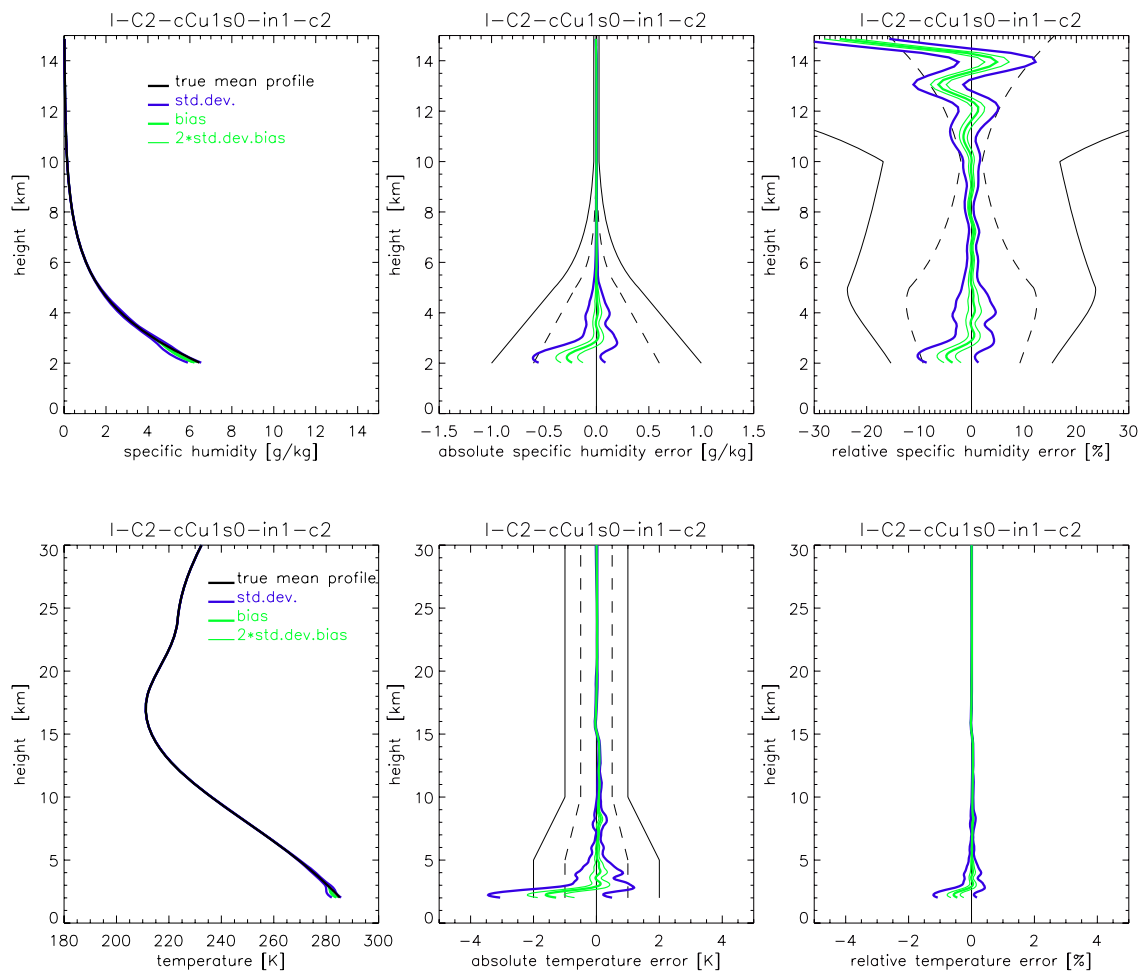


Fig. 3.2.8. Humidity (upper panels) and temperature (lower panels) retrieval results for the mid-lat summer case (C2), instrumental errors (ine) scenario (therm. noise, C/No 67 dBHz, ampl. drift 0.33%/20sec, 1/f noise 0.01*T%, T=1-20sec). Statistics performance results (standard deviation, bias, 2 x std.deviation of bias) for an ensemble of 40 profiles are shown. The std.deviation is shown as +/- envelopes about the bias profiles. In the middle panels (for humidity and temperature) and the right panel (for humidity) the observational requirements, as set by the ACE+ MRD (v2.1/Jan 2004), are shown for reference (solid black, threshold requirements; dashed black, target requirements).

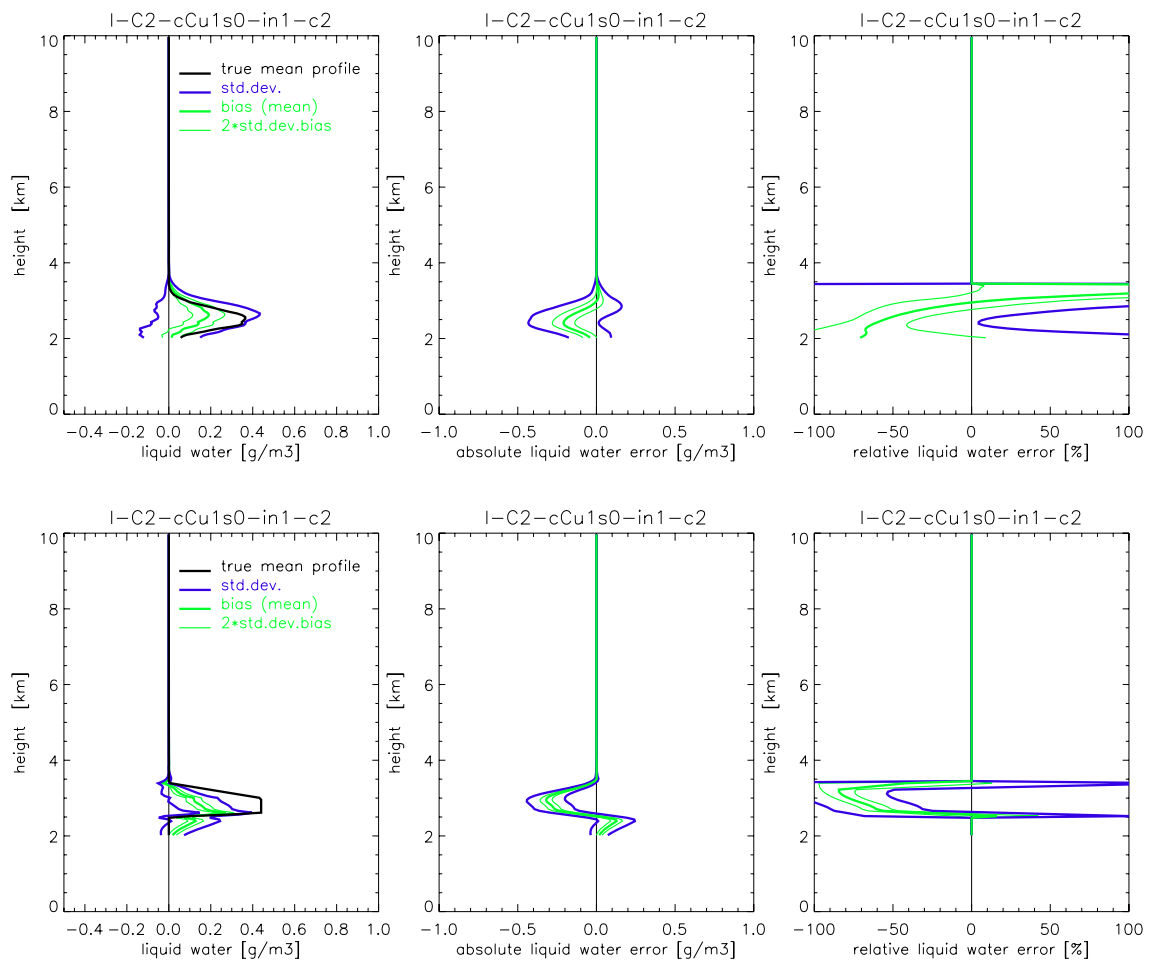


Fig. 3.2.9. Liquid water sample of reference profiles (upper panels) and single reference profile (lower panels) retrieval results for the mid-lat summer case (C2), instrumental errors (ine) scenario (therm. noise, C/No 67 dBHz, ampl. drift 0.33%/20sec, 1/f noise 0.01*T%, T=1-20sec). Statistics performance results (standard deviation, bias, 2 x std.deviation of bias) for an ensemble of 40 profiles are shown. The std.deviation are shown as +/- envelopes about the bias profiles. In the middle panels (for humidity and temperature) and the right panel (for humidity) the observational requirements, as set by the ACE+ MRD (v2.1/Jan 2004), are shown for reference (solid black, threshold requirements; dashed black, target requirements).

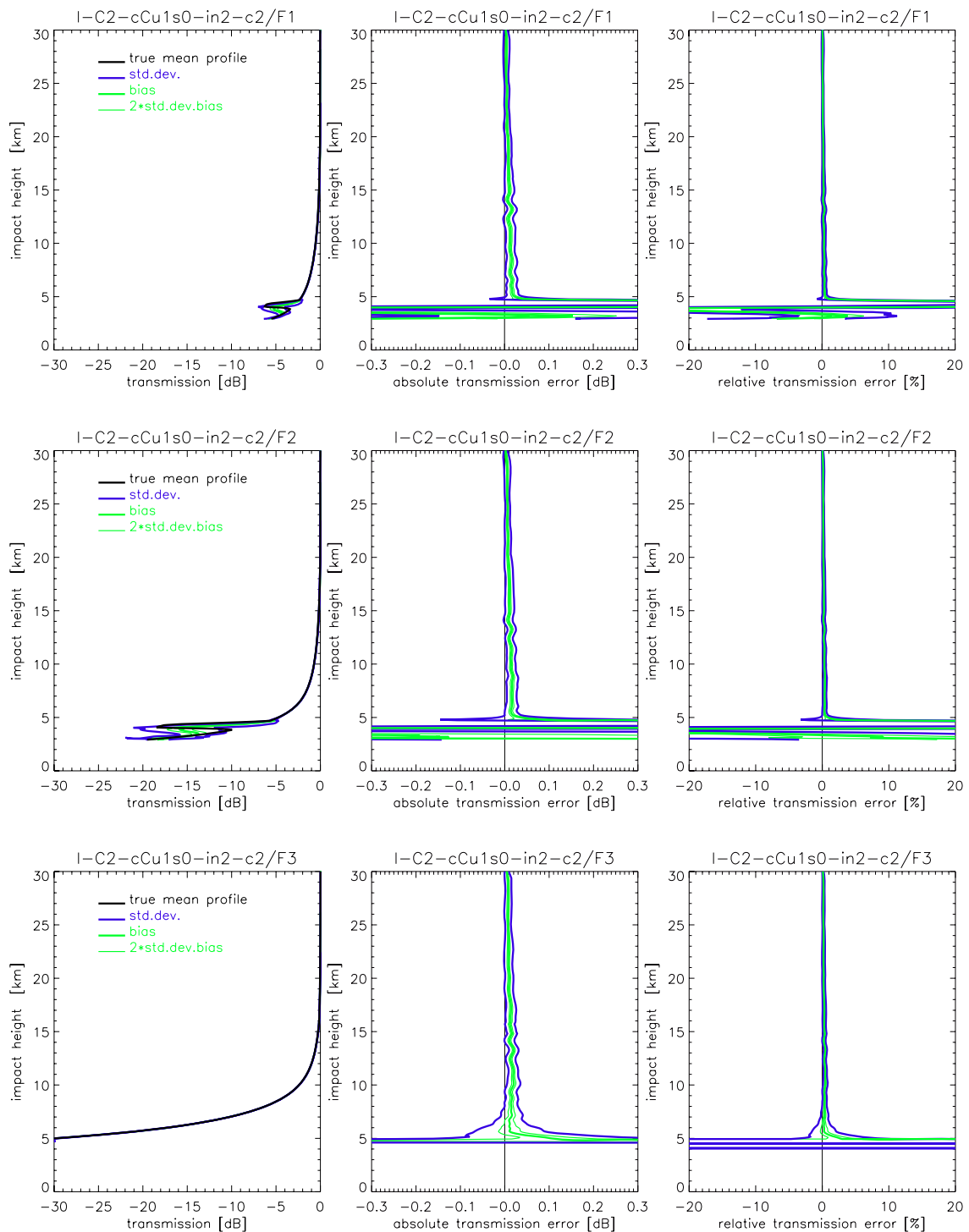


Fig. 3.2.10 Transmission retrieval results for the ACE+ frequencies F1 = 9.7 GHz (top panels), F2 = 17.25 GHz (middle panels), and F3 = 22.6 GHz (bottom panels) for the mid-lat summer case (C2), instrumental errors (ine) scenario (therm. noise, C/No 67 dBHz, ampl. drift 0.62%/20sec, 1/f noise 0.02*T%, T=1-20sec). Statistics performance results (standard deviation, bias, 2 x std.deviation of bias) for an ensemble of 40 profiles are shown. The std.deviation is shown as +/- envelopes about the bias profile.

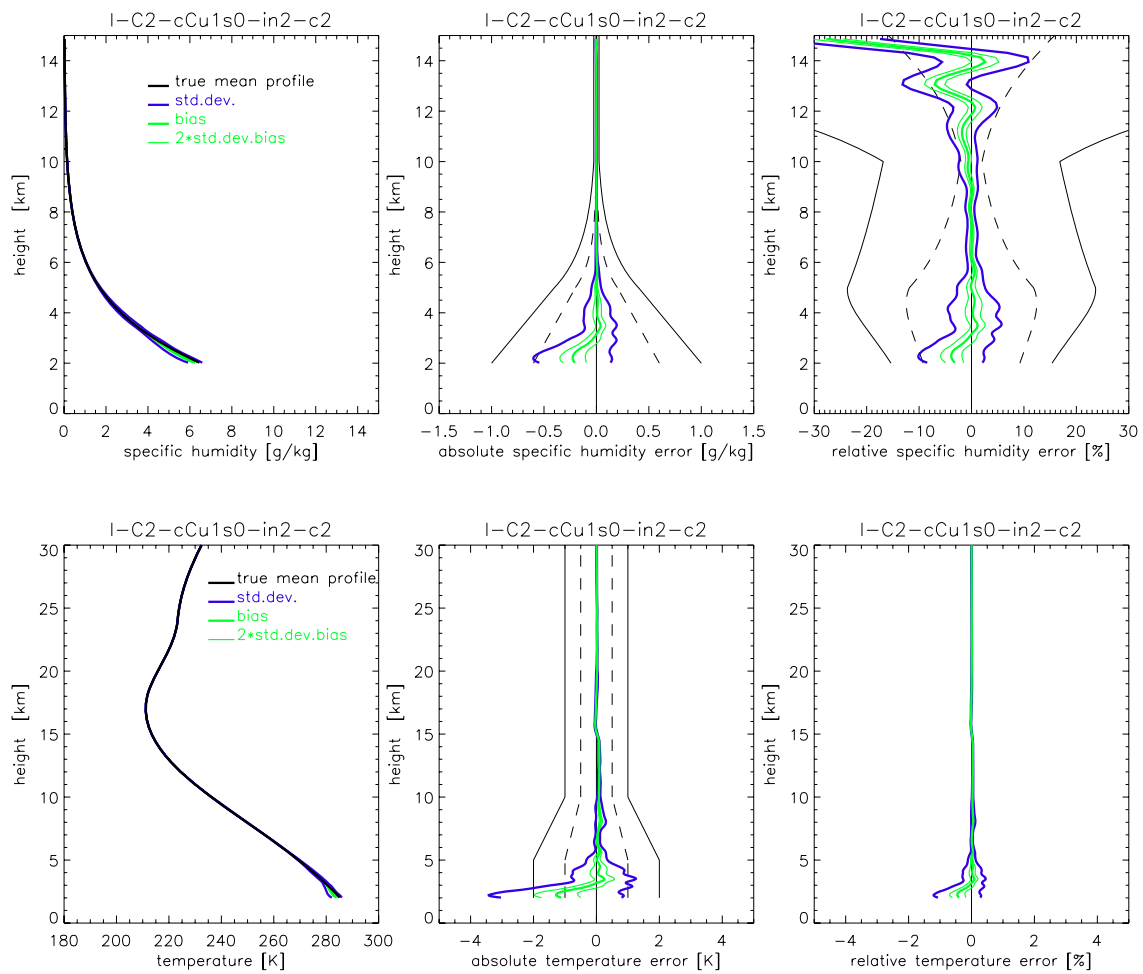


Fig. 3.2.11. Humidity (upper panels) and temperature (lower panels) retrieval results for the mid-lat summer case (C2), instrumental errors (ine) scenario (therm. noise, C/No 67 dBHz, ampl. drift 0.62%/20sec, 1/f noise 0.02*T%, T=1-20sec). Statistics performance results (standard deviation, bias, 2 x std.deviation of bias) for an ensemble of 40 profiles are shown. The std.deviation are shown as +/- envelopes about the bias profiles. In the middle panels (for humidity and temperature) and the right panel (for humidity) the observational requirements, as set by the ACE+ MRD (v2.1/Jan 2004), are shown for reference (solid black, threshold requirements; dashed black, target requirements).

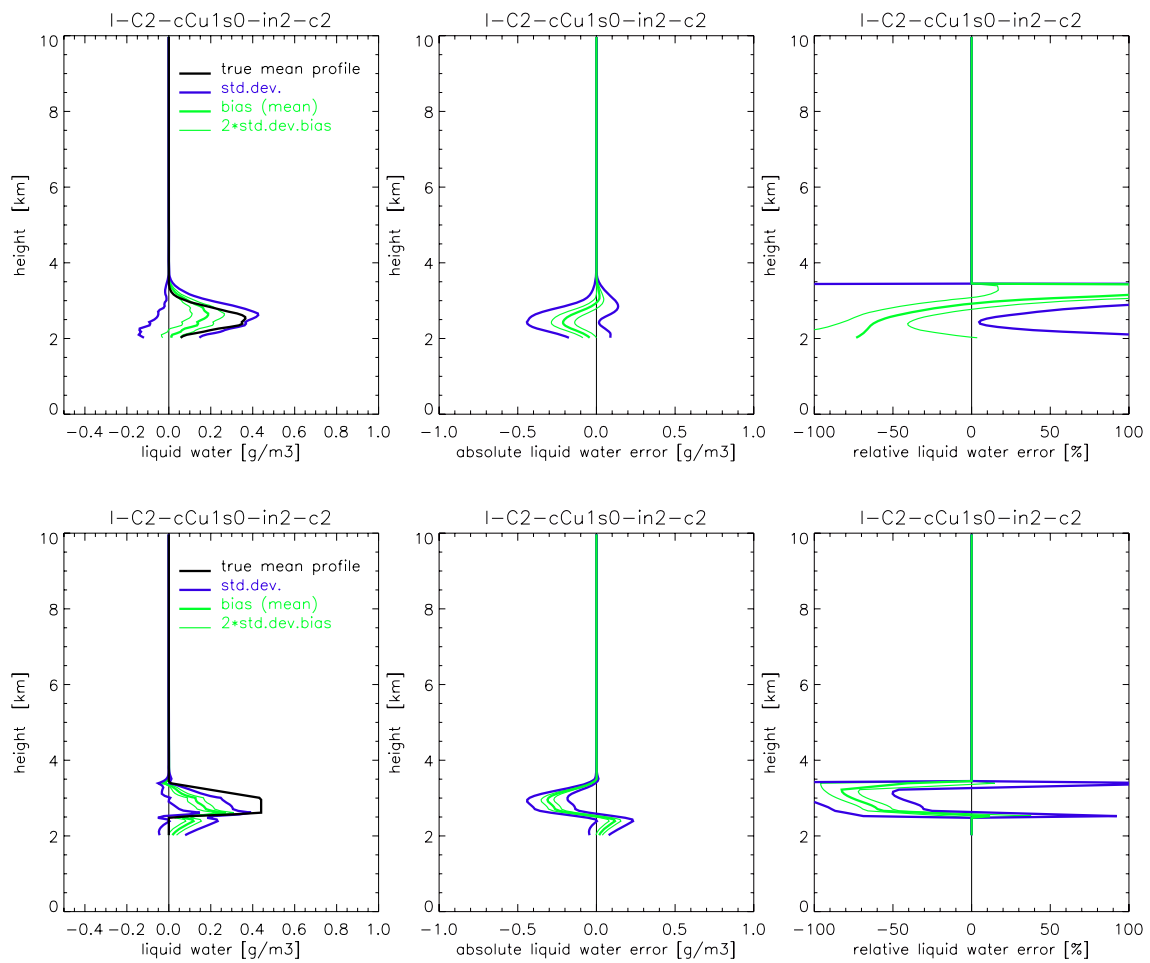


Fig. 3.2.12. Liquid water sample of reference profiles (upper panels) and single reference profile (lower panels) retrieval results for the mid-lat summer case (C2), instrumental errors (ine) scenario (therm. noise, C/No 67 dBHz, ampl. drift 0.62%/20sec, 1/f noise 0.02*T%, T=1-20sec). Statistics performance results (standard deviation, bias, 2 x std.deviation of bias) for an ensemble of 40 profiles are shown. The std.deviations are shown as +/- envelopes about the bias profiles. In the middle panels (for humidity and temperature) and the right panel (for humidity) the observational requirements, as set by the ACE+ MRD (v2.1/Jan 2004), are shown for reference (solid black, threshold requirements; dashed black, target requirements).

3.3. Results on Retrieval Performance in Presence of Clouds and Atmospheric Turbulence

This section shows transmission, humidity, temperature, and liquid water retrieval results for the mid-latitude summer case (C2) in presence of randomized clouds, 3D As and 3D Cu respectively, plus mean-case scintillations (Mea) due to atmospheric turbulence superposed. Furthermore, two different kinds of total instrumental errors were superposed. These 2×2 scenarios (2 atmospheric cases, each with 2 instrumental error cases) were then processed with the inversion/retrieval processing system using two different retrieval algorithms. For a detailed description of the specifications for these scenarios see the introduction to section 3 on pages 29 – 30.

The results of the $2 \times 2 \times 2$ cloudy-turbulent air retrieval scenarios are shown on the following pages 105 – 124.

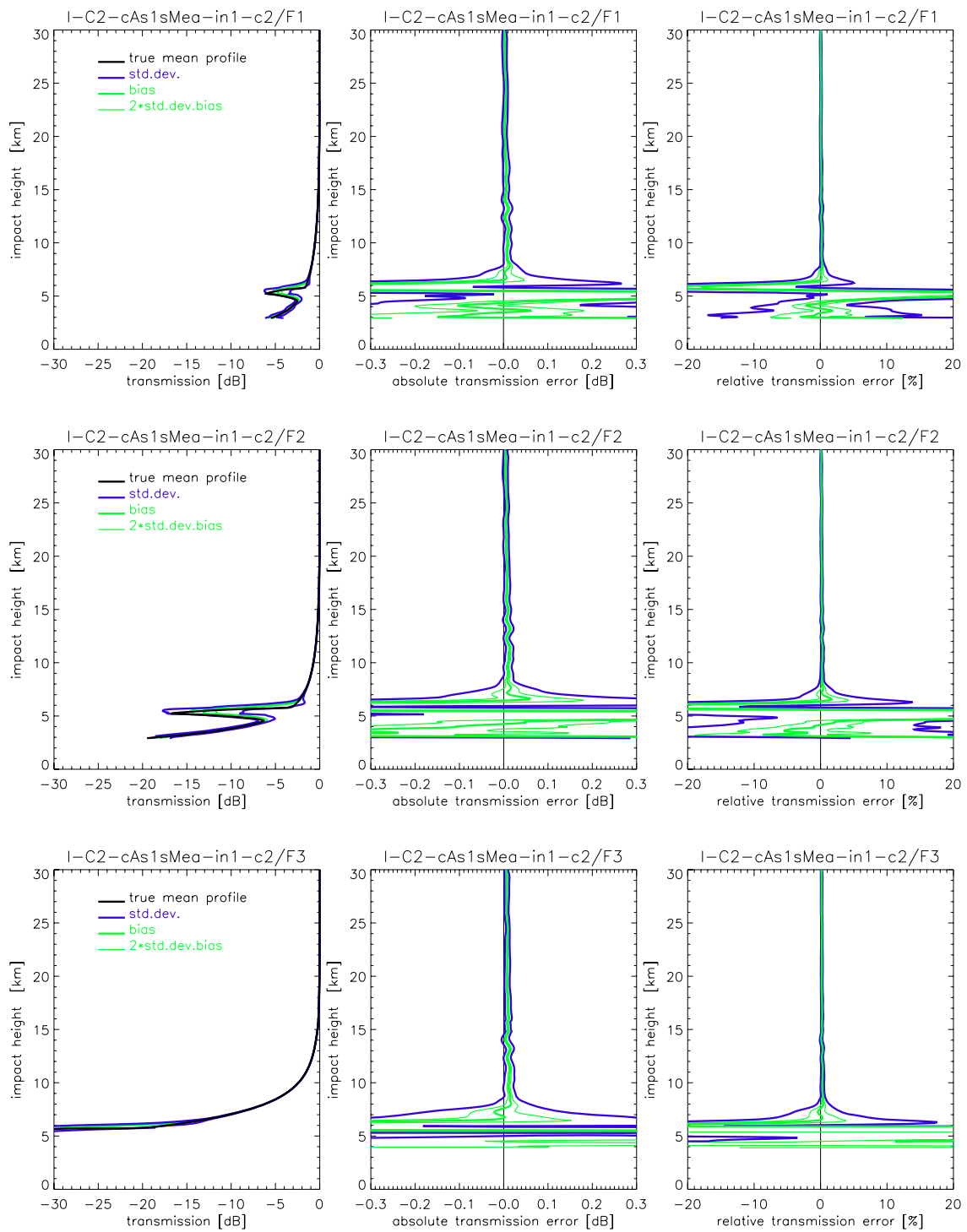


Fig. 3.3.1 Transmission retrieval results for the ACE+ frequencies F1 = 9.7 GHz (top panels), F2 = 17.25 GHz (middle panels), and F3 = 22.6 GHz (bottom panels) for the mid-lat summer case (C2), instrumental errors (in1) scenario (therm. noise, C/No 67 dBHz, ampl. drift 0.33%/20sec, 1/f noise 0.01*T%, T=1-20sec). Statistics performance results (standard deviation, bias, 2 x std.deviation of bias) for an ensemble of 40 profiles are shown. The std.deviation are shown as +/- envelopes about the bias profile.

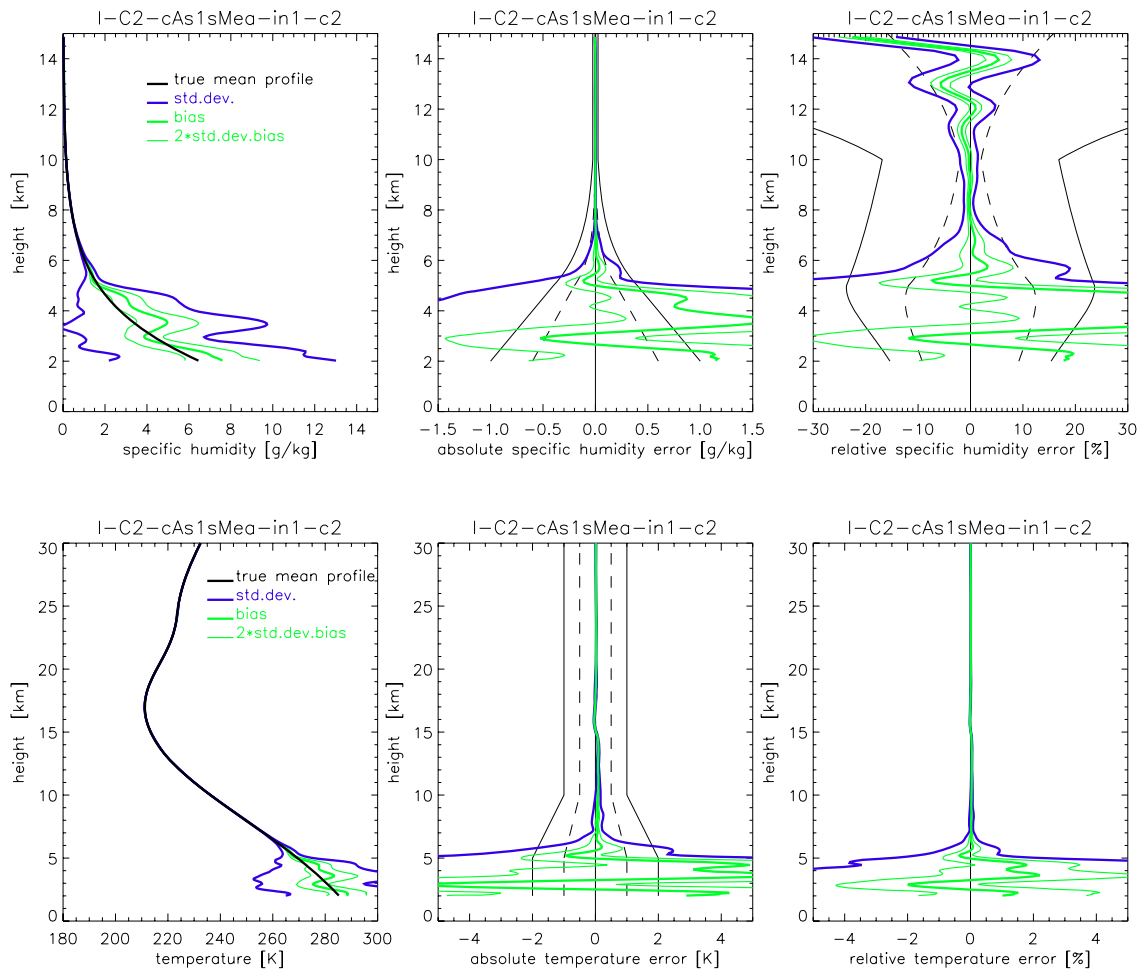


Fig. 3.3.2. Humidity (upper panels) and temperature (lower panels) retrieval results for the mid-lat summer case (C2), instrumental errors (in1) scenario (therm. noise, C/No 67 dBHz, ampl. drift 0.33%/20sec, 1/f noise 0.01*T%, T=1-20sec, standard cloudy air retrieval). Statistics performance results (standard deviation, bias, 2 x std.deviation of bias) for an ensemble of 40 profiles are shown. The std.deviation is shown as +/- envelopes about the bias profiles. In the middle panels (for humidity and temperature) and the right panel (for humidity) the observational requirements, as set by the ACE+MRD (v2.1/Jan 2004), are shown for reference (solid black, threshold requirements; dashed black, target requirements).

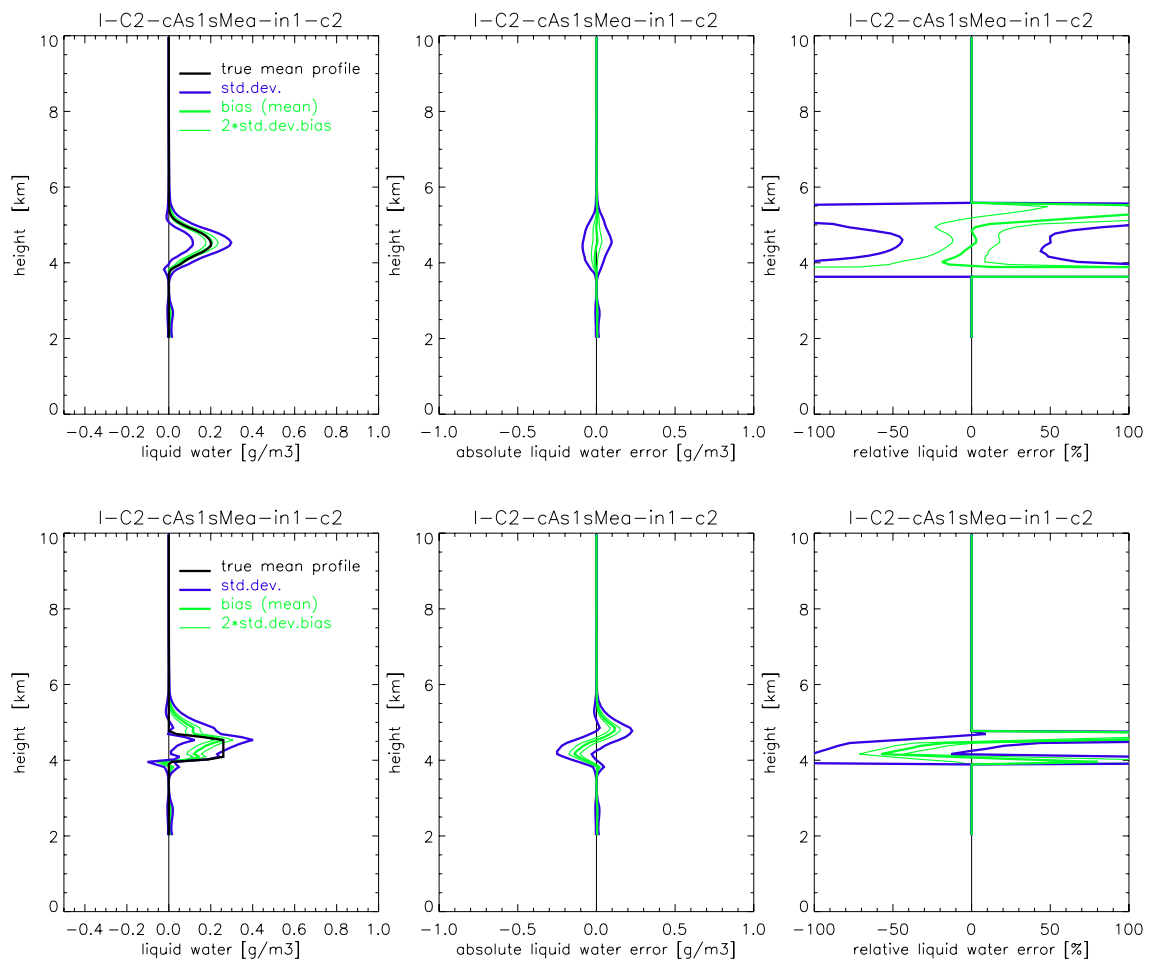


Fig. 3.3.3. Liquid water sample of reference profiles (upper panels) and single reference profile (lower panels) retrieval results for the mid-lat summer case (C2), instrumental errors (in1) scenario (therm. noise, C/No 67 dBHz, ampl. drift 0.33%/20sec, 1/f noise 0.01*T%, T=1-20sec, standard cloudy air retrieval). Statistics performance results (standard deviation, bias, 2 x std.deviation of bias) for an ensemble of 40 profiles are shown. The std.deviation is shown as +/- envelopes about the bias profiles. In the middle panels (for humidity and temperature) and the right panel (for humidity) the observational requirements, as set by the ACE+ MRD (v2.1/Jan 2004), are shown for reference (solid black, threshold requirements; dashed black, target requirements).

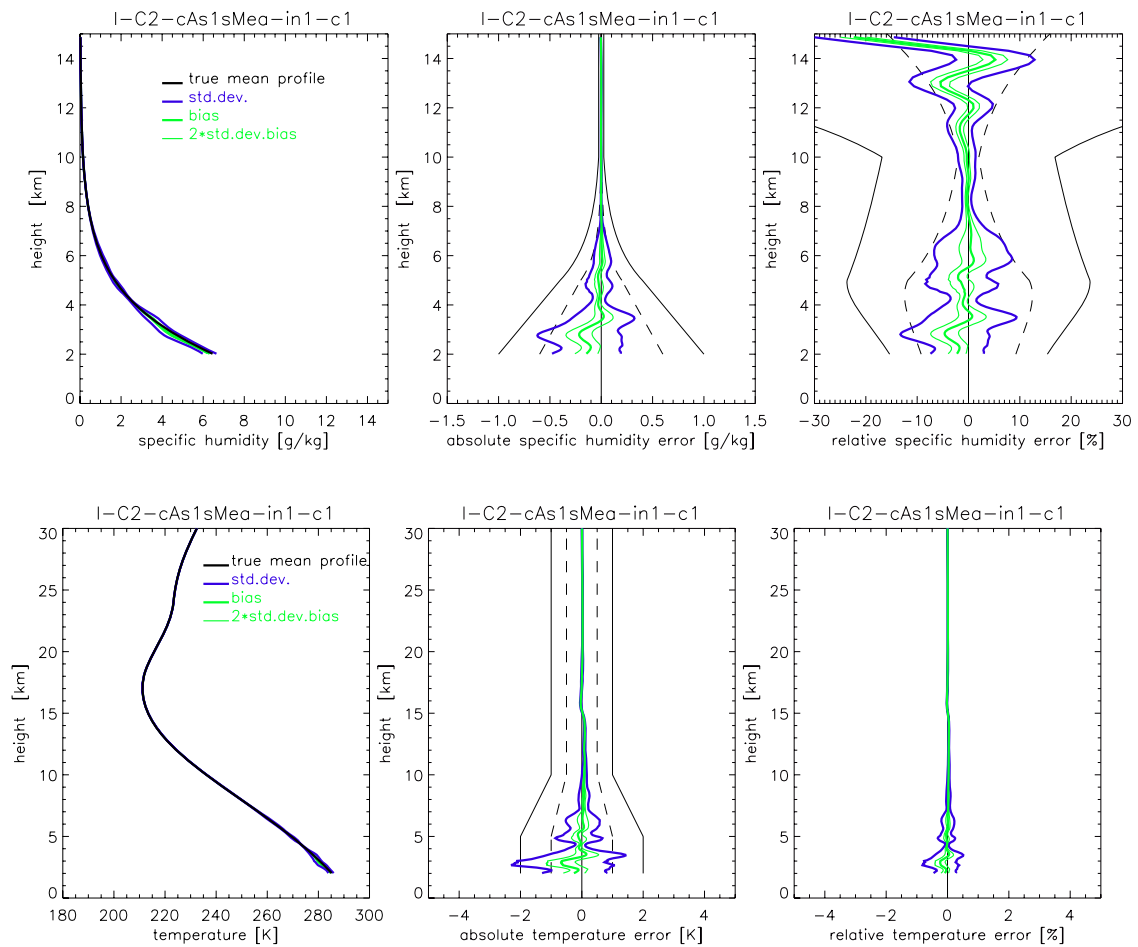


Fig. 3.3.4. Humidity (upper panels) and temperature (lower panels) retrieval results for the mid-lat summer case (C2), instrumental errors (in1) scenario (therm. noise, C/No 67 dBHz, ampl. drift 0.33%/20sec, 1/f noise 0.01*T%, T=1-20sec, advanced cloudy air retrieval). Statistics performance results (standard deviation, bias, 2 x std.deviation of bias) for an ensemble of 40 profiles are shown. The std.deviation is shown as +/- envelopes about the bias profiles. In the middle panels (for humidity and temperature) and the right panel (for humidity) the observational requirements, as set by the ACE+MRD (v2.1/Jan 2004), are shown for reference (solid black, threshold requirements; dashed black, target requirements).

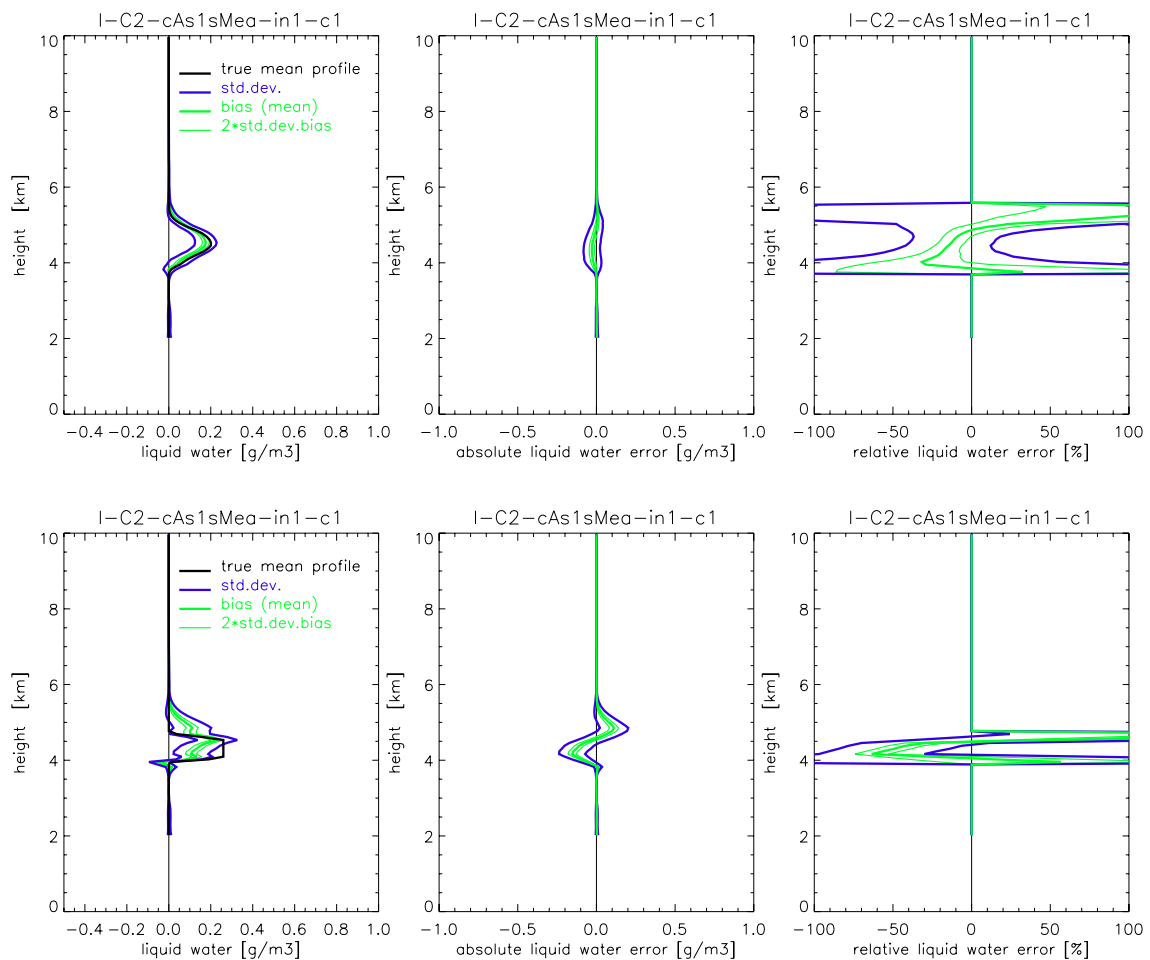


Fig. 3.3.5. Liquid water sample of reference profiles (upper panels) and single reference profile (lower panels) retrieval results for the mid-lat summer case (C2), instrumental errors (in1) scenario (therm. noise, C/No 67 dBHz, ampl. drift 0.33%/20sec, 1/f noise 0.01*T%, T=1-20sec, advanced cloudy air retrieval). Statistics performance results (standard deviation, bias, 2 x std.deviation of bias) for an ensemble of 40 profiles are shown. The std.deviation is shown as +/- envelopes about the bias profiles. In the middle panels (for humidity and temperature) and the right panel (for humidity) the observational requirements, as set by the ACE+ MRD (v2.1/Jan 2004), are shown for reference (solid black, threshold requirements; dashed black, target requirements).

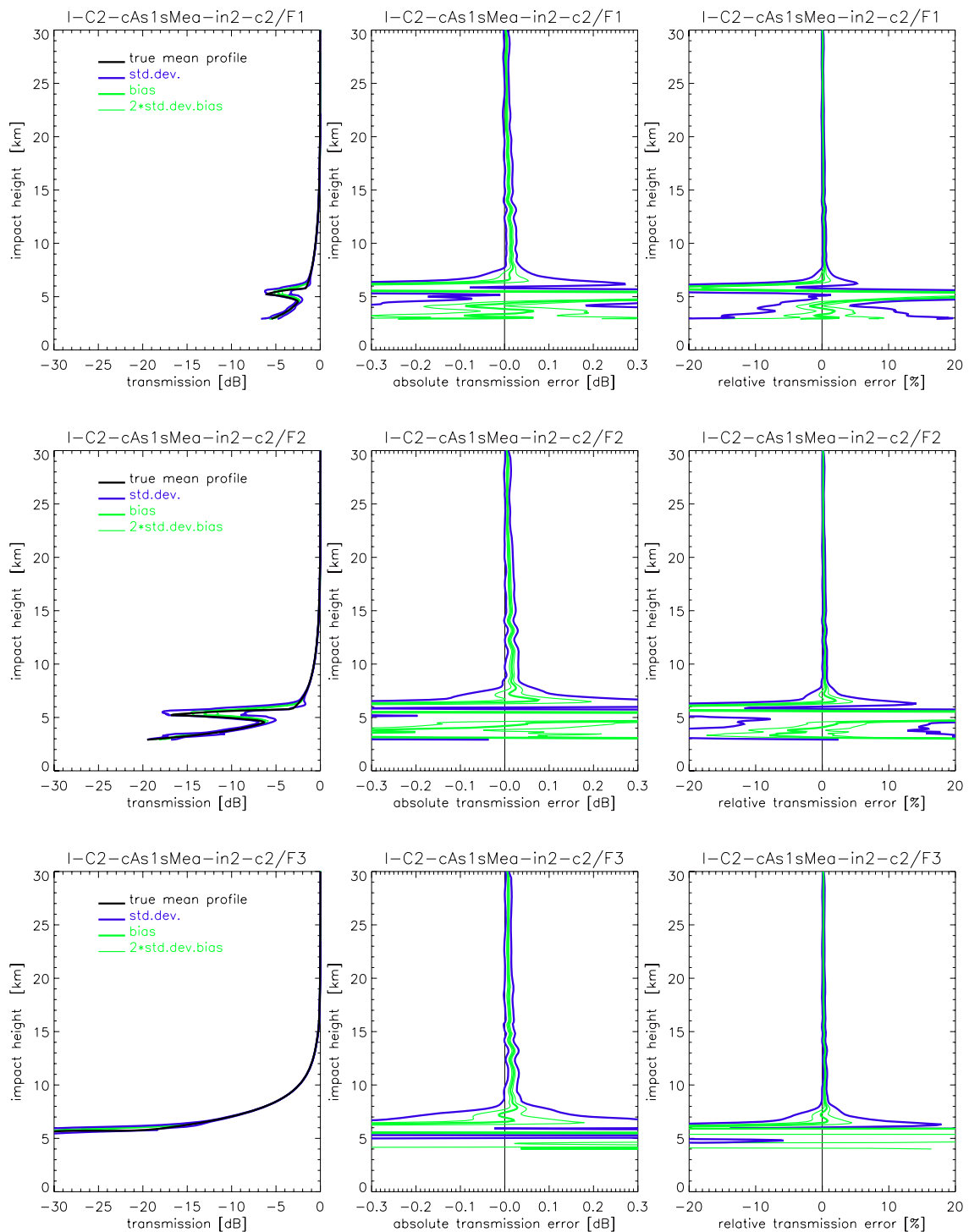


Fig. 3.3.6 Transmission retrieval results for the ACE+ frequencies F1 = 9.7 GHz (top panels), F2 = 17.25 GHz (middle panels), and F3 = 22.6 GHz (bottom panels) for the mid-lat summer case (C2), instrumental errors (in2) scenario (therm. noise, C/No 67 dBHz, ampl. drift 0.62%/20sec, 1/f noise 0.02*T%, T=1-20sec). Statistics performance results (standard deviation, bias, 2 x std.deviation of bias) for an ensemble of 40 profiles are shown. The std.deviation is shown as +/- envelopes about the bias profile.

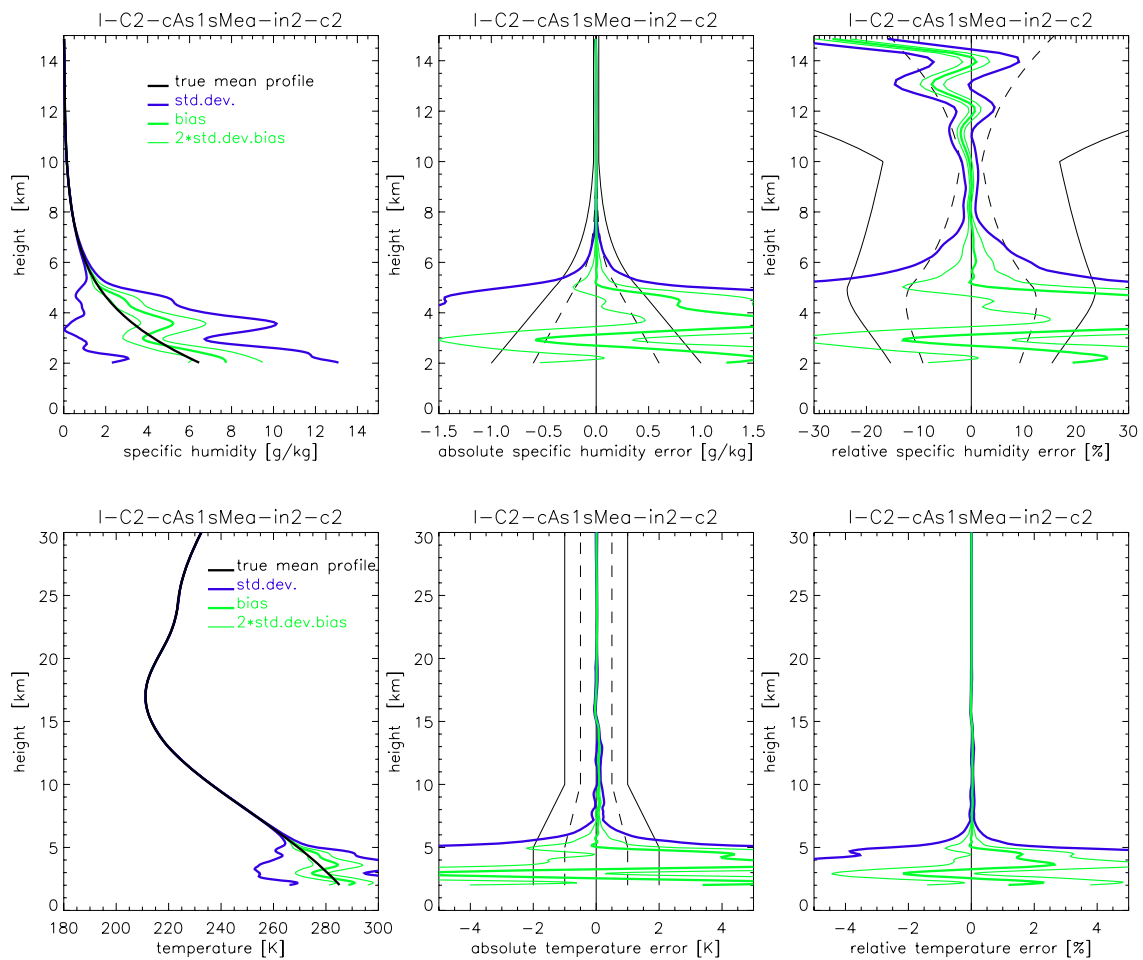


Fig. 3.3.7. Humidity (upper panels) and temperature (lower panels) retrieval results for the mid-lat summer case (C2), instrumental errors (in2) scenario (therm. noise, C/No 67 dBHz, ampl. drift 0.62%/20sec, 1/f noise 0.02*T%, T=1-20sec, standard cloudy air retrieval). Statistics performance results (standard deviation, bias, 2 x std.deviation of bias) for an ensemble of 40 profiles are shown. The std.deviation is shown as +/- envelopes about the bias profiles. In the middle panels (for humidity and temperature) and the right panel (for humidity) the observational requirements, as set by the ACE+MRD (v2.1/Jan 2004), are shown for reference (solid black, threshold requirements; dashed black, target requirements).

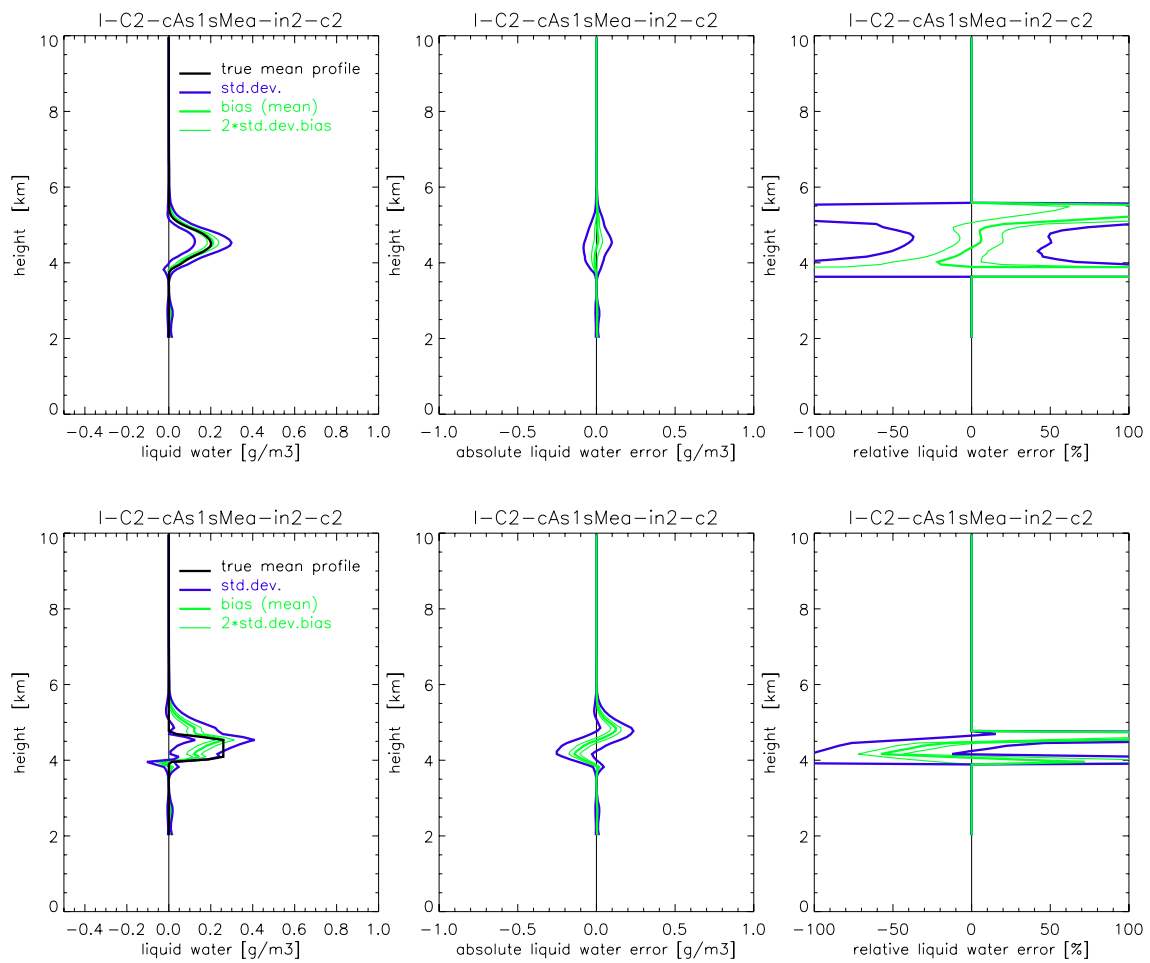


Fig. 3.3.8. Liquid water sample of reference profiles (upper panels) and single reference profile (lower panels) retrieval results for the mid-lat summer case (C2), instrumental errors (in2) scenario (therm. noise, C/No 67 dBHz, ampl. drift 0.62%/20sec, 1/f noise 0.02*T%, T=1-20sec, standard cloudy air retrieval). Statistics performance results (standard deviation, bias, 2 x std.deviation of bias) for an ensemble of 40 profiles are shown. The std.deviation is shown as +/- envelopes about the bias profiles. In the middle panels (for humidity and temperature) and the right panel (for humidity) the observational requirements, as set by the ACE+ MRD (v2.1/Jan 2004), are shown for reference (solid black, threshold requirements; dashed black, target requirements).

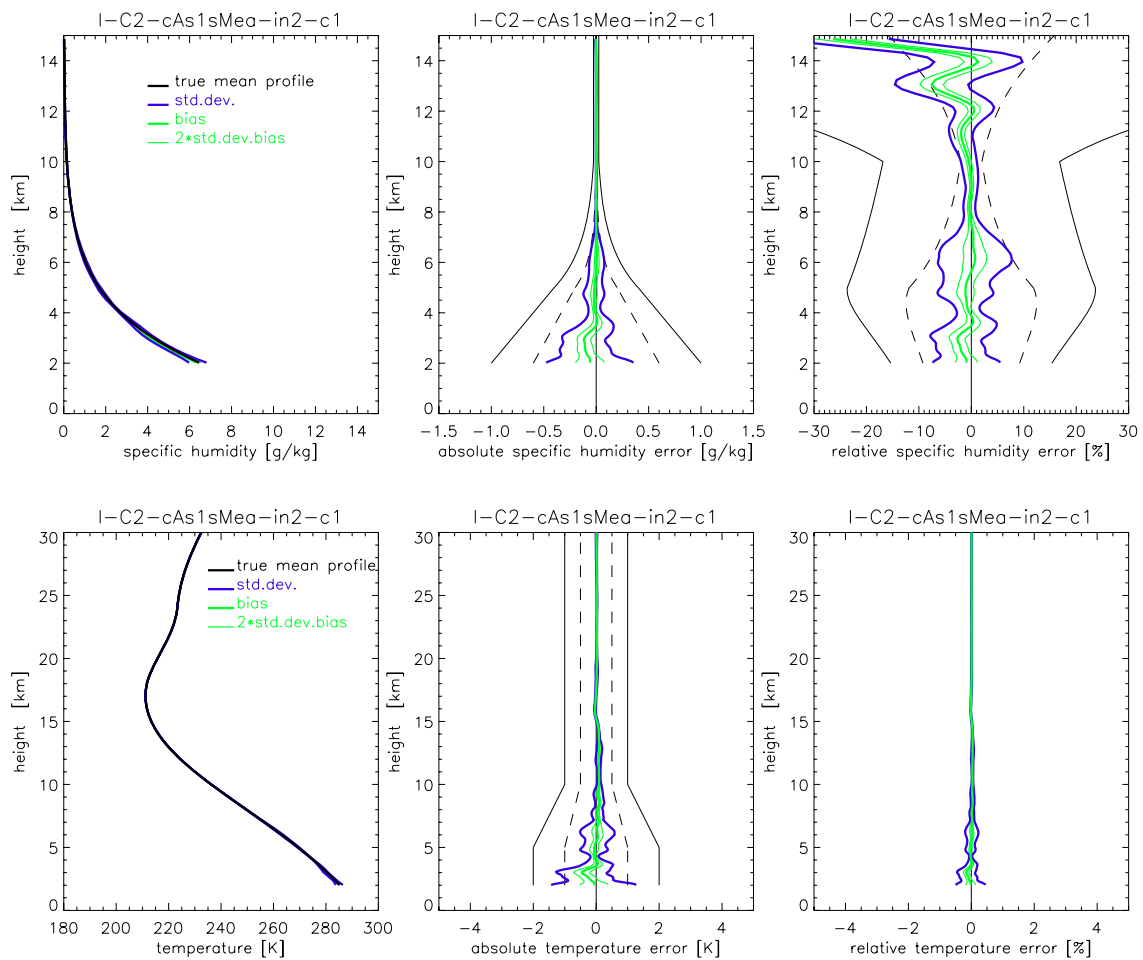


Fig. 3.3.9. Humidity (upper panels) and temperature (lower panels) retrieval results for the mid-lat summer case (C2), instrumental errors (in2) scenario (therm. noise, C/No 67 dBHz, ampl. drift 0.62%/20sec, 1/f noise 0.02*T%, T=1-20sec, advanced cloudy air retrieval). Statistics performance results (standard deviation, bias, 2 x std.deviation of bias) for an ensemble of 40 profiles are shown. The std.deviation is shown as +/- envelopes about the bias profiles. In the middle panels (for humidity and temperature) and the right panel (for humidity) the observational requirements, as set by the ACE+MRD (v2.1/Jan 2004), are shown for reference (solid black, threshold requirements; dashed black, target requirements).

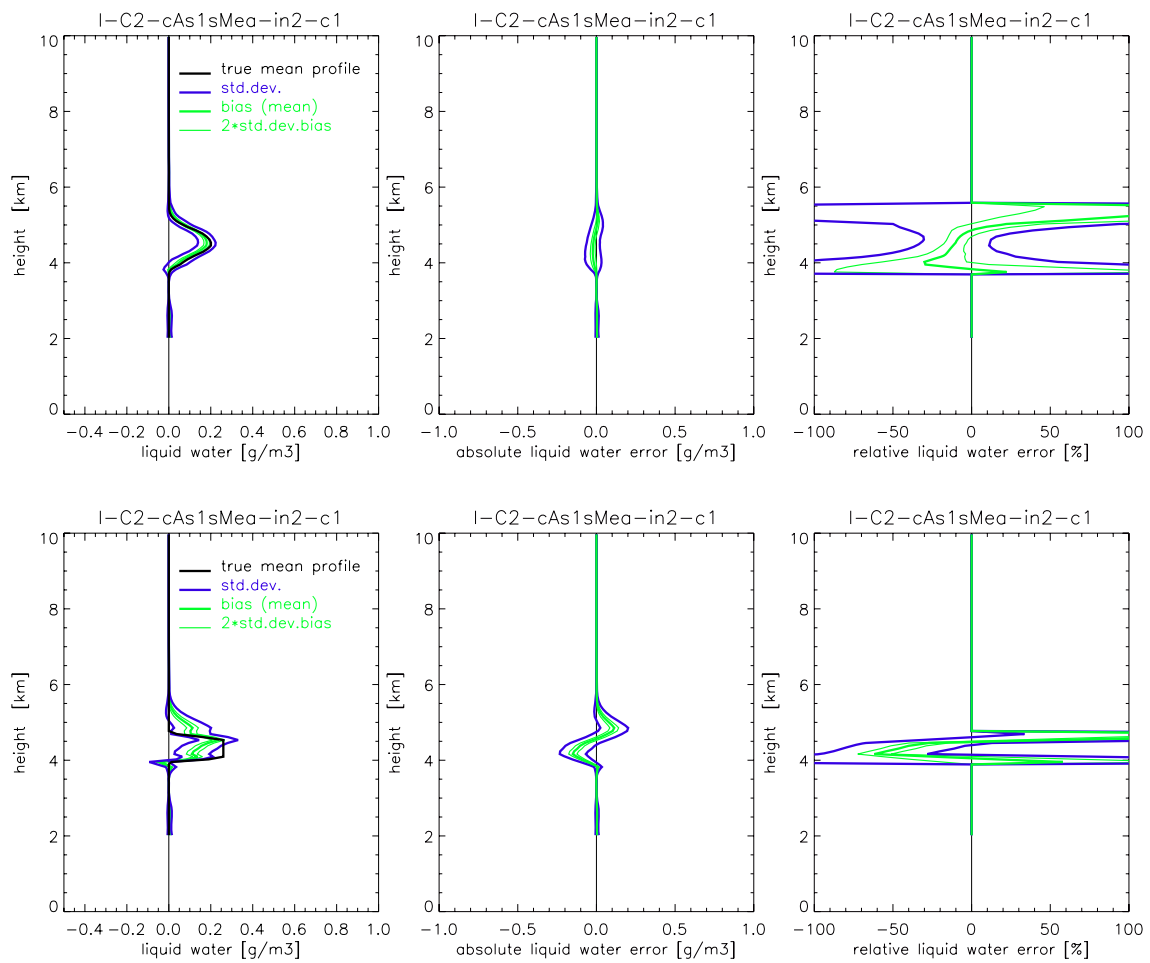


Fig. 3.3.10. Liquid water sample of reference profiles (upper panels) and single reference profile (lower panels) retrieval results for the mid-lat summer case (C2), instrumental errors (in2) scenario (therm. noise, C/No 67 dBHz, ampl. drift 0.62%/20sec, 1/f noise 0.02*T%, T=1-20sec, advanced cloudy air retrieval). Statistics performance results (standard deviation, bias, 2 x std.deviation of bias) for an ensemble of 40 profiles are shown. The std.deviation is shown as +/- envelopes about the bias profiles. In the middle panels (for humidity and temperature) and the right panel (for humidity) the observational requirements, as set by the ACE+ MRD (v2.1/Jan 2004), are shown for reference (solid black, threshold requirements; dashed black, target requirements).

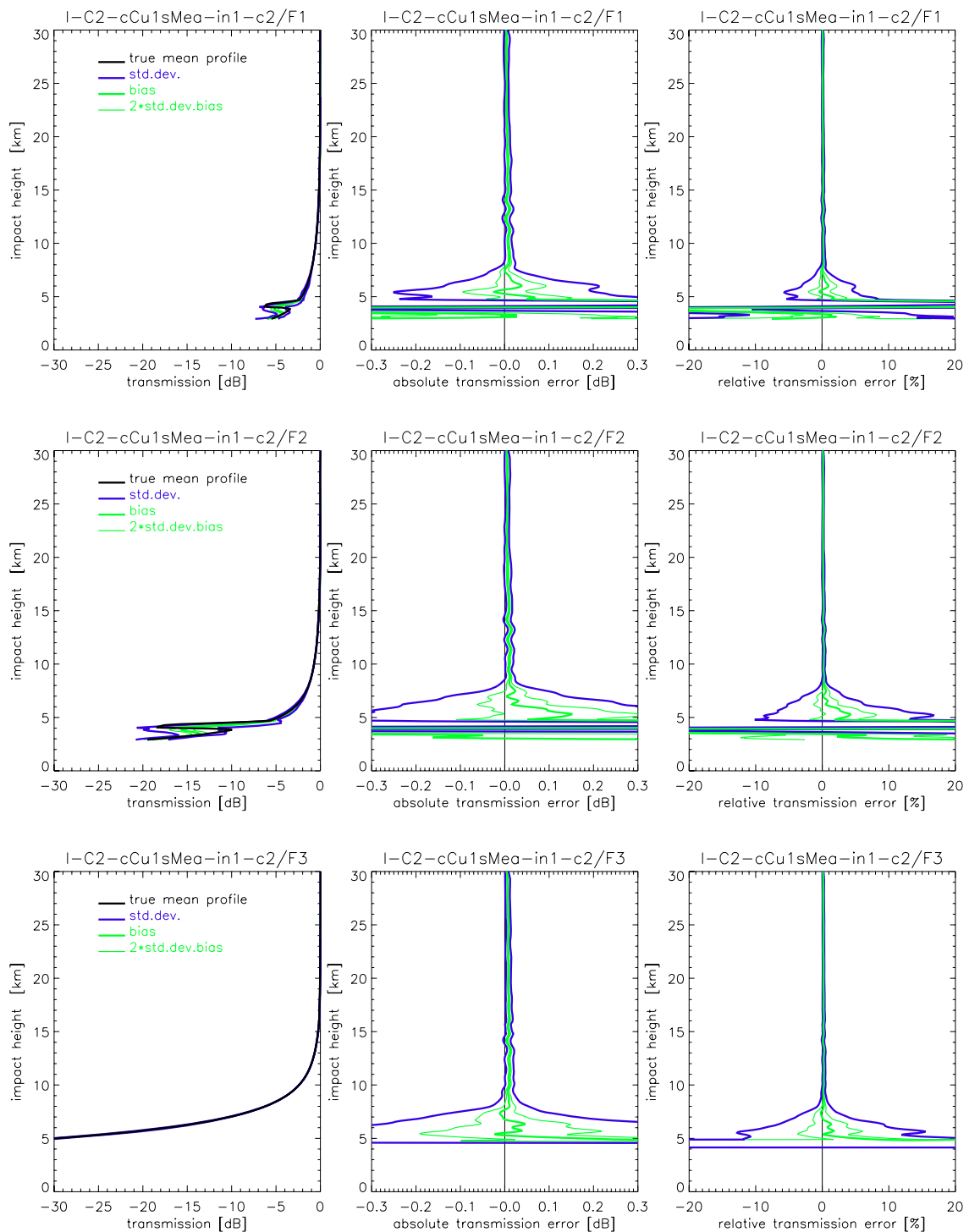


Fig. 3.3.11 Transmission retrieval results for the ACE+ frequencies F1 = 9.7 GHz (top panels), F2 = 17.25 GHz (middle panels), and F3 = 22.6 GHz (bottom panels) for the mid-lat summer case (C2), instrumental errors (in1) scenario (therm. noise, C/No 67 dBHz, ampl. drift 0.33%/20sec, 1/f noise 0.01*T%, T=1-20sec). Statistics performance results (standard deviation, bias, 2 x std.deviation of bias) for an ensemble of 40 profiles are shown. The std.deviation is shown as +/- envelopes about the bias profile.

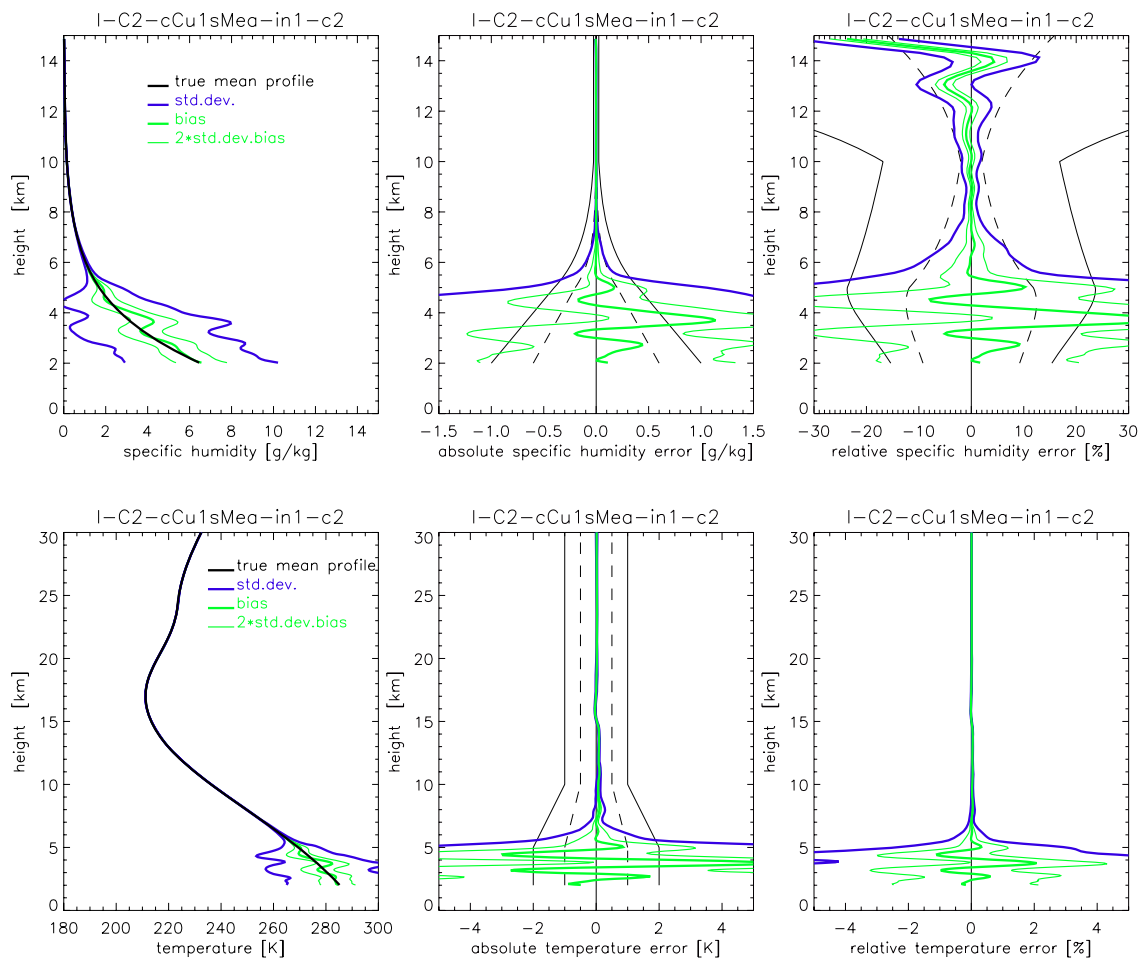


Fig. 3.3.12. Humidity (upper panels) and temperature (lower panels) retrieval results for the mid-lat summer case (C2), instrumental errors (in1) scenario (therm. noise, C/No 67 dBHz, ampl. drift 0.33%/20sec, 1/f noise 0.01*T%, T=1-20sec, standard cloudy air retrieval). Statistics performance results (standard deviation, bias, 2 x std.deviation of bias) for an ensemble of 40 profiles are shown. The std.deviation is shown as +/- envelopes about the bias profiles. In the middle panels (for humidity and temperature) and the right panel (for humidity) the observational requirements, as set by the ACE+MRD (v2.1/Jan 2004), are shown for reference (solid black, threshold requirements; dashed black, target requirements).

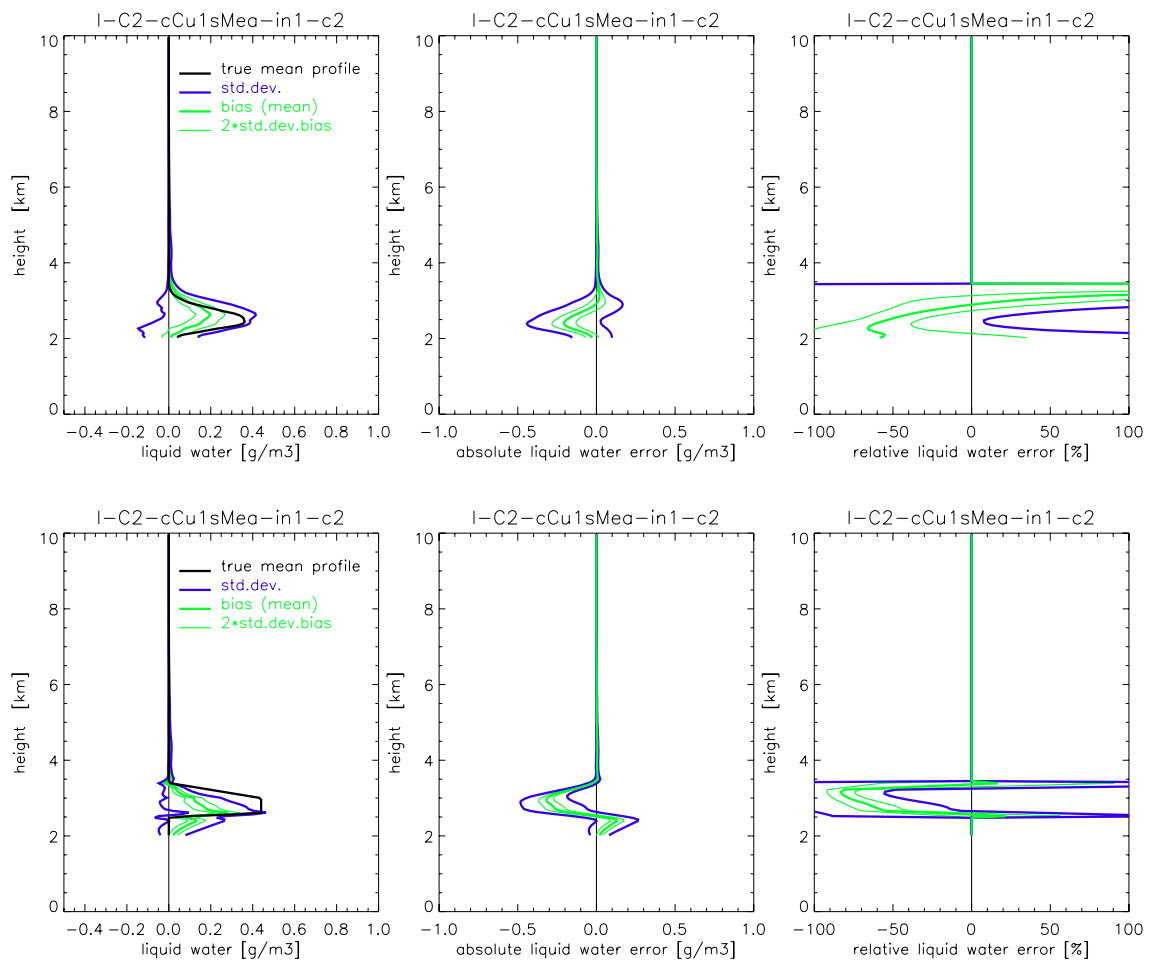


Fig. 3.3.13. Liquid water sample of reference profiles (upper panels) and single reference profile (lower panels) retrieval results for the mid-lat summer case (C2), instrumental errors (in1) scenario (therm. noise, C/No 67 dBHz, ampl. drift 0.33%/20sec, 1/f noise 0.01*T%, T=1-20sec, standard cloudy air retrieval). Statistics performance results (standard deviation, bias, 2 x std.deviation of bias) for an ensemble of 40 profiles are shown. The std.deviation is shown as +/- envelopes about the bias profiles. In the middle panels (for humidity and temperature) and the right panel (for humidity) the observational requirements, as set by the ACE+ MRD (v2.1/Jan 2004), are shown for reference (solid black, threshold requirements; dashed black, target requirements).

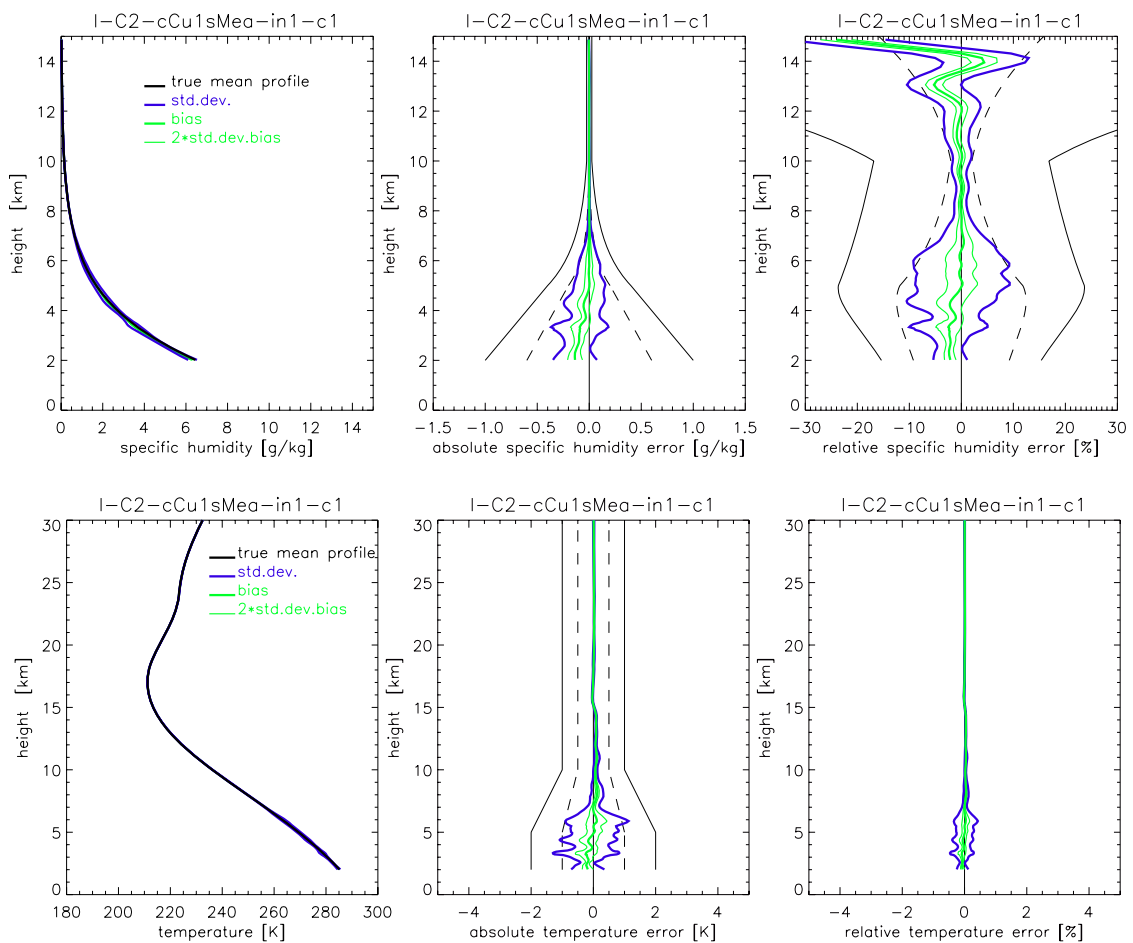


Fig. 3.3.14. Humidity (upper panels) and temperature (lower panels) retrieval results for the mid-lat summer case (C2), instrumental errors (in1) scenario (therm. noise, C/No 67 dBHz, ampl. drift 0.33%/20sec, 1/f noise 0.01*T%, T=1-20sec, advanced cloudy air retrieval). Statistics performance results (standard deviation, bias, 2 x std.deviation of bias) for an ensemble of 40 profiles are shown. The std.deviation is shown as +/- envelopes about the bias profiles. In the middle panels (for humidity and temperature) and the right panel (for humidity) the observational requirements, as set by the ACE+MRD (v2.1/Jan 2004), are shown for reference (solid black, threshold requirements; dashed black, target requirements).

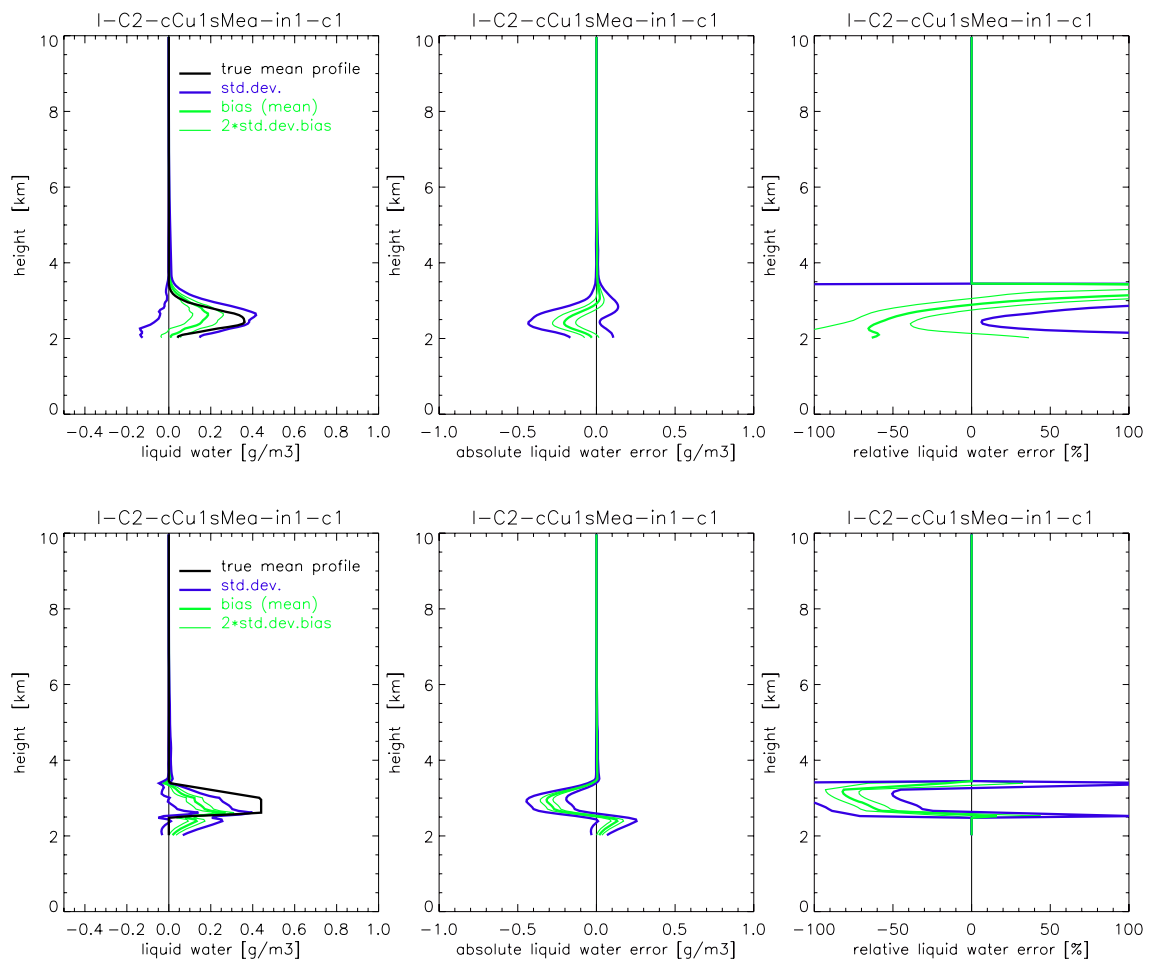


Fig. 3.3.15. Liquid water sample of reference profiles (upper panels) and single reference profile (lower panels) retrieval results for the mid-lat summer case (C2), instrumental errors (in1) scenario (therm. noise, C/No 67 dBHz, ampl. drift 0.33%/20sec, 1/f noise 0.01*T%, T=1-20sec, advanced cloudy air retrieval). Statistics performance results (standard deviation, bias, 2 x std.deviation of bias) for an ensemble of 40 profiles are shown. The std.deviation is shown as +/- envelopes about the bias profiles. In the middle panels (for humidity and temperature) and the right panel (for humidity) the observational requirements, as set by the ACE+ MRD (v2.1/Jan 2004), are shown for reference (solid black, threshold requirements; dashed black, target requirements).

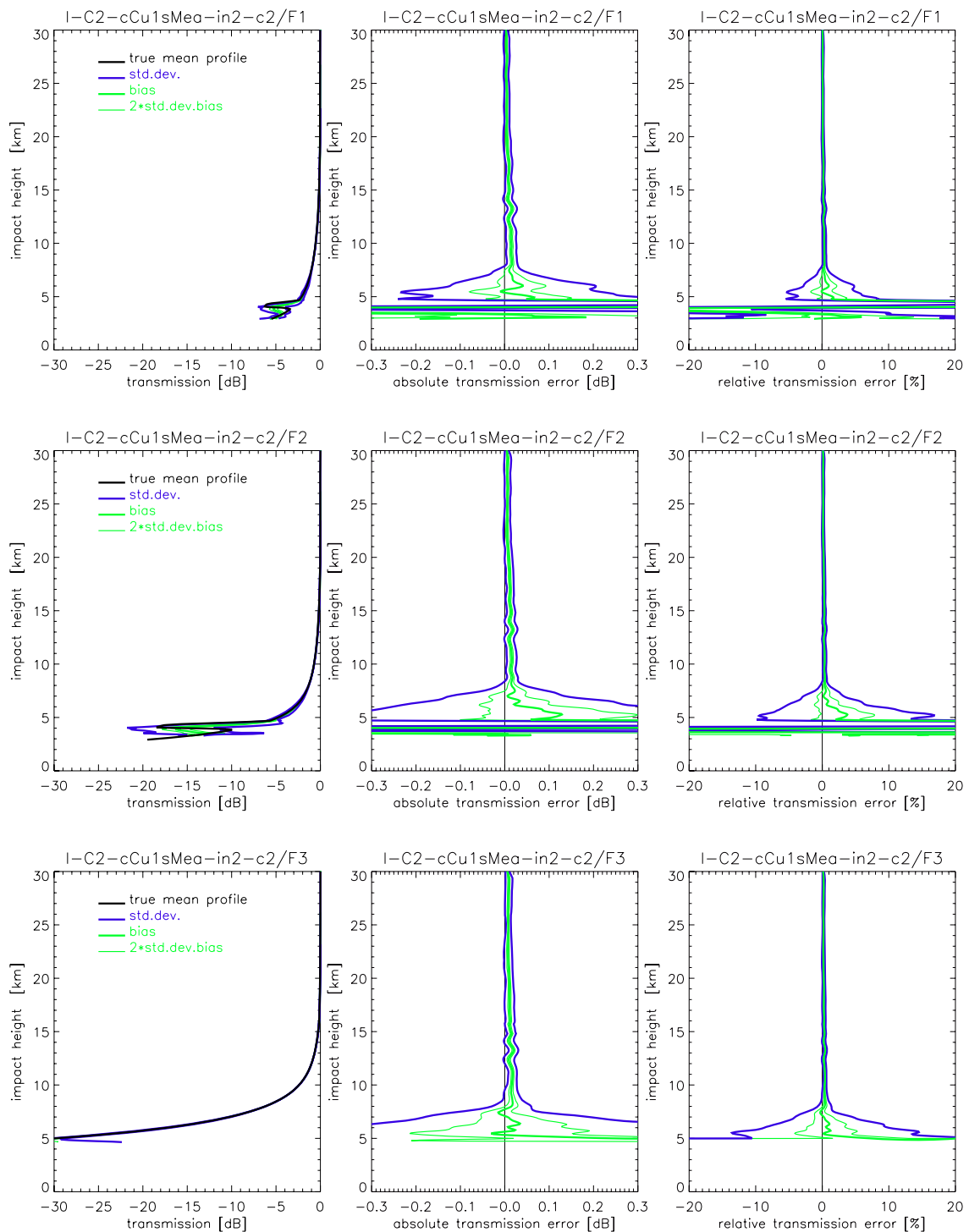


Fig. 3.3.16 Transmission retrieval results for the ACE+ frequencies F1 = 9.7 GHz (top panels), F2 = 17.25 GHz (middle panels), and F3 = 22.6 GHz (bottom panels) for the mid-lat summer case (C2), instrumental errors (in2) scenario (therm. noise, C/No 67 dBHz, ampl. drift 0.62%/20sec, 1/f noise 0.02*T%, T=1-20sec). Statistics performance results (standard deviation, bias, 2 x std.deviation of bias) for an ensemble of 40 profiles are shown. The std.deviation is shown as +/- envelopes about the bias profile.

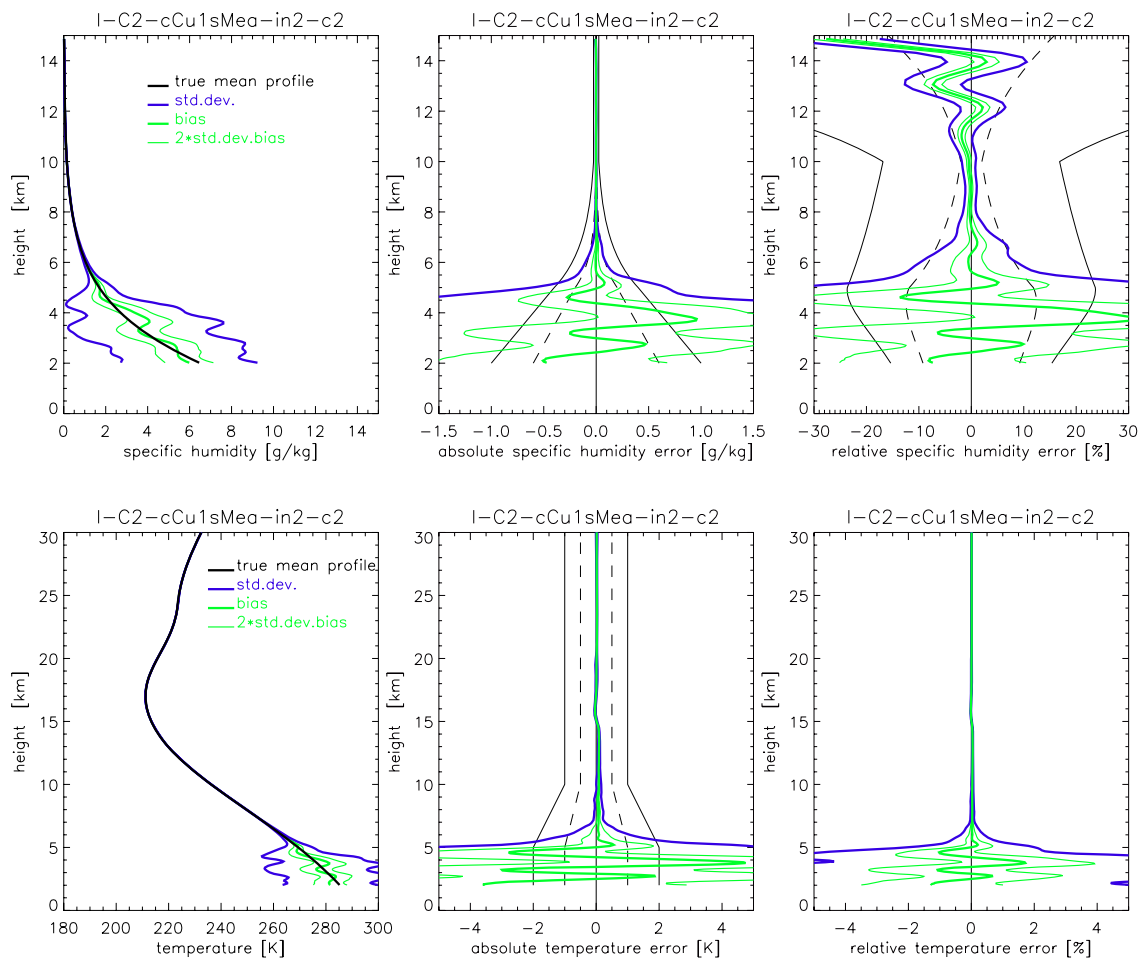


Fig. 3.3.17. Humidity (upper panels) and temperature (lower panels) retrieval results for the mid-lat summer case (C2), instrumental errors (in2) scenario (therm. noise, C/No 67 dBHz, ampl. drift 0.62%/20sec, 1/f noise 0.02*T%, T=1-20sec, standard cloudy air retrieval). Statistics performance results (standard deviation, bias, 2 x std.deviation of bias) for an ensemble of 40 profiles are shown. The std.deviation is shown as +/- envelopes about the bias profiles. In the middle panels (for humidity and temperature) and the right panel (for humidity) the observational requirements, as set by the ACE+MRD (v2.1/Jan 2004), are shown for reference (solid black, threshold requirements; dashed black, target requirements).

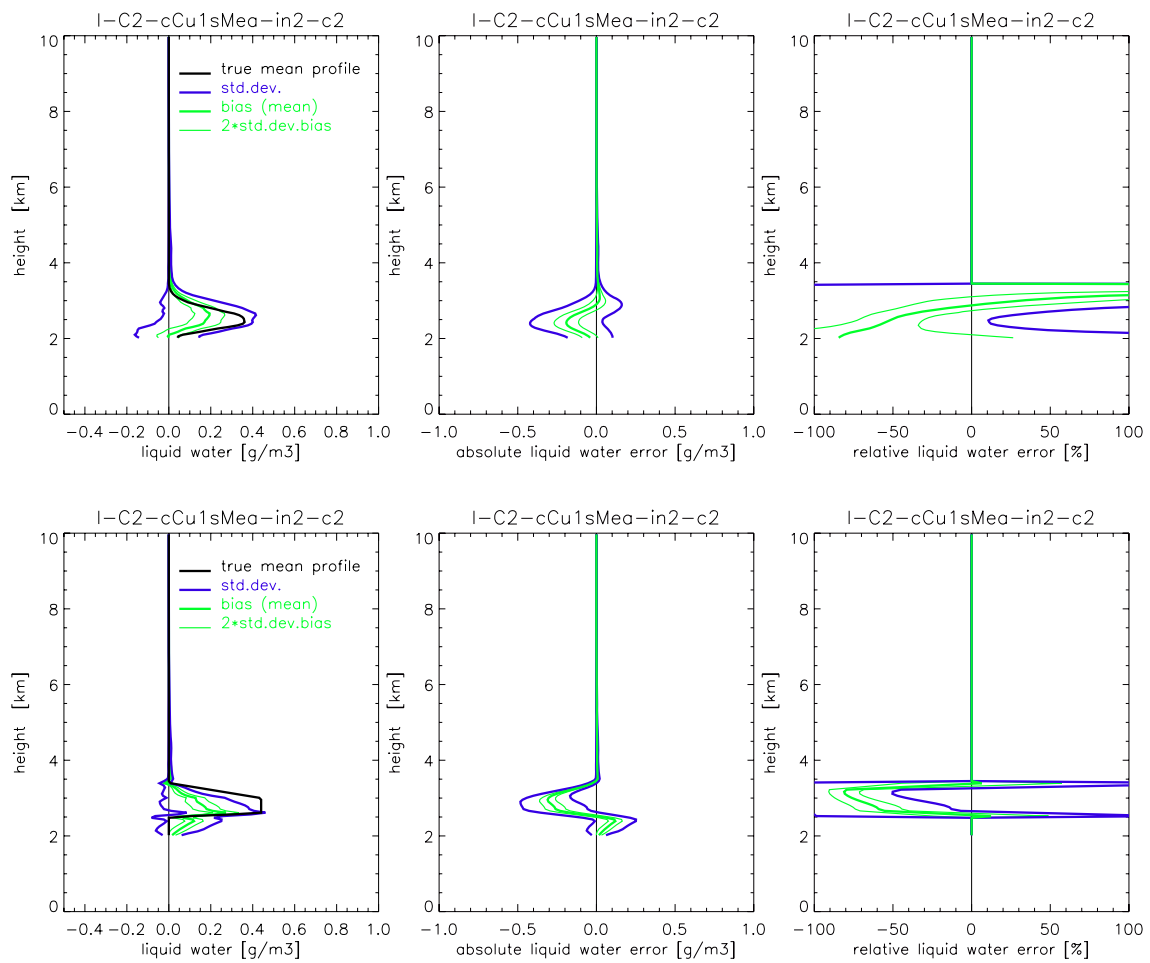


Fig. 3.3.18. Liquid water sample of reference profiles (upper panels) and single reference profile (lower panels) retrieval results for the mid-lat summer case (C2), instrumental errors (in2) scenario (therm. noise, C/No 67 dBHz, ampl. drift 0.62%/20sec, 1/f noise 0.02*T%, T=1-20sec, standard cloudy air retrieval). Statistics performance results (standard deviation, bias, 2 x std.deviation of bias) for an ensemble of 40 profiles are shown. The std.deviation is shown as +/- envelopes about the bias profiles. In the middle panels (for humidity and temperature) and the right panel (for humidity) the observational requirements, as set by the ACE+ MRD (v2.1/Jan 2004), are shown for reference (solid black, threshold requirements; dashed black, target requirements).

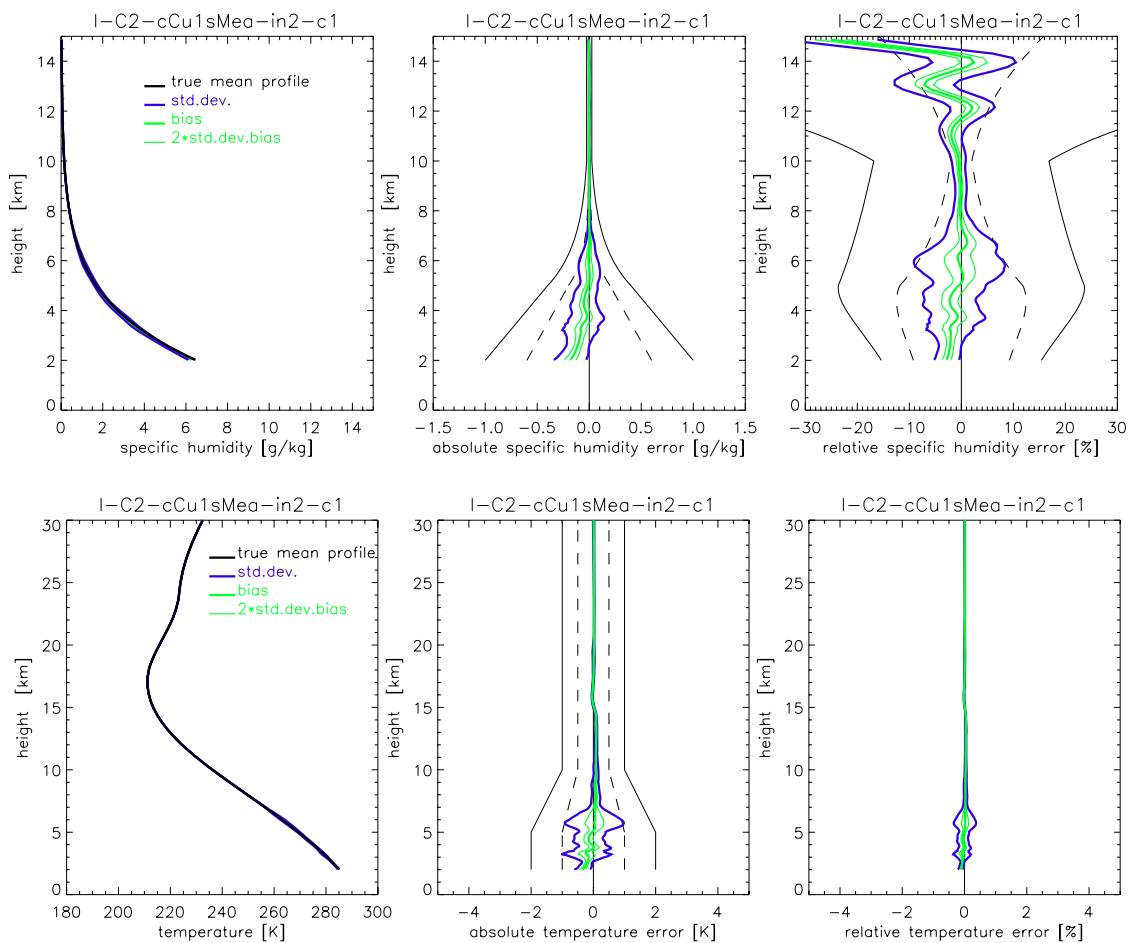


Fig. 3.3.19. Humidity (upper panels) and temperature (lower panels) retrieval results for the mid-lat summer case (C2), instrumental errors (in2) scenario (therm. noise, C/No 67 dBHz, ampl. drift 0.62%/20sec, 1/f noise 0.02*T%, T=1-20sec, advanced cloudy air retrieval). Statistics performance results (standard deviation, bias, 2 x std.deviation of bias) for an ensemble of 40 profiles are shown. The std.deviation is shown as +/- envelopes about the bias profiles. In the middle panels (for humidity and temperature) and the right panel (for humidity) the observational requirements, as set by the ACE+MRD (v2.1/Jan 2004), are shown for reference (solid black, threshold requirements; dashed black, target requirements).

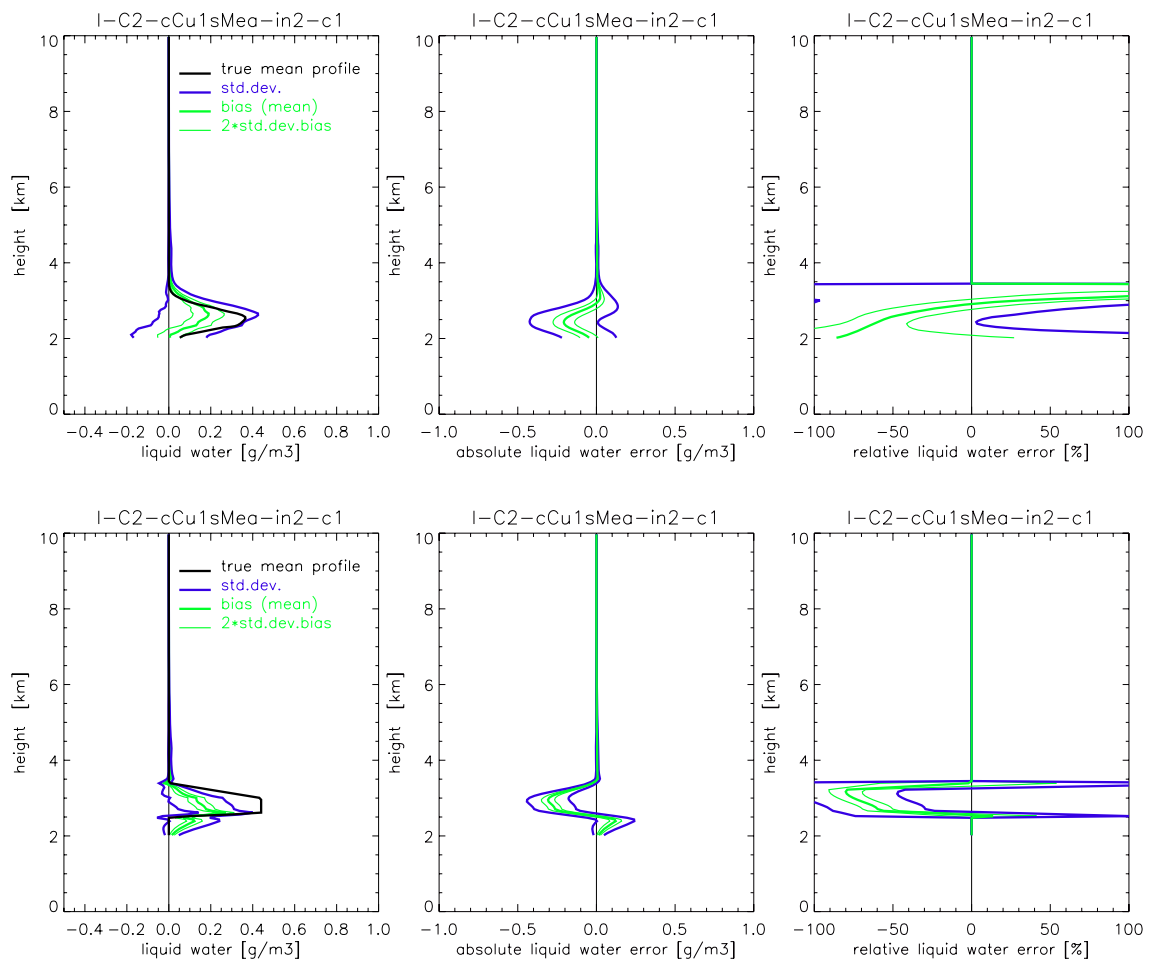


Fig. 3.3.20. Liquid water sample of reference profiles (upper panels) and single reference profile (lower panels) retrieval results for the mid-lat summer case (C2), instrumental errors (in2) scenario (therm. noise, C/No 67 dBHz, ampl. drift 0.62%/20sec, 1/f noise 0.02*T%, T=1-20sec, advanced cloudy air retrieval). Statistics performance results (standard deviation, bias, 2 x std.deviation of bias) for an ensemble of 40 profiles are shown. The std.deviation is shown as +/- envelopes about the bias profiles. In the middle panels (for humidity and temperature) and the right panel (for humidity) the observational requirements, as set by the ACE+ MRD (v2.1/Jan 2004), are shown for reference (solid black, threshold requirements; dashed black, target requirements).

4. Summary and Conclusions

This study addressed the expected quality of atmospheric profiles retrieved from ACE+ LEO-LEO occultation data. A performance analysis for instrumental errors using geometric optics processing (GOP) was carried out and retrieval results inspected for a whole range of scenarios in moist (clear) air as well as in the presence of clouds and in the presence of scintillations due to atmospheric turbulence.

The humidity and temperature retrieval results have been assessed relative to the observational requirements laid out in the ACE+ Mission Requirements Document (ACE+ MRD, 2004). From this assessment also inference is possible as to how adequate the main system requirements, as presently formulated in the appendix of the ACE+ MRD, are for achieving the observational requirements. In other words, the study results establish a much needed link between system requirements, guiding the EGOPS5 input parameter settings in observational system modeling, and observational requirements, which are set on the humidity and temperature retrieval results.

The main conclusion of the study is that the system requirements as currently laid in the ACE+ MRD are adequate to achieve the observational requirements. On one specific issue, namely doubts raised on the possibility of adequate retrieval below 7 km in the presence of scintillations, these are cleared by the evidence of this study. It is found that under median to mean scintillation conditions adequate retrieval is possible down to about 2 – 4 km, i.e., well into the lower troposphere, without prior information.

Using a further advanced retrieval algorithm involving weak prior temperature information below about 3 to 6 km (“best-fit temperature extrapolation”), statistical simulations with profile ensembles demonstrated that adequate retrieval is possible down towards the boundary layer also under severe turbulence, including mixed cloudy-turbulent conditions.

Other than radiometric atmospheric sounders, including advanced ones like the AIRS and IASI sensors, which by concept rely on prior information and provide no geopotential height explicitly, the ACE+ system thus is expected to furnish the unique capability of upper and middle troposphere sounding of consistent humidity, temperature, and geopotential height (or pressure) as function of altitude independent of prior information. In part of the lower troposphere below about 3 to 6 km the need for background temperature information is expected under adverse conditions, as in these cases the major information will be extracted from the bending angle rather than the transmission data.

Furthermore, the performance analysis demonstrated the essentially bias-free character of the retrieval products. This is a key characteristic rooting in the self-calibrating nature of the ACE+ occultation data, as detailed in the algorithmic description sections.

The overall evidence from this first end-to-end performance study under reasonably realistic conditions is that ACE+ can fulfil its scientific objectives laid out in the ACE+ MRD.

Acknowledgments. The authors thank U. Foelsche, A. Gobiet, A.K. Steiner (all IGAM/UG), and M. Gorbunov (IAP Moscow, IGAM/UG) for support in preparing some auxiliary software used in the study, and in particular for their various contributions to the EGOPS5 software. The EGOPS5 software, the core tool of the study, was developed by an international consortium led by IGAM/UG and involving partner teams at Danish Meteorological Institute, Denmark, Chalmers University of Technology, Sweden, and IEP/University of Bremen, Germany, and also all colleagues in these partner teams are thanked for their important contributions. EGOPS5 is based on strong heritage from EGOPS4, which was developed 1996–2003 by a consortium led by IGAM/UG and involving partner teams at Danish Meteorological Institute and TERMA Elektronik A/S, Denmark, the Met. Office, U.K., and Austrian Aerospace GmbH, Austria, with the major funding provided by the European Space Agency. The major funding for this study and for the development of EGOPS5 was provided by the European Space Agency under ESA/ESTEC Contract No. 16743/02/NL/FF. Furthermore, co-funding was received for the work from the START research award of G.K. funded by the Austrian Ministry for Education, Science, and Culture and managed under Program No. Y103-N03 of the Austrian Science Fund.

References

- ACE+ MRD**, ACE+ Atmosphere and Climate Explorer Mission Requirements Document (for Phase A), *Doc.No. ESD/ACE+/MRD/001/TW-Issue 2 rev. 1*, 51 p., ACE+ Mission Advisory Group, ESA/ESTEC, Noordwijk, Netherlands, 2004.
- Bjørck, Å.**, Numerical methods for least square problems, *society of industrial and applied mathematics*, 1996.
- Budden, K.G.**, The propagation of radio waves - The theory of radio waves of low power in the ionosphere and magnetosphere, Cambridge Univ. Press, Cambridge, U.K., 1985.
- Fjeldbo, G., A. Kliore, and V.R. Eshleman**, The neutral atmosphere of Venus as studied with the Mariner V radio occultation experiments, *Astron. J.*, 76, 2, 123-140, 1971.
- Foelsche, U.**, Tropospheric water vapor imaging by combination of ground-based and spaceborne GNSS sounding data (Ph.D. thesis), *Wissenschaftl. Ber. No. 10*, 164 p., Inst. Meteorol. Geophys., Univ. of Graz, Austria, 1999.
- Foelsche, U., G. Kirchengast, A.K. Steiner, L. Kornblueh, E. Manzini, and L. Bengtsson**, Klimawandel-Monitoring mit satellitengetragenen GNSS Okkultationssensoren, *Proc. CD-Rom DACH (deutsch-österreich.-schweiz.) Meteorologentagung 2001*, Sept. 2001, Vienna, Austria, 19p., 2001.
- Giering, R., and T. Kaminski**, Recipes for Adjoint Code Construction, *ACM Trans. On Math. Software*, 24(4), p. 437-474, 1998.
- Gobiet, A., and G. Kirchengast**, Sensitivity of atmospheric profiles retrieved from GNSS occultation data to ionospheric residual and high-altitude initialization errors, *Techn. Report for ESA/ESTEC No. 1/2002*, Inst. for Geophys., Astrophys., and Meteorol., Univ. of Graz, Austria, 2002.
- Gobiet, A., G. Kirchengast, J. Wickert, C. Retscher, D. Wang, and A. Hauchecorne**, Evaluation of Stratospheric Radio Occultation Retrieval Using Data from CHAMP, MIPAS, GOMOS, and ECMWF Analysis Fields, *Springer Proc. Book, 2nd CAHMP Science Meeting, Sept. 2003*, Potsdam, Germany, accepted, 2004.

- Gorbunov, M.E.**, Radioholographic methods for processing radio occultation data in multi-path regions, *DMI Tech. Report 01-02*, Danish Met. Inst., Copenhagen, Denmark, 2001a.
- Gorbunov, M.E.**, Radio-holographic analysis and validation of Mircrolab-1 radio occultation data in the lower troposphere, *J. Geophys. Res.*, submitted manuscript, 2001b.
- GRAS-SAG**, The GRAS instrument on METOP, *ESA/EUMETSAT Rep. (ESA No. VR/3021 /PI, EUM.No. EPS/MIS/IN/9)*, 38 pp., ESA/ESTEC, Noordwijk, Netherlands, 1998.
- Healy, S.B., and J.R. Eyre**, Retrieving temperature, water vapour and surface pressure information from refractive-index profiles derived by radio occultation: A simulation study, *Quart. J. Roy. Meteorol. Soc.*, 126, 1661-1683, 2000.
- Healy, S.B.**, Smoothing radio occultation bending angles above 40 km, *Ann. Geophys.*, 19, 459-468, 2001.
- Hedin, A.E.**, Extension of the MSIS thermosphere model into the middle and lower atmosphere, *J. Geophys. Res.*, 96, 1159-1172, 1991.
- Hoeg, P., A.S. Jensen, H. Vedel, E. Kaas, and G. Kirchengast**, ACE (Atmosphere Climate Experiment) Scientific Support Study, *Proposal to ESA/ESTEC*, 40p., Danish Met. Institute, Copenhagen, Denmark, 2000.
- Jensen, A.S., M. Lohmann, H.-H. Benzon, and A. Nielsen**, Full spectrum inversion of radio occultation signals, *Radio Sci.*, 38, 763, doi: 10.1029/2002RS002, 2003.
- Kirchengast, G.**, End-to-end GNSS Occultation Performance Simulator overview and exemplary applications, *Wissenschaftl. Ber. No. 2/1998*, Inst. for Meteorol. and Geophys., Univ. of Graz, Austria, 1998.
- Kirchengast, G., and P. Hoeg**, The ACE+ Mission: An Atmosphere and Climate Explorer based on GPS, GALILEO, and LEO-LEO Radio Occultation, *Proc. Book, 1st Int'l Workshop on Occultations for Probing Atmosphere and Climate (OPAC-1)*, Sept. 2002, Graz, Austria, Springer Verlag, in press, 2004.
- Kirchengast, G., J. Hafner, and W. Poetzi**, The CIRA86aQ_UoG model: An extension of the CIRA-86 monthly tables including humidity tables and a Fortran95 global moist air climatology model, *Techn. Report for ESA/ESTEC No. 8/1999*, 18p., Inst. Meteorol. Geophys., Univ. of Graz, Austria, 1999.
- Kirchengast, G., J. Fritzer, and J. Ramsauer**, End-to-end GNSS Occultation Performance Simulator Version 4 (EGOPS4) Software User Manual (Overview and Reference Manual), *Techn. Report for ESA/ESTEC No. 5/2001*, Inst. for Geophys., Astrophys., and Meteorol., Univ. of Graz, Austria, 2001.
- Kirchengast, G., et al., P. Hoeg et al., G. Elgered et al., and S. Buehler et al.**, ESA-ACEPASS: ACE+ Phase A Scientific Support Study on LEO-LEO Occultation Characterization, *Proposal to ESA*, 67 p., Inst. for Geophys., Astrophys., and Meteorol., Univ. of Graz, Austria, 2002.
- Kuhn, T.**, Atmospheric Scintillation, *Draft Report to ESA/ESTEC-Feb.2003*, 59 p., IEP/Univ. of Bremen, Germany, 2003a.
- Kuhn, T.**, TurbScintModel – the EGOPS scintillation model for LEO-LEO occultations, *Draft Report to ESA/ESTEC-Oct.2003*, 22 p., IEP/Univ. of Bremen, Germany, 2003b.

- Kursinski, E.R., G.A. Hajj, J.T. Schofield, R.P. Linfield, and K.R. Hardy**, Observing Earth’s atmosphere with radio occultation measurements using the Global Positioning System, *J. Geophys. Res.*, 102, D19, 23429 - 23465, 1997.
- Kursinski, E.R., S. Leroy, and B. Herman**, The radio occultation technique, *J. Atmos. Solar-Terr. Phys.*, 11, 53-114, 2000.
- Kursinski, E.R., S. Syndergaard, D. Flittner, D. Feng, G. Hajj, B. Herman; D. Ward and T. Yunck**, A microwave occultation observing system optimized to characterize atmospheric water, temperature and geopotential via absorption, *J. Atmos. Oceanic Technol.*, 19(12), 1897-1914, 2002.
- Landolt-Börnstein**, *Geophysics of the Solid Earth, the Moon and the Planets – Numerical Data and Functional Relationships in Science and Technology*, Vol. V/2a (Fuchs, K., and H. Stoffel, Eds.), 332–336, Springer Verlag, Berlin–Heidelberg, 1984.
- Leroy, S.**, Amplitude of an occultation signal in three dimensions, *Unpublished Script (pers. communications)*, 2001.
- Liebe, H.J., G. Hufford, and M. Cotton**, Propagation Modeling of moist air and suspended water/ice particles at frequencies below 1000 GHz, in *52nd Specialists Meeting of the Electromagnetic Wave Propagation Panel*, p. 542, AGARD, 1993.
- Melbourne, W.G., E. Davis, C. Duncan, G. Hajj, K. Hardy, E. Kursinski, T. Meehan, L. Young, and T. Yunck**, The application of space borne GPS to atmospheric limb sounding and global change monitoring, *JPL Publ.*, 94-18, 147 pp., Pasadena, California, 1994.
- Nielsen, A.S. et al., T. Kuhn et al., and P. Eriksson et al.**, Characterization of ACE+ LEO-LEO Radio Occultation Measurements, *Draft Report, ESTEC contract no. 16743/02/NL/FF (ACEPASS study)*, 2003.
- Ramsauer, J. , and G. Kirchengast**, Sensitivity of atmospheric profiles retrieved from GNSS radio occultation data to instrumental errors, *Techn. Report for ESA/ESTEC No. 6/2001*, 62p., Inst. for Geophys., Astrophys., and Meteorol., Univ. of Graz, Austria, 2001.
- Rieder, M.J., and G. Kirchengast**, Error analysis for mesospheric temperature profiling by absorptive occultation sensors, *Ann. Geophys.*, 19, 71–81, 2001a.
- Rieder, M.J., and G. Kirchengast**, Error analysis and characterization of atmospheric profiles retrieved from GNSS occultation data, *J. Geophys. Res.*, 106, 31, 755–31,770, 2001b.
- Rodgers, C.**, Characterization and error analysis of profiles retrieved from remote sounding measurements, *J. Geophys. Res.*, 95, 5587-5595, 1990.
- Rodgers, C.**, *Inverse Methods for atmospheric sounding – Theory and Practice*, World Scientific Publishing, Signapore, 2000.
- Salby, M.L.**, *Fundamentals of Atmospheric Physics*, Academic Press, San Diego, 1996.
- Schanda, E.**, *Physical fundamentals of remote sensing*, Springer, Berlin, 1986.
- Smith, E.K., and S. Weintraub**, The constants in the equation for atmospheric refractive index at radio frequencies, *Proceedings of the I.R.E.*, 41, 1035-1037, 1953.
- Sokolovskiy, S.**, Inversion of radio occultation amplitude data, *RS*, 35(1), 97-105, 2000.

- Steiner, A.K.**, High-resolution sounding of key climate variables using the radio occultation technique, *IGAM Wissenschaftl. Ber.-3/1998*, Inst. for Geophys., Astrophys., and Meteorol., Univ. of Graz, Austria, 1998.
- Steiner, A.K., G. Kirchengast, and H.P. Ladreiter**, Inversion, error analysis and validation of GPS/MET occultation data, *Ann. Geophysicae*, 17, 122-138, 1999.
- Steiner, A.K., G. Kirchengast, U. Foelsche, L. Kornblueh, E. Manzini, and L. Bengtsson**, GNSS occultation sounding for climate monitoring, *Phys. Chem. Earth (A)*, 26, 113–124, 2001.
- Steiner, A.K., and G. Kirchengast**, Ensemble-based analysis of errors in atmospheric profiles retrieved from GNSS occultation data, *Springer Proc. Book, 1st Int'l Workshop on Occultations for Probing Atmosphere and Climate (OPAC-1)*, Sept. 2002, Graz, Austria, in press, 2004.
- Syndergaard, S.**, Modeling the impact of the Earth's oblateness on the retrieval of temperature and pressure profiles from limb sounding, *J. Atmos. Terr. Phys.*, 60, 171-180, 1998.
- Syndergaard, S.**, Retrieval analysis and methodologies in atmospheric limb sounding using the GNSS radio occultation technique. *DMI Scient. Report 99-6*, 131 pp., Danish Meteorol. Institute, Copenhagen, Denmark, 1999.
- Vorob'ev, V.V., and T.G. Krasnil'nikova**, Estimation of the accuracy of the atmospheric refractive index recovery from doppler shift measurements at frequencies used in the NAVSTAR system, *Phys. of Atmos. and Oceans*, 29, 602-609, 1994.

(intentionally left blank, back page if double-sided print)

Appendix A.

A.1. ACE+ Constellation Two Line Element (TLE) Files

ACE+ transmitter (Tx) satellites

```
ACE+TX1-800km          H1          betalim = 10.0
1      1  99003USR 99001.00000000 .00000000 00000-0 00000-0 0 0010
2      1  98.6300 243.6000 0001000 90.0000 0.0000 14.31502844 0
ACE+TX2-800km          H2          betalim = 10.0
1      1  99004USR 99001.00000000 .00000000 00000-0 00000-0 0 0010
2      1  98.6300 243.6000 0001000 90.0000 180.0000 14.31502844 0
```

ACE+ receiver (Rx) satellites

```
ACE+RX1-650km          L1          betalim = 10.0
1      1  99001USR 99001.00000000 .00000000 00000-0 00000-0 0 0010
2      1  97.9500 63.6000 0001000 90.0000 0.0000 14.74733736 0
ACE+RX2-650km          L2          betalim = 10.0
1      1  99002USR 99001.00000000 .00000000 00000-0 00000-0 0 0010
2      1  97.9500 63.6000 0001000 90.0000 80.0000 14.74733736
```

A.2. Mission Analysis/Planning input (example)

```
[*Project-Id and Task-Id*]
EGOPS Input File Version = 5.0.3
Creation Date & Time      = 2004-02-02 18:38:00
Task-Type                 = MAnPl
Project-Id                = SDECMWF1
Task-Id                   = M-GCM1

[*Data Type Selection*]
Data Type                 = LEO-LEO Occultation Data

[*UT Range*]
Start_Time                = 020915.000000 [yyymmdd.hhmmss]
Simul_Time_Range         = 0240000 [hhmmss]

[*Height Levels*]
Hlo1 Hhi1 HStep1 dh1     = 1.0 12.0 1.0 0.10 [km]
Hlo2 Hhi2 HStep2 dh2     = 12.0 30.0 2.0 0.20 [km]
Hlo3 Hhi3 HStep3 dh3     = 30.0 80.0 10.0 1.00 [km]

[*Geographic Area of Interest*]
GeogrAreaChoice           = Global

[*Earth Figure Model*]
EarthFigModelChoice       = Ellip.WGS84

[*Tx-to-Rx Ray Treatment*]
RayTreatmentChoice        = Bended Rays (Exp. Atmos.)

[*Tx System and Orbit Specifications*]
Tx SatSystemChoice        = ACE+
Tx OrbitModelChoice       = SGP Orbits (Impr. Kepler)
Tx1 OrbitElemFilename     = Tx-ACE-Plus_1999001.tle

[*Tx Antennae Specifications*]
Tx -V AntennaChoice       = Used
```

```
Tx -V BoresightElevation = 27.0 [deg]
Tx -V BoresightAzimuth  = 180.0 [deg]
Tx -V FOVChoice         = Ell_Cartes
Tx -V TPBW Vertical     = 10.0 [deg]
Tx -V TPBW Horizontal   = 90.0 [deg]
Tx +V AntennaChoice     = Used
Tx +V BoresightElevation = 27.0 [deg]
Tx +V BoresightAzimuth  = 0.0 [deg]
Tx +V FOVChoice         = Ell_Cartes
Tx +V TPBW Vertical     = 10.0 [deg]
Tx +V TPBW Horizontal   = 90.0 [deg]

[*Rx System and Orbit Specifications*]
Rx SatSystemChoice      = ACE+
Rx OrbitModelChoice     = SGP Orbits (Impr. Kepler)
Rx OrbitElemFilename    = Rx-ACE-Plus_1999001.tle

[*Rx Antennae Specifications*]
Rx -V AntennaChoice     = Used
Rx -V BoresightElevation = 27.0 [deg]
Rx -V BoresightAzimuth  = 180.0 [deg]
Rx -V FOVChoice         = Ell_Cartes
Rx -V TPBW Vertical     = 10.0 [deg]
Rx -V TPBW Horizontal   = 90.0 [deg]
Rx +V AntennaChoice     = Used
Rx +V BoresightElevation = 27.0 [deg]
Rx +V BoresightAzimuth  = 0.0 [deg]
Rx +V FOVChoice         = Ell_Cartes
Rx +V TPBW Vertical     = 10.0 [deg]
Rx +V TPBW Horizontal   = 90.0 [deg]

[*Visibility Infos on Differencing*]
DiffVisInfChoice        = No_Diff_Vis_info
TrackVisInfChoice       = No_Track_Vis_info

[* EOF *]
```

A.3. Forward Modeling input (example)

```
[*Project-Id and Task-Id*]
EGOPS Input File Version = 5.0.3
Creation Date & Time     = 2004-02-02 19:27:12
Task-Type                = FoMod
Project-Id               = SDRef1
Task-Id                  = F-C2-c0s0

[*Occ. Event Simulation Type/Specifications*]
OccEventSimulType       = Single Event/Ideal Geometry
OccEv.HeightRange       = 1.0 80.0 [km]
TangPointLoc (Lat Lon)  = 40.0 0.0 [deg]
AziOccPlane (N over W)  = 0 [deg]
EventStart Date/Time    = 030715.120000 [yymmdd.hhmmss]
SatHeights (hRx hTx)    = 650 850 [km]

[*Tx Channels and FoMod Sampling Rate Specification*]
Tx ChannelSetChoice     = ACE+ Standard (NChan= 3 F1-F3)
FoMod Sampling Rate     = 10.0 [Hz]

[*Atmospheric Models Choice/Specifications*]
AtmModelChoice          = HLat 2D Atmosphere (CIRA86aQ_UoG)
AtmModelStructureChoice = Sph. Symmetry (no horizontal var.)
HumidityChoice          = Humidity included (moist air)
```

CloudsandRainChoice = No Clouds+Rain
AtmDistModelChoice = No Atmos. Disturbance superposed

[*Ionospheric Models Choice/Specifications*]

IonModelChoice = No Ionosphere

[*Signal Propagation Simulator Specifications*]

PropSimulatorType = Full-3D Ray Tracer
PropSimulatorAccuracy = < ~1 mm
Extended Data Output = Dopp-Tran-Bend-pLC1 Data

[*Earth Figure Model*]

EarthFigModelChoice = Spherical

[* EOF *]

A.4. Observation System Modeling input (example)

[*Project-Id and Task-Id*]

EGOPS Input File Version = 5.0.3
Creation Date & Time = 2004-02-02 19:58:28
Task-Type = OSMod
Project-Id = SDRef1
Task-Id = O-C2-c0s0-in1

[*Occ. Event Simulation Type/Specifications*]

OccEventSimulType = Single Event/Ideal Geometry
OccEv.HeightRange = 1.0 80.0 [km]
ReferenceFoMod/Task-Id = F-C2-c0s0
OccNoRange = 1 1 0

[*Tx Channels and Rx Sampling Rate Specification*]

Tx ChannelSetChoice = ACE+ Standard (NChan= 3 F1-F3)
Rx Sampling Rate = 10.0 [Hz]

[*POD Error Modeling/Specifications*]

PODErrorModelChoice = No POD Errors

[*Tx-Rx System Simulator Specifications*]

TxRx SysSimulatorType = Parameterized Receiving System Simulator
Extended Data Output = C/N0 and Antenna Data

[*Tx Antennae Specifications*]

Tx -V AntennaChoice = Used
Tx -V BoresightElevation = 27.0 [deg]
Tx -V BoresightAzimuth = 180.0 [deg]
Tx -V FOVChoice = Ell_Cartes
Tx -V HPBW Vertical = 90.0 [deg]
Tx -V HPBW Horizontal = 90.0 [deg]
Tx -V AntGain/Boresight = 24.8 [dB]
Tx -V BoresightTracking = Yes
Tx +V AntennaChoice = Used
Tx +V BoresightElevation = 27.0 [deg]
Tx +V BoresightAzimuth = 0.0 [deg]
Tx +V FOVChoice = Ell_Cartes
Tx +V HPBW Vertical = 90.0 [deg]
Tx +V HPBW Horizontal = 90.0 [deg]
Tx +V AntGain/Boresight = 24.8 [dB]
Tx +V BoresightTracking = Yes

[*Tx Performance Modeling*]

TxPerformModelChoice = No Transmitter Perf. Model

```
[*Rx Antennae Specifications*]
Rx -V AntennaChoice          = Used
Rx -V BoresightElevation    = 27.0 [deg]
Rx -V BoresightAzimuth     = 180.0 [deg]
Rx -V FOVChoice             = Ell_Cartes
Rx -V HPBW Vertical         = 10.0 [deg]
Rx -V HPBW Horizontal       = 40.0 [deg]
Rx -V AntGain/Boresight     = 24.8 [dB]
Rx -V BoresightTracking     = Yes
Rx +V AntennaChoice         = Not Used

[*Rx Performance Modeling*]
RxThermNoiseModelChoice     = LEO-LEO Thermal Noise Model
ChannelsC/N0Adjustment     = -2.40 -1.70 -0.80 [dBHz]
AntennaNoiseTemp10GHz      = 80.0 [K]
ReceiverNoiseTemp10GHz     = 160.0 [K]
Rx1/fNoiseModelChoice      = 1/f Amplitude Noise Model
1/fReferenceHeight         = 25.0 [km]
PeriodInterval TMin TMax   = 1.00 20.00 [sec]
ErrorSlopePeriodDomain     = 0.050 [dB/min]
RxPolyAmplDriftModel       = Polynomial Ampl. Drift Model
DriftApplicationType       = As specified
PolyReferenceHeight        = 25.0 [km]
LinearDriftSlope           = 0.060 [dB/min]
QuadrDriftCurvature       = 0.0000 [dB/min2]
3rdOrderDriftCurvChange   = 0.00000 [dB/min3]
RxSinAmplDriftModel       = No Sinusoidal Ampl. Drifts

[*Local Multipath Modeling*]
LocalMultipModelChoice     = No Local Multipath

[*Differencing Treatment/Clocks Modeling*]
DiffTreatClocksChoice     = Perfect Clocks (No Differencing)

[*Atmospheric Models Choice/Specifications*]
AtmModelChoice            = HLat 2D Atmosphere (CIRA86aQ_UoG)
AtmModelStructureChoice   = Sph. Symmetry (no horizontal var.)
HumidityChoice            = Humidity included (moist air)
CloudsandRainChoice       = No Clouds+Rain
AtmDistModelChoice        = No Atmos. Disturbance superposed

[*Ionospheric Models Choice/Specifications*]
IonModelChoice            = No Ionosphere

[*Earth Figure Model*]
EarthFigModelChoice       = Spherical

[* EOF *]
```

A.5. Inversion/Retrieval input (example)

```
[*Project-Id and Task-Id*]
EGOPS Input File Version = 5.0.3
Creation Date & Time     = 2004-02-02 20:29:49
Task-Type                = InRet
Project-Id               = SDRfl1
Task-Id                  = I-C2-c0s0-in0-m1

[*Occ. Event Type/Specifications*]
OccDataType              = SimData
OccEventType             = Sample of Events/Realistic Geometry
```

ACE+ LEO-LEO Occultation: Statistical Performance Analysis

“ESA-ACEPASS – Analysis of instrumental and GOP performance impacts”

```
OccNoRange           =      1      1      0
OccEv.HeightRange    =      1.0  80.0 [km]
ReferenceOSMod/Task-Id = O-C2-c0s0-in0

[*Tx Channels and Rx Sampling Rate Specification*]
Tx ChannelSetChoice  = ACE+ Standard (NChan= 3 F1-F3)
Rx Sampling Rate     =      10.0 [Hz]

[*Bending Angle and Transmission Retrieval Specifications*]
BendAngleRetToolChoice = Advanced Geom.Optics Bend.Angle Retrieval
IonoCorrectionType     = Phase Correction
StatOptimizationType  = Optimize invoking MSIS90_DMI
TransmRetToolChoice    = Standard Channel Transmission Retrieval
I/I0 RefHeightperChannel = 25.0 25.0 25.0 [km]
IOValue AvHeightInterval = 4.0 [km]

[*Refractivity Profiles Retrieval Specifications*]
RefProfRetToolChoice  = Abel Transform Complex Refr.Profiles Retrieval

[*Atmospheric Profiles Retrieval Specifications*]
AtmProfRetToolChoice  = Complex Refr.Based Atmos. Profiles
ComplRefrInvRetType   = T,q,e,p,rho,w by Opt.Inverse Estimation
RealRefrErrorModelChoice = 1/z (<zRef) + exp(z) (>zRef) Errors
RealRefrRMSError_zRef = 0.10 [%] (zRef: 15 km)
ImagRefrErrorModelChoice = fac*dNi(z0)*W(z) SNR-based Errors
ImagRefrRMSError_spec = 1.00 [1] (scale factor)
AtmProfRetrievalMode  = p+T+q (moist air) Retrieval

[*Atmospheric Models Choice/Specifications*]
AtmModelChoice        = HLat 2D Atmosphere (CIRA86aQ_UoG)
AtmModelStructureChoice = Sph. Symmetry (no horizontal var.)
HumidityChoice         = Humidity included (moist air)
CloudsandRainChoice    = No Clouds+Rain
AtmDistModelChoice     = No Atmos. Disturbance superposed

[*Ionospheric Models Choice/Specifications*]
IonModelChoice         = No Ionosphere

[*Earth Figure Model*]
EarthFigModelChoice    = Spherical

[* EOF *]
```

Ω end of document Ω